NASA/CR—2003-212369

Design and Test of Fan/Nacelle Models Quiet High-Speed Fan Design

Russ Repp, David Gentile, David Hanson, and Srinivas Chunduru
Honeywell Engines, Systems and Services

July 2003

The NASA STI Program Office . . . in Profile

Since its founding, NASA has been dedicated to the advancement of aeronautics and space science. The NASA Scientific and Technical Information (STI) Program Office plays a key part in helping NASA maintain this important role.

The NASA STI Program Office is operated by Langley Research Center, the Lead Center for NASA's scientific and technical information. The NASA STI Program Office provides access to the NASA STI Database, the largest collection of aeronautical and space science STI in the world. The Program Office is also NASA's institutional mechanism for disseminating the results of its research and development activities. These results are published by NASA in the NASA STI Report Series, which includes the following report types:

- TECHNICAL PUBLICATION. Reports of completed research or a major significant phase of research that present the results of NASA programs and include extensive data or theoretical analysis. Includes compilations of significant scientific and technical data and information deemed to be of continuing reference value. NASA's counterpart of peer-reviewed formal professional papers but has less stringent limitations on manuscript length and extent of graphic presentations.

- TECHNICAL MEMORANDUM. Scientific and technical findings that are preliminary or of specialized interest, e.g., quick release reports, working papers, and bibliographies that contain minimal annotation. Does not contain extensive analysis.

- CONTRACTOR REPORT. Scientific and technical findings by NASA-sponsored contractors and grantees.

- CONFERENCE PUBLICATION. Collected papers from scientific and technical conferences, symposia, seminars, or other meetings sponsored or cosponsored by NASA.

- SPECIAL PUBLICATION. Scientific, technical, or historical information from NASA programs, projects, and missions, often concerned with subjects having substantial public interest.

- TECHNICAL TRANSLATION. English-language translations of foreign scientific and technical material pertinent to NASA's mission.

Specialized services that complement the STI Program Office's diverse offerings include creating custom thesauri, building customized databases, organizing and publishing research results . . . even providing videos.

For more information about the NASA STI Program Office, see the following:

- Access the NASA STI Program Home Page at ***http://www.sti.nasa.gov***

- E-mail your question via the Internet to help@sti.nasa.gov

- Fax your question to the NASA Access Help Desk at 301–621–0134

- Telephone the NASA Access Help Desk at 301–621–0390

- Write to:
  NASA Access Help Desk
  NASA Center for AeroSpace Information
  7121 Standard Drive
  Hanover, MD 21076

NASA/CR—2003-212369

Design and Test of Fan/Nacelle Models Quiet High-Speed Fan Design

Russ Repp, David Gentile, David Hanson, and Srinivas Chunduru
Honeywell Engines, Systems and Services

Prepared under Contract NAS3–27752

National Aeronautics and
Space Administration

Glenn Research Center

July 2003

Available from

NASA Center for Aerospace Information
7121 Standard Drive
Hanover, MD 21076

National Technical Information Service
5285 Port Royal Road
Springfield, VA 22100

Available electronically at http://gltrs.grc.nasa.gov

TABLE OF CONTENTS

TABLE OF CONTENTS (Contd)

LIST OF FIGURES

LIST OF FIGURES (Contd)

LIST OF FIGURES (Contd)

LIST OF FIGURES (Contd)

LIST OF FIGURES (Contd)

LIST OF FIGURES (Contd)

LIST OF FIGURES (Contd)

LIST OF FIGURES (Contd)

LIST OF FIGURES (Contd)

LIST OF FIGURES (Contd)

LIST OF TABLES

LIST OF TABLES (Contd)

NAS3-27752, NASA AST AOI 14
DESIGN AND TEST OF FAN/NACELLE MODELS
QUIET HIGH-SPEED FAN
DESIGN REPORT

1.0 SUMMARY

1.1 Purpose

The primary objective of the Quiet High-Speed Fan (QHSF) program was to develop an advanced high-speed fan design that will achieve a 6 dB reduction in overall fan noise over a baseline configuration while maintaining similar performance. The program applies and validates acoustic, aerodynamic, aeroelastic, and mechanical design tools developed by NASA, US industry, and academia. The successful fan design will be used in an AlliedSignal Engines (AE) advanced regional engine to be marketed in the year 2000 and beyond. This technology is needed to maintain US industry leadership in the regional turbofan engine market.

1.2 Conclusions

The AE/QHSF was designed to match the baseline rotor design point performance and yet achieve a 6 dB reduction. Innovative techniques in coupling the aerodynamic and mechanical analyses, along with design of experiments (DOE's) involving multiple engineering disciplines accomplished the effort. The result was a fan stage design with a forward swept rotor with 50 degrees of leading edge sweep that matched the baseline aerodynamic performance and achieved all mechanical and aeroelastic design criteria; and, a stator lean tailored for minimum rotor-stator acoustic interaction.

1.3 Design Procedure

The design technique used for the QHSF involved early design input from the Aerodynamic, Mechanical, Acoustic, and Aeroelastic disciplines through the use of design of experiments. Additional optimization procedures were used to enhance and verify the DOE analyses and results. Four DOE's were completed for the rotor and two for the stator which focused on achieving the design goals without violating established design criteria.

1.4 Design Summary/Perspective

In order to obtain the design goal of a 6 dB reduction, the design concentrated on three aspects. Reduction of the inlet relative normal Mach number, position of the shock within the passage, and minimizing rotor-stator interaction effects. Leading edge effective sweep was used to reduce the inlet relative normal Mach number, while mean-camber line blade angle distributions were used to correctly position the shock in the blade-to-blade passage. Although some design constraints were imposed on the stator design, rotor-stator interaction effects were minimized by controlling the rotor wake impingement on the stator leading edge.

The AE/QHSF is a forward swept rotor designed to match the design point performance of the baseline. It incorporates relatively large amounts of leading edge effective sweep, and yet with the use of statistical analyses and optimization procedures has reduced stress and weight while maintaining adequate aeroelastic and critical vibration margins relative to the baseline. Table 1.4-1 shows a summary of the AE/QHSF design features at the aerodynamic design point.

TABLE 1.4-1 AE/QHSF SUMMARY
AERODYNAMIC DESIGN POINT

Performance Parameters:					
Inlet corrected flow ……..	98.65 lbm/s				
Bypass ratio ……	3.78				
	DAWES Results in AXCAPS				Test
	QHSF		Baseline		Baseline
	Rotor	Stage	Rotor	Stage	Stage
Bypass pressure ratio …….	1.839	1.813	1.839	1.811	1.844
Core pressure ratio ……	1.845	1.817	1.777	1.741	1.718
Bypass efficiency (ad) …….	0.883	0.860	0.888	0.865	0.889
Core efficiency (ad) ……	0.960	0.934	0.961	0.923	0.918
O/A pressure ratio ……..		1.813		1.796	1.818
O/A efficiency (ad) ……..		0.874		0.875	0.895
Rotor Parameters:					
Number of blades ……..…	22				
Corrected RPM ……..…	15358				
Inlet tip diameter ……..…	22.0 inches				
Corrected tip speed ……..…	1474 ft/s				
Hub - tip ratio ……	0.35				
Aspect ratio ……	1.35				
Inlet specific flow ……..…	42.6 lbm/s/ft^2				
Hub and tip slope ……..……..	28^o, -7^o				
Hub work coefficient ……	2.5				
Inlet tip rel Mach no. ……..…	1.43				
Stator Parameters:					
Number of vanes ……..…	52				
Aspect ratio ……..	2.42				
Exit Mach no. (avg.) ……...	0.52				
Exit air angle (avg.) ……	0^o				

2.0 INTRODUCTION AND BACKGROUND

2.1 AST Area of Interest 14

Area of Interest 14 specifically addresses two level-three milestones to support "Model Tests for Code Validation/Concept Evaluation" in the Noise Reduction element of the NASA Advanced Subsonic Technology (AST) Program:

- Select second-generation, low-noise concepts for model tests (4Q, FY 1997)
- Complete second-generation model tests for low noise designs (4Q, FY 1999)

A 2-year effort was originally proposed for this effort. During the first year, a calibration of the acoustic and aerodynamic prediction methods was performed and a baseline fan definition was established and evaluated. The second year activities were to include evaluation of several candidate noise reduction concepts using combinations of rotor and stator lean and sweep. The program scope has since been expanded. The program roadmap is illustrated in Figure 2.1-1. Three fan designs are used in the program. The existing NASA-Lewis QF-12 fan and an AE TFE derivative fan serve as baseline configurations. Data from these fans will aid in design tool validation. A new advanced fan was designed by AE. The program will lead to a model scale test using the Ultra High Bypass (UHB) Propulsion Simulator in the NASA-Lewis 9 x 15-foot wind tunnel.

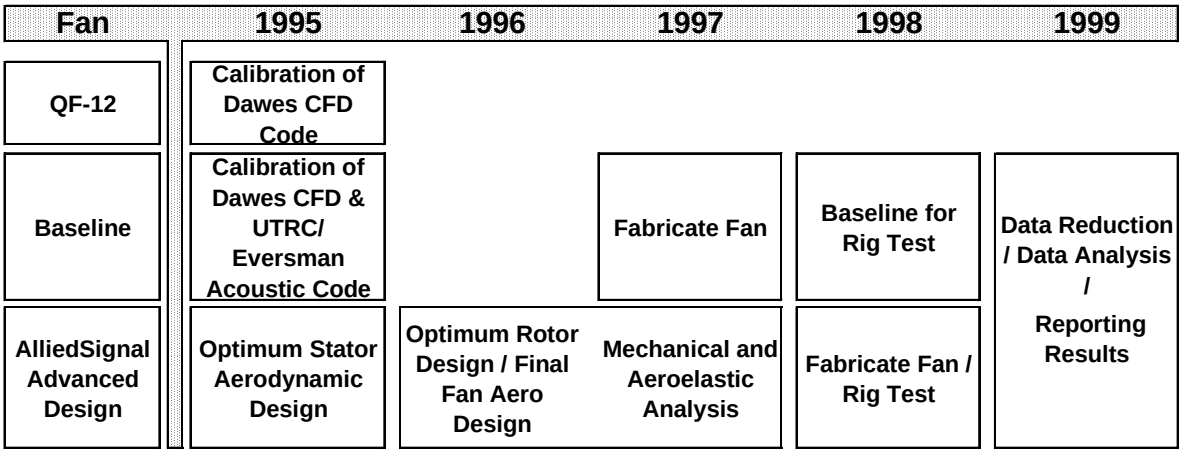

Figure 2.1-1. The Quiet High-Speed Fan Program Roadmap Targets a Wind Tunnel Test in October of 1998.

2.2 Quiet High Speed Fan Program

The QHSF program is a cooperative effort between AE and the NASA Lewis Research Center. Both NASA and AE will design an advanced high-speed fan that will be tested on the Universal Propulsion Simulator in the NASA Lewis 9 x 15 foot wind tunnel, currently scheduled for the third quarter of 1998. An AE scaled TFE derivative fan design will be used as a baseline. A nacelle model will be provided that will be characteristic of a typical, modern regional aircraft nacelle and meet all of the program test objectives.

The quiet high-speed fan is an advanced single-stage fan designed for a 5K to 20K pound thrust turbofan regional airline application. Advanced aerodynamic, mechanical, aeroelastic, and computational fluid dynamic (CFD) tools will be used to meet aggressive performance goals while achieving at least a 6 dB reduction in fan noise at a critical takeoff noise condition. Three fans will be built for evaluation at NASA; a baseline TFE derivative, an advanced NASA design, and an advanced AE design. A 22-in. diameter fan nacelle for the UHB Propulsion Simulator in the NASA-Lewis 9 x 15 foot wind tunnel will integrate NASA and AE aerodynamic designs and instrumentation to fulfill all aerodynamic, mechanical, distortion sensitivity, and acoustic test needs.

2.3 Baseline Fan

The baseline consists of a damperless, low-aspect- ratio, moderately aft swept rotor and full-span aft swept composite stator vanes. The geared fan configuration allows the fan to run at a tip speed optimized for best performance, stall margin, and noise.

The baseline fan was the subject of considerable acoustic evaluation early in the design phase. Blade and vane counts, rotor/stator spacing, and stator vane sweep were selected to minimize the noise signature within the fan design constraints. Fan rig spinning-mode measurements were made to verify the design constraints and provide acoustic treatment design criteria. The acoustic effort was concluded with a full-scale engine acoustic test which verified that the acoustic design goals, including the acoustic treatment, were satisfied.

Installed performance of the baseline fan was a critical issue. Measuring fan component performance accurately during flight was required. The engine nacelle and inlet section of the flight test engine were custom tailored and instrumented for flow measurement. The engine front frame was also instrumented so fan performance could be measured without impacting fan or engine performance. The fan performance measured in flight at appropriate Reynolds numbers during the extensive flight test program agreed very well with rig and engine data acquired on the ground using conventional fluid metering techniques. The experience gained on these programs will be used on the Quiet High-Speed Fan program.

2.4 Historical Background

The presence of a shock at the inlet of the fan rotor in a turbofan engine can result in acoustic phenomena that represent substantial noise sources. Multiple Pure Tone (MPT) noise, for example, results when the pressure disturbances from the inlet shock move upstream out of the rotor blade passage. One approach to reducing these shock-related noise sources is to eliminate the formation of the inlet shock in the fan by tailoring the rotor blade shape. The introduction of sweep in the fan rotor blade can reduce the relative velocity component normal to the blade to subsonic values, much as a swept wing on an aircraft can produce subsonic velocities normal to the wing leading edge, even when the resultant velocity is supersonic.

This noise minimization technique was applied by AlliedSignal Engines (formerly AVCO Lycoming) and Bolt, Beranek and Newman, Inc. (BBN) to the design of the QF-12 quiet high-speed fan, as part of a NASA-sponsored program performed between 1974 and 1977 (Reference 1). The fan rotor featured a compound forward-and-aft sweep to eliminate the leading edge shock. However, although shock-induced MPT noise was reduced, the aerodynamic performance of the fan did not meet design goals. The reasons for the performance deficiencies were not determined, but the source was found to be localized in the rotor. Figure 2.4-1 shows a summary of the results of the acoustic evaluation of the QF-12.

The ability to accurately predict, during the fan rotor design, the speed range over which the MPT noise will occur can provide a valuable tool for acoustically tailoring the design of the rotor to minimize the effect of this noise source.

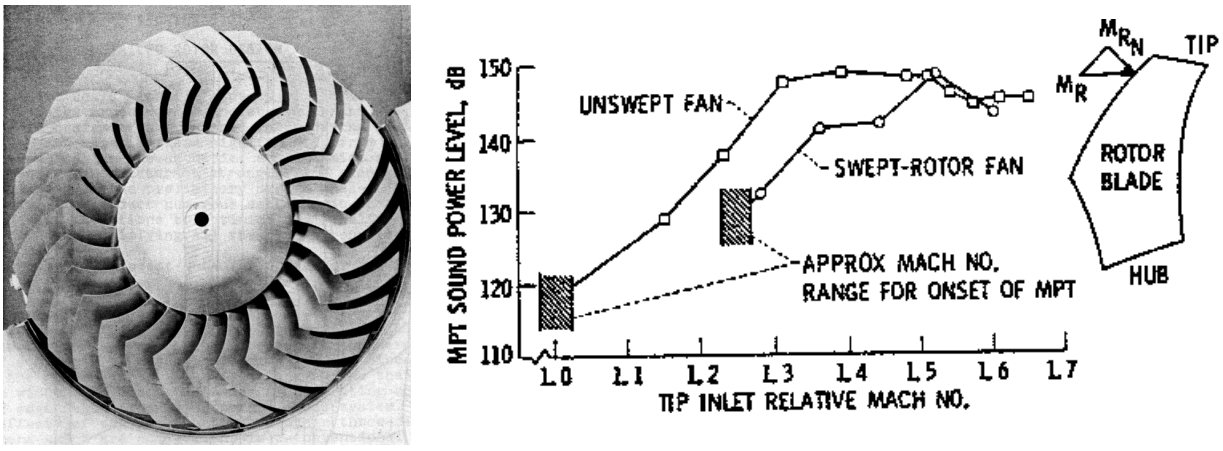

Figure 2.4-1. The QF-12 Fan Demonstrated the Feasibility of Using Blade Leading Edge Sweep to Reduce Fan Noise.

3.0 DESIGN OBJECTIVES / CRITERIA

3.1 Overall

The AE/QHSF stage design included design objectives from the acoustic, aerodynamic, mechanical, and aeroelastic disciplines. Acoustic objectives included a 6 dB reduction in effective perceived noise (EPNdB) at takeoff relative to the baseline. This was to be accomplished without the known benefits of vane count reduction and increased axial spacing (hub and tip) between rotor TE and vane LE. The intent of the design was focused on obtaining noise reductions through the use of more unconventional design techniques such as: controlling the rotor wake impinging on the stator LE, reducing rotor normal inlet relative Mach number, and controlling shocks within blade passage. Aerodynamic objectives were to obtain baseline performance (or better) with a forward swept rotor and acoustically matched vanes. Mechanical and aeroelastic objectives were to obtain AE and NASA criteria for stress and burst margins, proper positioning of mode / harmonic crossings to minimize high vibratory strains, and provide sufficient flutter margin throughout the operating region.

3.2 Specific

Specific aerodynamic design criteria is shown in Table 3.2-1. Mechanical criteria is shown in Table 3.2-2 and Figure 3.2-1.

Table 3.2-1. Specific Aerodynamic Design Criteria

Fan Aero Design Point (100% Nc)

	22" DIA
Wcorr, lbm/s	98.9
Wc/A, lbm/s/ft^2	42.7
Utcorr, ft/s	1474
Bypass ratio	3.8
P/P, overall	1.82
Eff ad, overall	> .895
Stall margin (N_{1C}=C)	15%
Hub/Tip ratio	.35
Rotor blade count	22
Stator vane count	52

Table 3.2-2. Specific Mechanical Design Criteria

- Airfoil and Attachment LCF Life > 10^5 cycles
  - Peak Stress in Attachment and Airfoil
- HCF Life > 10^7 Cycles
  - Frequency, Excitation (Inlet Distortion Harmonics, Speed @Resonance)
- Bird-Ingestion Capability
  - Bird Weight, LE Thickness
- Flutter Margin Exceeds Baseline
  - Reduced Frequency, Twist/Flex, and Incidence
- Blade Weight Equal to Or Less Than Baseline

- High Speed Resonances Must Be Avoided
  - Rotor
    - Mode 1 / 2E Crossing < 50 percent speed
    - Mode 2 / 4E Crossing < 70 percent speed
- 10% Frequency Margin at Maximum Engine Operating Speed
- Modified Goodman Approach used for HCF Calculation

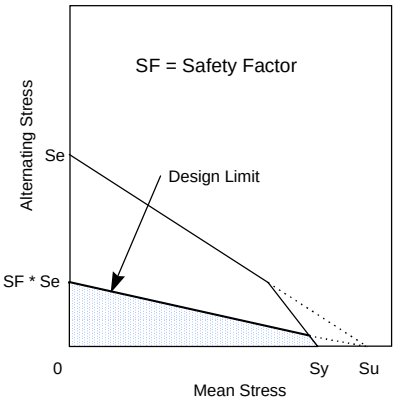

Figure 3.2-1. Mechanical Criteria for High-Cycle Fatigue

4.0 PRELIMINARY DESIGN

4.1 Cycle Point Selection

An engine cycle design point was originally established for the AE/QHSF to correspond to a regional type application for the AE Small Engine Technology (SET) engine concept. However, during the initial study efforts, it became apparent that although the cycle point originally selected would benefit the AST program in terms of a regional application; it would make comparisons relative to the baseline (design and test) much more difficult. Therefore, the baseline design cycle was selected which would provide the best and cleanest 'back-to-back' test to verify Area of Interest 14 technology goals.

4.2 Rotor

4.2.1 Blade Harmonic Selection

Analyses were completed to determine whether the rotor should be a "1/rev" design (similar to the baseline) or a "2/rev". The 1/rev design offers the advantage of less weight but, without a midspan damper, increases the susceptibility to flutter. An optimization process using ANSYS was completed for both designs in order to minimize weight while maintaining all other design criteria.

A parametric model of the airfoil was defined to allow aeromechanical optimization via ANSYS. The value of maximum airfoil thickness (Tmax/C) and its chordwise position were varied at several spanwise locations, including the hub and tip. A cubic spline fit through these control points was used to define these distributions at 5% span increments.

X-cg and Y-cg distributions were defined along 4^{th}-order polynomial functions fixed at the airfoil hub. The X-cg at the tip was fixed at 1.07 inches forward. The coefficients of the polynomials were used as design variables. X-cg and Y-cg were defined at 5% span increments.

The blade geometric parameters were used to create an AXCAPS (AE's radial equilibrium streamline flow solver) input file, with the resulting airfoil geometry automatically meshed and analyzed. These geometric parameters were defined as independent design variables for the optimization procedure. A single objective function is available with ANSYS, thus additional "objectives" were forced with constraints.

The first optimization was for a blade with a 1/rev crossing (1E/4E). The initial analyses were conducted with the Tmax/C and position of Tmax design variables defined at 4 equally-spaced, spanwise sections. The resulting optimized airfoil was approximately 23 percent heavier than the baseline design. The spanwise resolution was subsequently increased to 6 sections. A cubic spline fit through these control points was used to define these distributions at 5% span increments. Using the new spanwise resolution, the optimized blade was only 1 percent heavier than the baseline blade.

Table 4.2.1-1. AE/QHSF Preliminary 1/rev Design

Parameter	QHSF 1/Rev Airfoil (Fixed-root; no root fillet)	Relative to Baseline
Airfoil Weight	1.27 lb	+ 1.2 %
Max Principal Stress	82 ksi	-10.8 %
Max Deflection	0.31 in	-19.5 %
Mode 1/2E crossing	48 percent speed	-28 %
Flutter Margin	-0.44	+10 %
Tip Tmax/C	0.02	Same

Initial optimization analyses for the 2/rev crossing (2E/4E) were also conducted with Tmax/C and position of Tmax design variables defined at 4 equally-spaced, spanwise sections. The best, near-feasible solution obtained was 31 percent heavier than baseline blade. Based on the success of the 1E/4E study, the spanwise Tmax/C and position of Tmax design variables were defined up to 11 sections. A cubic spline fit through these control points was used to define these distributions at 5% span increments. The total number of design variables (DV's) was 29 for the 11 point case even though ANSYS recommends no more than 20 DV's.

The weight of the 2E/4E design was relatively unaffected by an increase in spanwise sections. The best design was slightly low on mode 1 frequency margin, 14 percent vs. the desired 15 percent, but met all other mechanical constraints. The blade was still 22 percent heavier than the baseline blade; and, was obtained only after reducing Tmax/C at the tip to 0.01, well below the design criteria of 0.02.

Table 4.2.1-2. AE/QHSF Preliminary 2/rev Design

Parameter	QHSF 2/Rev Airfoil (Fixed-root; no root fillet)	Relative to Baseline
Airfoil Weight	1.53 lb	+22%
Max Stress	67 ksi	-27%
Max Deflection	0.39 in	0
Mode 2/4E freq margin	14 percent (require 15%)	
Flutter Margin	-0.32	+18%
Tip Tmax/C	0.01	-50%

4.2.2 DAWES Model

The DAWES program is a finite-volume time-marching solver for the 3-D thin-layer Navier-Stokes equations. The version of the program used by AE for the QHSF was the same version previously used on the baseline rotor design. To maintain close compatibility, the same grid and flow size were used for the two designs. All DAWES analyses, rotor and stator, were completed at the baseline engine flow size.

The blade and flowpath geometry descriptions for the fan rotor were obtained from AE's axisymmetric streamline curvature program, AXCAPS. This program provides a discrete-point definition of the blade geometry along specified stream surfaces intersected with the blade surface. Endwall definition is also provided in terms of radial and axial coordinates at discrete points. The AXCAPS model of the flowpath is shown in Figure 4.2.2-1.

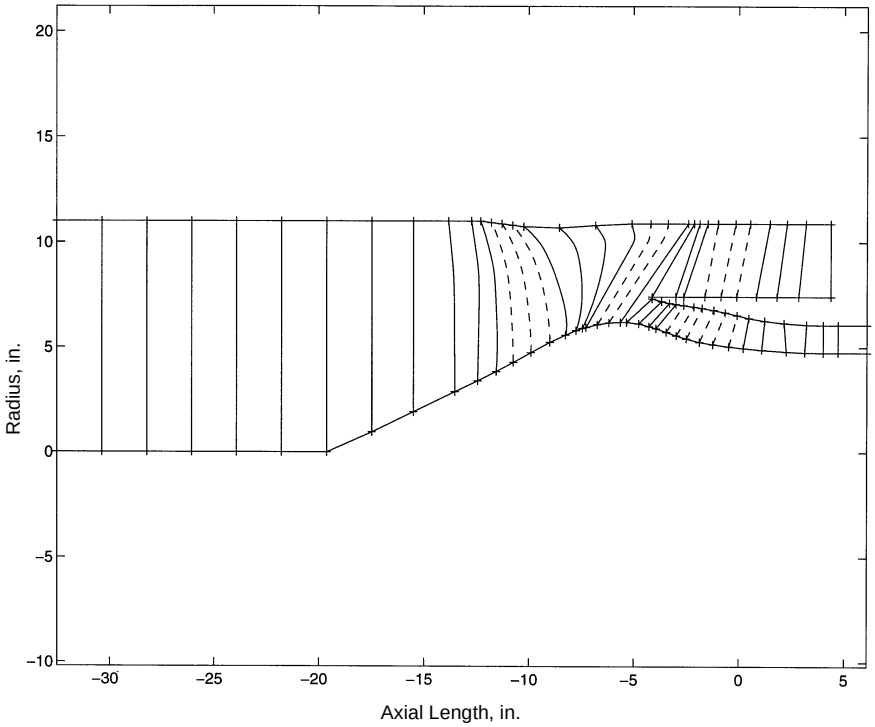

Figure 4.2.2-1. AXCAPS Flowpath Model Used

The geometry represented in the AXCAPS model was the deflected aerodynamic blade shape at 100 percent wheel speed. Hub fillets were not modeled in DAWES; and, the blade tip was modeled as tapered, rather than squared-off, which is required by a gridding limitation within the program.

The computational domain consisted of a single rotor blade passage, with the suction surface of one blade forming one pitchwise boundary, and the pressure surface of the adjacent blade forming the other pitchwise boundary. The inlet to the computational domain was positioned upstream (approximately one tip chord) to reduce impacting the development of the upstream shock structure. The exit of the computational domain was located the same, relative to the rotor TE, as the baseline. Because of the rotor forward sweep, the exit plane did not include the outer 40% span of the stator leading edge. Analyses were completed late in the design with an extended grid which showed there was no impact on the previously completed rotor wake/stator interaction study.

The computational grid for the DAWES program is a structured single-block skewed H-grid. Typical sections of the computational grid are presented in Figure 4.2.2-2. The grid size employed for the final set of rotor analyses was specified as:

Pitchwise:	25 Nodes
Spanwise:	71 Nodes (with 8 cells in the clearance gap)
Streamwise:	131 Nodes

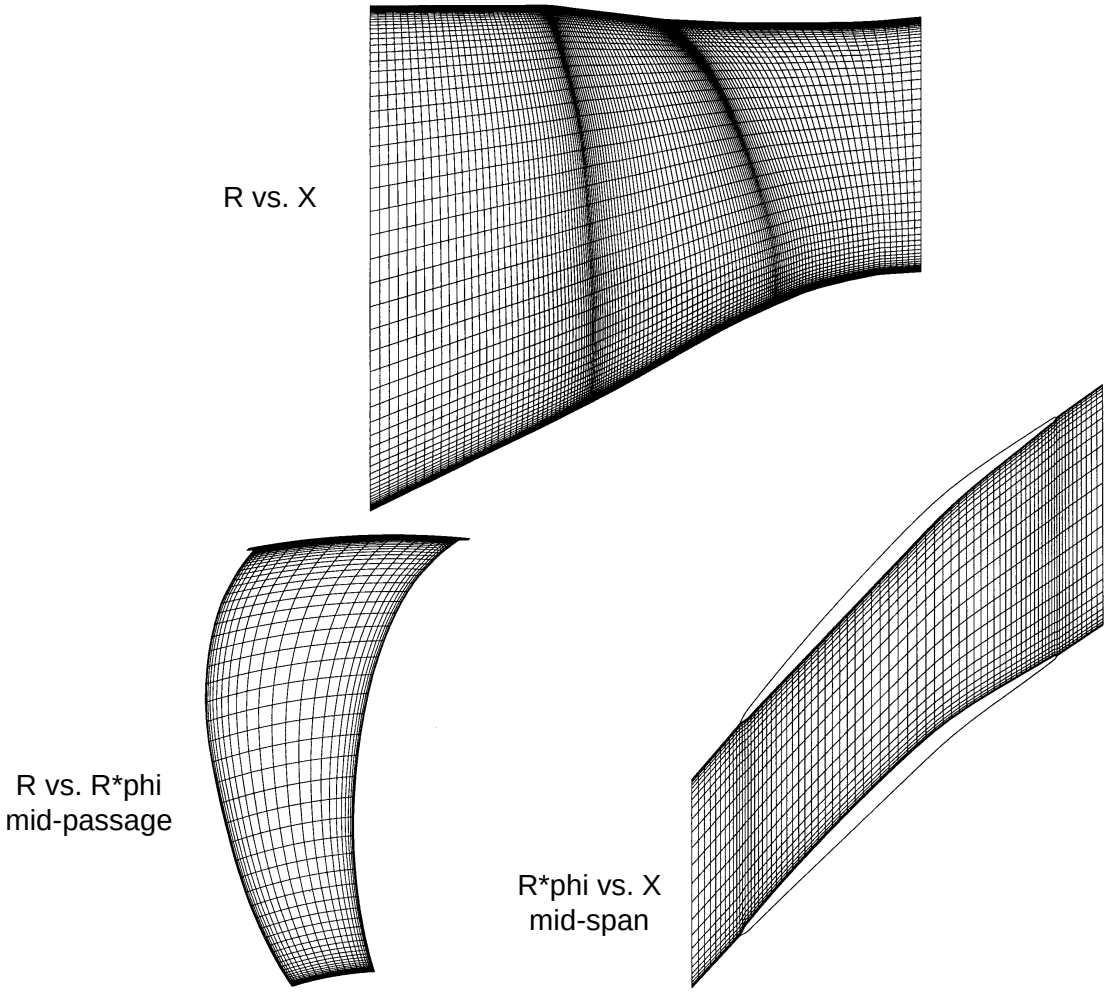

Figure 4.2.2-2. Rotor DAWES Computational Grid

4.2.3 Design of Experiment 1

4.2.3.1 Purpose

The first statistical design of experiment (DOE) was created to determine the extent of forward sweep required to obtain the 6 dB noise reduction with marginal violation of the other performance goals. (It was believed that the performance goals would be achieved in subsequent DOE's planned.) The DOE involved analyses from the Aerodynamic, Mechanical, Acoustic, and Aeroelastic disciplines.

4.2.3.2 Description

Because of the perceived non-linearity of the axial and tangential leans, the DOE was created to consist of 4 factors (Xcg-tip, Ycg-tip, Xcg-midspan, Ycg-midspan) with 3 levels each. The 9 cases are described in Table 4.2.3-1, with the CG orientation shown in Figure 4.2.3-1. Figures 4.2.3-2 and 4.2.3-3 show the CG distribrutions of the nine cases. The blade geometry and the mean flow properties were determined using AXCAPS. The intent was to analyze the cases at design speed (100% Nc) and 80% Nc using DENTON (Denton's 3D inviscid Euler code) to obtain the aerodynamic and acoustic quality characteristics. It was believed, based on past experience, that DENTON could be used to provide accurate solutions for flow, and shock locations; and, because of the fast turnaround time would be advantages for the DOE. For solution verification, several cases were analyzed using DAWES which showed some differences in flow and passage shock locations. The differences were believed to be caused by using convergence factors (time step, pitch and axial smoothing, damping, and inlet smoothing) in DENTON which deviated from experience but were required for case convergence. DAWES was therefore used to analyze the cases; however, because of the CPU time required, only the design speed was analyzed for the DOE.

Table 4.2.3-1. DOE 1 Forward Sweep Analysis X-Factors

Case No.	X-cg tip	Y-cg tip	X-cg mid	Y-cg mid
1	-1.50	-1.0	-0.25	-0.50
2	-1.50	0	0	0
3	-1.50	+1.0	+0.60	+0.50
4	-0.75	-1.0	0	+0.50
5	-0.75	0	+0.60	-0.50
6	-0.75	+1.0	-0.25	0
7	0	-1.0	+0.60	0
8	0	0	-0.25	+0.50
9	0	+1.0	0	-0.50

Dimensions are in inches and relative to Baseline engine size (30.7 in Dia.). Negative X-cg is axial forward direction, positive Y-cg is in direction of rotation

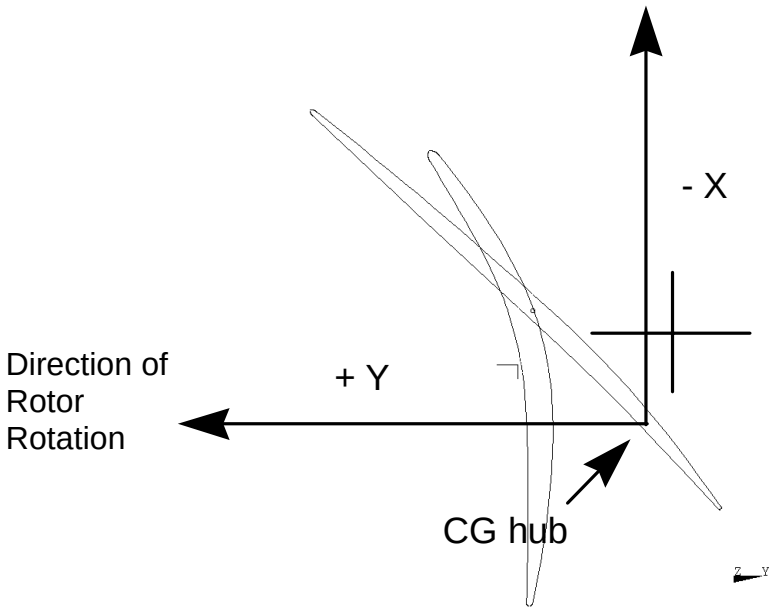

Figure 4.2.3-1. Blade CG Orientation Definition.

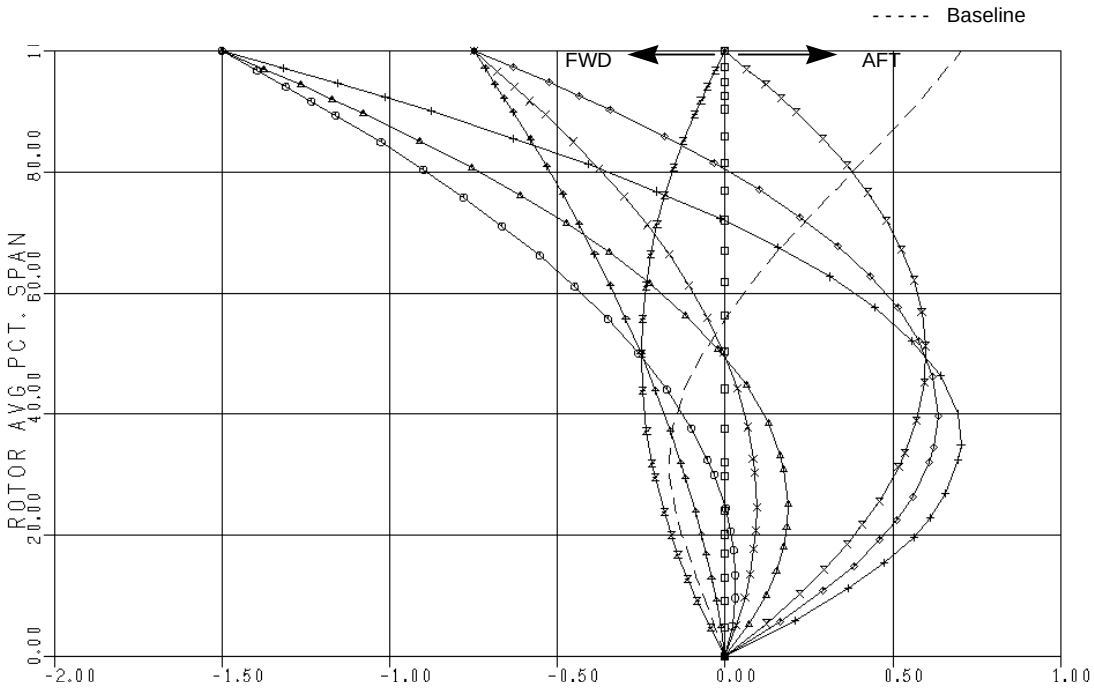

Figure 4.2.3-2. Xcg distributions used in DOE 1.

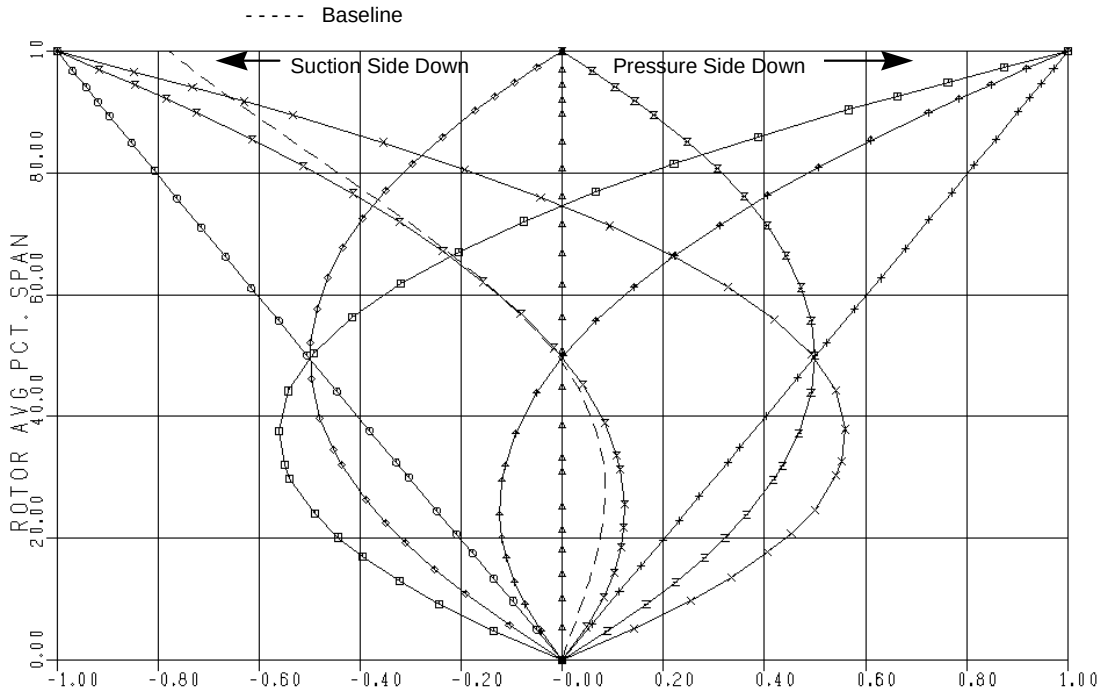

Figure 4.2.3-3. Ycg distributions used in DOE 1.

4.2.3.3 Analysis

Response variables (Y-factors) were compiled based on analyses from the four engineering disciplines. These factors became somewhat dynamic in that some were deleted, while others were added or calculated slightly differently. The final list of Y-factors with a brief description is shown in Table 4.2.3-2 with results tabulated in Table 4.2.3-3. Vector solutions for each case were created at 55.9% corrected fan speed using an off-design model from the design point. This speed corresponds to an approach condition where interaction noise is likely to be the dominant fan noise source (buzzsaw noise cutoff). Predictions of rotor/stator interaction noise were performed using the NASA code V072. The baseline stator was used for all rotor design studies.

Table 4.2.3-2. DOE 1 Forward Sweep Analysis Y-Factors

	Discipline	Y-factor	Description	Analysis Tool	% N1c
1	Acoustic	dB	Interaction noise sound power level	V072	55.9
2	Acoustic	eff swp le	Rotor LE effective sweep	AXCAPS	100.0
3	Acoustic	%c 50	Passage shock location at 50% span	DAWES	100.0
4	Acoustic	%c 60	Passage shock location at 60% span	DAWES	100.0
5	Acoustic	%c 70	Passage shock location at 70% span	DAWES	100.0
6	Acoustic	%c 80	Passage shock location at 80% span	DAWES	100.0
7	Acoustic	%c 90	Passage shock location at 90% span	DAWES	100.0
8	Acoustic	%c 95	Passage shock location at 95% span	DAWES	100.0
9	Acoustic	delz 50	Axial distance RTE - VLE midspan	AXCAPS	
10	Acoustic	delz 100	Axial distance RTE - VLE tip	AXCAPS	
11	Aero	Wc	Inlet corrected flow (top of choke)	DAWES	100.0
12	Aero	PR	Rotor pressure ratio (top of choke)	DAWES	100.0
13	Aero	Eff	Rotor efficiency (top of choke)	DAWES	100.0
14	Aero	Mpeak 50	Suction surface peak Mach 50% span	DAWES	100.0
15	Aero	Mpeak 60	Suction surface peak Mach 60% span	DAWES	100.0
16	Aero	Mpeak 70	Suction surface peak Mach 70% span	DAWES	100.0
17	Aero	Mpeak 80	Suction surface peak Mach 80% span	DAWES	100.0
18	Aero	Mpeak 90	Suction surface peak Mach 90% span	DAWES	100.0
19	Aero	Mpeak 95	Suction surface peak Mach 95% span	DAWES	100.0
20	Aero	ws 50	Wennerstrom shock loss 50% span	AXCAPS	100.0
21	Aero	ws 75	Wennerstrom shock loss 75% span	AXCAPS	100.0
22	Aero	ws 100	Wennerstrom shock loss 100% span	AXCAPS	100.0
23	Aero	spds	Speedline slope out of choke	DAWES	100.0
24	Aeroelastic	flut 1	Empirical flutter parameter mode 1	ANSYS	100.0
25	Aeroelastic	flut 2	Empirical flutter parameter mode 2	ANSYS	100.0
26	Aeroelastic	twf 1	Twist/flex ratio mode 1	ANSYS	100.0
27	Mechanical	ssavg1	Avg suction surface stress 4 - 20%	ANSYS	100.0
28	Mechanical	ssavg2	Avg suction surface stress 21 - 40%	ANSYS	100.0
29	Mechanical	ssavg3	Avg suction surface stress 41 - 60%	ANSYS	100.0
30	Mechanical	ssavg4	Avg suction surface stress 61 - 80%	ANSYS	100.0
31	Mechanical	ssavg5	Avg suction surface stress 81 - 100%	ANSYS	100.0
32	Mechanical	psavg1	Avg pressure surface stress 4 - 20%	ANSYS	100.0
33	Mechanical	psavg2	Avg pressure surface stress 21 - 40%	ANSYS	100.0
34	Mechanical	psavg3	Avg pressure surface stress 41 - 60%	ANSYS	100.0
35	Mechanical	psavg4	Avg pressure surface stress 61 - 80%	ANSYS	100.0
36	Mechanical	psavg5	Avg pressure surface stress 81 - 100%	ANSYS	100.0
37	Mechanical	umax tip	Max tip deflection	ANSYS	100.0
38	Mechanical	freq 1	Frequency margin mode 1	ANSYS	100.0
39	Mechanical	freq 2	Frequency margin mode 2	ANSYS	100.0
40	Mechanical	freq 3	Frequency margin mode 3	ANSYS	100.0
41	Mechanical	fec 1	Placement of 2/rev crossing mode 1	ANSYS	100.0
42	Mechanical	fec 2	Placement of 4/rev crossing mode 2	ANSYS	100.0

The process flowchart used for DOE 1 is shown in Figure 4.2.3-4. The flowchart shows how the traditional "experiment" analysis is coupled with the ANSYS optimization technique.

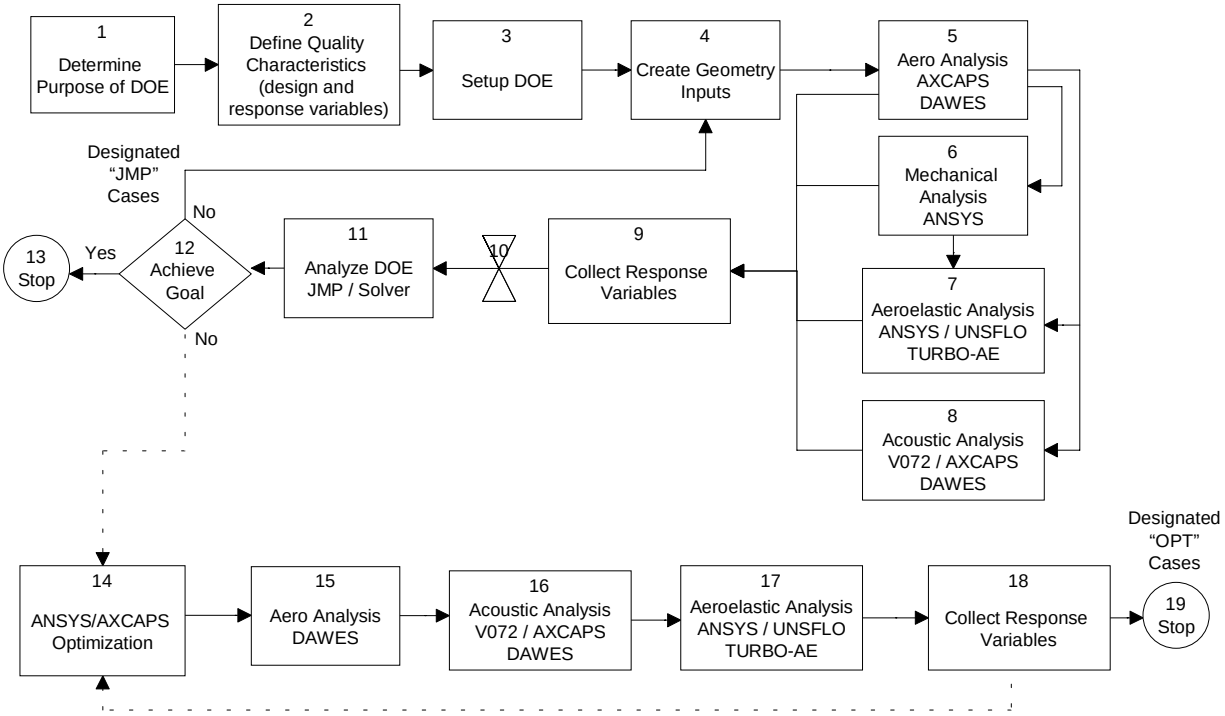

Figure 4.2.3-4. The process flow diagram for the QHSF design shows the combined use of design of experiments and ANSYS parametric optimization.

After all the response variables were collected, the data was input into the statistical program JMP. A second order polynomial was used to fit the data, and coefficients were generated for each Y-factor. Because of some deficiencies in the JMP program, the coefficients were input into EXCEL and used with the SOLVER function. SOLVER works by maximizing, minimizing, or iterating to a specified value for one Y-factor and can extrapolate outside the X-factor envelope. To obtain a feasible solution, limits were set for the other Y-factors and weighting was somewhat controlled by the range of these limits. Various feasible solutions were obtained by optimizing different Y-factors. Several new rotor geometry cases (go-forward cases) were created based on these results and analyzed. Go-forward cases created using EXCEL Solver and the statistical program JMP were designated jmp(number), while cases created from the ANSYS optimization were designated opt(letter).

4.2.3.4 Results

Acoustic response variables, overall power level at 55.9% N1c relative to the baseline rotor and blade effective sweep at the leading edge and at the suction surface impingement point of the adjacent blade, are shown in Figure 4.2.3-5. Although the figure shows only one case (case #4) to have lower noise than the baseline, the purpose of the DOE was to acquire sensitivities of the design variables and response variables. The sensitivities were the objective of the experiment such that go-forward cases could be created. The figure also shows two important aspects of effective sweep: the large effect of tangential lean, and the importance of the suction surface impingement point. Figure 4.2.3-2 showed that only one case (case #8) had a small amount of aft sweep; however Figure 4.2.3-5 shows that cases with large amounts of tangential lean (suction side down) can cause the effective sweep to be in the opposite direction thereby (potentially) mitigating benefits of the forward swept blade.

The blade effective sweep was calculated based on Art Wennerstroms' oblique shock angle (OBA) calculation at the leading edge and the shock impingement on the adjacent airfoil's suction surface. In AE's coordinate system, oblique shock angles greater than 90 degrees represent forward sweep, and are shown in the figure as a negative value (relative to 90 degrees). The desired amount of effective sweep was based on the amount required to reduce the normal component of the inlet relative Mach number at 90% N1c (maximum obtainable fan speed up to 4000 feet elevation) to a Mach number of 1.0. Effective sweep described here is the delta between the angle of the shock surface relative to the engine center line and 90 degrees. The shock surface at the leading edge is created as the shock travels from the leading edge of one blade and impinges on the adjacent blade's suction surface at some distance aft of the leading edge. Therefore, the shock loss (at a particular radius) is a function of the oblique shock angle at the leading edge and the impingement point on the suction surface. Because the shock surface impingement point on the adjacent blade is aft of the blade leading edge, the oblique shock angle at the impingement point will always be less than the oblique shock angle at the leading edge. Therefore, for aft swept and forward swept blades with the same absolute value of leading edge effective sweep, the aft swept blade will have lower shock losses.

Aerodynamic response variables, inlet corrected flow and rotor efficiency, are shown in Figure 4.2.3-6. Several empirical aeroelastic response variables for Mode 1, twist/flex ratio and empirical flutter parameter (EFP), are shown in Figure 4.2.3-7. The EFP is the ratio of the actual reduced frequency and the desired reduced frequency for a twist/flex ratio, based on AE's empirical data base. Figure 4.2.3-8 shows two, of many, mechanical response variables. The two variables shown are the maximum tip deflection and the average bending stress between 41 and 60% radial span. The tip deflection is the vector summation of the radial, axial, and tangential components and is relative to the baseline engine size. The goal of +/- 0.4 inches shown is also relative to the baseline engine size. The dominant component of the deflection vector is axial, while the radial component is much less (approximately 0.060 inches). Positive values of tip deflection indicate bending toward the suction side. The bending stress goal of less than +/- 40 ksi on the suction and pressure surfaces was used to keep the maximum principal stresses on the blade below 85 ksi.

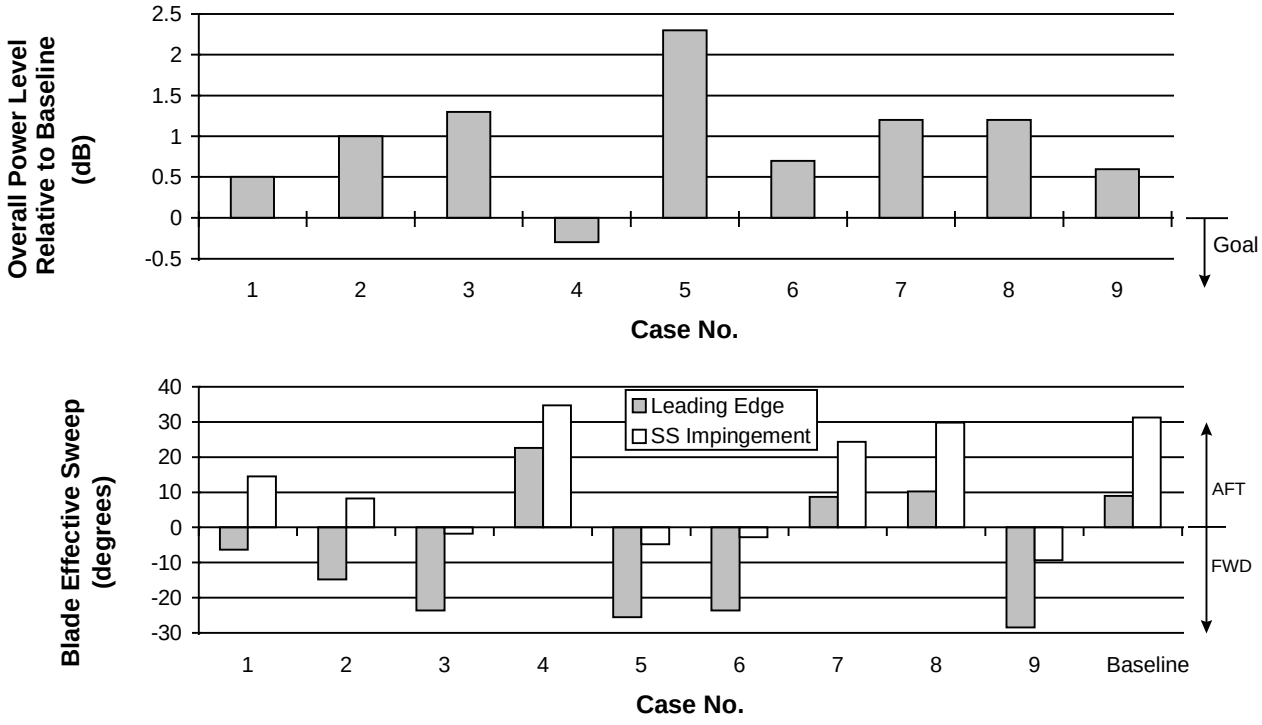

Figure 4.2.3-5. Result of the Acoustic Assessment of the Configurations for Rotor DOE 1.

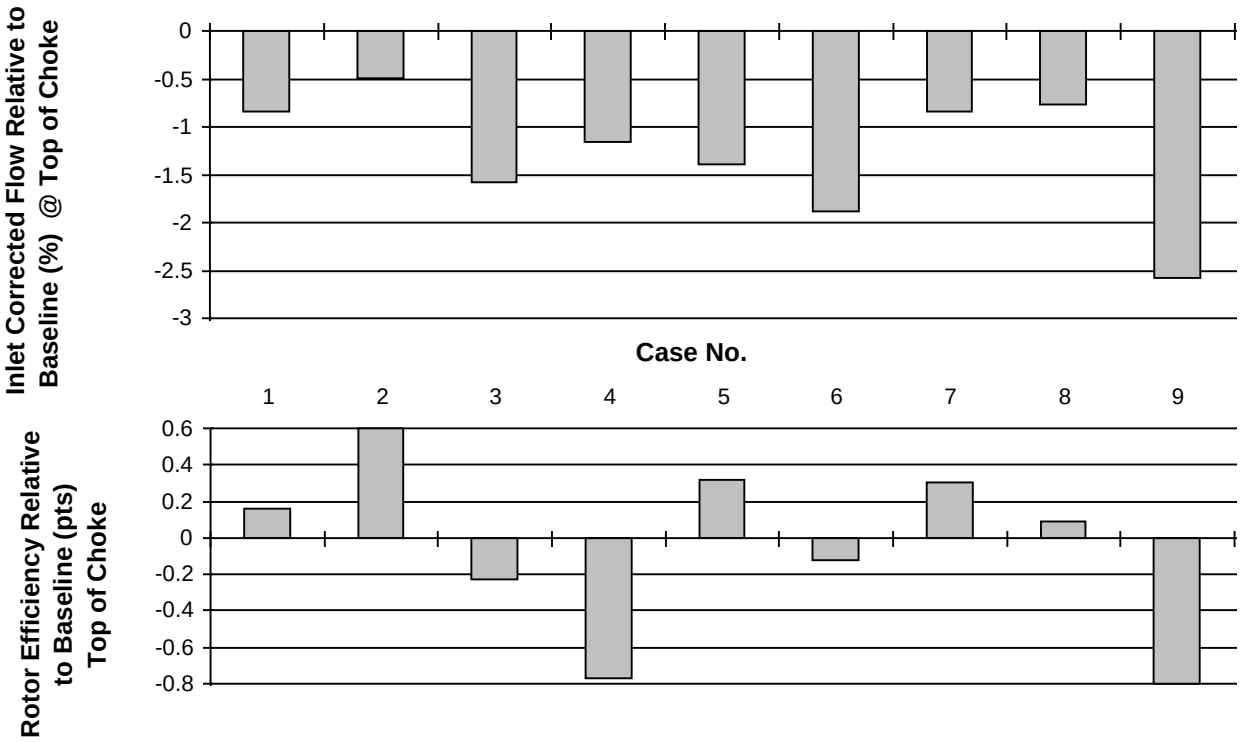

Figure 4.2.3-6. Result of the Aerodynamic Assessment of the Configurations for Rotor DOE 1.

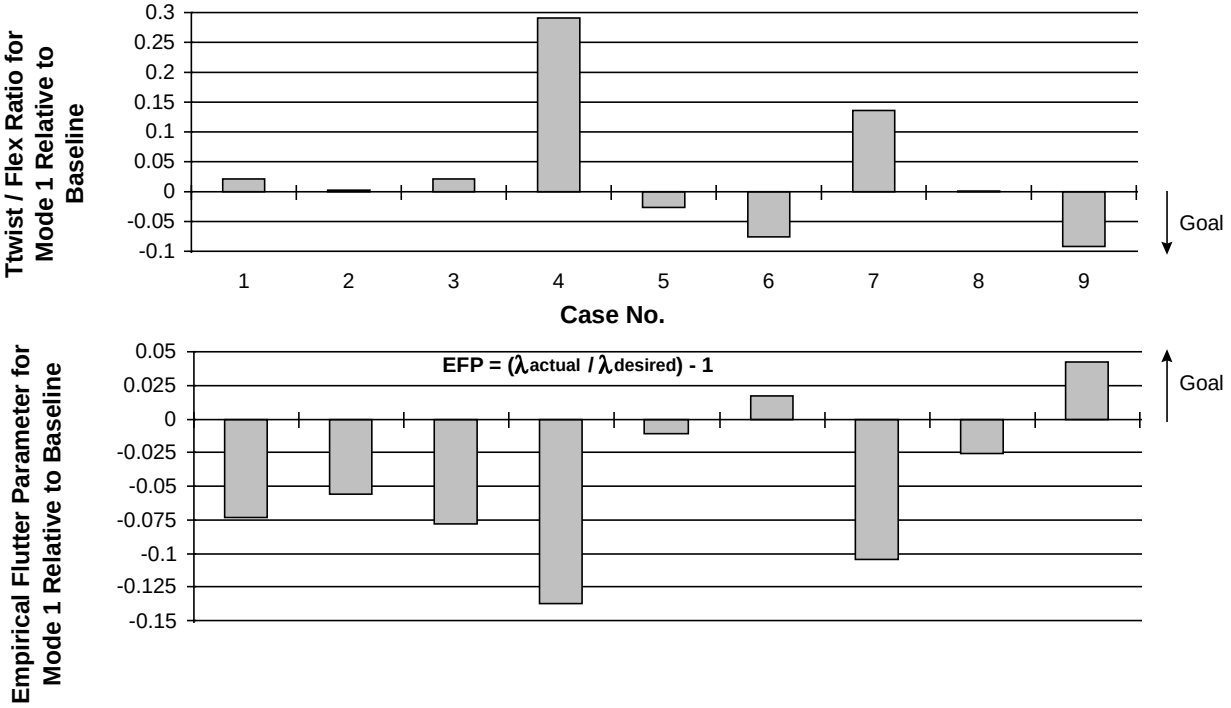

Figure 4.2.3-7. Result of the Aeroelastic Assessment of the Configurations for Rotor DOE 1.

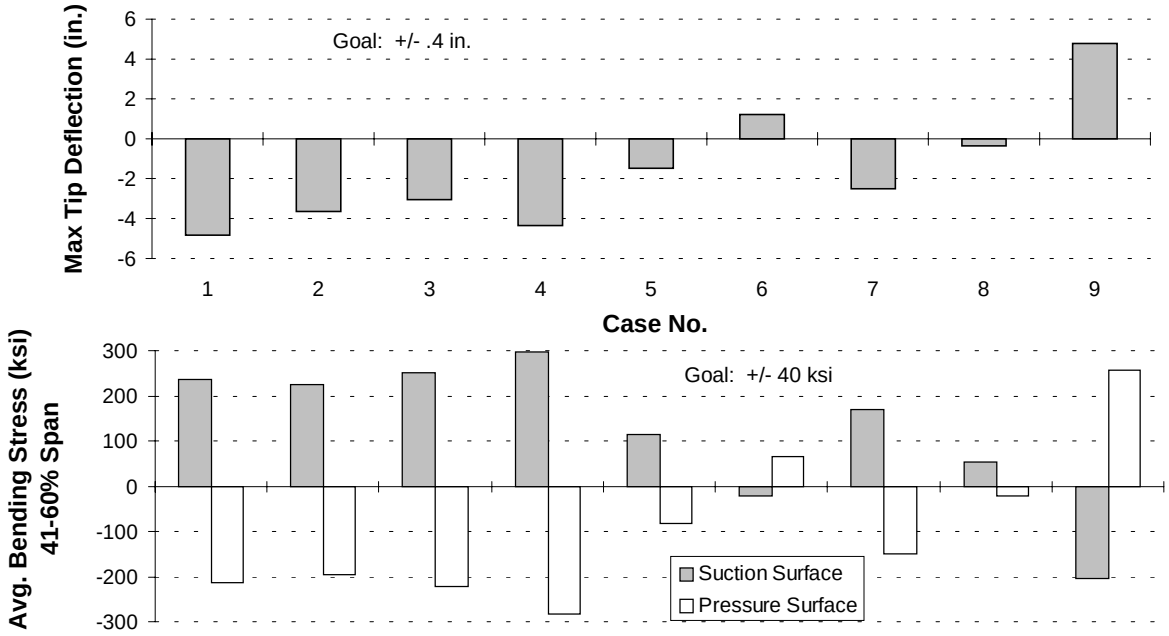

Figure 4.2.3-8. Result of the Mechanical Assessment of the Configurations for Rotor DOE 1.

Table 4.2.3-3. Tabulated Results of DOE 1 Forward Sweep Analysis

	Config #	1	2	3	4	5	6	7	8	9
1	dB	132.4	132.8	133.0	131.4	133.8	132.1	133.1	132.8	132.1
2	eff swp le	-6.27	-14.70	-23.53	22.61	-25.50	-23.57	8.73	10.28	-28.40
3	%c 50	28.80	31.26	33.66	35.85	31.00	26.49	35.79	30.91	21.83
4	%c 60	33.61	36.29	39.09	43.65	36.19	33.56	46.53	38.36	28.30
5	%c 70	41.13	47.06	47.42	48.86	44.33	43.87	52.07	46.42	38.11
6	%c 80	46.65	55.76	59.04	51.82	53.06	52.46	60.46	52.40	46.26
7	%c 90	55.96	66.79	69.56	55.31	66.93	68.87	68.49	55.96	65.99
8	%c 95	58.55	73.37	75.69	55.48	73.39	73.26	70.63	58.83	70.62
9	delz 50	3.827	3.601	3.024	3.526	3.004	3.757	2.944	3.767	3.516
10	delz 100	6.862	6.784	6.737	6.228	5.950	6.036	5.298	5.465	5.235
11	Wc	191.01	191.69	189.59	190.39	189.94	188.99	191.02	191.16	187.67
12	PR	1.899	1.901	1.894	1.811	1.898	1.890	1.852	1.854	1.891
13	Eff	.9038	.9082	.8999	.8945	.9054	.9010	.9052	.9031	.8942
14	Mpeak 50	1.429	1.464	1.470	1.470	1.453	1.404	1.480	1.422	1.423
15	Mpeak 60	1.452	1.480	1.491	1.496	1.483	1.432	1.504	1.441	1.440
16	Mpeak 70	1.454	1.464	1.475	1.503	1.468	1.432	1.545	1.444	1.448
17	Mpeak 80	1.445	1.460	1.475	1.514	1.459	1.426	1.550	1.454	1.429
18	Mpeak 90	1.467	1.527	1.535	1.510	1.554	1.545	1.574	1.517	1.503
19	Mpeak 95	1.493	1.534	1.532	1.465	1.586	1.631	1.571	1.488	1.613
20	ws 50	.023	.028	.034	.016	.029	.024	.019	.019	.026
21	ws 75	.055	.046	.031	.045	.043	.040	.053	.046	.039
22	ws 100	.081	.076	.055	.040	.048	.045	.077	.059	.029
23	spds	-9.5e-4	2.79e-3	3.90e-3	-2.84e-3	3.01e-3	9.34e-3	-1.09e-3	7.35e-4	-9.5e-4
24	flut 1	-0.563	-0.546	-0.568	-0.627	-0.501	-0.473	-0.594	-0.516	-0.448
25	flut 2	-0.105	-0.008	-0.129	-0.181	-0.005	-0.005	-0.008	0.319	-0.200
26	twf 1	0.581	0.562	0.581	0.851	0.533	0.484	0.696	0.561	0.468
27	ssavg1	152.5	71.9	-14.5	92.2	21.4	-1.3	48.1	21.2	-50.3
28	ssavg2	221.0	164.1	110.5	232.5	49.6	-25.5	120.6	54.8	-152.9
29	ssavg3	235.1	223.6	250.7	296.9	115.8	-21.4	169.4	54.0	-205.0
30	ssavg4	173.5	184.0	241.9	200.6	113.6	-12.1	149.1	28.4	-138.9
31	ssavg5	39.5	45.1	63.4	48.3	31.8	-3.3	38.0	4.0	-35.7
32	psavg1	-110.6	-14.8	92.9	-45.5	30.6	69.8	3.4	44.1	108.7
33	psavg2	-191.9	-126.8	-66.3	-207.8	-6.5	82.0	-87.6	-9.8	213.9
34	psavg3	-211.6	-195.9	-221.4	-283.4	-81.2	65.3	-150.1	-22.5	256.3
35	psavg4	-152.1	-160.0	-215.2	-192.9	-88.6	38.2	-133.8	-6.9	165.3
36	psavg5	-32.4	-38.1	-57.0	-45.2	-24.5	11.8	-31.7	3.6	44.1
37	umax tip	-4.83	-3.64	-3.05	-4.35	-1.48	1.22	-2.50	-0.35	4.78
38	freq 1	1.478	1.491	1.461	1.478	1.559	1.504	1.606	1.586	1.527
39	freq 2	3.541	3.630	3.448	3.242	3.775	3.751	3.640	3.827	3.166
40	freq 3	0.692	0.533	0.802	0.785	0.423	0.589	0.498	0.304	0.958
41	fec 1	0.420	0.457	0.436	0.423	0.556	0.518	0.579	0.610	0.407
42	fec 2	0.724	0.784	0.673	0.522	0.899	0.896	0.828	0.930	0.560

Two cases emerged from DOE 1 as the go-forward designs: jmp08 and optc. A comparison of some mechanical and geometry parameters is shown in Table 4.2.3-4. Also shown in the table is another optimization design, opta, because it revealed an important aspect of integrating all the design disciplines. Although it had some highly desirable features in terms of stress and sweep, rotor-stator interaction noise results from the NASA - Acoustic code V072 showed the case to be unacceptable. (A comparison of the opta, optc and jmp08 results is shown with the DOE 2 results, Section 4.2.4.4). Results from DOE 1 go-forward cases; jmp08, opta, and optc showed that at the conclusion of DOE 1, the aerodynamic performance was below the design goal, and would have to be increased in the other DOE's planned. Although the results of these cases looked promising, additional blade effective sweep was required.

Table 4.2.3-4. DOE 1 Go-Forward Case Comparison

	Desired	OPTA	OPTC	JMP08
Optimization		Acoustic Performance	Aero Performance	DOE #1
Stresses	< 85 Ksi	93 Ksi	73 Ksi	120 Ksi
Defln.	< 0.4 in.	0.35 in.	0.47 in.	0.55 in.
YCG* Tip		1.475 in.	1.774 in.	1.343 in.
YCG* Mid		-0.443 in.	-0.152 in.	-0.446 in.
XCG Tip**	Fwd (-)	-1.5 in.	-1.871 in.	-1.871 in.
XCG Mid**	Fwd (-)	+0.281 in.	-0.333 in.	-0.279 in.
OBA075	> |-34°|	-39°	-25°	-22°
OBA100	> |-41°|	-50°	-49°	-41°

* Positive Toward Pressure Side
** Positive Toward Aft

Late in the design process (after completion of the rotor design and half of the stator design effort), it was discovered that the V072 input parameter ACLS, the relative flow angle at the stator leading edge, was being input incorrectly. Time allowed for recalculation of the baseline engine calibration, the original rotor DOE 1, and all pertinent stator DOE cases. Although incorrect predictions were used to direct the rotor design process, the general conclusions derived from these analyses were supported by the corrected predictions.

V072 predictions were generated for the rotor DOE 1 cases 1-9 and the optimized cases jmp08 and optc. All the rotor DOE cases used the baseline stator design. The inlet and aft duct power levels for 2 and 3 times the bladepass frequency are shown in Figure 4.2.3-9 as deltas from the baseline predicted power levels.

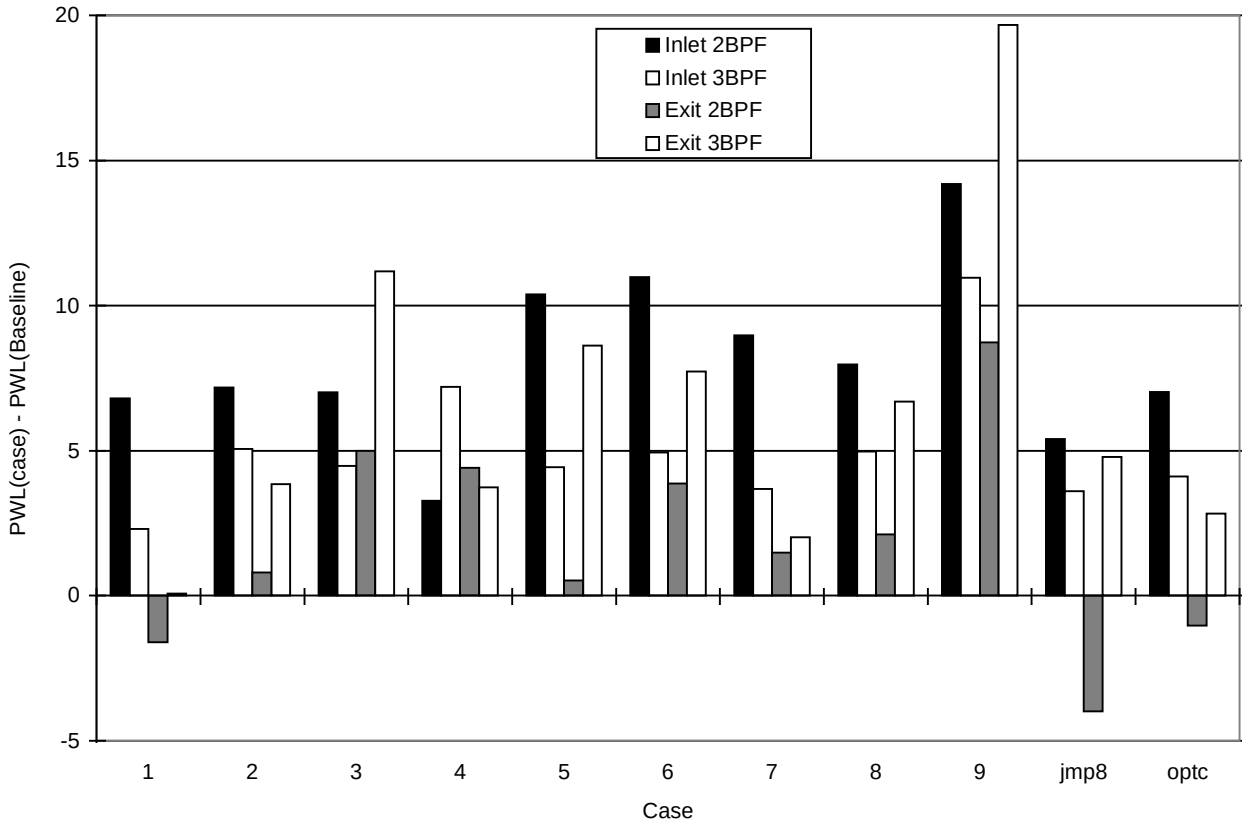

Figure 4.2.3-9. V072 Predictions for Cases in Rotor DOE 1, All Use Baseline Stator (1*BPF cutoff)

4.2.4 Design of Experiment 2

4.2.4.1 Purpose

The second DOE was created to minimize flutter. Although the goal was to use aeroelastic programs (FREPS, UNSFLO, and TURBO-AE) to calculate the aerodynamic damping at various points on the performance map, unfortunately the codes either had problems running or were considered not well enough calibrated to use in the DOE. Empirical data was used as the aeroelastic quality factors and direct the blade design.

4.2.4.2 Description

The second DOE consisted of 7 factors (position of max thickness at hub, mid, and tip; Tmax/C at hub, mid, and tip; and Ycg-tip) with 2 levels each. The 8 cases are described in Table 4.2.4-1. Although DOE 1 had shown that Ycg had little impact on aeroelastic empirical data, it was included to alleviate potential weight increase produced by thickness increases required to reduce stress and not flutter. Values of Ycg tip were selected based on DOE 1 results. Because the DOE 1 go-forward case optc was designed slightly after jmp08, and the need to initiate DOE 2; jmp08 was used as the QHSF baseline in DOE 2 even though the peak stresses and maximum tip deflection were above desired levels. Ranges for the other values in the table were selected based on previous analyses using the ANSYS optimization process completed to determine whether the blade design should be a 1/rev or a 2/rev, (Section 4.2.1). Spanwise thickness and position of max thickness for these analyses, compared to the baseline, are shown in Figures 4.2.4-1 and 4.2.4-2.

Table 4.2.4-1. DOE 2 Aeroelastic Analysis X-Factors

Case No.	Tmax Loc Hub	Tmax Loc Mid	Tmax Loc Tip	Tmax/c Hub	Tmax/c Mid	Tmax/c Tip	Y cg*
1	0.25	0.30	0.50	0.04	0.065	0.030	1.80
2	0.25	0.30	0.70	0.08	0.030	0.015	1.80
3	0.25	0.65	0.50	0.08	0.030	0.030	1.00
4	0.25	0.65	0.70	0.04	0.065	0.015	1.00
5	0.60	0.30	0.50	0.08	0.065	0.015	1.00
6	0.60	0.30	0.70	0.04	0.030	0.030	1.00
7	0.60	0.65	0.50	0.04	0.030	0.015	1.80
8	0.60	0.65	0.70	0.08	0.065	0.030	1.80

*Y-cg are in inches and relative to Baseline engine size (30.7 in Dia.) positive in direction of rotation

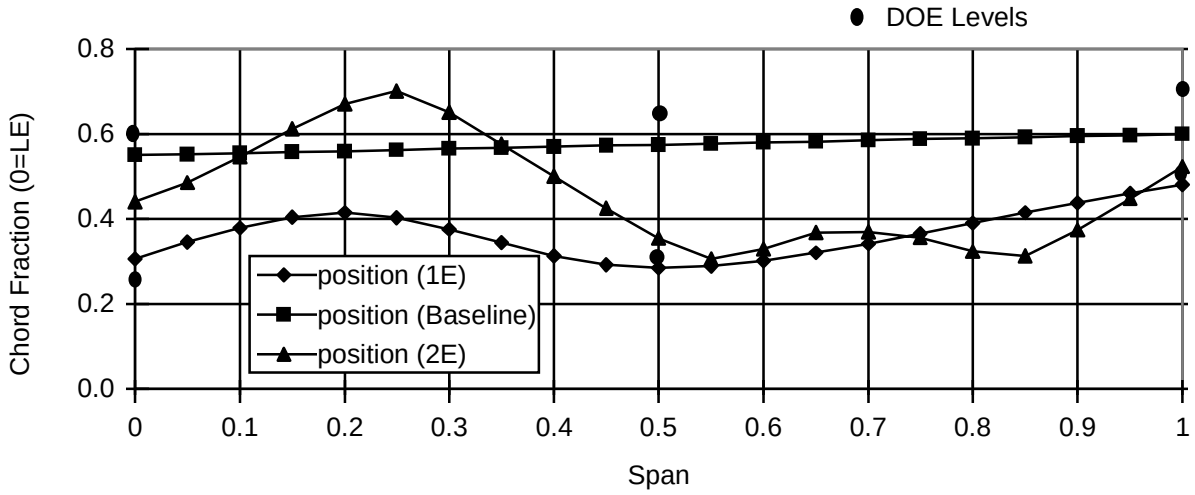

Figure 4.2.4-1. Levels Selected for Position of Maximum Thickness

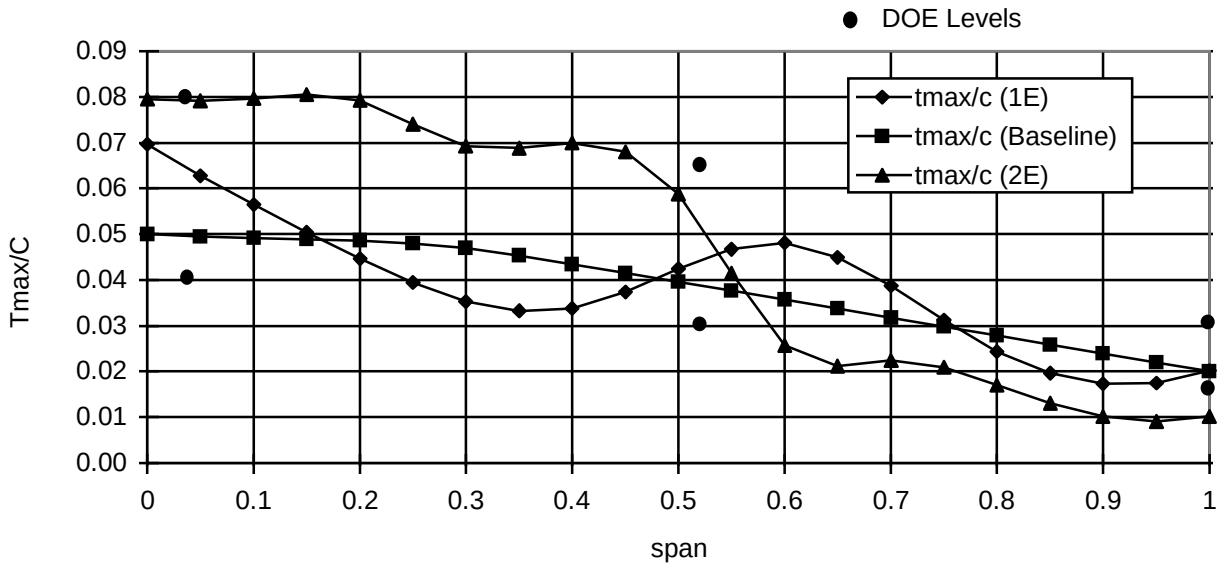

Figure 4.2.4-2. Levels Selected for Maximum Thickness

4.2.4.3 Analysis

The DOE 2 cases were analyzed using the same techniques and same response variables (Y-factors) as DOE 1, shown in Table 4.2.3-2.

4.2.4.4 Results

For consistency, the same response variables are shown as presented in Section 4.2.4.4. Included also in the figures are the go-forward cases from DOE 1; jmp08, opta, and optc. Again, it is the sensitivities of the design and response variables which were the objective of the DOE. Results from DOE 2, as well as jmp08, opta, and optc are shown in Figures 4.2.4-3 through 4.2.4-6. Acoustic response variables for interaction noise and MPT's are shown in Figure 4.2.4-3. Rotor-stator interaction noise was again calculated using V072 at 55.9% N1c, and was compared relative to the baseline such that a negative value was desired. The figure shows why opta, which looked good based on the other discipline design criteria, was not used as a go-forward design. The reason why it had such high interaction noise levels was that in an effort to create more effective sweep the blade was allowed to sweep aft at midspan prior to sweeping forward. The reduction in rotor-stator axial spacing caused the increased noise. The figure shows the large amount of effective sweep being considered relative to the aft-swept baseline rotor.

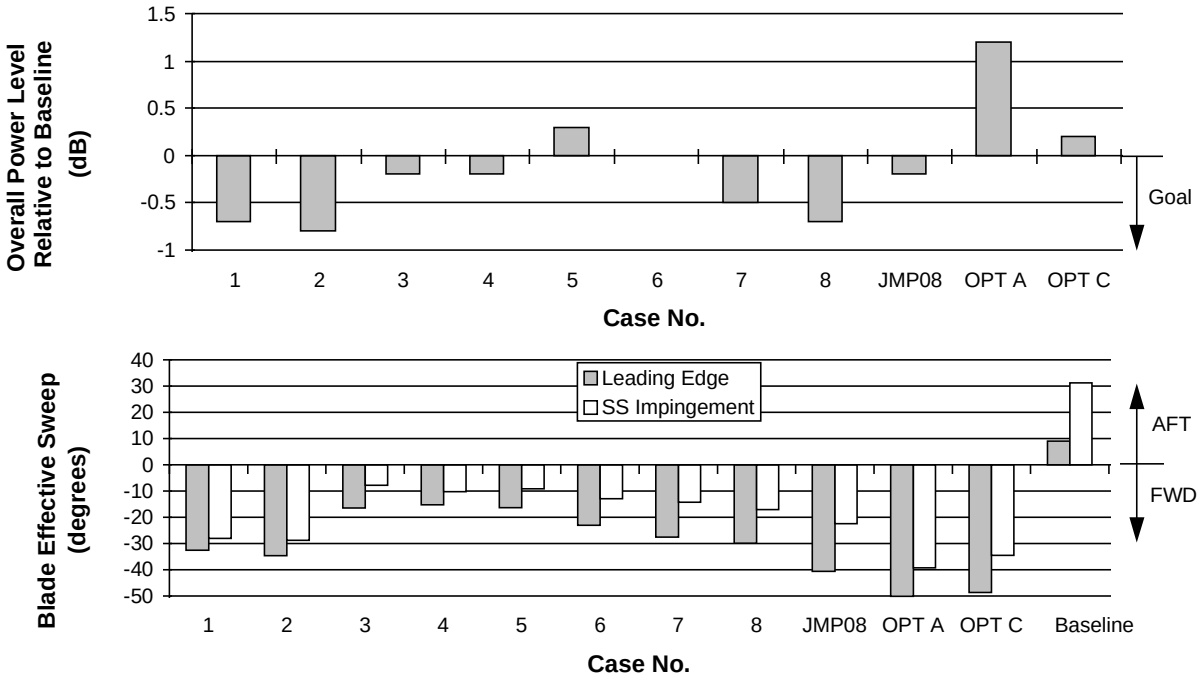

Figure 4.2.4-3. Result of the Acoustic Assessment of the Configurations for Rotor DOE 2.

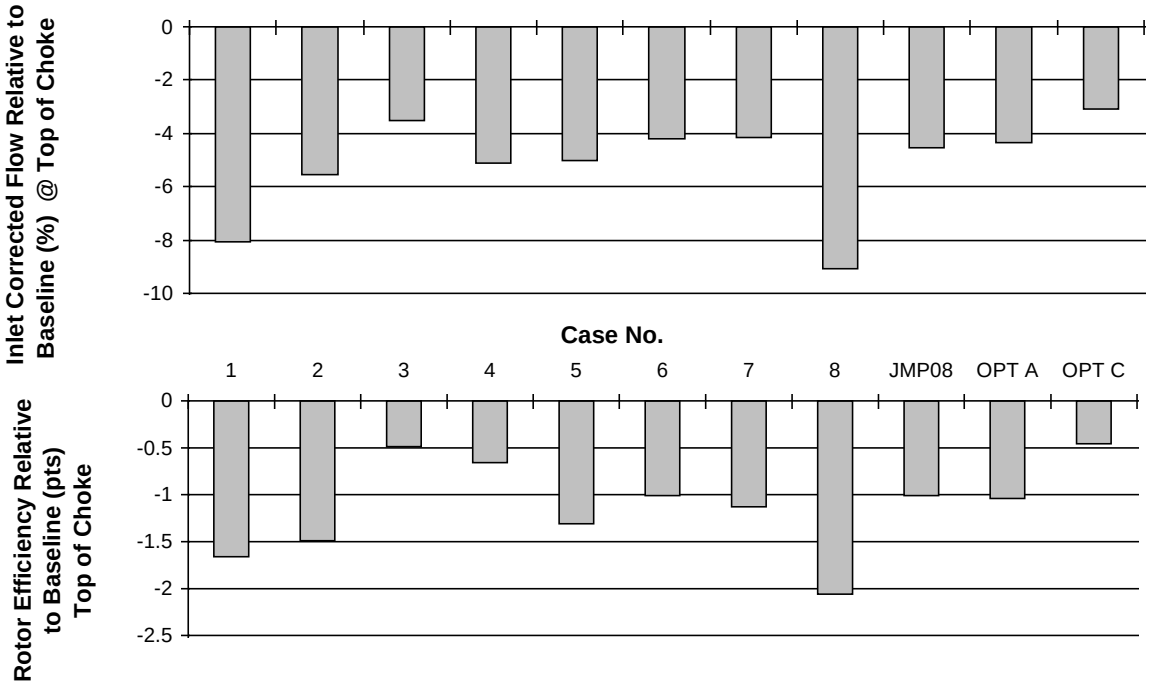

Figure 4.2.4-4. Results of the Aerodynamic Assessment of the Configurations for Rotor DOE 2.

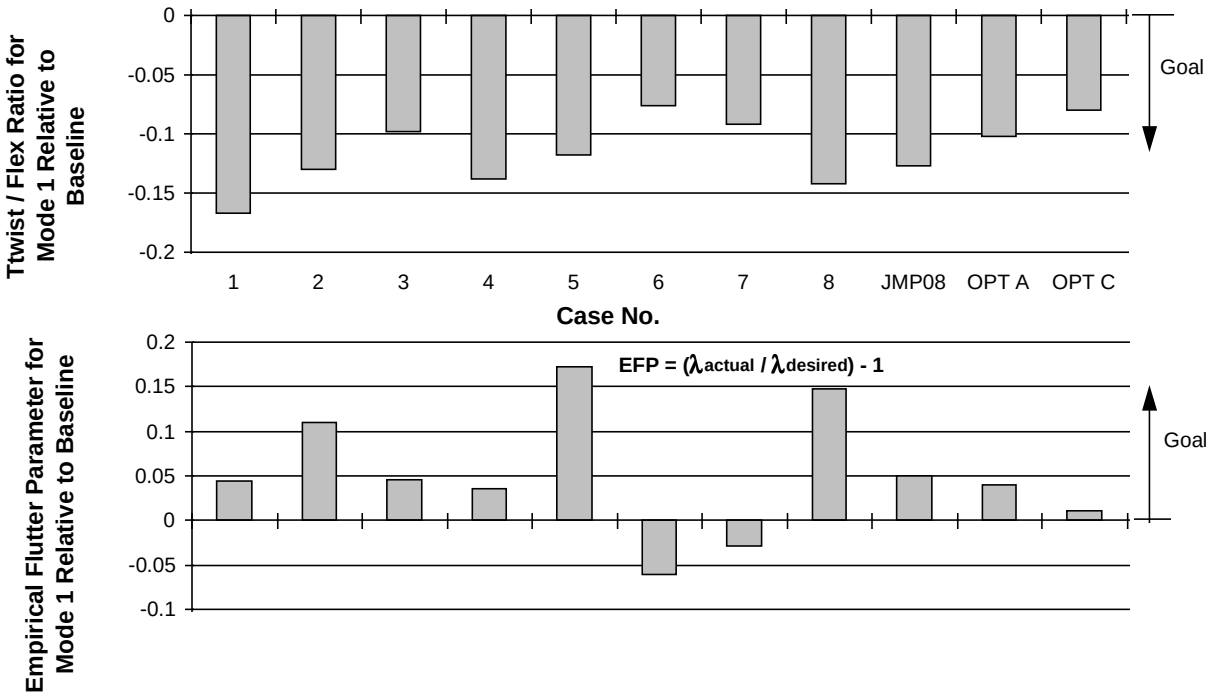

Figure 4.2.4-5. Results of the Aeroelastic Assessment of the Configurations for Rotor DOE 2.

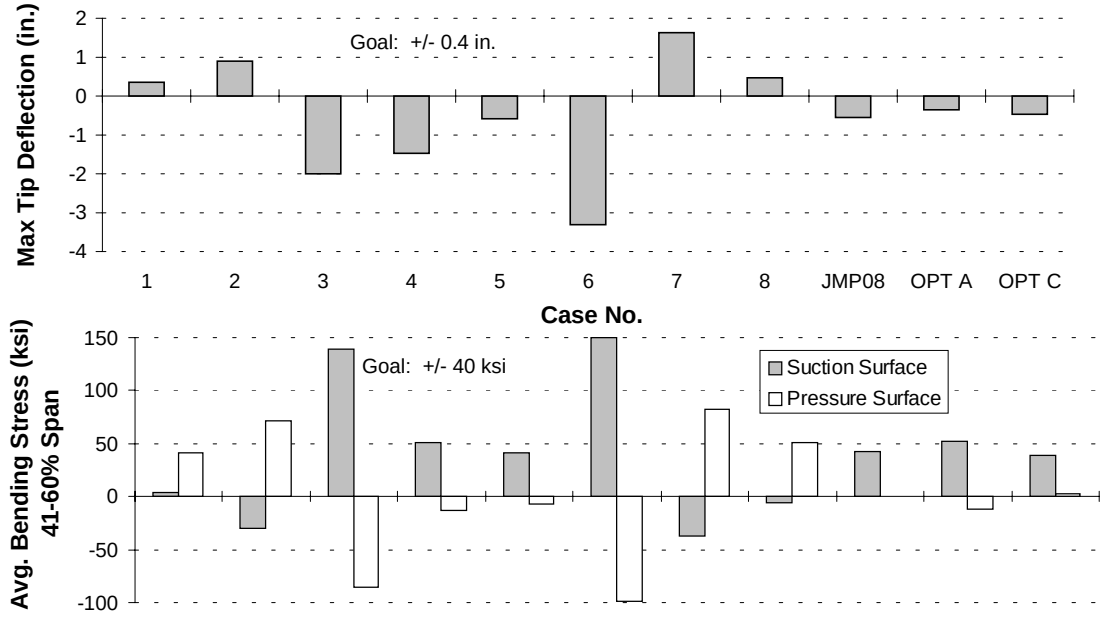

Figure 4.2.4-6. Results of the Mechanical Assessment of the Configurations for Rotor DOE 2.

A new methodology was required to complete rotor DOE 2. Because the blade geometry was created by stacking airfoil section centers of gravity (cg) on a radial line from the engine center line through the hub section cg, any change to the hub section maximum thickness (tmax), or position of tmax would cause the hub cg to shift and the airfoil geometry to change - in particular, the leading edge (LE) metal angle. Because the LE metal angle was changing between the cases, the aerodynamic quality characteristics (flow, efficiency, etc.) could not be directly related to the x-factors. A long and unsuccessful attempt was made to stack the optc airfoil from DOE 1 on the LE which would, if successful, allow direct comparisons between the x-factors and y-factors of DOE 2. Although this technique was successful for the stator, the large hub slope of the rotor proved too much for AXCAPS and back-to-back geometry generation cases could not be duplicated.

In order to solve this problem, a technique was developed which generated the blade geometry in an ANSYS script using the airfoil generation routines from AXCAPS. This procedure forced the airfoil section mean camber lines to be the same as optc. Ranges were determined for the x-factors, and the internal ANSYS optimization procedure was used to minimize flutter. This was essentially the same optimization procedure described in the process flowchart (Figure 4.2.3-4) and used in DOE 1 and the first part of DOE 2, except AXCAPS was not used to generate the airfoil. Go-forward cases, based on the mechanical and empirical aeroelastic criteria, were then analyzed using DAWES to obtain the aerodynamic quality characteristics. The final go-forward case from DOE 2 was designated optm. Results of optm relative to the two go-forward cases from DOE 1 (jmp08 and optc) are shown in Figure 4.2.4-7. The figures show that relative to the baseline, substantial improvements in empirical flutter parameters were achieved while reducing weight; without any additional flow reduction.

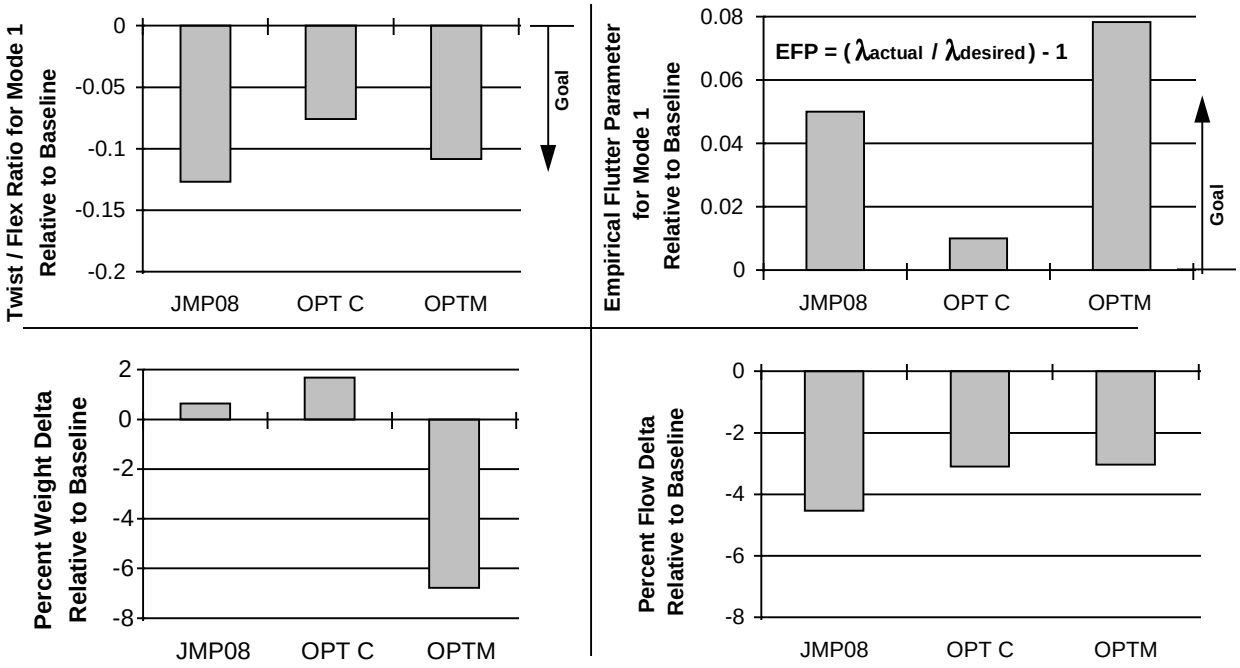

Figure 4.2.4-7. Rotor summary from DOE 2

4.2.5 Design of Experiment 3

4.2.5.1 Purpose

The purpose of DOE 3 was to increase flow and achieve desirable efficiency characteristics by optimizing the incidence.

4.2.5.2 Description

The base level used for DOE 3 was optm. In order to optimize the incidence across the radial span, five spans were chosen (0%, 25%, 50%, 75%, and 95%) with three levels at each span as shown in Table 4.2.5-1. The tip (100% span) was not included because of an inlet boundary layer which was being modeled in the analysis; however, the tip was adjusted to remain consistent with the 95% span level. The magnitude in incidence was also reduced from hub to 95% span to satisfy an additional flutter criteria involving excessive positive tip incidence. The minimum fractional factorial orthogonal matrix for 5 factors with 3 levels produced 27 different geometry's; and, because four or more runs were required for each geometry to determine the

speedline shapes, it resulted in over 108 runs. Because of the time required to run such a large number of cases, DENTON (3-D inviscid analysis) was again reviewed as a possible analysis tool.

Table 4.2.5-1. DOE 3 Design Point Rotor Performance Analysis

Incidence Values in Degrees
(Values represent differences from base case - OPTM)

Case #	0% Span	25%	50%	75%	95%
1	-4.0	-3.5	-3.0	-2.5	-2.0
2	-4.0	-3.5	0.0	2.5	2.0
3	-4.0	-3.5	3.0	0.0	0.0
4	-4.0	0.0	-3.0	2.5	2.0
5	-4.0	0.0	0.0	0.0	0.0
6	-4.0	0.0	3.0	-2.5	-2.0
7	-4.0	3.5	-3.0	0.0	0.0
8	-4.0	3.5	0.0	-2.5	-2.0
9	-4.0	3.5	3.0	2.5	2.0
10	0.0	-3.5	-3.0	2.5	0.0
11	0.0	-3.5	0.0	0.0	-2.0
12	0.0	-3.5	3.0	-2.5	2.0
13	0.0	0.0	-3.0	0.0	-2.0
14	0.0	0.0	0.0	-2.5	2.0
15	0.0	0.0	3.0	2.5	0.0
16	0.0	3.5	-3.0	-2.5	2.0
17	0.0	3.5	0.0	2.5	0.0
18	0.0	3.5	3.0	0.0	-2.0
19	4.0	-3.5	-3.0	0.0	2.0
20	4.0	-3.5	0.0	-2.5	0.0
21	4.0	-3.5	3.0	2.5	-2.0
22	4.0	0.0	-3.0	-2.5	0.0
23	4.0	0.0	0.0	2.5	-2.0
24	4.0	0.0	3.0	0.0	2.0
25	4.0	3.5	-3.0	2.5	-2.0
26	4.0	3.5	0.0	0.0	2.0
27	4.0	3.5	3.0	-2.5	0.0

4.2.5.3 Analysis

DENTON was run with the optc geometry and speedlines were compared with those previously completed using DAWES. Although the total pressure and efficiency levels were considerably different (as expected), choke flow and speedline shapes of efficiency and pressure compared reasonably well. Therefore DENTON was used to complete DOE 3. After completing the analysis, the JMP program and EXCEL Solver were used to predict go-forward cases which would achieve the desirable results. The y-factors were choke flow, a flow delta between deep choke and design-point, and a qualitative assessment of the efficiency speed line shape.

4.2.5.4 Results

Statistical correlations of the data were not very good, but several go-forward cases were completed. The final go-forward case from DOE 3 was designated optm3 and is shown compared to three representative cases from the DOE: Cases 1, 9, and 19 in Figure 4.2.5-1. The figure shows that, in general, cases with large amounts of choke flow (Case 9) had poor efficiency shapes that reduced in level from choke to stall, while those with lower amounts of choke flow (Case 1) had efficiency shapes that increased in level from choke to stall. The go-forward case optm3 was selected to provide maximum flow while still exhibiting good efficiency speedline shape characteristics.

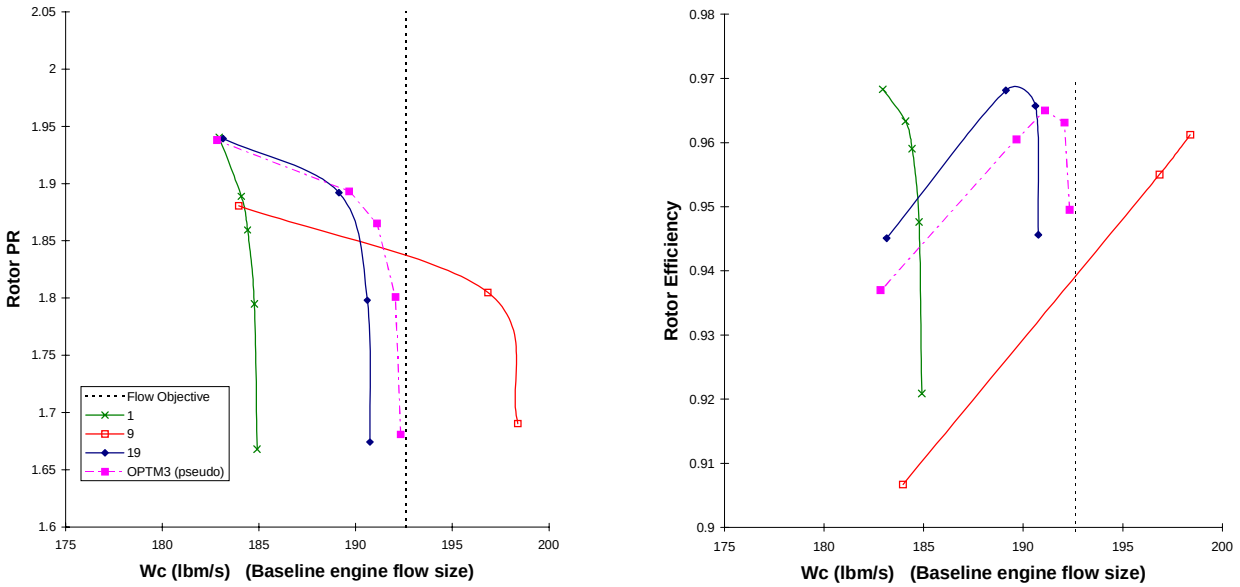

Figure 4.2.5-1. Representative Results from DOE 3 Compared to the Go-Forward Case OPTM3.

4.2.6 Design of Experiment 4

4.2.6.1 Purpose

The purpose of DOE 4 was to increase design point flow and efficiency by optimizing the blade metal angle (beta) distributions along the mean camber.

4.2.6.2 Description

A fractional factorial L-16 was used incorporating fifteen x-factors with two levels each. (Although 3 levels for each x-factor would have been preferred, completion time associated with using DAWES prevented it.) Go-forward case optm3 (from DOE 3) was used as the base level. DAWES analyses performed on optm3 showed that efficiency levels could be increased across the span and therefore dictated the complete spanwise range for DOE 4 design factors. A description of the x and y-factors selected are included in Table 4.2.6-1 along with the matrix description in Table 4.2.6-2. The x-factors are shown graphically in Figure 4.2.6-1 as ranges from the base configuration (optm3). For the blade metal angles on streamlines between those being modified, the betas were linearly interpolated for a smooth transition.

Table 4.2.6-1. DOE 4 Design Point Rotor Performance Analysis
Quality Characteristics

(Values represent differences from base case - OPTM3)

X-factors		Y-factors
1 Beta SL1 LE	+/- 3.0 deg.	Design point flow
2 Beta SL1 25% m	+/- 3.0 deg.	Peak efficiency
3 Beta SL1 50% m	+/- 3.0 deg.	Design point efficiency radial profile (10, 30, 50, 70, 90% radial spans)
4 Beta SL12 LE	+/- 2.5 deg.	Aerodynamic loadings (10, 30, 50, 70, 90% radial spans)
5 Beta SL12 25% m	+/- 2.5 deg.	Suction surface passage shock location (50, 70, 90% radial spans)
6 Beta SL12 50% m	+/- 2.5 deg.	Surge margin assessment
7 Beta SL12 75% m	+/- 2.5 deg.	Part-speed efficiency
8 Beta SL24 LE	+/- 2.0 deg.	
9 Slope of Beta to x-f 14 loc.	0, -20.5 deg.	
10 Beta SL24 50% m	+/- 2.0 deg.	
11 Beta SL24 75% m	+/- 2.0 deg.	
12 Beta location of x-factor 5	15%, 25%	
13 Beta location of x-factor 6	40%, 60%	
14 Beta location of x-factor 9	10%, 25%	
15 Beta location of x-factor 10	40%, 60%	

Table 4.2.6-2. DOE 4 Design Point Rotor Performance Analysis
X-Factor Levels

(Values represent differences from base case - OPTM3)

Case #	X1	X2	X3	X4	X5	X6	X7	X8	X9	X10	X11	X12	X13	X14	X15
1	-3.0	-3.0	-3.0	-2.5	2.5	-2.5	-2.5	2.0	-20.5064	2.0	2.0	4.0	13.0	6.0	13.0
2	-3.0	-3.0	-3.0	2.5	-2.5	2.5	2.5	-2.0	0.0	-2.0	-2.0	4.0	13.0	6.0	13.0
3	-3.0	-3.0	3.0	-2.5	-2.5	2.5	2.5	-2.0	-20.5064	2.0	2.0	6.0	9.0	3.0	13.0
4	-3.0	-3.0	3.0	2.5	2.5	-2.5	-2.5	2.0	0.0	-2.0	-2.0	6.0	9.0	3.0	13.0
5	-3.0	3.0	-3.0	-2.5	-2.5	2.5	-2.5	2.0	0.0	-2.0	2.0	6.0	9.0	6.0	9.0
6	-3.0	3.0	-3.0	2.5	2.5	-2.5	2.5	-2.0	-20.5064	2.0	-2.0	6.0	9.0	6.0	9.0
7	-3.0	3.0	3.0	-2.5	2.5	-2.5	2.5	-2.0	0.0	-2.0	2.0	4.0	13.0	3.0	9.0
8	-3.0	3.0	3.0	2.5	-2.5	2.5	-2.5	2.0	-20.5064	2.0	-2.0	4.0	13.0	3.0	9.0
9	3.0	-3.0	-3.0	-2.5	-2.5	-2.5	2.5	2.0	0.0	2.0	-2.0	6.0	13.0	3.0	9.0
10	3.0	-3.0	-3.0	2.5	2.5	2.5	-2.5	-2.0	-20.5064	-2.0	2.0	6.0	13.0	3.0	9.0
11	3.0	-3.0	3.0	-2.5	2.5	2.5	-2.5	-2.0	0.0	2.0	-2.0	4.0	9.0	6.0	9.0
12	3.0	-3.0	3.0	2.5	-2.5	-2.5	2.5	2.0	-20.5064	-2.0	2.0	4.0	9.0	6.0	9.0
13	3.0	3.0	-3.0	-2.5	2.5	2.5	2.5	2.0	-20.5064	-2.0	-2.0	4.0	9.0	3.0	13.0
14	3.0	3.0	-3.0	2.5	-2.5	-2.5	-2.5	-2.0	0.0	2.0	2.0	4.0	9.0	3.0	13.0
15	3.0	3.0	3.0	-2.5	-2.5	-2.5	-2.5	-2.0	-20.5064	-2.0	-2.0	6.0	13.0	6.0	13.0
16	3.0	3.0	3.0	2.5	2.5	2.5	2.5	2.0	0.0	2.0	2.0	6.0	13.0	6.0	13.0

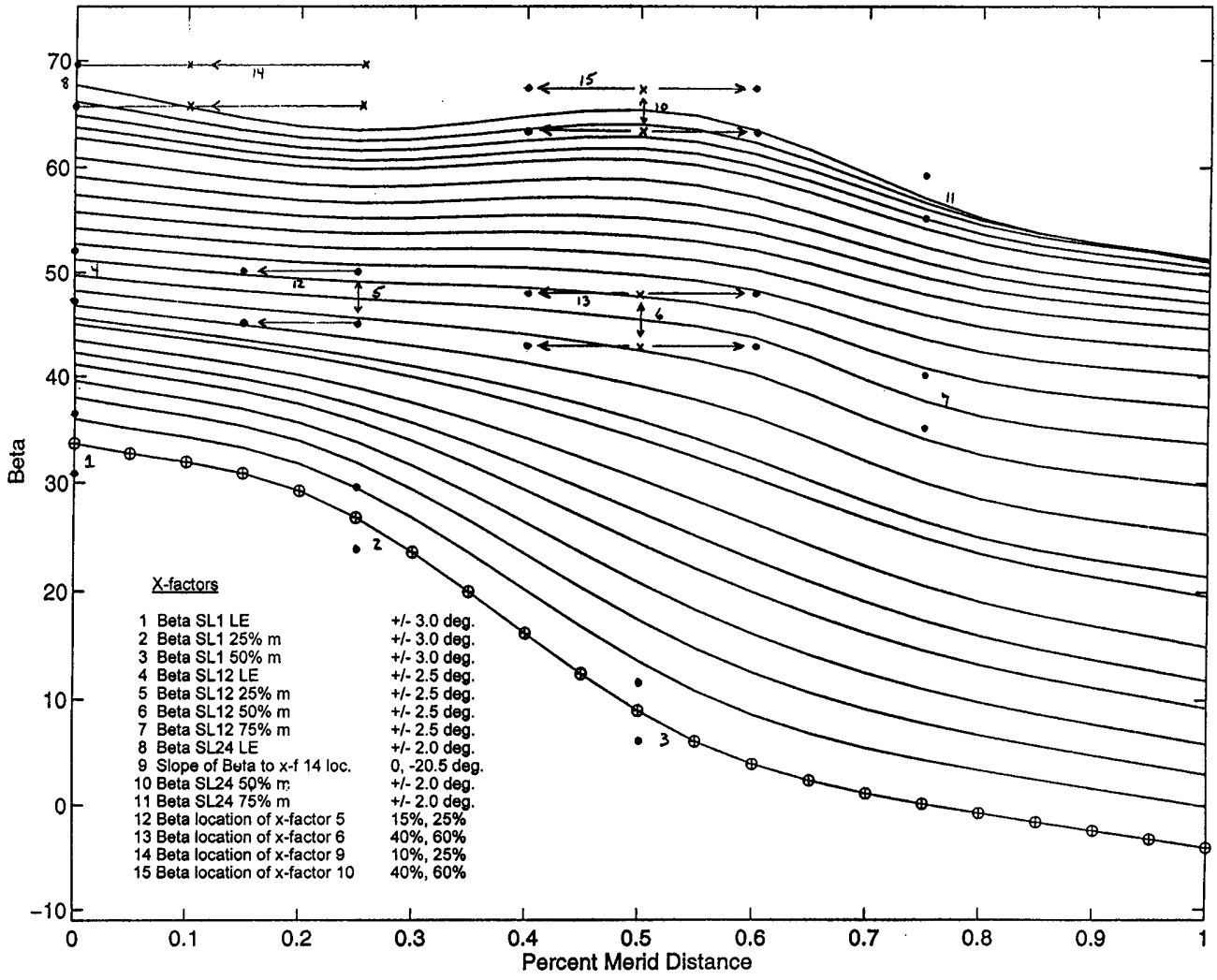

Figure 4.2.6-1. Graphical Description of the X-Factors Used in Rotor DOE 4.

4.2.6.3 Analysis

DAWES results were analyzed and compared for the 64 runs (16 cases with 4 different backpressures) at the design speed. Y-factors of flow, efficiency, pressure ratio, and work were calculated and plotted. Spanwise efficiency profiles were compared and tabulated at 10, 30, 50, 70, and 90 percent span. Aerodynamic blade loadings were also compared at the same spans and were qualitatively assigned values for the DOE. The loadings were judged on suction surface

peak Mach number, suction surface diffusion rate, leading edge assessment (choke/stall), and pressure surface Mach number distribution. Passage shock locations (on the suction surface) were calculated and tabulated at 50, 70, and 90 percent span. Once the y-factors had been tabulated, JMP and EXCEL were used to create go-forward cases.

One potential problem in using DOE's with two levels is that it assumes that the solution is linear, which is typically not the case. This results in extrapolated values with excessive ranges which would not be feasible. To address this, constraints were imposed on the amount that the design factors could permeate. This forced the optimization procedure to find a feasible solution (all design criteria met) within the specified range.

4.2.6.4 Results

The tabulated results are shown in Table 4.2.6-3. A representative sample of the cases (low flow, high flow, and max efficiency) are shown at the design point relative to the baseline rotor DAWES analysis in Figure 4.2.6-2.

Table 4.2.6-3. DOE 4 Tabulated Results

Case	Wc 17.0	Eff pk	Eff 10%	Eff 30%	Eff 50%	Eff 70%	Eff 90%	L 10%	L30%	L 50%	L 70%	L 90%	S L 50%	S L 70%	S L 90%	S M
1	183.78	0.8914	0.9797	0.9415	0.8992	0.8784	0.8136	13	9	2	8	2	0.247	0.343	0.649	-0.0215
2	188.24	0.8931	0.9767	0.9279	0.8829	0.8831	0.8451	12	14	11	10	13	0.246	0.170	0.701	-0.0094
3	185.40	0.8772	0.9762	0.9055	0.8425	0.8595	0.8783	16	16	16	16	8	0.166	0.189	0.595	0.0000
4	180.95	0.8832	0.9819	0.9474	0.8956	0.8556	0.6982	14	6	6	13	10	0.291	0.418	0.596	-0.0074
5	183.33	0.8845	0.9790	0.9225	0.8844	0.8734	0.8294	15	15	13	6	12	0.185	0.343	0.650	-0.0215
6	188.68	0.9040	0.9802	0.9493	0.8948	0.8916	0.8405	11	3	14	2	16	0.339	0.210	0.700	-0.0128
7	190.02	0.8994	0.9803	0.9458	0.8983	0.8931	0.8603	10	5	3	1	5	0.269	0.296	0.699	0.0000
8	186.04	0.8965	0.9795	0.9306	0.8830	0.8855	0.8616	9	11	12	5	7	0.225	0.189	0.675	-0.0322
9	184.90	0.8859	0.9775	0.9300	0.8840	0.8775	0.8416	4	12	4	4	3	0.205	0.295	0.649	-0.0196
10	188.76	0.9072	0.9790	0.9462	0.8925	0.8836	0.8589	1	7	15	12	9	0.316	0.210	0.700	-0.0120
11	186.55	0.8984	0.9801	0.9456	0.8944	0.8689	0.8431	5	2	10	15	15	0.248	0.134	0.700	-0.0149
12	187.91	0.8909	0.9773	0.9355	0.8830	0.8771	0.8479	3	13	7	14	1	0.291	0.319	0.699	-0.0139
13	183.81	0.8995	0.9786	0.9518	0.9034	0.8795	0.8649	8	1	1	11	4	0.248	0.418	0.675	-0.0314
14	189.80	0.8982	0.9803	0.9419	0.8897	0.8926	0.8353	7	8	8	3	14	0.292	0.189	0.722	-0.0098
15	194.05	0.8970	0.9791	0.9380	0.8848	0.8925	0.8766	6	10	5	7	6	0.247	0.250	0.674	0.0000
16	177.01	0.8938	0.9797	0.9458	0.8957	0.8612	0.6605	2	4	9	9	11	0.269	0.446	0.700	-0.0087

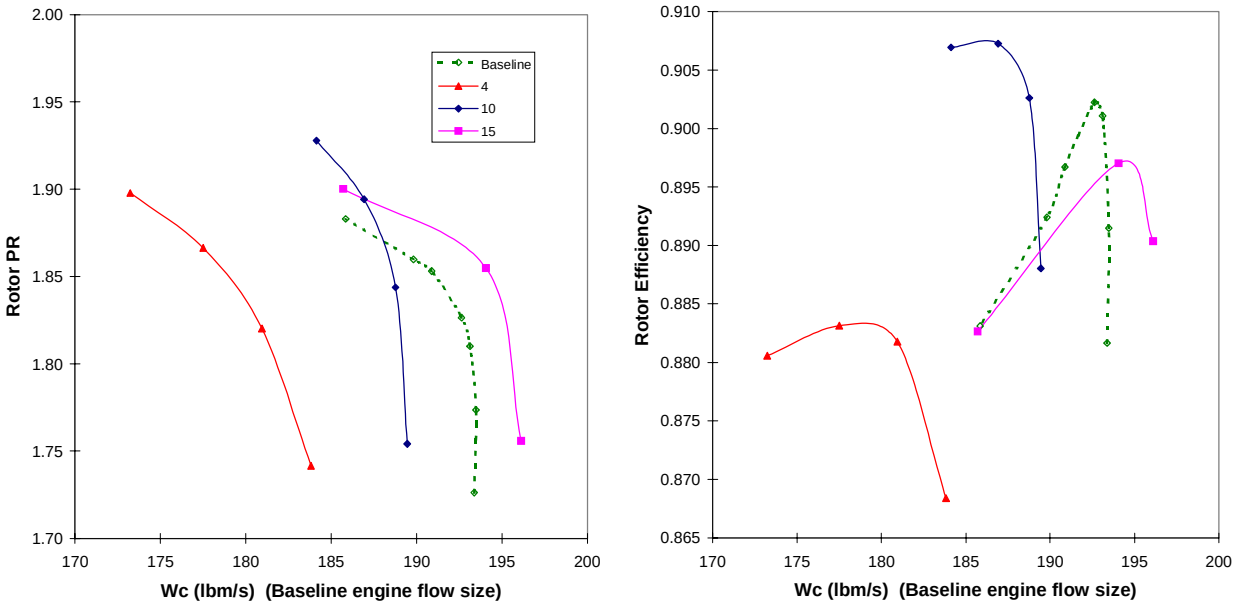

Figure 4.2.6-2. Representative Results from Rotor DOE 4 Compared to Baseline Rotor

As Table 4.2.6-3 shows, the calculated efficiency and the qualitative value given to the aerodynamic loading, for the same spanwise location, varied considerably in some instances. Therefore, go-forward cases were created based on the other y-factors combined with either the efficiency at radial spans or the loadings. DAWES results for the go-forward cases at the design point are shown in Figure 4.2.6-3 compared to the starting case from DOE 3 (optm3) and the performance objective (baseline rotor). The initial two cases (gf01, and gf02) were completed using EXCEL and were predicted to match the design flow objective; however, DAWES results showed insufficient flow. Y-factors from these cases were added to the model and two new go-forward cases were created, gf03 and gf04. The four cases were also analyzed at 85% N1c to verify good part-speed performance with results shown in Figure 4.2.6-4. The results indicated a reduction in part-speed efficiency with increased choke flow at 100% N1c. In order to best match the baseline rotor performance goals, and provide the best back-to-back test for acoustic comparisons, go-forward case 3 (gf03) was selected as the final design (details reported in Section 5.0).

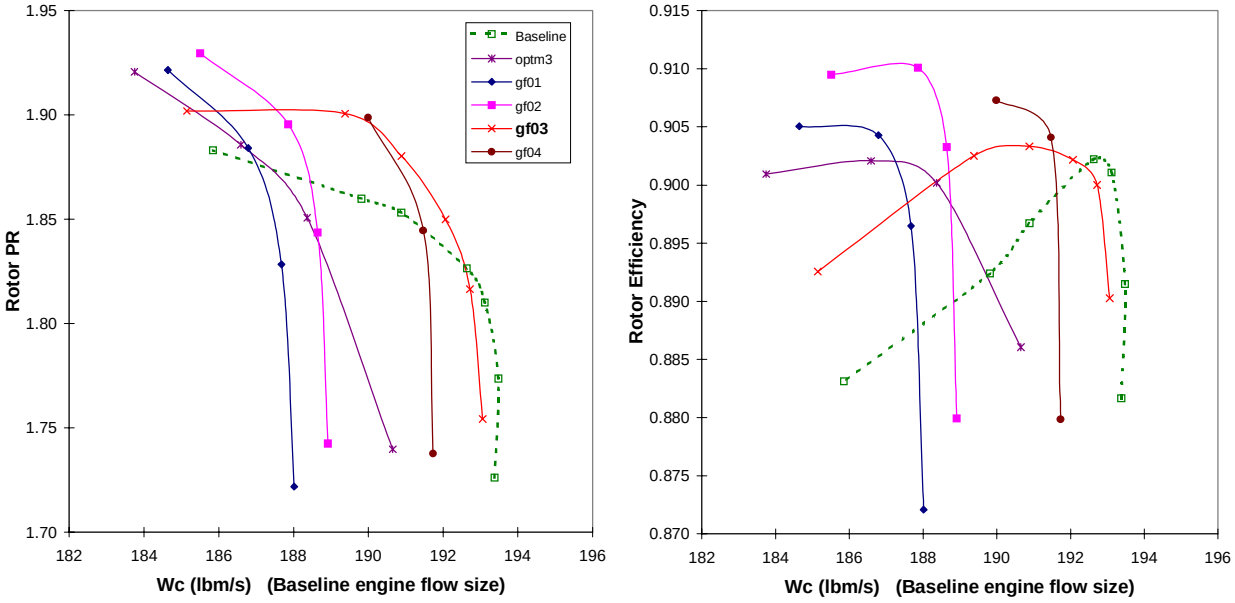

Figure 4.2.6-3. Effect of Beta Distribution on Flow and Efficiency on DOE 4 Go-Forward Cases at 100% N1c.

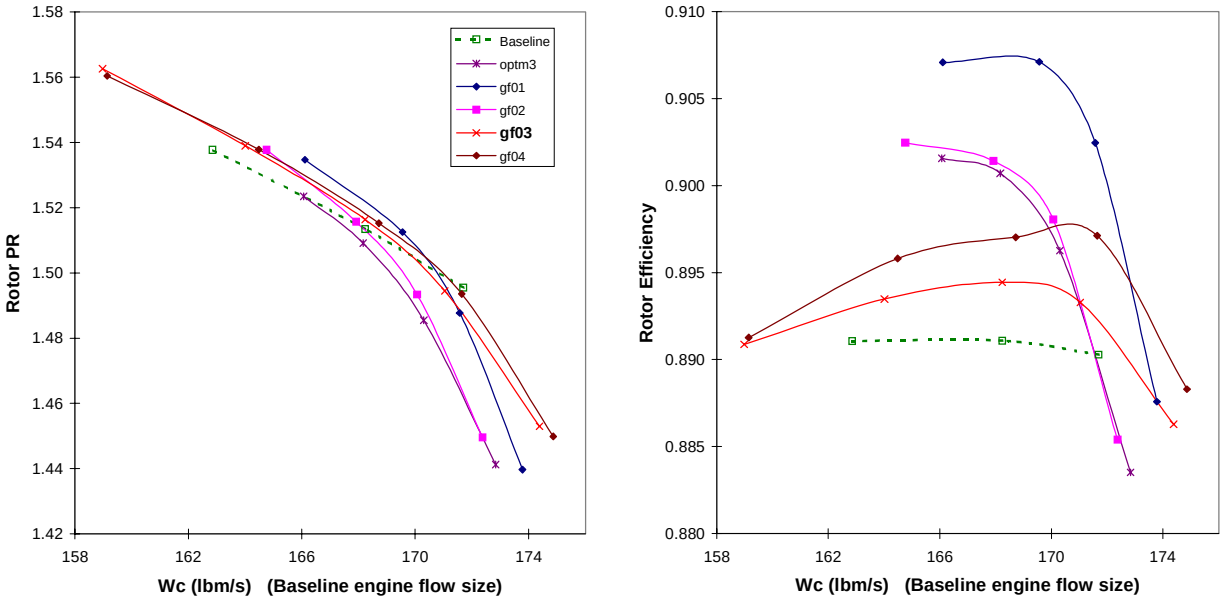

Figure 4.2.6-4. Effect of Beta Distribution on Flow and Efficiency on DOE 4 Go-Forward Cases at 85% N1c.

4.2.7 Bird Ingestion Analysis

A preliminary Foreign-Object-Damage (FOD) assessment performed on the QHSF blade indicated leading-edge thickness parameters to be well within successful AE experience. This analysis is comparative in nature and considers only spanwise geometric characteristics, LE thickness distribution, blade count, metal angles, bird weight, as well as other parameters. The computed damage tolerance factors are compared with a database consisting of very successful, marginal, and poor designs. This preliminary analysis however, can not account for the high degree of forward sweep and tangential lean built into the QHSF, which will be accounted for using NOSAPM (Section 5.1.4.6).

4.3 Stator

4.3.1 Design Ground Rules and Goals

The stator design emphasizes the reduction of rotor wake interaction noise while meeting aerodynamic, mechanical, and producibility goals. The ground rules required:

1.) Use the baseline vane count (52 vanes). The acoustic effects of varying vane count would confuse the analysis of the effects of vane design.

2.) Don't sweep the stator aft or move it downstream relative to the baseline stator. The fan will be able to replace the baseline fan without a change in engine dimensions.

3.) Use the baseline front frame unchanged.

4.) Use the baseline stator solidity. The inflow from the AE/QHSF was similar to the baseline fan so that the baseline solidity would provide good loadings.

5.) Control vane stacking by specifying the shape of the leading edge. Since this is what affects wake trace speed, it seemed simpler to specify the shape of the leading edge.

6.) Design for composite construction. This requirement puts some restrictions on leading and trailing edge radius and maximum thickness.

The stator was to reduce rotor wake interaction noise to the greatest extent possible while still having acceptable aerodynamic loadings, losses similar to the baseline stator, and acceptable stress, frequency margin, flutter margin, and composite producibility.

4.3.2 Strategy

The vane stacking would be set first since this was important acoustically and since it was likely to be radical enough that it would be good to find out up front about any aerodynamic or mechanical problems it caused. DOE 1 would be used to experiment with different vane stacks. As originally planned, this DOE varied vane stacking tangentially and axially. Axial stacking changes were outside the ground rules, but knowledge of these trends was desirable anyway. Acoustic, aerodynamic, and mechanical quality factors would be collected and their trends with vane stacking would be used to design the final vane stack. The vane incidence, vane section mean camber line angle chordwise distributions, deviation, chord, and thicknesses for this DOE would come from the baseline vane in the beliefs that it was a good starting point. Aerodynamic quality characteristics would be calculated by the DAWES 3D viscous CFD code.

Once the stacking had been decided, the second vane DOE would be used to optimize vane incidence and mean camber line angle chordwise distributions for good aerodynamic performance with this stacking.

The vane trailing edge angle would then be set to produce axial (zero swirl) stator exit flow. This would not require a DOE. The vane trailing angle would be set to remove any residual DAWES-predicted exit swirl. This angle usually produces exit swirl acceptably close to axial in just a few iterations. Loadings and loss are then re-checked to make sure they're still acceptable in spite of any increased flow turning required to produce axial flow.

The vane leading and trailing edge radius and maximum thicknesses would then be adjusted to meet composite vane producibility criteria. Composite vanes require control of the vane thickness as measured normal to the vane suction and pressure surfaces, as opposed to the design tools which specify thickness in the tangential direction. The tangential thickness varies from the normal thickness by the cosine of the lean angle. Since the lean angle everywhere but the leading edge is affected by both the vane stacking and the vane section stagger angles, the thickness modification is performed after the stagger angles have been determined. After thickness has been adjusted, the loadings, loss, and exit swirl are re-checked.

The composite construction provides flexibility to produce a vane with combinations of high axial and tangential leans with minimum weight penalty. The current production vanes on the baseline stator have symmetric lay-up or taped construction. Recently, a braided vane has been developed at AE as a part of the ENCORE (Engine Cost Reduction) program. In addition, the braided vane has better FOD characteristics than the taped vane. However, it has lower flutter margins due to decreased torsional rigidity. The QHSF exit vane will be a braided composite vane. A preliminary layout of the vane is shown in Figure 4.3.2-1.

The AE in-house design tool CADS (Composite Airfoil Design System) will be used for the composite vane design. As shown in the flowchart in Figure 4.3.2-2, CADS uses the airfoil geometry from the aero bank file to generate an ANSYS input (prep7) file. This system was used to design the baseline stator.

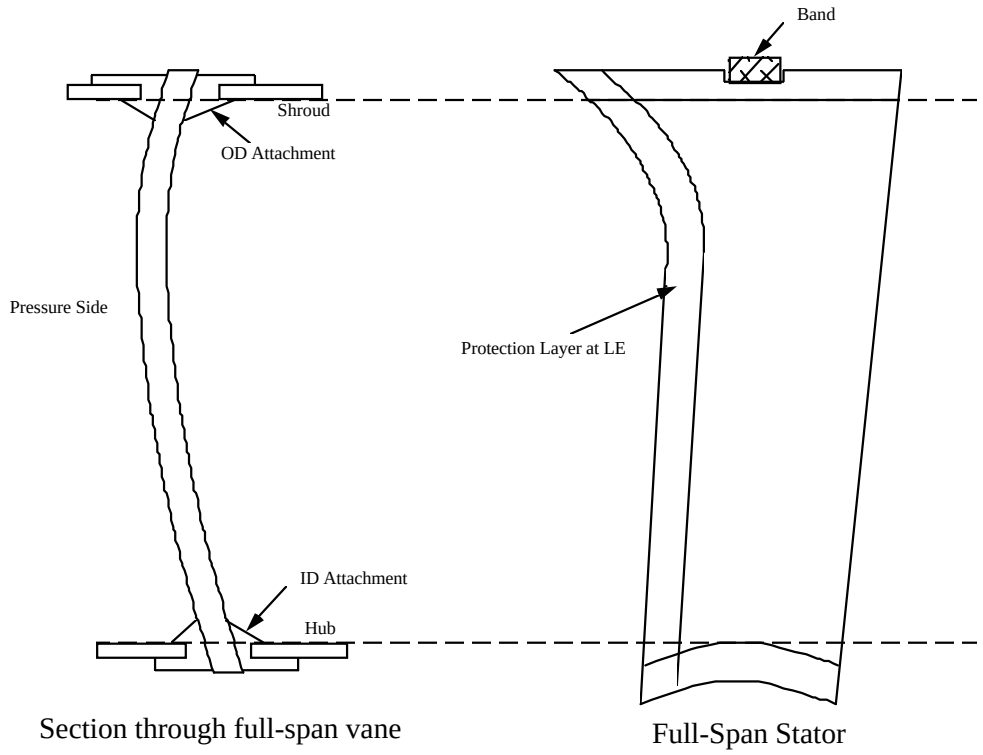

Figure 4.3.2-1. Preliminary Layout of the Composite Vane

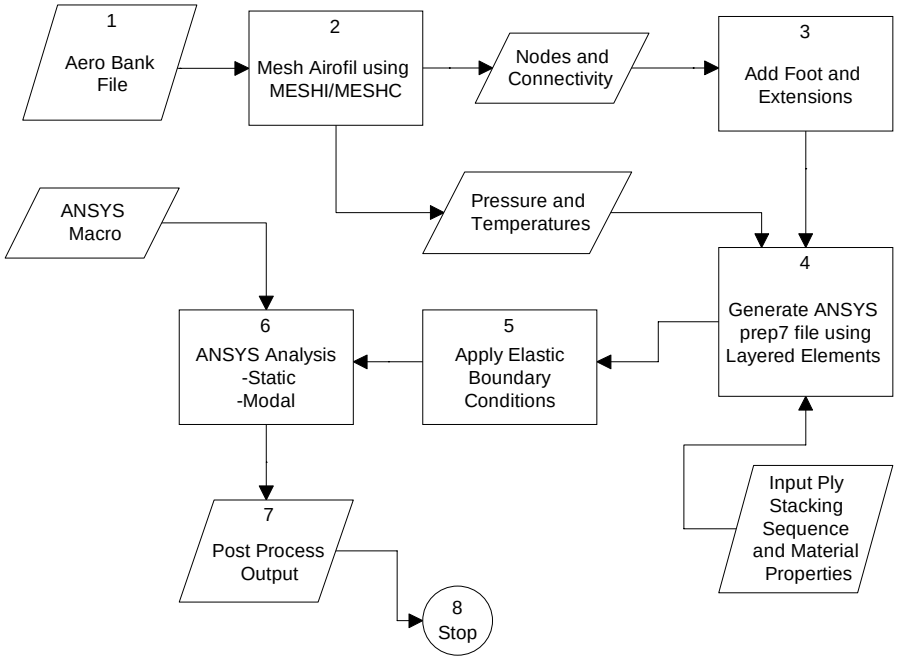

Figure 4.3.2-2. The AE Composite Stator Design System will Design a Composite Vane that Will Incorporate the Optimum Aerodynamic and Acoustic Features.

4.3.3 Stacking DOE

The vanes used in the stacking DOE were designed to operate behind the "optc" fan rotor. Initially, an L18 Taguchi matrix was chosen with 2 levels for axial sweep at the vane midspan and tip and 3 levels for the tangential stacking at the midspan and tip. The 2 sweep levels represented the baseline vane axial sweep and a 14 degree increase. This DOE couldn't be completed because the great variation in rotor-stator axial spacing between the hub and the shroud created convergence problems in the axisymmetric flow solver (AXCAPS). The matrix was modified so the sweep now varied between the baseline sweep and a radial leading edge, which would still provide information about the effects of sweep. Work on the modified DOE was abandoned due to schedule constraints and since decreasing axial sweep had noticeable acoustic and aerodynamic penalties.

The baseline axial sweep was then chosen for the vane and only the effect of tangential lean and bow was studied. Tangential stacking was controlled at the midspan and the shroud with three levels at each location representing lean with the direction of rotor rotation, no lean, and lean against the direction of rotor rotation. Since this only produced 9 different vanes, a full factorial was used to examine all 9 vanes.

In full factorial stator DOE 1 (FF 1), tip tangential displacement equivalent to 30 deg of lean from the radial were tried. This had acoustic benefits but vanes leaned 30 deg with the rotor rotation (i.e., with the suction surface leaned down facing the hub) showed serious flow separation near the hub in DAWES. Since the 30 deg lean was infeasible from a performance standpoint, a second full factorial, FF 2, was used which had vane section tangential tip displacements equivalent to 15 deg of lean from the radial. The leading edges are shown in Fig. 4.3.3-1 and tabulated in Table 4.3.3-1. This figure also shows rev_3, which was the stacking eventually chosen after vane iterations using the acoustic, aerodynamic, and mechanical results of FF 2.

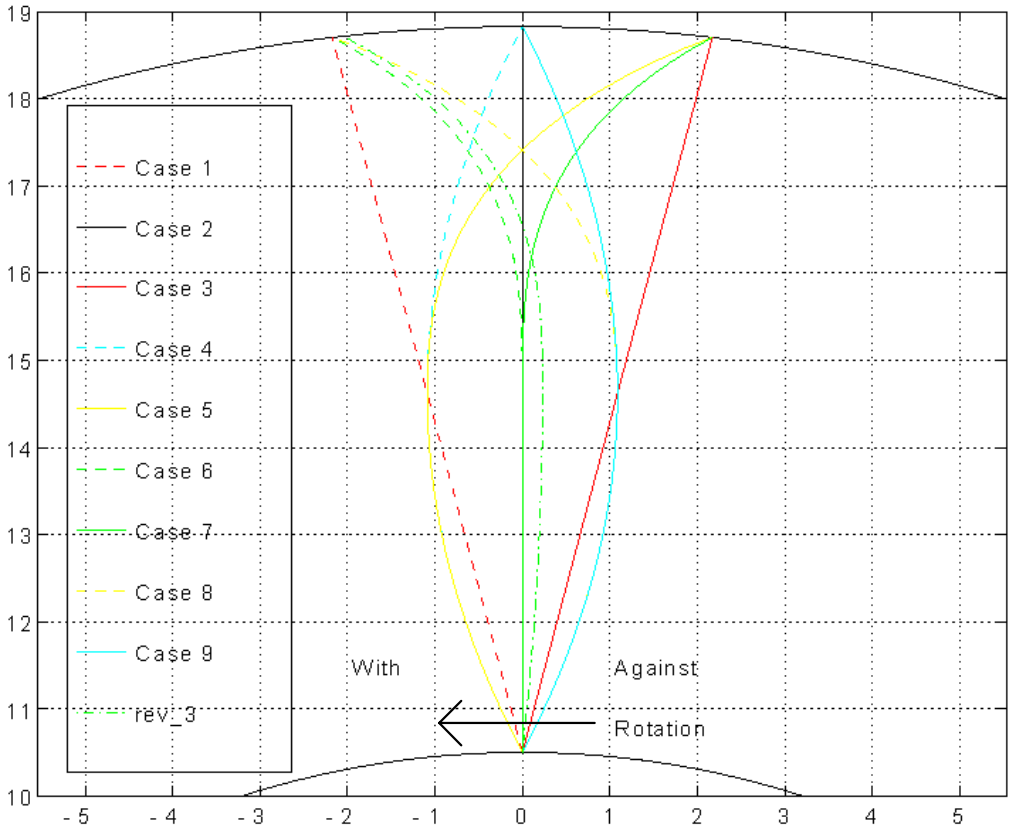

Figure 4.3.3-1. Stator Stacking Full Factorial 2 Vane Leading Edges

Table 4.3.3-1. Stator Stacking Full Factorial 2
CG Shifts in Baseline Engine Scale

Case	Midspan Ycg (in)	Shroud Ycg (in)	
1	-0.879	-1.758	15 deg lean with rotation
2	0.000	0.000	No lean
3	0.879	1.758	15 deg lean against rotation
4	-0.879	0.000	Bow with rotation
5	-0.879	1.758	Compound bow w/ and against rotation
6	0.000	-1.758	Compound lean with rotation
7	0.000	1.758	Compound lean against rotation
8	0.879	-1.758	Compound bow against and w/ rotation
9	0.879	0.000	Bow against rotation

Ycg: +ve=shifted against direction of rotation
0=unshifted
-ve=shifted with direction of rotation

The quality characteristics used for the vane stacking iterations were:

Acoustic: V072-predicted rotor wake-stator interaction sound power levels (SPL) at 2 and 3 times blade passing frequency (BPF), radiated towards the fan inlet and exit, at a representative approach point at 55.9% corrected fan design speed were used. The stator inlet velocity triangles used in V072 were predicted by an off-design model of the optc rotor in AXCAPS. The acoustic results are shown in Figures 4.3.3-2 through 4.3.3-5 for inlet 2*BPF, inlet 3*BPF, exit 2*BPF, and exit 3*BPF respectively. These figures also show the acoustic predictions for rev_3, the final vane stack.

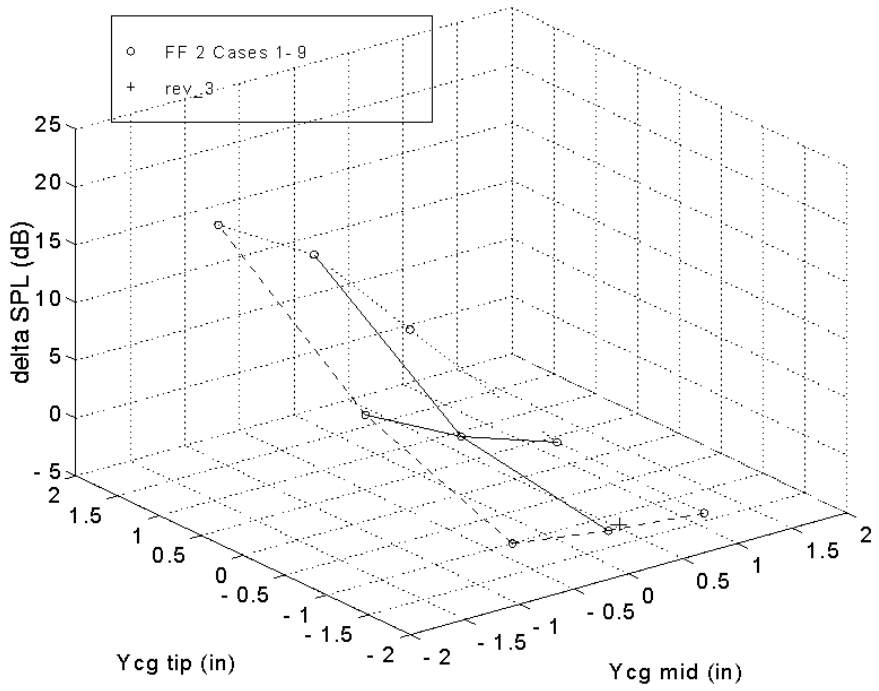

Figure 4.3.3-2. Stator Stacking Full Factorial 2 Inlet 2*BPF SPL Predictions

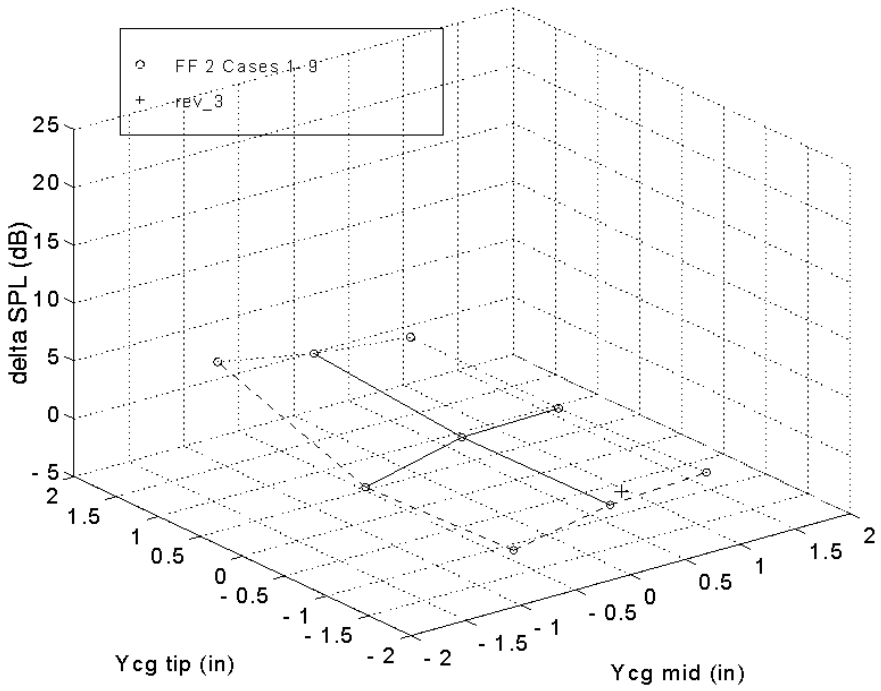

Figure 4.3.3-3. Stator Stacking Full Factorial 2 Inlet 3*BPF SPL Predictions

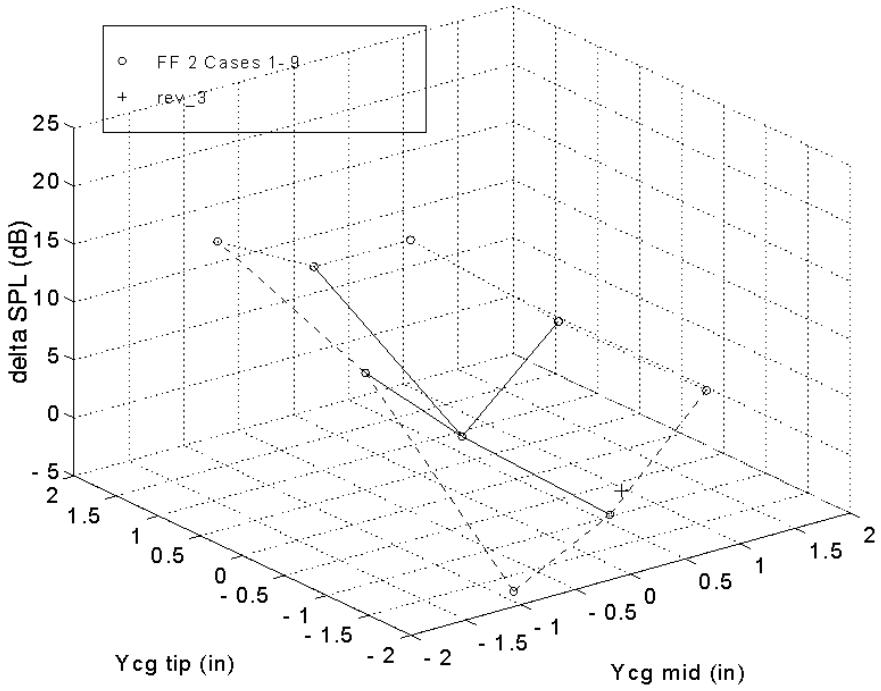

Figure 4.3.3-4. Stator Stacking Full Factorial 2 Exit 2*BPF SPL Predictions

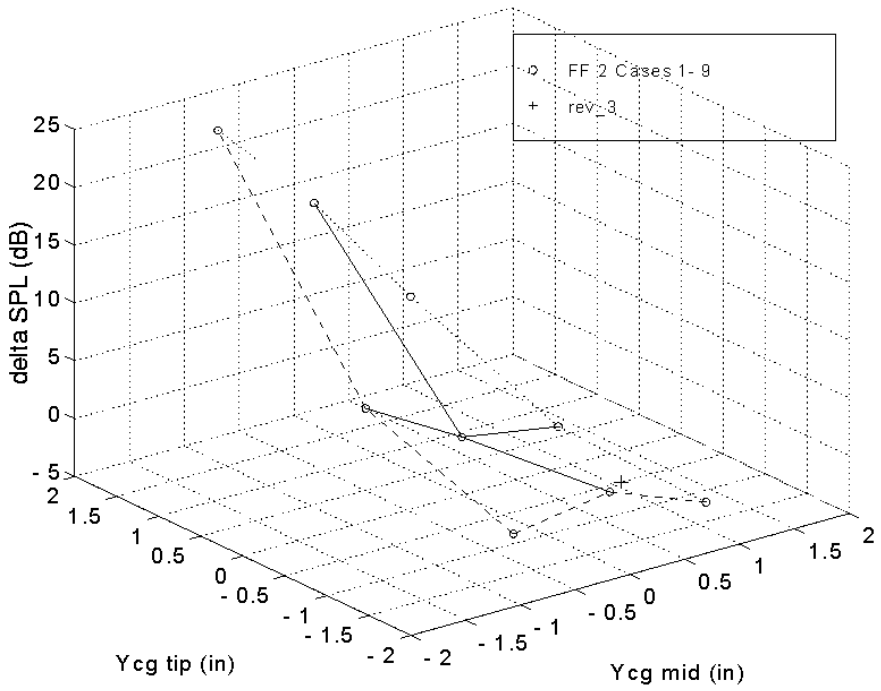

Figure 4.4.3-5. Stator Stacking Full Factorial 2 Exit 3*BPF SPL Predictions

The acoustic results were difficult to optimize. Generally, any stacking that reduced one sound power level increased others. A reduction in inlet sound power level was favored over a reduction in exit because the exit radiated sound can be more easily attenuated with acoustic treatment. The inlet 2*BPF results favored leaning the midspan against rotation and the tip with rotation as in rev_3.

Aerodynamic: Design point stator loss and stator exit swirl as estimated by DAWES were used as quality factors. Stator loadings were used as a qualitative guide. Figure 4.3.3-6 shows the DAWES predicted loss for the 9 stators in FF 2 as well as for the rev_3 stator.

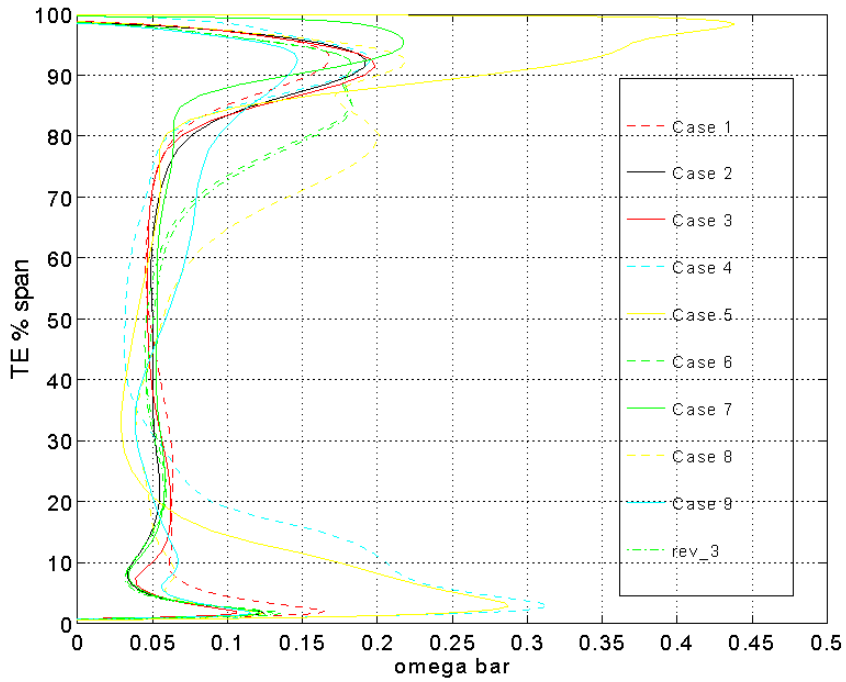

Figure 4.3.3-6. Stator Stacking Full Factorial 2 Stator Loss

The loss profiles show that leaning the suction surface towards the endwalls should be avoided because of flow separation from the suction surface and high hub loss (Cases 1, 4, and 5) and shroud loss (Cases 5 and 7). This result was an important aerodynamic driver in the stacking iterations.

The loss profiles also show a high-loss region from about 60% to 80% span for Cases 6, 8, and (to a lesser extent) 9. At first, this appeared to be a problem with stacks that lean with rotation over the outer 50% span but examination of the flow vectors in the vane-to-vane surface in this region showed flow separation from the pressure surface due to large negative incidence. Figure 4.3.3-7 shows incidence calculated using DAWES leading edge swirl angles. Figures 4.3.3-8 and 4.3.3-9 show the vane leading edge geometric angles and the vane leading edge swirl angles that resulted in this incidence.

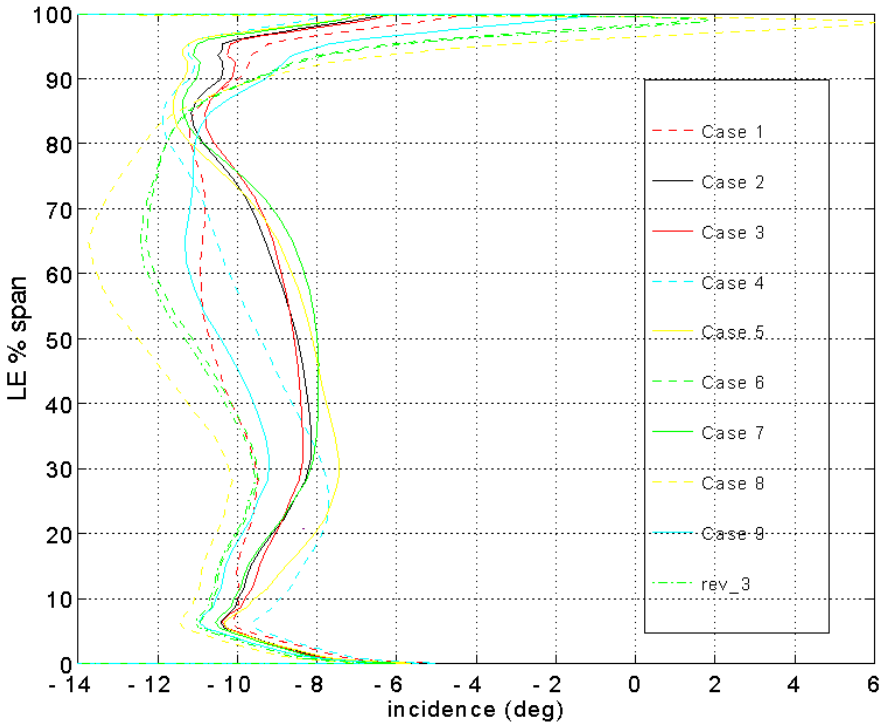

Figure 4.3.3-7. Stator Stacking Full Factorial 2 Stator Incidence

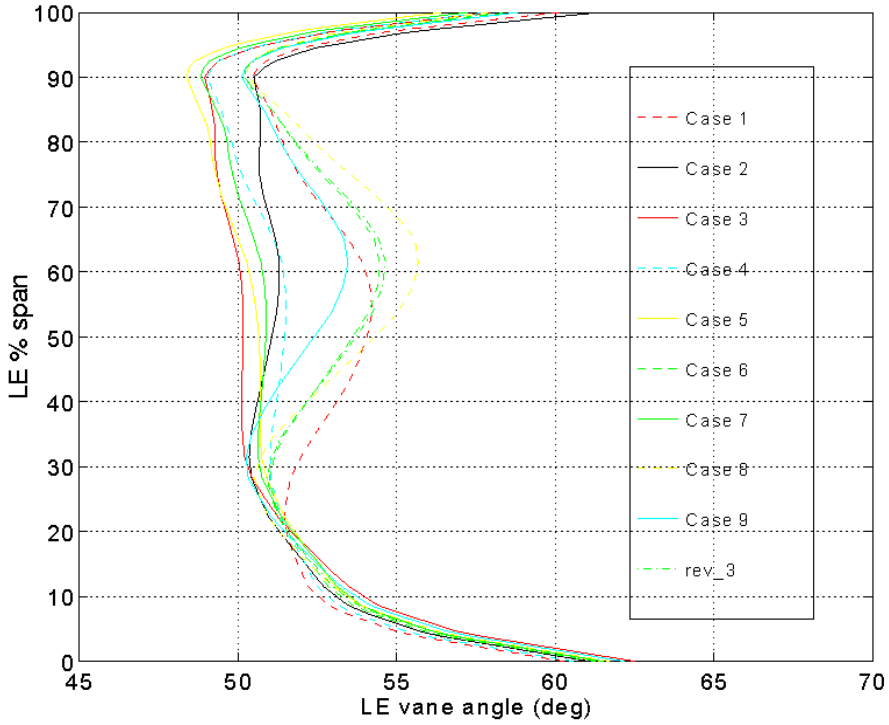

Figure 4.3.3-8. Stator Stacking Full Factorial 2 Vane LE Angle

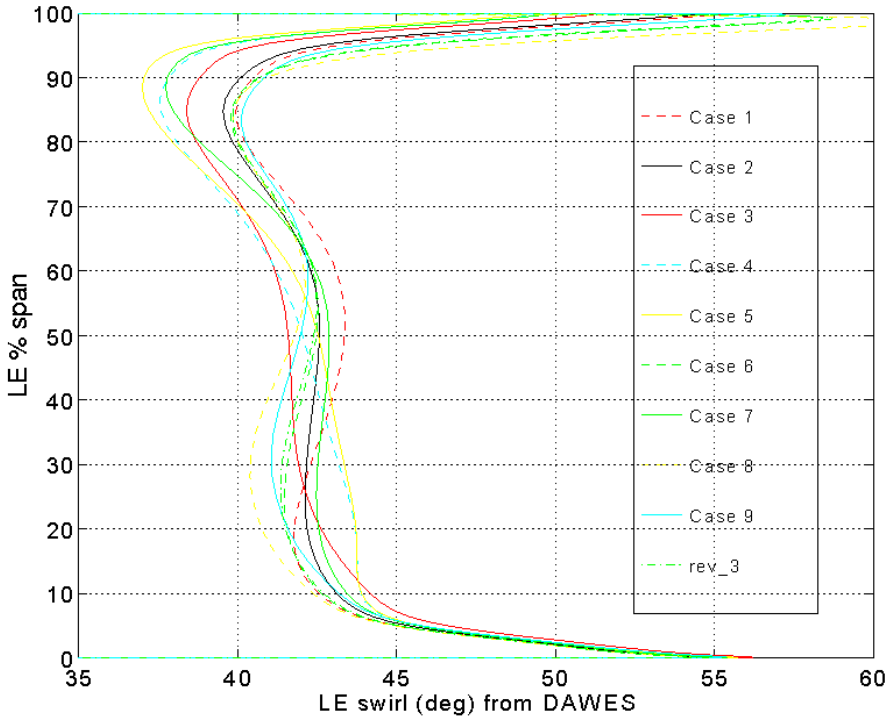

Figure 4.3.3-9. Stator Stacking Full Factorial 2 Stator LE Swirl Angle

The vane leading edge geometric angles in Figure 4.3.3-8 were calculated by AXCAPS. The intended stator incidence for FF 2 was the baseline design point stator incidence. AXCAPS was used to calculate the required vane leading edge angles to achieve this incidence given the rotor exit swirl angles from the OPTC rotor DAWES model. The varying vane stacks produced varying stator leading edge swirl profiles in AXCAPS since AXCAPS applies vane body radial forces to shift the flow radially, which changes the stator leading edge meridional velocity profile according to how the vane is stacked. Since all 9 cases have the same incidence, the variation in vane leading edge geometric angle in Figure 4.3.3-8 represents the variation in leading edge swirl angle in AXCAPS, which can be slightly over 5 degrees between 60% and 80% span.

The air angles in Figure 4.3.3-9 were obtained from the stator DAWES models. Each DAWES model used the exit swirl profile predicted by the OPTC rotor DAWES model at the design point. The swirl profile variation from case to case at the stator leading edge represents DAWES' estimate of how vane stacking affects the radial distribution of flow upstream of the stator. In DAWES, the variation due to vane stacking is only 2-3 degrees.

The high loss in this region results from setting the vane leading edge angles too high for these cases. This happened because the streamline code which was used to generate vane geometry over-estimated the effect of vane stacking on the stator leading edge swirl angles. Stator loss in this region was, therefore, not considered in the vane stacking evaluation. Figure 4.3.3-6 shows that the final vane stack, rev_3, also has high loss. This issue was resolved in the next DOE where incidence would be optimized.

Figure 4.3.3-10 shows stator exit swirl estimated by DAWES. The ultimate intent of the design was to set this as close to axial (0 deg) as practical, which was done in the baseline vane design. The vane trailing edge geometric angles for this DOE were taken from the baseline vane and were not adjusted to reduce the exit swirl. Exit swirl was still used as a quality characteristic since stators with swirl already close to axial would require less trailing edge angle adjustment.

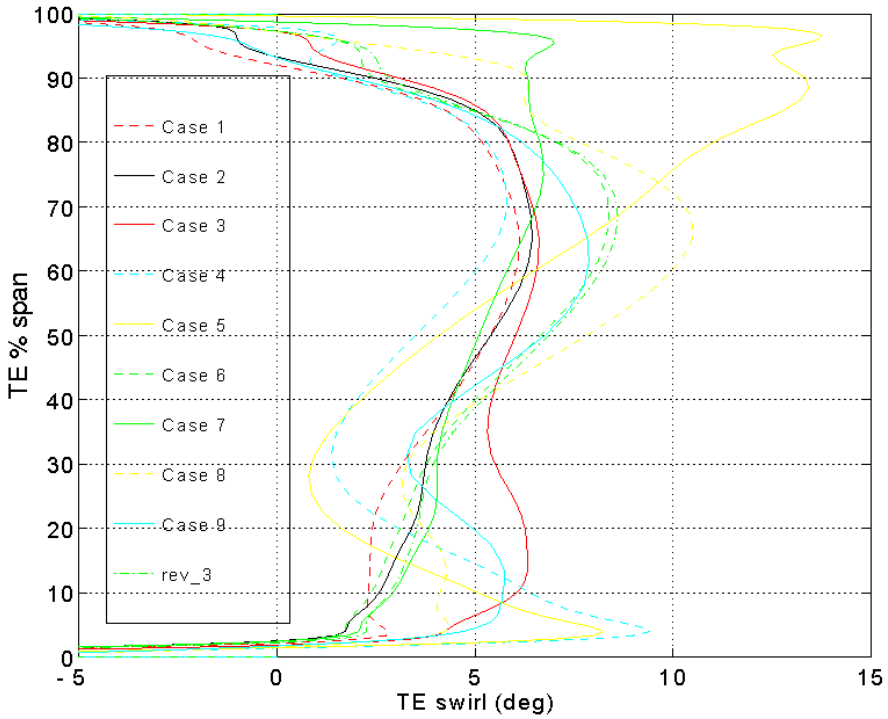

Figure 4.3.3-10. Stator Stacking Full Factorial 2 Stator TE Swirl Angle

Since all the vanes in this study have the same trailing edge geometric vane angle, Figure 4.3.3-10 shows the expected result that vanes with higher loss have higher deviation. Although exit swirl was examined in the design process, it was not used directly in the DOE since it is another way of representing loss.

Vane displacements, static strains on pressure and suction surfaces, vibration and flutter margins were used in the DOE as mechanical inputs. In addition, the static stresses and strains in the vane foot were monitored for abnormalities. The strain and displacement limits were defined based on AE experience. As seen from Figures 4.3.3-11 and 4.3.3-12, there were no surprises with both strain levels and the maximum displacements. Further, the maximum strains and displacements were within acceptable limits for all the go-forward cases that emerged out of the stator DOE.

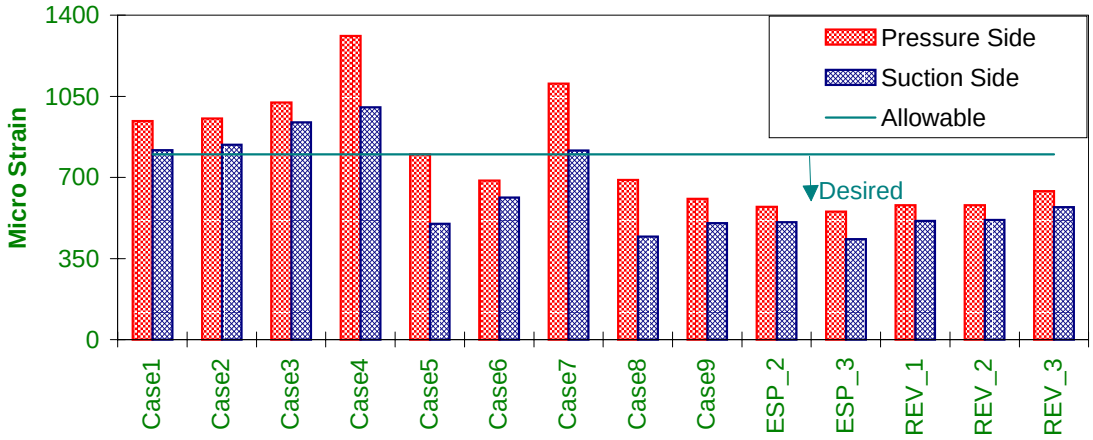

Figure 4.3.3-11 Stator Stacking Full Factorial Maximum Static Strain Predictions

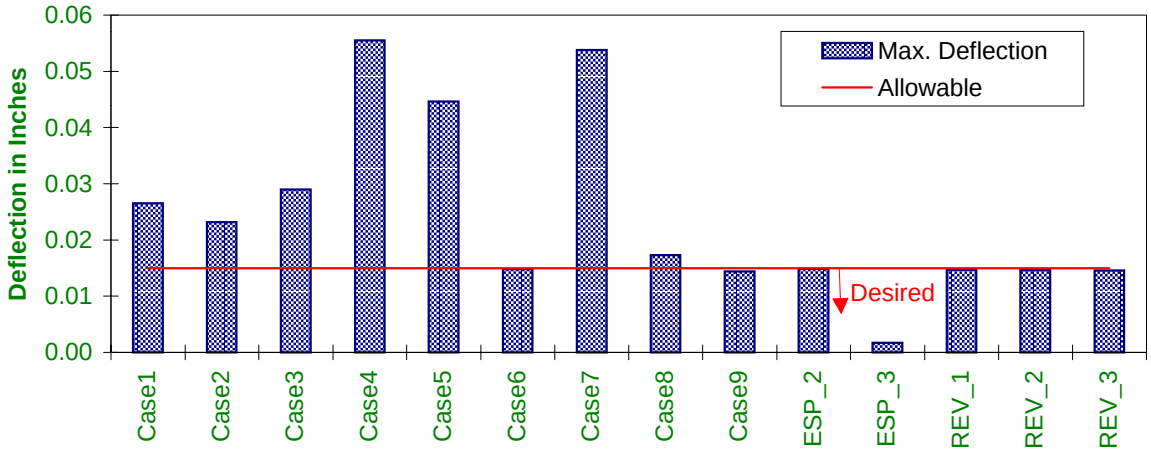

Figure 4.3.3-12 Stator Stacking Full Factorial Maximum Deflection Predictions

Satisfying the AE empirical flutter criteria for vanes conflicted with the aerodynamic and acoustic design. From an aerodynamic/acoustics perspective, a high degree of tangential bow is desirable. However, the addition of bow causes a significant change in the mode shape of the fundamental vibration mode. With small amounts of bow this mode is predominantly a flexure mode, while a larger degree of bow changes it into a torsion mode (see Figure 4.3.3-13). The problem arises because the flutter criteria based on reduced frequency, fc/V, is dependent on mode shape, with the torsion mode being much more difficult to satisfy. Fundamental mode flutter parameters were found to be at least 25% lower than AE recommended values for most of the go-forward designs (see Figure 4.3.3-14).

A number of approaches were investigated to increase the frequency of the bowed stator vane, such as thickness increases, changing airfoil chord, attachment boundary conditions, etc. Table 4.3.3-2 summarizes the flutter predictions for all the cases investigated. Initial attempts to increase flutter margin by thickening the vanes resulted in rapidly increasing stator weight with some moderate aerodynamic loss increases predicted by DAWES. For example, the total weight of the case_6 stator (52 vanes) increased from 5.68 to 7.07 lb. to drive the torsion mode flutter from 0.89 to 0.96. Increasing the chord further increased the weight with negligible change to the flutter margins. The weight issue was considered a problem and the low flutter margin was not necessarily a problem. There was no data for stators that implied flutter was guaranteed at this level of the flutter parameter, it was simply below previous experience. A compromise was reached where the vanes would be left at the rev_3 flutter parameter level and the vanes would be strain gauged in the rig to watch for flutter. Vane hub and shroud attachment modifications have been identified analytically that will increase flutter margin to baseline levels if vane flutter is seen in the rig. The modification is to provide two retention bands instead of the conventional one-band retention scheme used in the previous designs. The approach was tested on a number of cases and was found to consistently increase the flutter parameter by about 10 to 13% (see Table 4.3.3-2). This approach helps keep stator weight under control and provides new knowledge about the limits of vane flutter parameter while providing an acceptable alternative if flutter actually occurs.

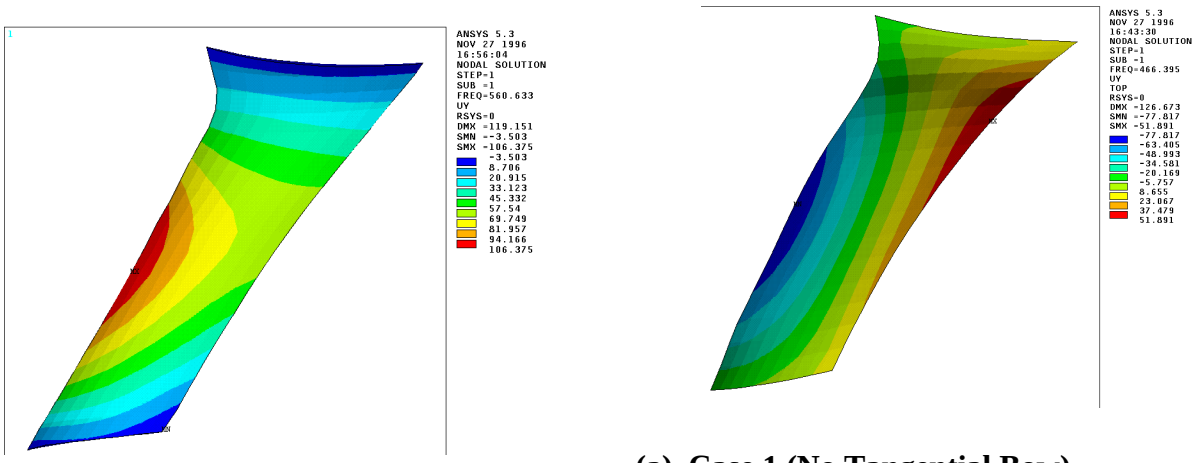

(a) Case 1 (No Tangential Bow) **(b) Rev_3**

Figure 4.3.3-13 Effect of Tangential Bow on the Mode Shape of Fundamental Vibration Mode

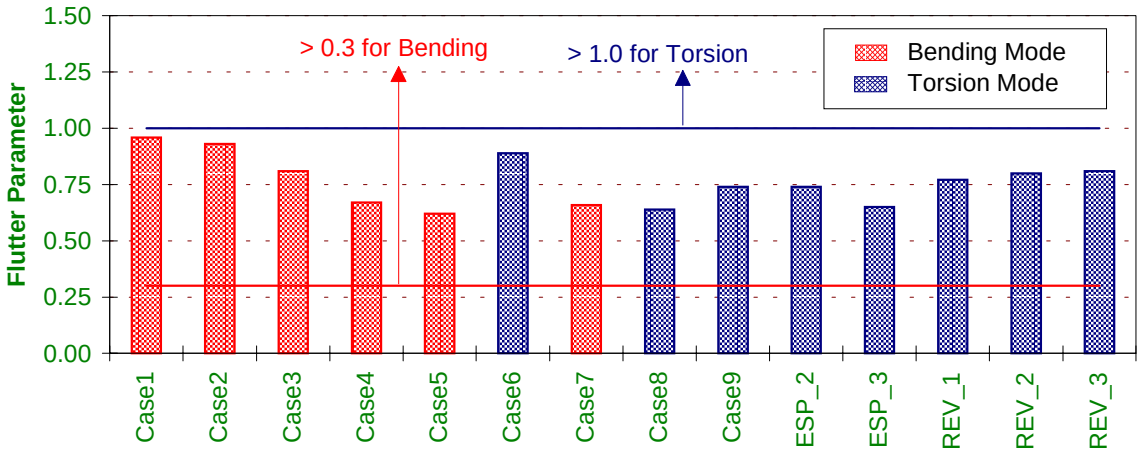

Figure 4.3.3-14. Stator Stacking Full Factorial Fundamental Mode Flutter Predictions

Table 4.3.3-2. Summary of Fundamental Modal Frequencies for Stator Vane

DOE Case	Mode 1			Total Wt. (lb.)	Comment
	Frequency (N/rev)	Type*	Flutter Parameter		
Case_1	3.31	B	0.96	5.64	
Case_2	3.28	B	0.93	5.60	
Case_3	2.96	B	0.81	5.63	
Case_4	2.39	B	0.67	5.63	
Case_5	2.26	B/T	0.62	5.56	
Case_6	3.01	T	0.89	5.68	
Case_6_Bnd	3.29	T	0.97	5.68	Two Bands
Case_6a	3.27	T	0.96	7.07	Inc. Thickness
Case_7	2.37	B	0.66	5.62	
Case_8	2.14	T	0.64	5.73	
Case_8c	2.50	T	0.76	8.45	Inc. Thickness
Case_9	2.56	T	0.74	5.65	
ESP_2	2.49	T	0.74	5.71	
ESP_2a	2.83	T	0.85	7.60	Inc. Thickness
ESP_2b	2.82	T	0.84	8.00	Inc. Thk & Chord
ESP_3	2.18	T	0.65	5.72	
REV_1	2.62	T	0.77	5.68	
REV_1_Bnd	2.94	T	0.87	5.68	Two Bands
REV_2	2.72	T	0.80	5.67	
REV_2_Bnd	3.04	T	0.89	5.67	Two Bands
REV_3	2.75	T	0.81	5.69	
REV_3_Bnd	3.11	T	0.92	5.69	Two Bands

*** Type:** B → Bending Mode; T → Torsion Mode

4.3.4 Incidence DOE

The next step has to set the incidence and mean camber line angle distribution. The vane mean camber line angle distributions were taken from the baseline vane. Although the mean camber line angle distribution optimization would render reduced stator loss and improved stator loadings, the stator losses predicted by DAWES for the rev_3 stator were already close to those predicted by DAWES for the baseline stator. Since the final rotor design (gf03) was available, the AXCAPS model was modified to use this rotor with its DAWES-predicted exit velocity triangles for the remaining stator design work.

The rev_3 stator behind the gf03 rotor was used as the base case for the incidence study. The vane leading edge angles were set to produce the baseline design point incidence with the stator leading edge swirl angles from the new gf03 rotor. A 9-case full factorial DOE was performed where vane leading edge angle was varied over three levels (-3 deg, 0 deg, and +3 deg) from the baseline at the vane hub, midspan, and tip. The vane leading edge angle was specified directly rather than allowing AXCAPS to try to calculate it from incidence. Figure 4.3.4-1 shows the vane leading edge geometric angles for the 9 cases (Case 5 is the baseline case) and for the rev_3 vane. Figure 4.3.4-1 also shows the vane leading edge angles for inc_1, which is the leading edge chosen from the results of this study. Figure 4.3.4-2 shows the resulting incidence profiles using DAWES stator leading edge swirl angles.

The effects of varying the vane leading edge angle on the mechanical and acoustic quality factors were insignificant so the leading edge angle was chosen based on stator loss and loading. Exit swirl was examined, but for a constant vane trailing edge angle, the deviation largely followed the loss as in the stacking study. Figures 4.3.4-3 and 4.3.4-4 show the stator loss and exit swirl estimated by DAWES.

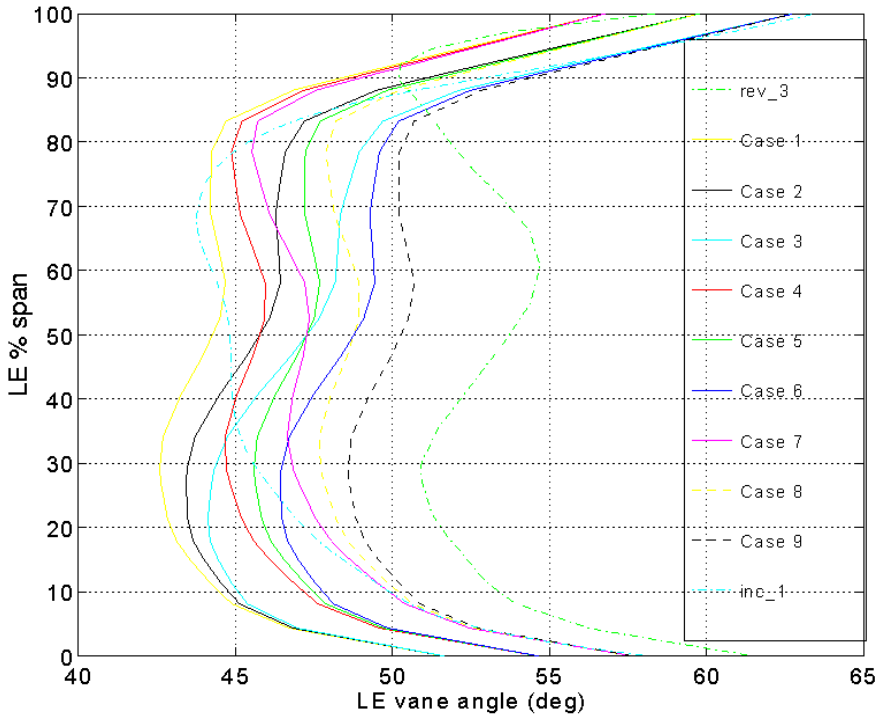

Figure 4.3.4-1. Stator Incidence Full Factorial Incidence

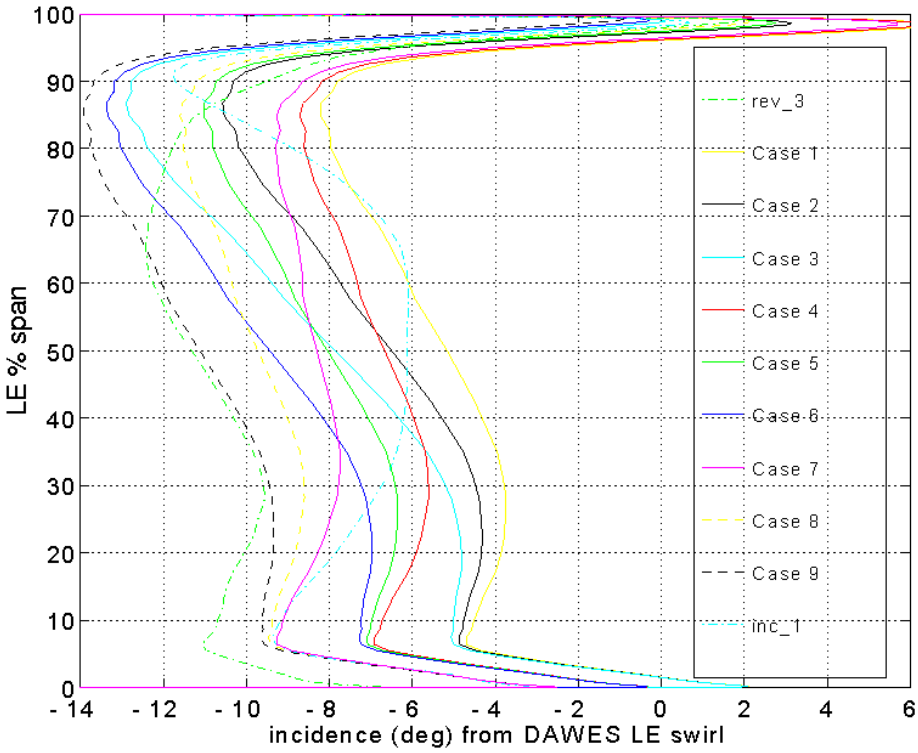

Figure 4.3.4-2. Stator Incidence FF Stator Incidence

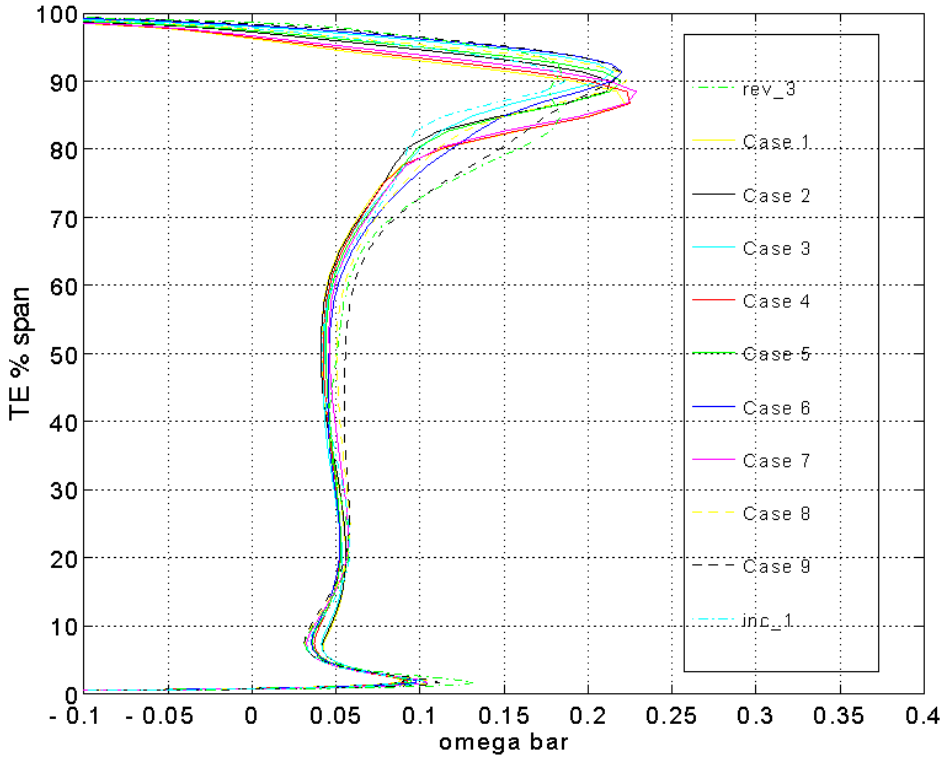

Figure 4.3.4-3. Stator Incidence FF Stator Loss

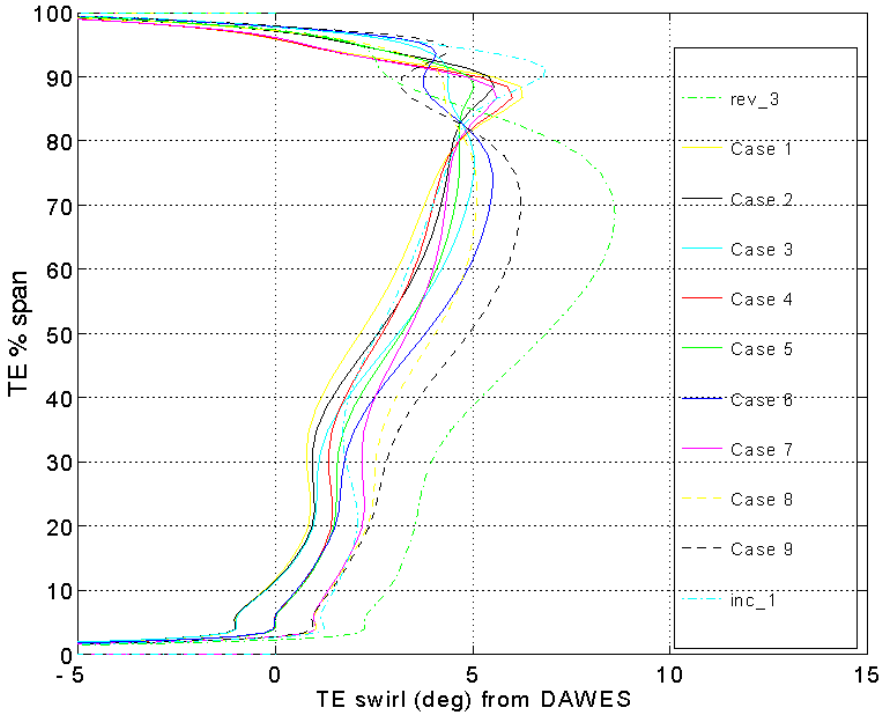

Figure 4.3.4-4. Stator Incidence FF Stator TE Swirl Angle

The loss was reduced from or equal to rev_3 over much of the span for all 9 cases, indicating that the biggest benefit of the incidence full factorial was due to correcting the way in which incidence was set. The leading edge angle was set by looking at curves of loss vs. leading edge angle and at vane loadings at different spanwise locations. Generally, leading edge angles that improve loss also improve loadings. If a section showed trends in loss but little effect on loading, loss was favored in setting the leading edge. The resulting leading edge angles are shown in Figure 4.3.4-1 as inc_1. Relative to the baseline (Case 5), the leading edge is overcambered 3.5 degrees at the hub and shroud and uncambered 3.5 degrees from 55% to 75% span. The inc_1 losses and exit swirl are shown in Figures 4.3.4-3 and 4.3.4-4.

The high-loss bump around 90% span was largely insensitive to incidence. Particle traces completed in the DAWES solution (Figure 4.3.4-5) showed that the high loss was coming from flow from the shroud boundary layer, the vane suction surface boundary layer, and the suction surface-shroud intersection. This flow was migrating down in span probably due to the vane lean and was unaffected by incidence at 90% span. This spanwise flow would be difficult to eliminate and may not be a problem relative to other stators. A similar loss source is probably present in all stators but isn't so distinctive since it would stay closer to the shroud for unleaned vanes.

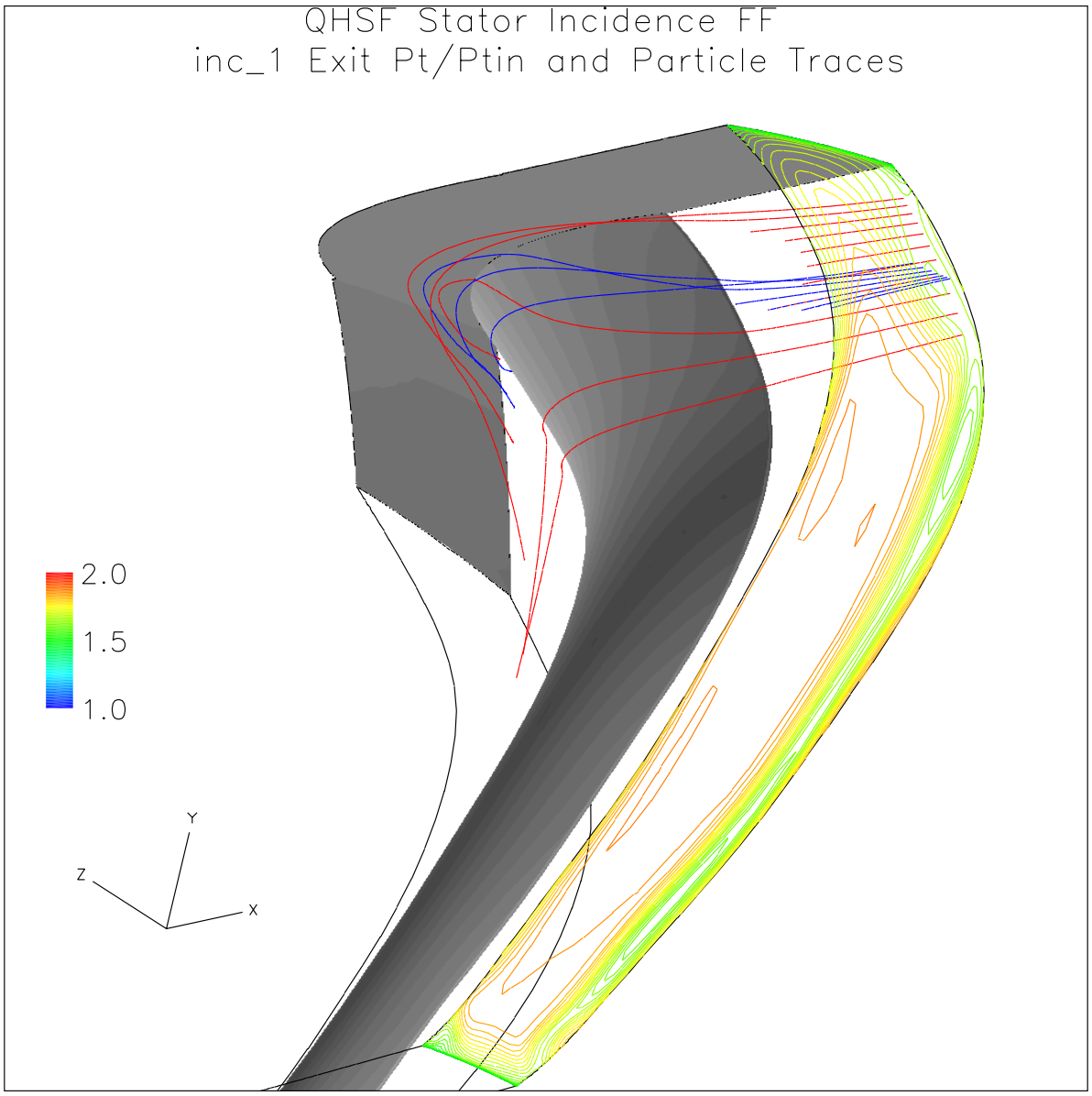

Figure 4.3.4-5. Stator Loss Bump

4.3.5 Trailing Edge Angle Setting

The vane trailing edge angle was adjusted to turn the flow as close to axial as practical. The trailing edge swirl angles from inc_1 were used to adjust the inc_1 vane trailing edge angle, DAWES was used to estimate the new trailing edge swirl, and within a couple of iterations the exit swirl was acceptably close to axial. Figure 4.3.5-1 shows the exit swirl for inc_1 and the exit swirl with the reset vane trailing edge (dev_2).

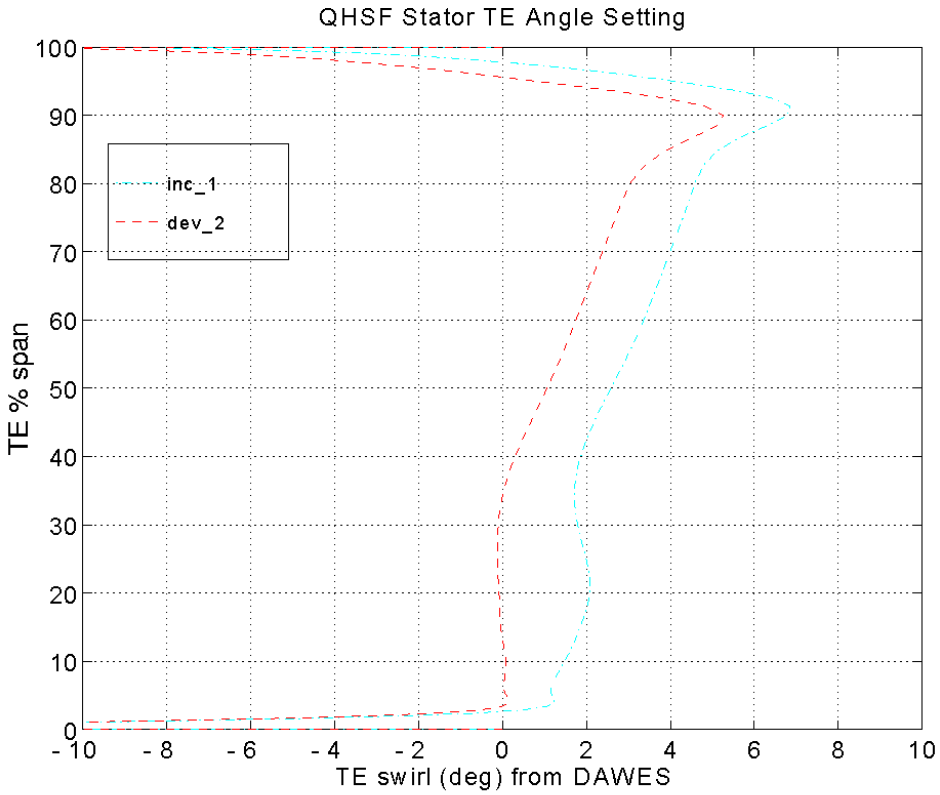

Figure 4.3.5-1. QHSF Stator Trailing Edge Angle Setting Swirl

The swirl is close to zero in the inner 30% span. Zero swirl in this region is important since the flow goes through a decreasing-radius transition duct to the core. Close control of the fan stator exit swirl in the core flow region is desirable to avoid mis-matching the compressor. The swirl farther out in span is considered acceptably close to zero. The swirl peak around 90% span is due to the shroud/vane intersection flow discussed previously and does not represent the actual stator flow turning in this region.

Figures 4.3.5-2 and 4.3.5-3 show the vane trailing edge angles and the deviation. Figure 4.3.5-4 shows the stator loss before and after the trailing edge angle was modified. Figure 4.3.5-4 shows that the loss changes caused by resetting the trailing edge angle were minor.

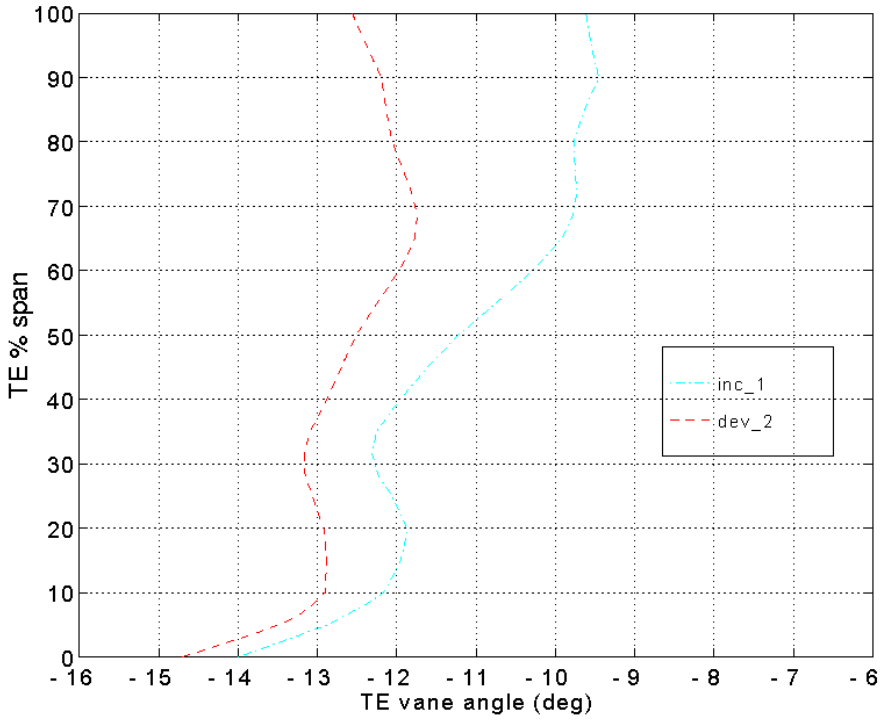

Figure 4.3.5-2. QHSF Stator Trailing Edge

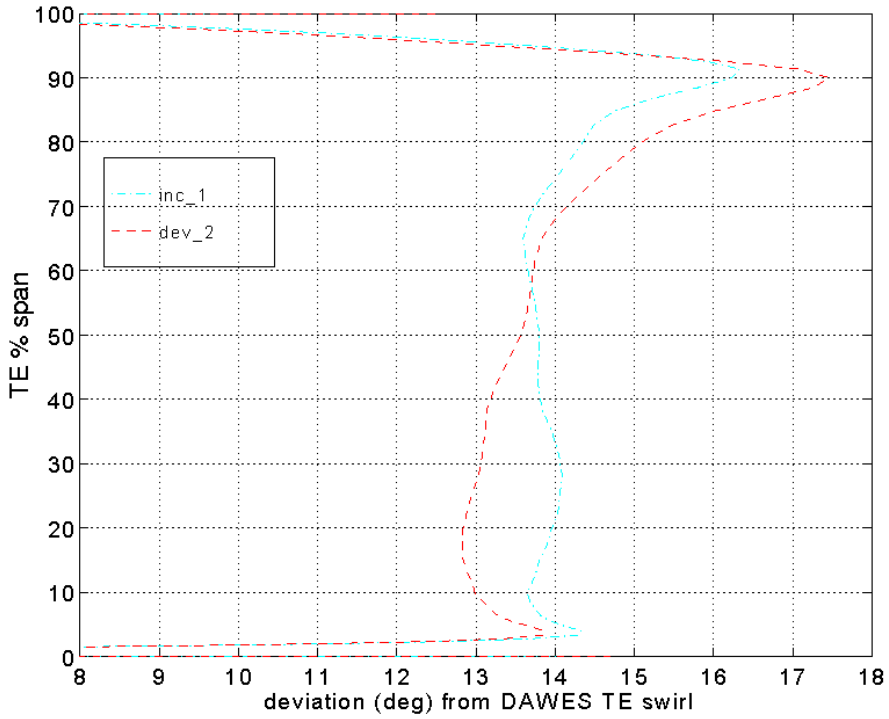

Figure 4.3.5-3. QHSF Stator Trailing Edge Angle Setting Deviation

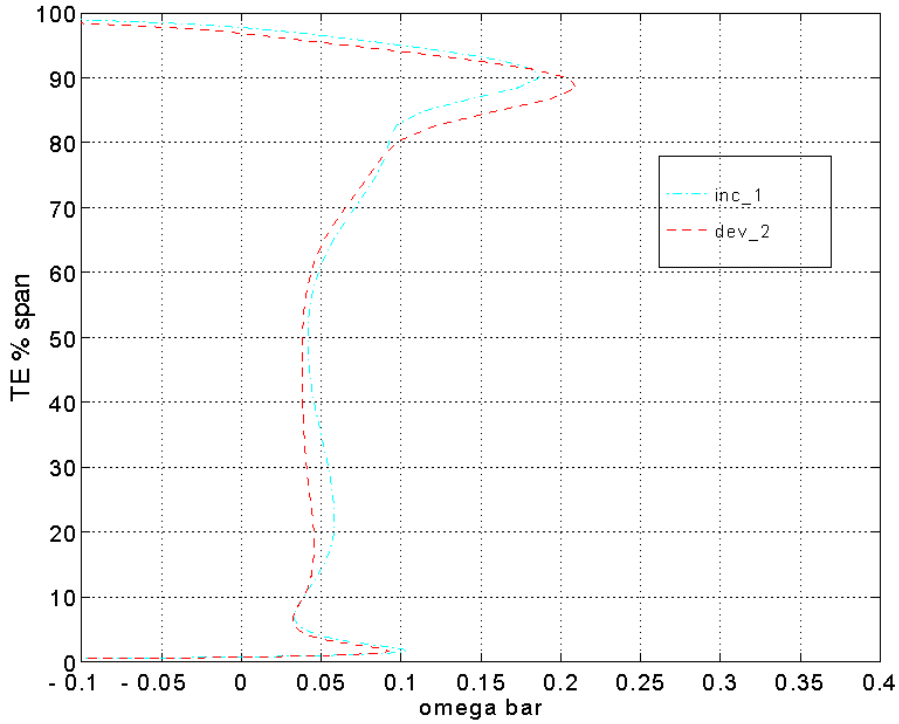

Figure 4.3.5-4. QHSF Stator Trailing Edge Angle Setting Loss

4.3.6 Composite Vane Thickness

The vane thicknesses were adjusted in the direction normal to the suction and pressure surfaces to allow for composite construction. The thickness adjustment was defined by the cosine of the local lean angle so it was necessary to consider it last since the lean angles depend on stacking and on vane section stagger.

Figures 4.3.6-1 and 4.3.6-2 show stator loss and exit swirl before (dev_2) and after the thickness change. Meeting the composite vane thickness criteria had only minor effects on loss and exit swirl. Examination of the vane section loadings showed little difference. This result was unexpected considering how much the tangential thicknesses were increased. This may be because the flow was not constrained to follow 2-dimensional streamsurfaces so the effect of the tangential thickness increase was reduced. The “effective” vane section thicknesses are probably somewhere between the tangential and the normal thicknesses. Figure 4.3.6-3 shows normal thickness distribution of the vane before (DEV_2) and after (THK_2d) thickness changes along with the recommended thickness distribution.

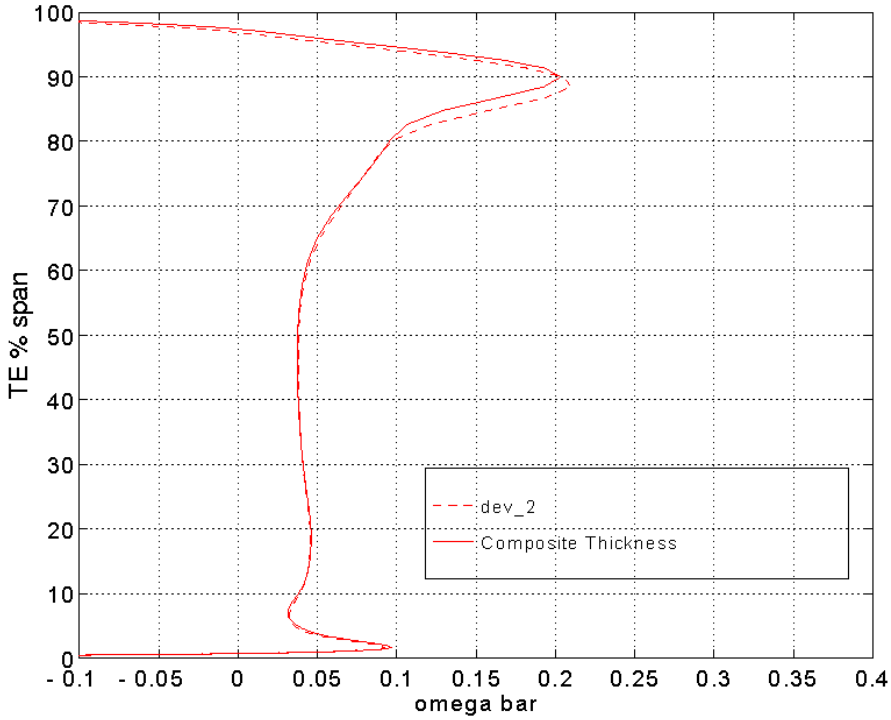

Figure 4.3.6-1. QHSF Stator Composite Thickness Loss

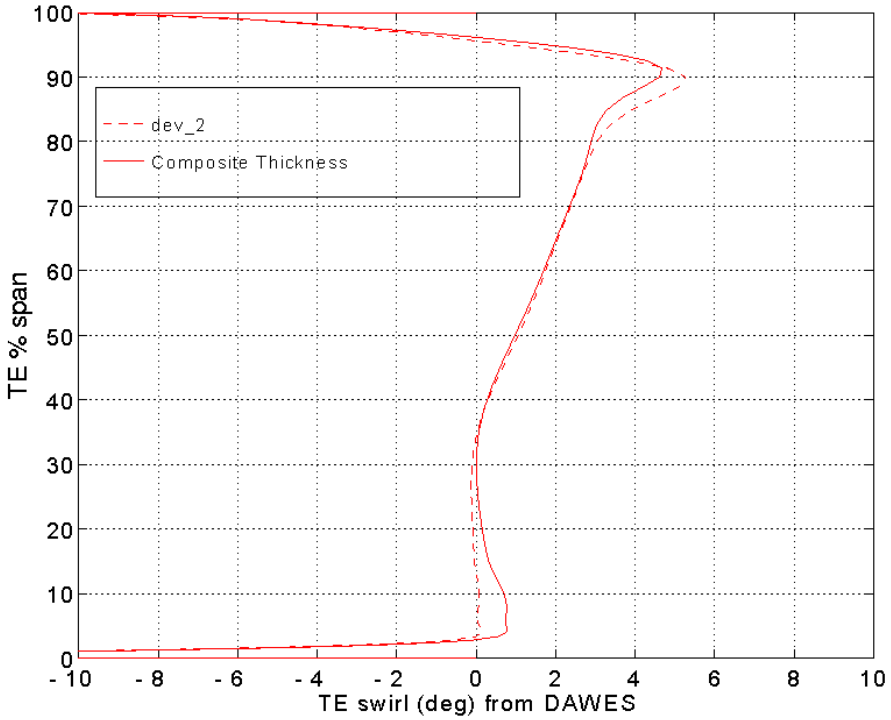

Figure 4.3.6-2. QHSF Stator Composite Thickness Exit Swirl

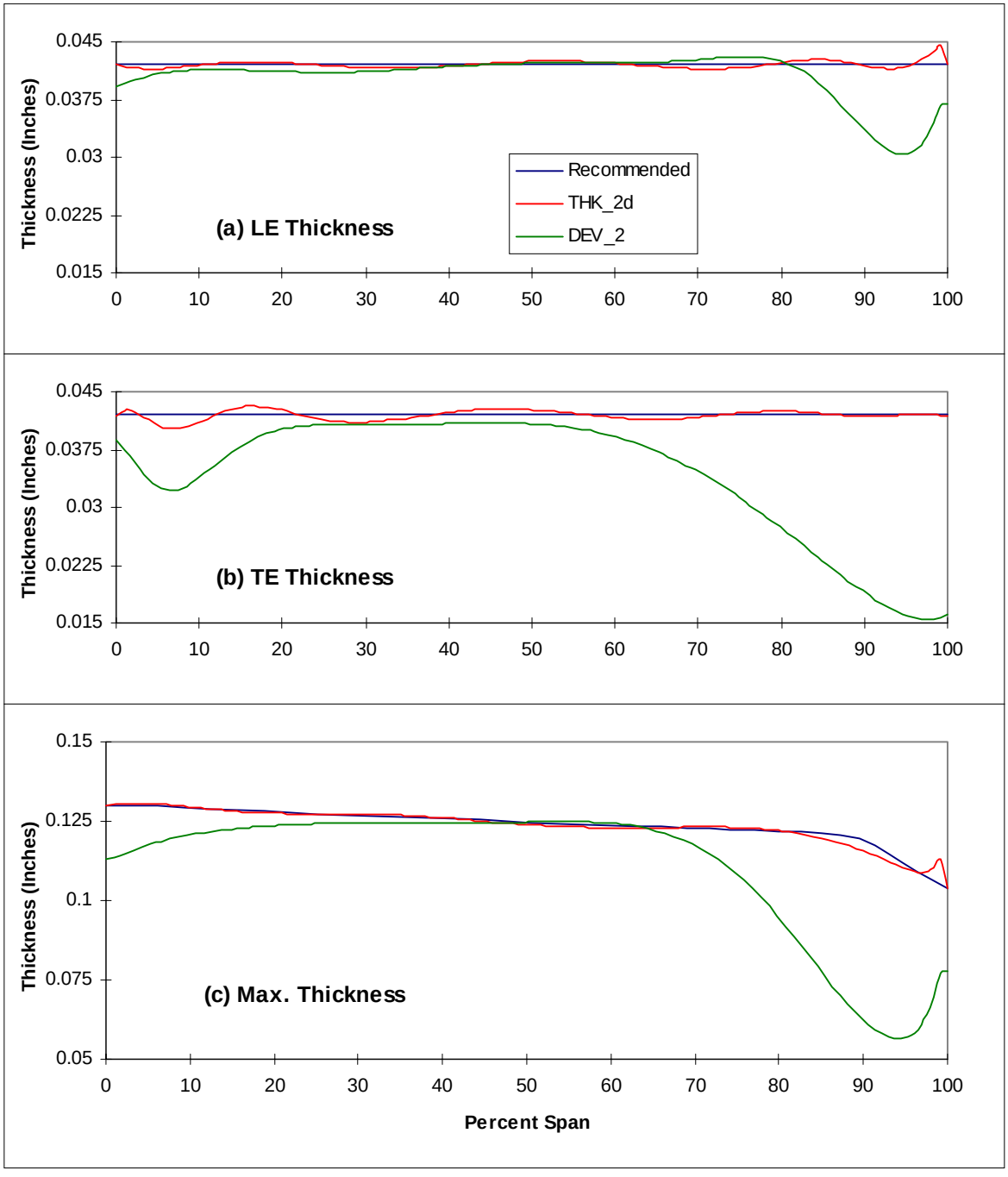

Fig. 4.3.6-3. Vane Normal Thickness Distribution for QHSF Stator Vane

4.4 Disk / Attachment

4.4.1 Initial Design Phase

Since both the AE/QHSF and baseline fans will be tested in the rig, it is desirable to have the same fan disk for both. The primary intent during this phase was to determine the feasibility of using the baseline disk for QHSF with minor modifications which include changes required to match the disk dimensions with the NASA rig dimensions.

The following points summarize the initial design parameter inputs for the disk design:

TFE engine size disk scaled down to NASA rig size (Scale Factor = 22/30.698)

- a rectangular cross section (no under cuts)
  Disk width and bore radius fixed to match the NASA rig dimensions
  (width = 3.4″; bore radius = 2.2″)
- titanium blades and attachment
- blade airfoil load based on OPTM blade
- blade attachment load assumed from baseline rotor configuration

4.4.2 Cyclic-Symmetric Model

A 2-D wedge section normal to the broach line was built using the baseline disk and dovetail geometry data. The bore diameter of the disk was trimmed to accommodate a 0.15″ thick torque sleeve. The 2-D geometry of the disk/dovetail was imported to HyperMesh in IGES format for the finite element (FE) meshing. The FE model from HyperMesh is output in ANSYS prep7 format for stress analysis.

Boundary Conditions: The nodes on the two edges of the wedge were positioned at identical radial locations, and the corresponding nodes on two edges were coupled both in radial and tangential directions to enforce cyclic symmetry in the disk. The blade and disk were coupled by constraining blade and disk nodes at the contact plane to have same displacement in the direction normal to the contact surface. The blade attachment and airfoil CF loads were applied as shown in Figure 4.4.2-1. The attachment geometry acts as a load transfer mechanism and was assumed to have zero density such that the attachment CF loads were not duplicated. The effects of slot broach were simulated by including a side load at the contact plane (see Figure 4.4.2-2). Finally, the nodes at the bore were constrained to have zero displacement in the tangential direction.

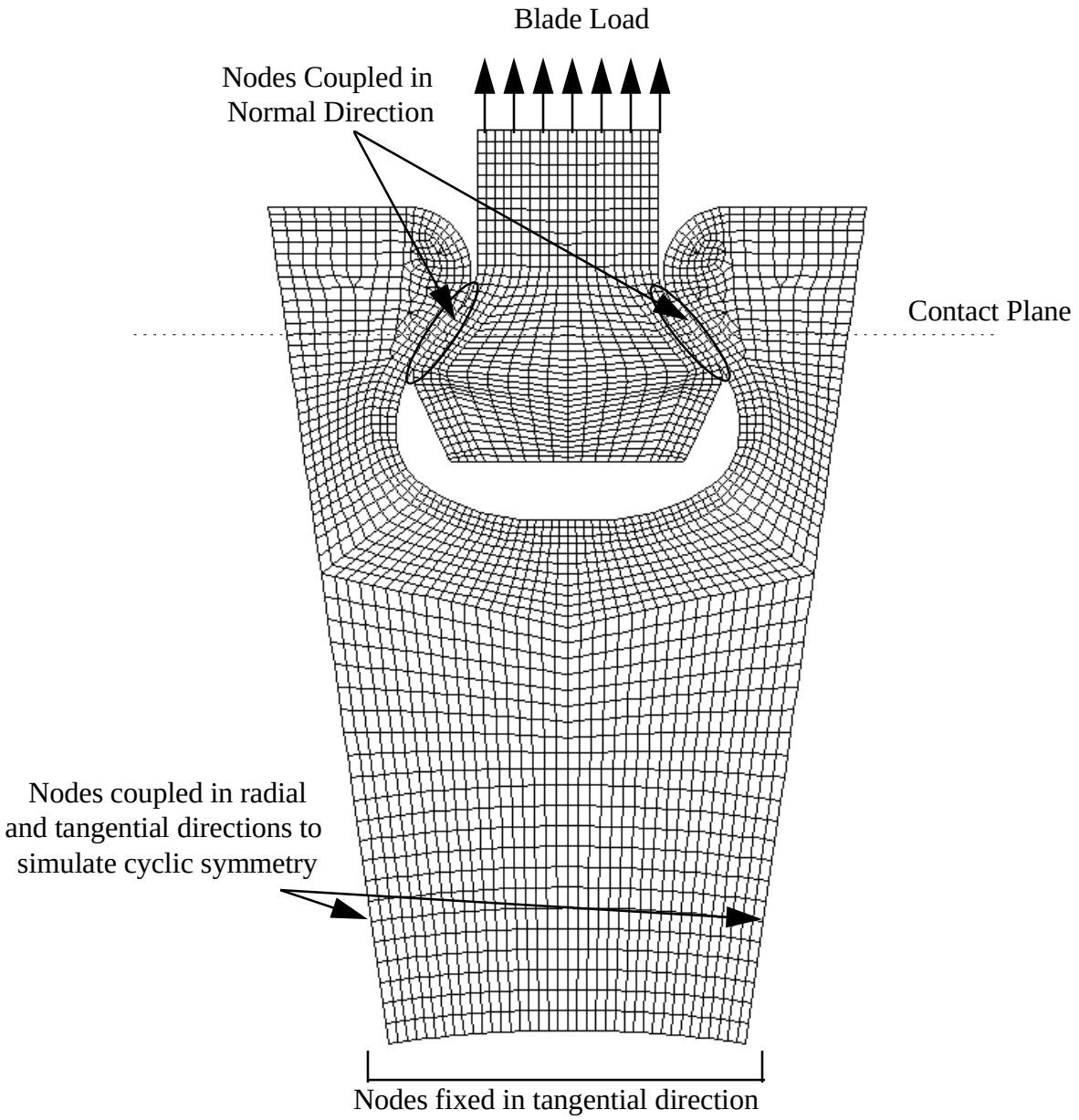

Figure 4.4.2-1. Cyclic Symmetric Model of the Fan Disk/Dovetail

4.4.3 Selection of Disk Material

Two different materials — titanium and C250 steel — were considered for the disk during test runs. Analysis was performed at three points:

- ***Mechanical Design Point:*** 100% physical speed (T_{tin} = 65 F) scaled to rig, *15444 RPM*
- ***Max. Test Speed:*** 110% Design Speed, *16988 RPM*
- ***Max. Operating Speed:*** 110% Max. Test Speed, based on NASA specification = 121% Design Speed, *18687 RPM*

Table 4.4.3-1. Material Properties for C250 Steel and Titanium at 75 F

Material Type	Iron	Titanium
Material Name	**Maraging Steel C250**	**TI-6AL-4V**
Process/Forming	Wrought	Wrought
Heat Treatment	Double ST+Aged	Annealed
Yield Strength (Ksi)	238.3	121.5
Ultimate Strength (Ksi)	247.2	129.1
Density (lb/in^3)	0.289	0.161

The results from 2-D cyclic symmetric analyses are presented in Table 4.4.3-2. With the titanium disk, the maximum radial stress was within the safe limits at the design speed. However, at maximum test speed, the maximum radial stress reached unacceptable limits (> 100 Ksi) as did the burst margin. The C250 steel disk had adequate stress as well as burst margins at all speed conditions. Based on this analysis, it was planned to proceed with the disk design using C250 steel. Figure 4.4.2-2 shows the principal stress distribution in the disk/dovetail at maximum operating speed for C250 steel disk case.

Table 4.4.3-2. Maximum Stresses for Various Cases – Rig-Size Model

Titanium Disk			
	Design Speed (100% N_{phy})	Max. Test Speed (110% N_{phy})	Max Operating Speed (121% N_{phy})
RPM	15444	16988	18687
Max. Deflection (inch)	0.0134	0.0162	0.0196
Max. Principal (Ksi)	87	105	127
Max. Radial Stress (Ksi)	84	101	122
Max. Tangential (Ksi)	71	86	104
Av. Tangential (Ksi)	57.8	69.9	84.6
Burst Margin*	1.42	1.29	1.18
C250 Steel Disk			
Max. Deflection (inch)	0.0105	0.0127	0.0154
Max. Principal (Ksi)	89.53	108.36	131.09
Max. Radial Stress (Ksi)	85.51	103.47	125.20
Max. Tangential (Ksi)	83.88	101.49	122.81
Av. Tangential (Ksi)	68.34	82.70	100.06
Burst Margin*	1.76	1.603	1.46

* Burst Margin requirements: AE > 1.25
NASA > 1.345 (when translated to AE criteria)

AE and NASA have different definitions of burst margin (BM); this merits some comments.

$$BM_{AE} = \sqrt{\frac{0.85 \times F_{tu}}{\sigma_{average}}} \geq 1.25$$

$$BM_{NASA} = \frac{0.7 \times F_{tu}}{\sigma_{average}} \geq 1.5$$

where F_{tu} is the ultimate strength of the material.

The AE design practice recommends a material utilization factor of 0.85, whereas NASA recommends a value of 0.7. The AE burst factor provides a margin on rotor speed (25% over speed) and NASA factor provides a 50% margin on average tangential stresses. When translated to the over speed condition, the NASA criterion is equivalent to $BM_{AE} \geq 1.345$.

4.4.4 Attachment Stresses and Post Unzip Capability

The margins of safety in various disk and attachment sections were obtained based on simple hand calculations. The sections represent the cross section that was most likely to fail under the given load. For example, the blade direct stresses were calculated at the blade minimum neck cross section. The margin of safety (MS) was defined (based on NASA guidelines) as

$$MS = \frac{Allowable\ Stress}{SF \times Calculated\ Stress} - 1$$

where SF = Safety Factor

Table 4.4.4-1 provides the margins of safety for various disk and attachment sectional stresses. The stresses are presented at Mechanical Design point (100% N_{phy}) and the margins of safety are presented at 100%, 110% and 121% N_{phy}.

Post unzip capability represents the failure resistance of the disk post due to combined bending and direct stresses during blade out condition. In other words, it is the capability of the disk to resist unzipping or losing adjacent blades. Figure 4.4.4-1 shows the unzip capability for the QHSF disk. The figure is analogous to well-known "Goodman diagram". In the figure, the y-axis represents a pure bending case and x-axis the pure tension case. For pure bending, failure occurs when bending stress exceeds 1.5 times yield strength of the material and for the pure tension case it occurs when the direct stress exceeds ultimate strength. For combined bending and direct stress case, failure occurs if the stresses are above the solid line or above the dotted line when safety factors are included. As seen in the figure, the QHSF disk post is safe under all three speed conditions.

4.4.5 Go-Forward Design

In summary, the preliminary design showed the baseline disk design can be used for the QHSF and should be manufactured with C250 steel material. It had adequate margins of safety, burst margin and unzip capability, and met both AE and NASA design criteria.

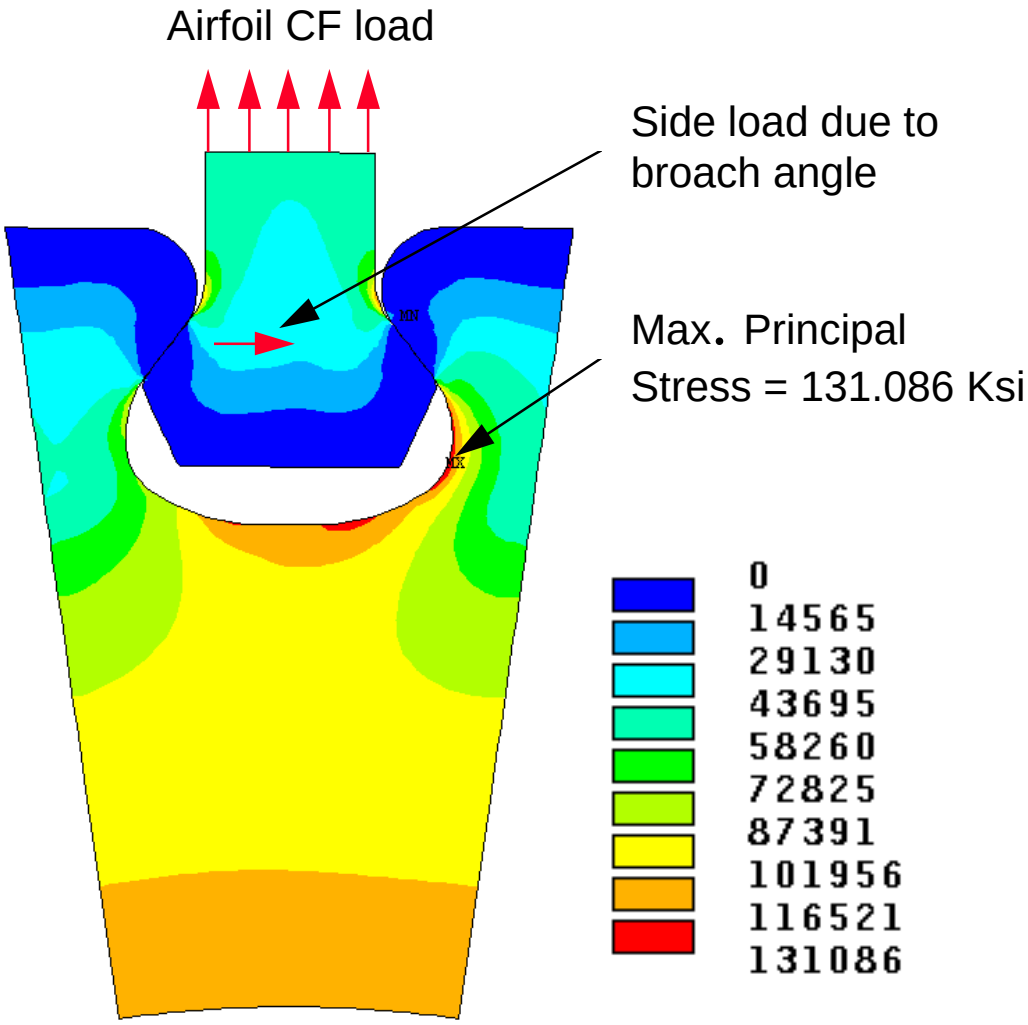

Figure 4.4.2-2 Principal Stress in disk/dovetail at 121% N_{phy}

Table 4.4.4-1. Attachment/Disk Stress Safety Margins

	Stress(Ksi)	Margin of Safety		
Percent Speed	100%	100%	110%	121%
Contact Stress	65.0290	0.5630	0.2917	0.0676
Blade Shear Stress	17.8972	2.2769	1.7082	1.2382
Blade Direct Stress	31.4828	2.2285	1.6682	1.2051
Blade Lobe Bending Stress	14.7769	5.8784	4.6846	3.6980
Disk Shear Stress	18.2269	5.6909	4.5297	3.5700
Disk Direct Stress	32.5291	5.4975	4.3699	3.4379
Disk Lobe Bending Stress	15.3263	12.7906	10.3972	8.4192
Yield Safety Factor (SF_y) =	1.1*			
Ultimate Safety Factor (SF_u) =	1.5*			

* Based on NASA guidelines

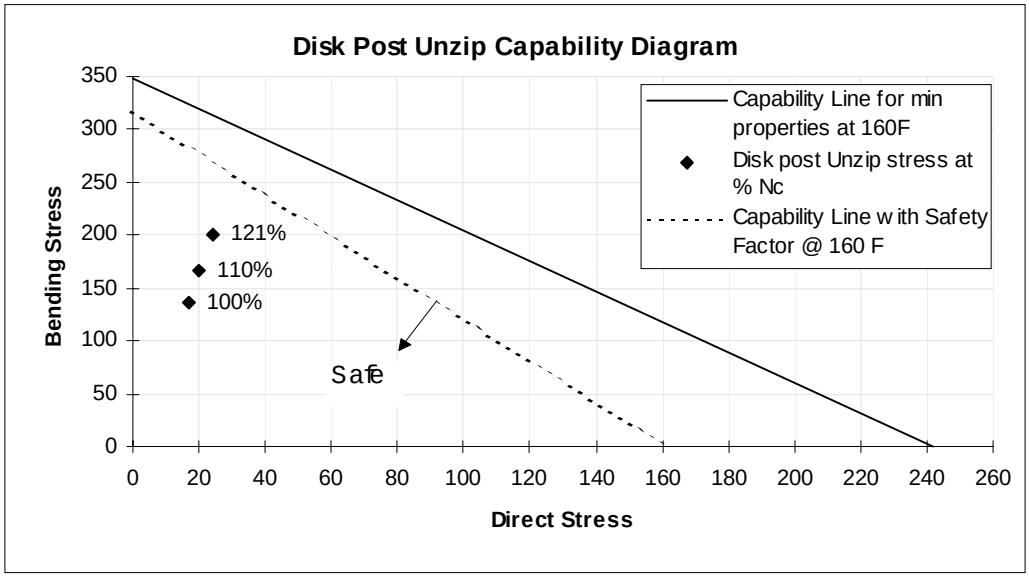

Figure 4.4.4-1 QHSF Disk is Designed to Withstand Unzipping During Blade-Out Condition

5.0 DETAILED DESIGN

5.1 Rotor

5.1.1 Geometry

The final QHSF design configuration was chosen based on the analyses from the "go-forward" cases of DOE 4. Go-forward case 3 was selected as the QHSF rotor design. Final blade geometry spanwise distributions are shown in Figure 5.1.1-1 through 5.1.1-5. Tabular geometry data of the blade is included in Appendix I. Values in the figures represent the NASA rig rotor design (22 inch diameter at the rotor leading edge tip). The incidence was calculated using DAWES at the design point. The large incidence increase at the tip was due to the endwall modeling of the boundary layer at the rotor inlet.

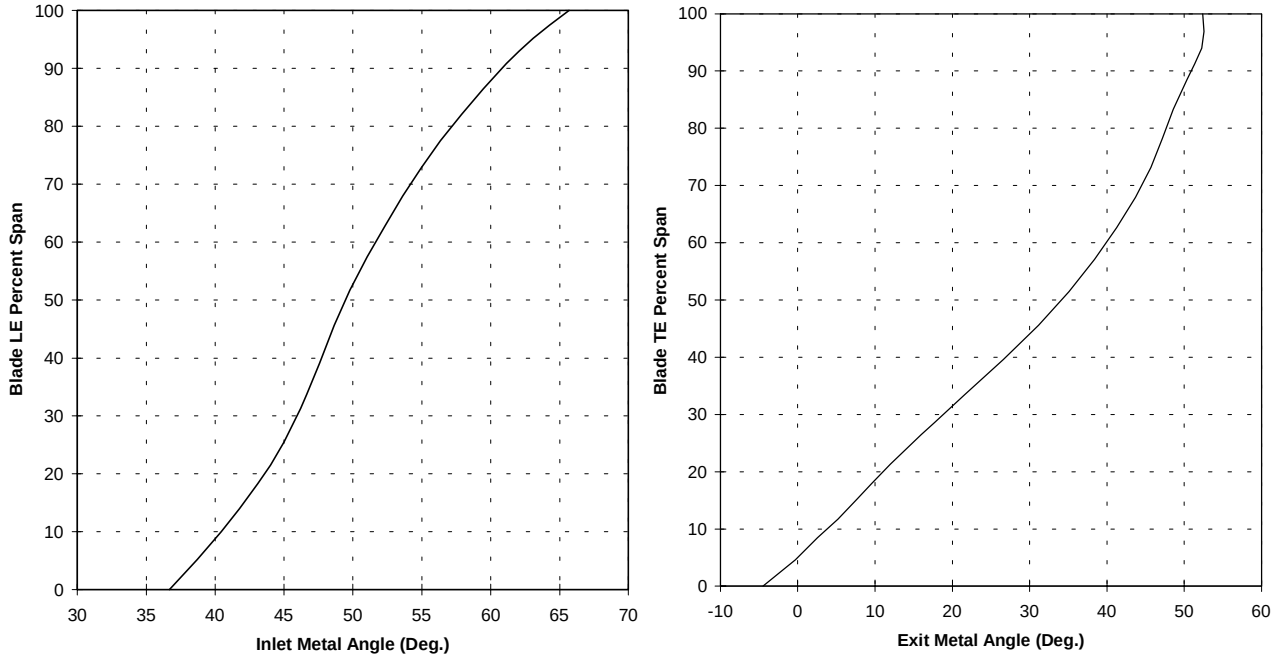

Figure 5.1.1-1. Blade Inlet and Exit Metal Angle

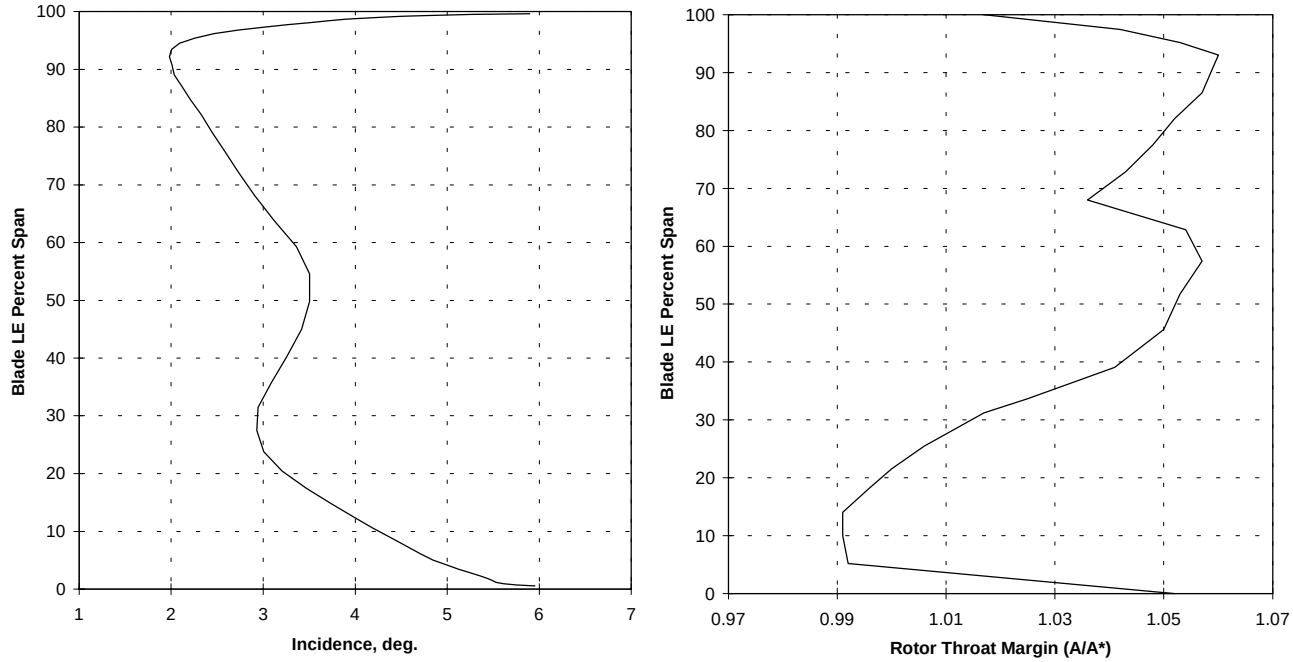

Figure 5.1.1-2. Blade Incidence and Throat Margin

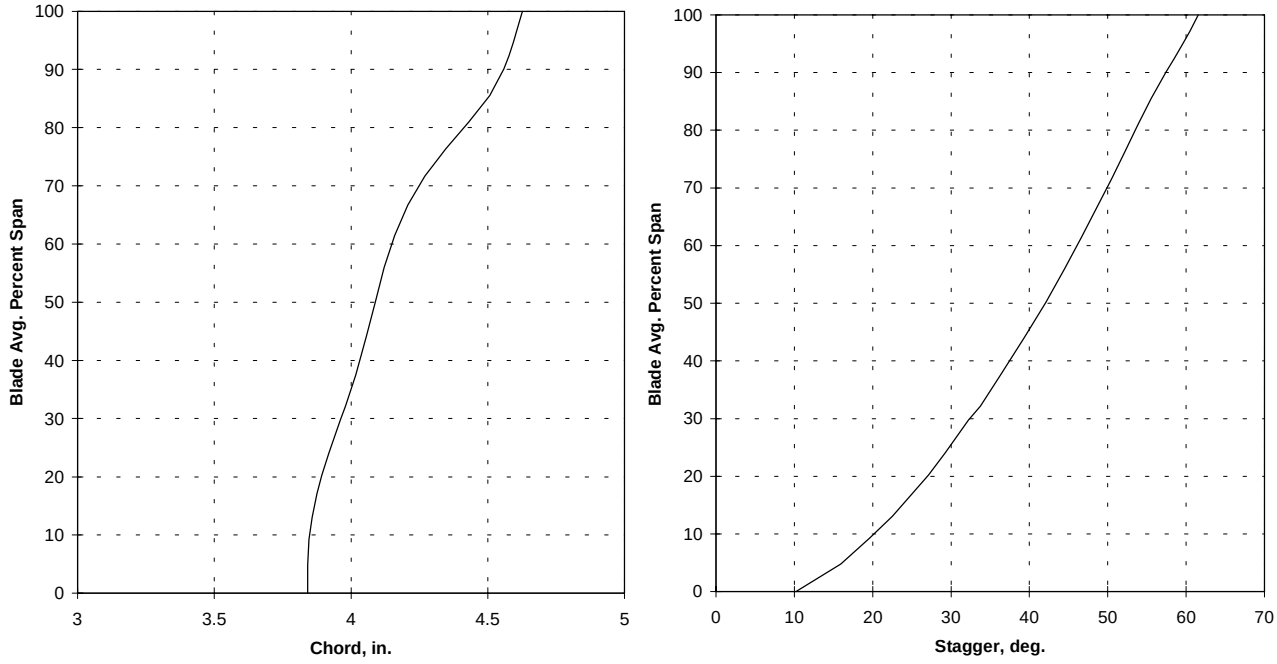

Figure 5.1.1-3. Blade Chord and Stagger Angle

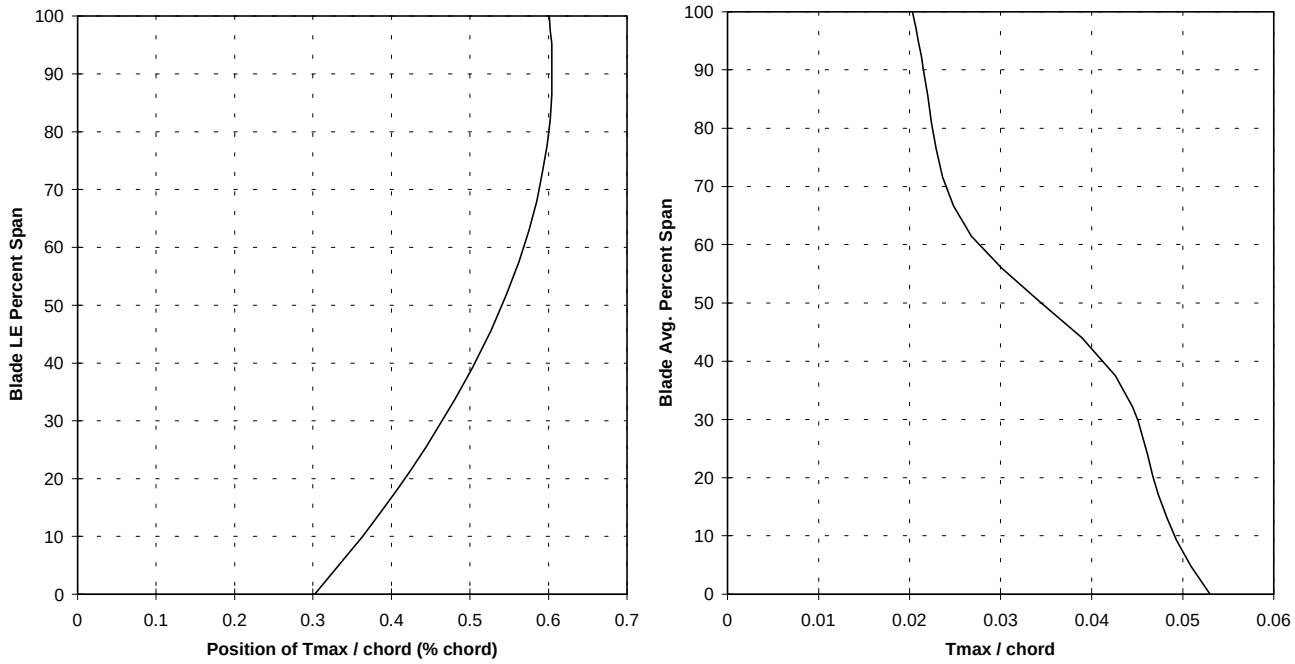

Figure 5.1.1-4. Blade Position of Maximum Thickness and Maximum Thickness / Chord Ratio

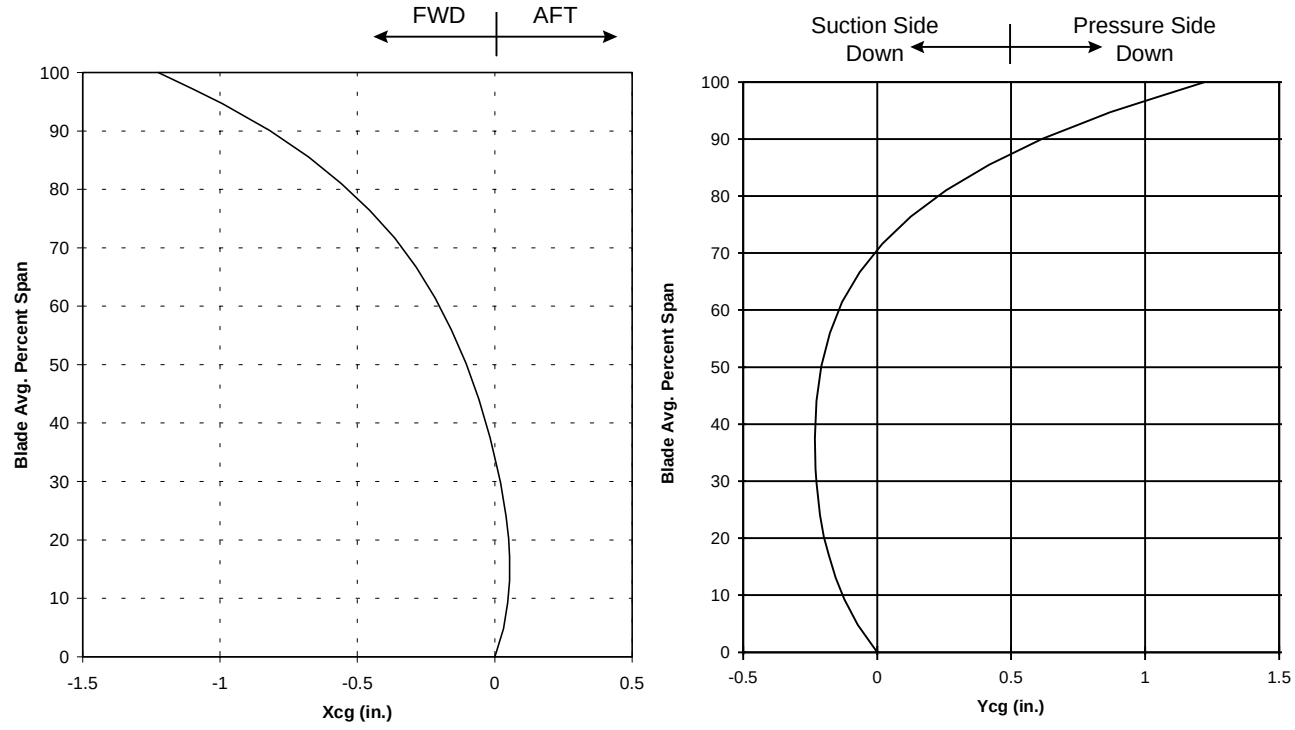

Figure 5.1.1-5. Blade CG Stacking

5.1.2 Aerodynamic Results

The design concentrated on achieving a close performance match relative to the baseline such that the acoustic benefits of the forward swept technology could be easily deduced from the test data. DAWES analyses at aerodynamic design point showed only a slight shift in speedline characteristics relative to the baseline. At the design efficiency goal, the flow was 0.3% lower than the design goal, while the pressure ratio was 1.3% higher. At the design flow goal, the efficiency was 0.2 points lower while the pressure ratio was 0.3% lower. However, analyses completed from choke to stall showed slightly higher peak efficiency than the baseline and approximately one point higher as the rotor was throttled up from peak efficiency to stall. Spanwise distributions of pressure ratio, temperature ratio, efficiency, deviation, omega-bar, and D-factor are shown in Figures 5.1.2-1 through 5.1.2-3, respectively. As previously mentioned, an endwall total pressure loss was being modeled at the rotor leading edge and the effect is evident in the figures.

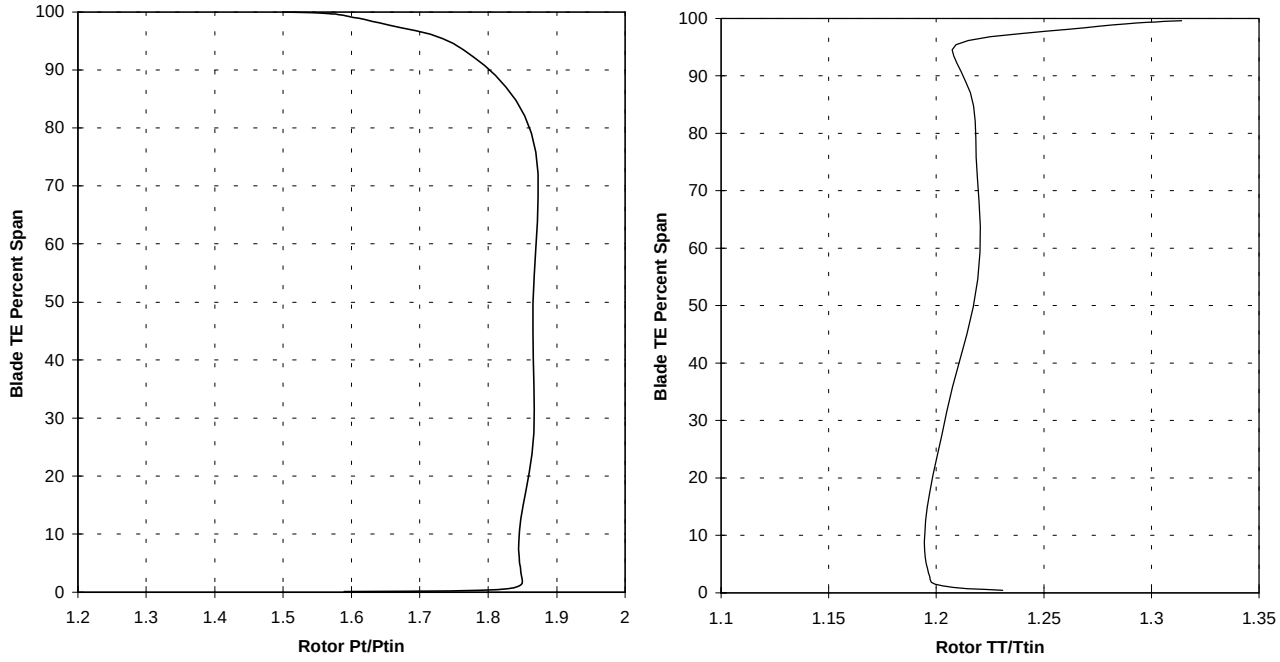

Figure 5.1.2-1. DAWES Calculated Rotor Pressure Ratio and Temperature Ratio at the Aerodynamic Design Point

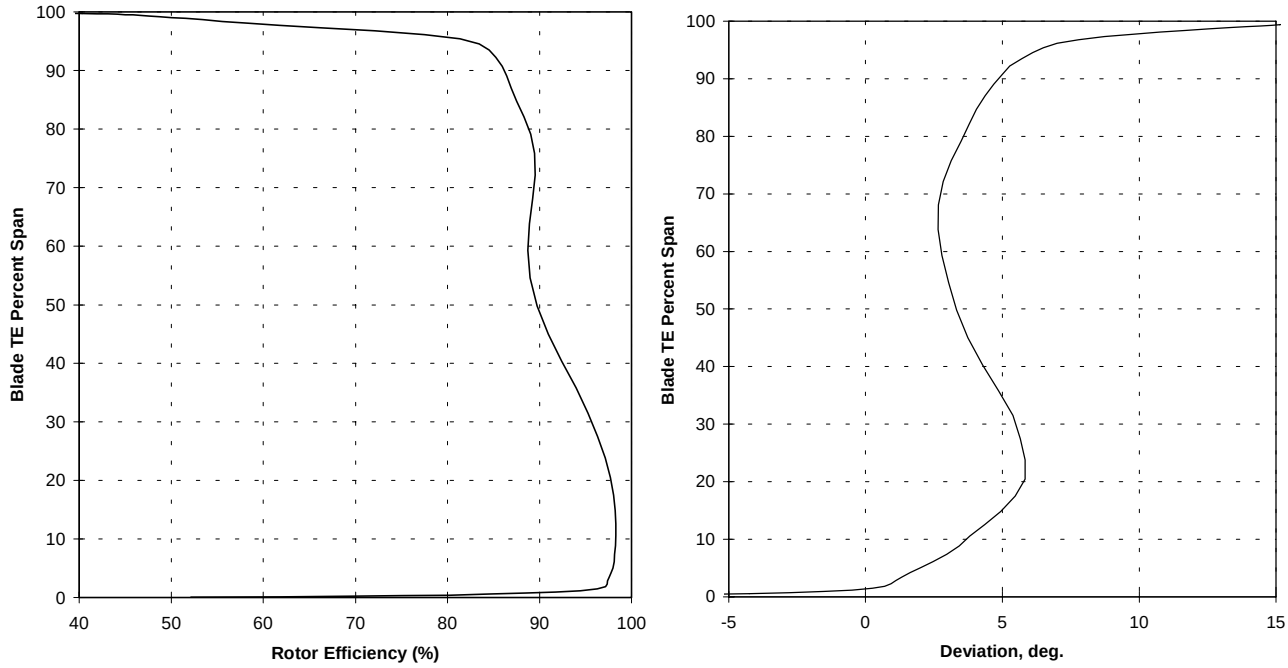

Figure 5.1.2-2. DAWES Calculated Rotor Efficiency and Deviation at the Aerodynamic Design Point

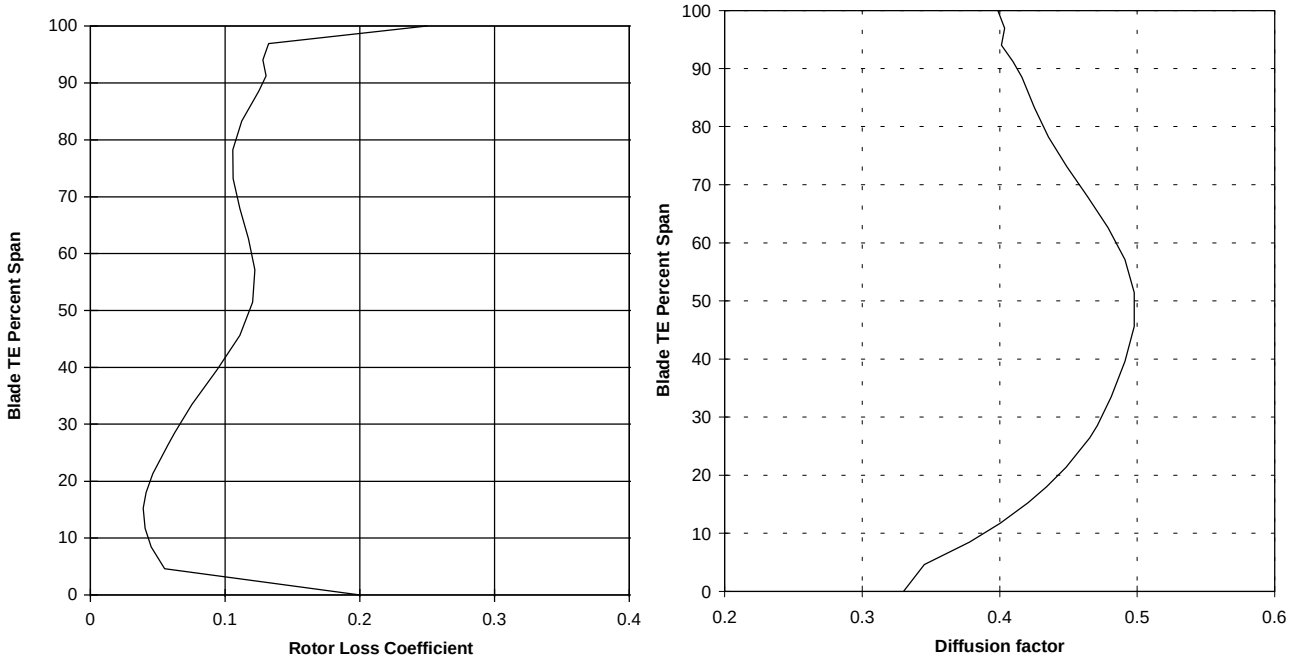

Figure 5.1.2-3. Rotor Omega-bar and D-factor at the Aerodynamic Design Point

The increase in loss coefficient near mid-span was due to an increase in shock loss as the blade effective sweep approached zero degrees. Effective sweep described within is the oblique shock angle which the inlet flow passes coming into the passage. The oblique shock angle is a function of stream surface angle, blade lean angle, station lean angle (blade sweep), and relative flow angle. When the shock angle is considered a shock surface, both the blade leading edge and the impingement point on the suction surface of the adjacent blade (across the passage) must be accounted. Figures 5.1.2-4 and 5.1.2-5 show the difference in the effective sweep calculation (in terms of normal inlet relative Mach number) between leading edge only and a simple average calculation of the leading edge and the suction surface impingement point. The figures also show an inherent difference between the forward swept QHSF and the aft swept baseline in that the shock surface will always reduce the benefit of a forward swept blade, while it will always increase the benefit of an aft swept blade. Although the QHSF design had significant benefits near the tip, it was slightly worse than the baseline near the mid-span.

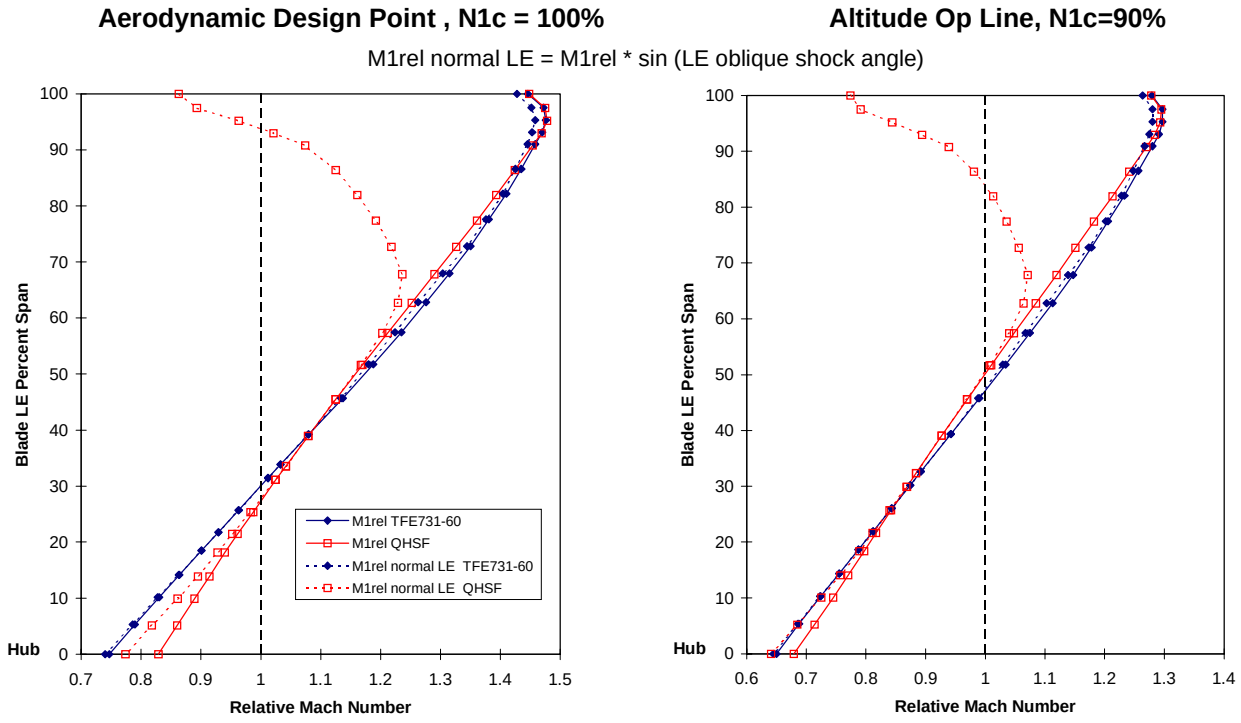

Figure 5.1.2-4. Effect of Blade Leading Edge Effective Sweep on Inlet Relative Normal Mach Number at 90 and 100% N1c

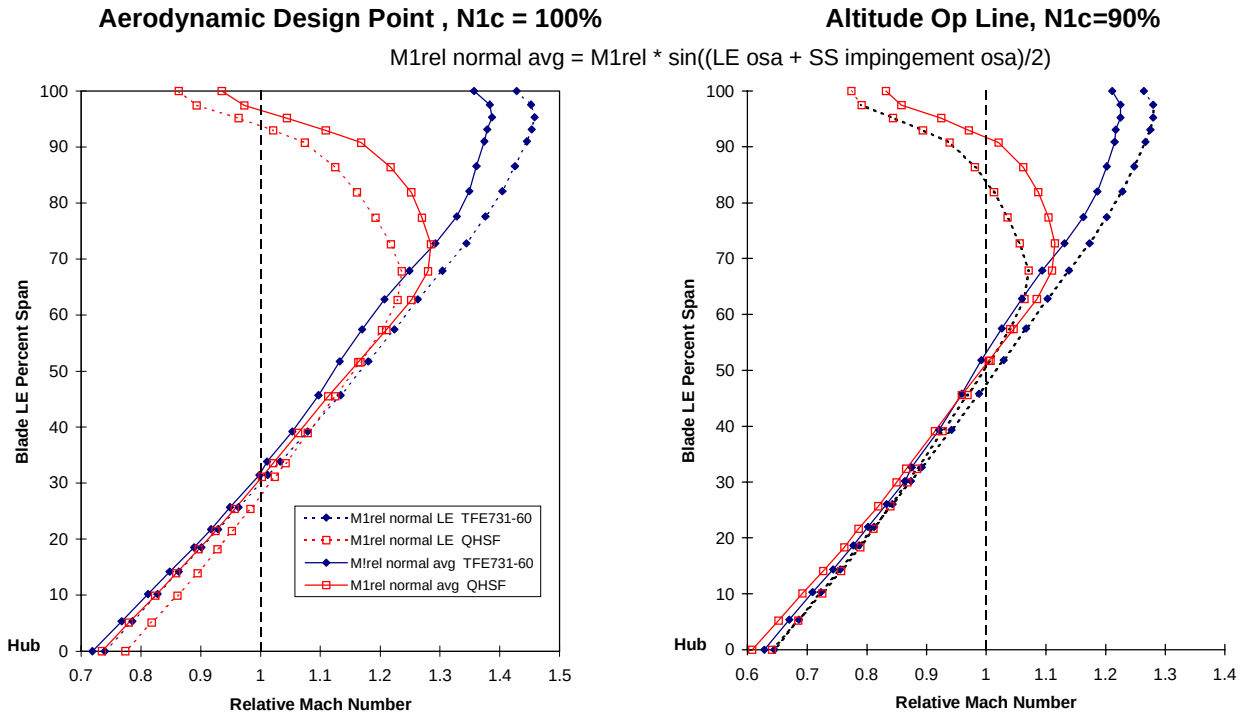

Figure 5.1.2-5. Effect of the Combination of Blade Leading Edge and Suction Surface Impingement Effective Sweep on Inlet Relative Normal Mach Number at 90 and 100% N1c

Airfoil loadings, represented as isentropic Mach number distributions along the suction and pressure surfaces, and the corresponding blade-to-blade Mach number contour plots are shown for 10, 30, 50, 70, and 90 percent spans at the aerodynamic design point in Figures 5.1.2-6 through 5.1.2-10. As previously mentioned, the QHSF design was chosen based on the design and part-speed performance results from DOE 4. In the DOE, many quality characteristics including airfoil loadings were examined and optimized for an overall best design. The loadings at 30, 50, and 90 percent spans show excessive diffusion with unnecessary re-acceleration on the suction surface. Additional work could be completed to improve these loadings and improve efficiency.

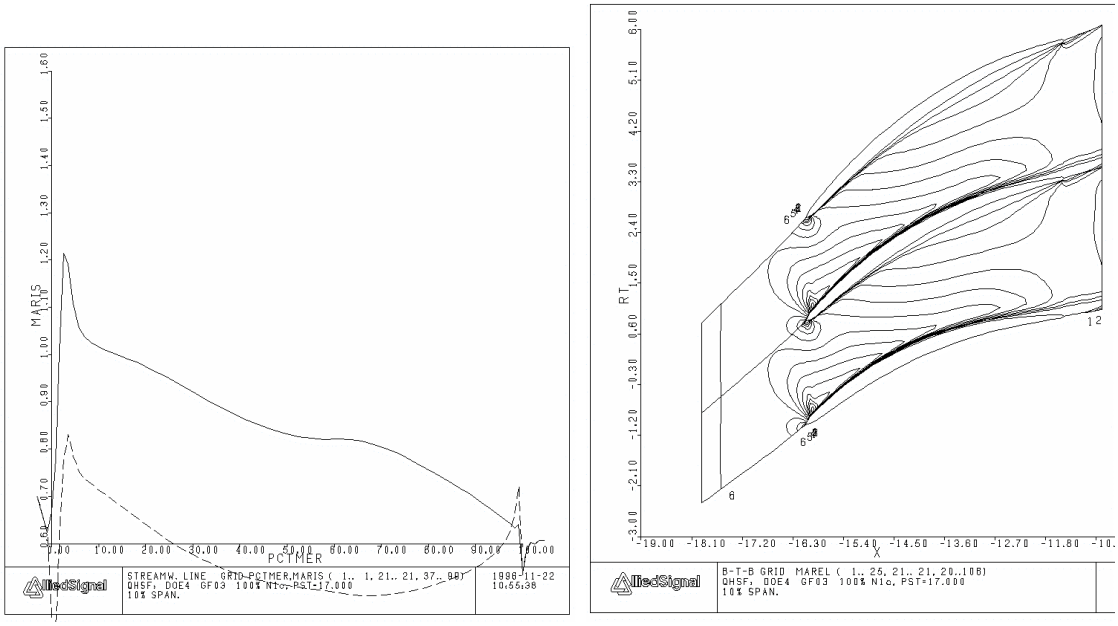

Figure 5.1.2-6. DAWES Calculated Isentropic Blade Loadings and Blade-to-Blade mach Number Contours at 10% Span at the Design Point

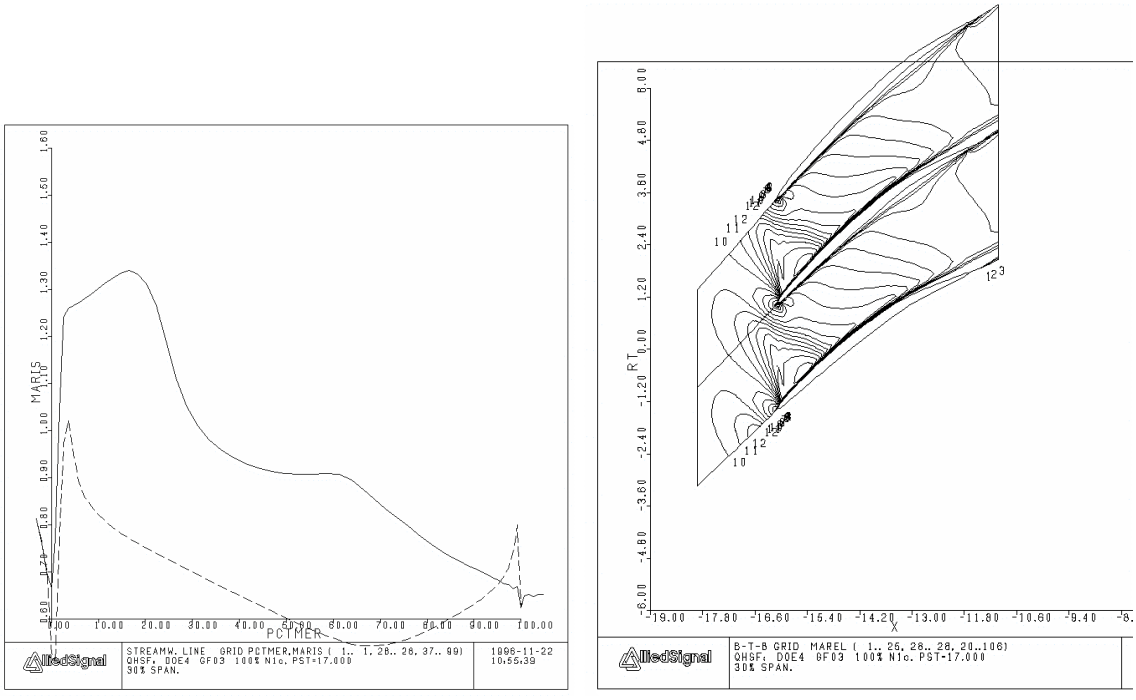

Figure 5.1.2-7. DAWES Calculated Isentropic Blade Loadings and Blade-to-Blade mach Number Contours at 30% Span at the Design Point

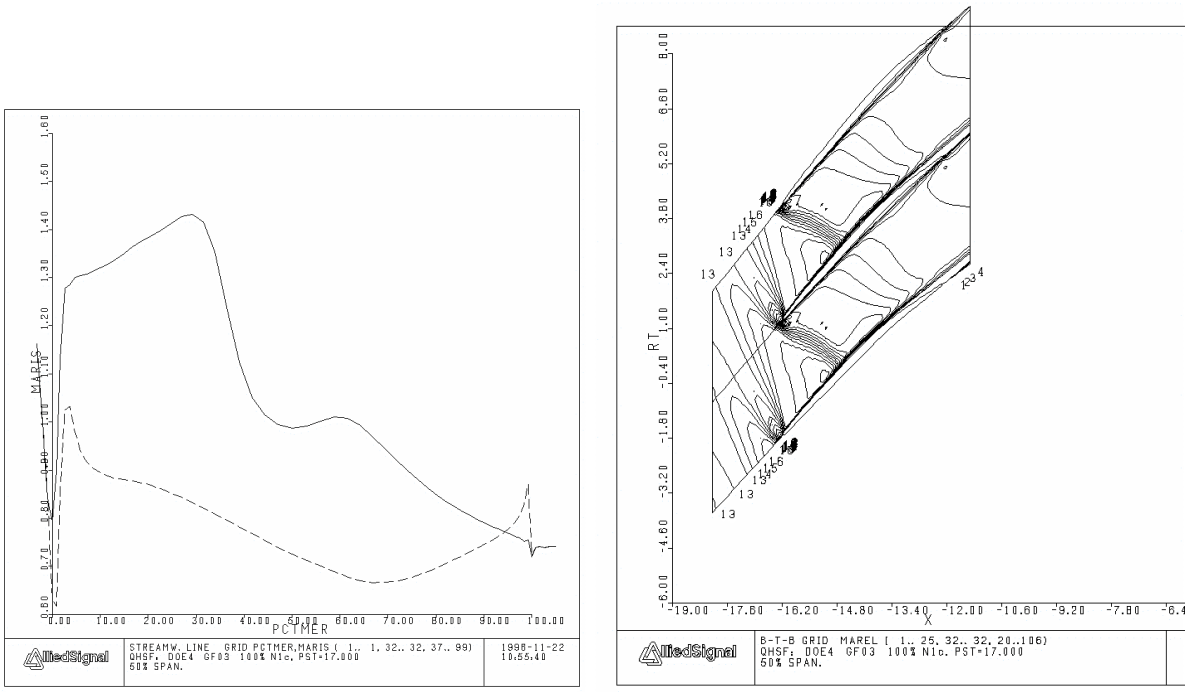

Figure 5.1.2-8. DAWES Calculated Isentropic Blade Loadings and Blade-to-Blade mach Number Contours at 50% Span at the Design Point

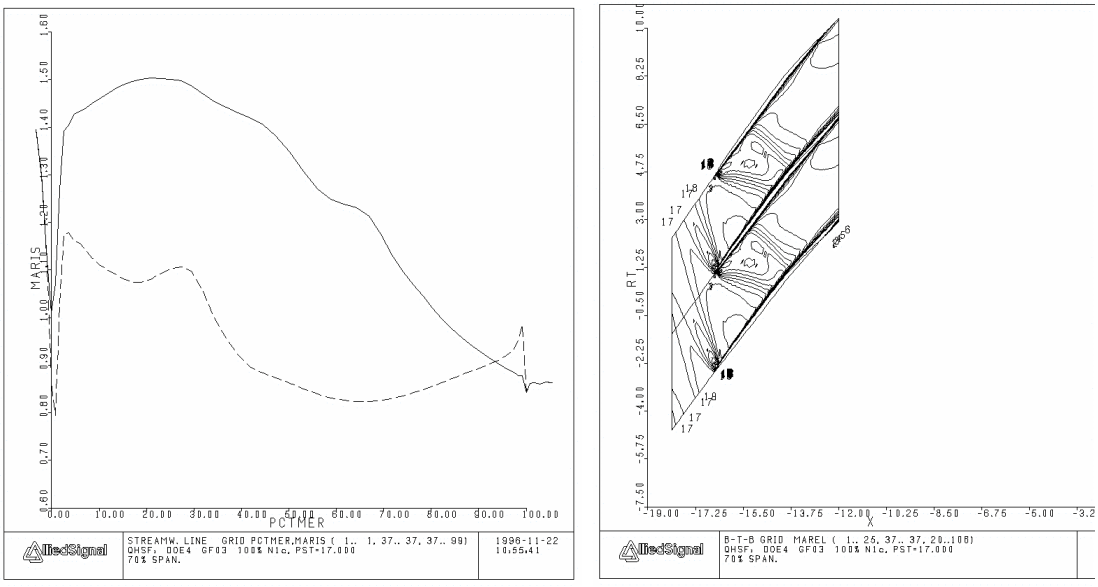

Figure 5.1.2-9. DAWES Calculated Isentropic Blade Loadings and Blade-to-Blade mach Number Contours at 70% Span at the Design Point

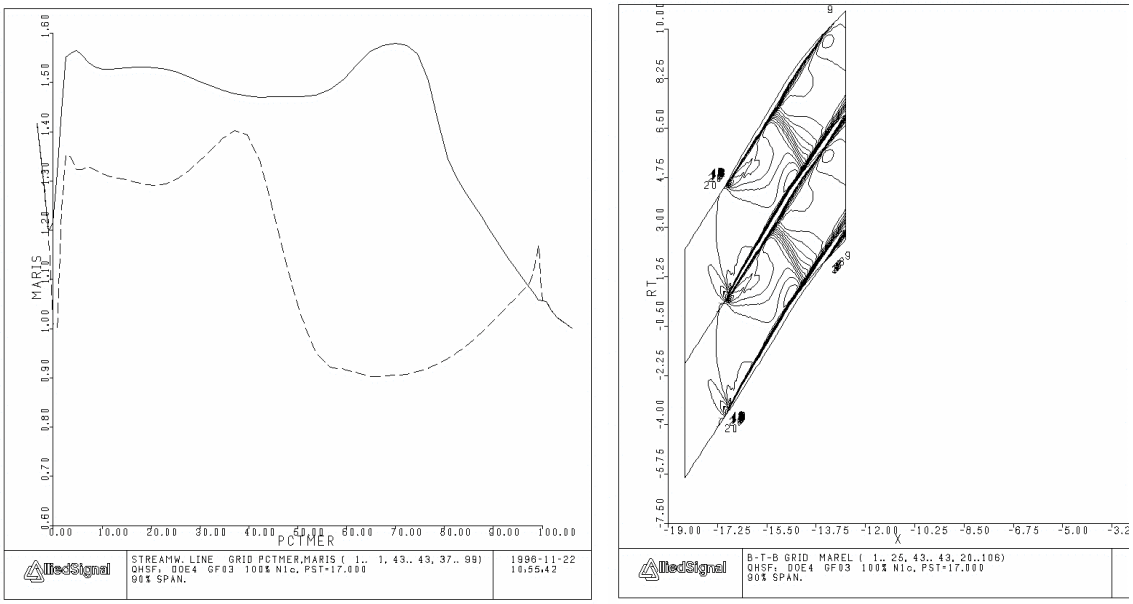

Figure 5.1.2-10. DAWES Calculated Isentropic Blade Loadings and Blade-to-Blade mach Number Contours at 90% Span at the Design Point

Blade-to-blade contour plots are shown for 50, 70, and 90 percent spans at choke, design point, and near stall in Figures 5.1.2-11 through 5.1.2-13, respectively. Relative to the baseline, the amount of blade effective sweep significantly reduced the strength of the shock. The figures show that the passage shock was well contained at the tip although it moved forward as span decreased and was positioned upstream of the leading edge at 70% span. Attempts in DOE 4 to keep the shock positioned back in the passage had negative impact on rotor efficiency.

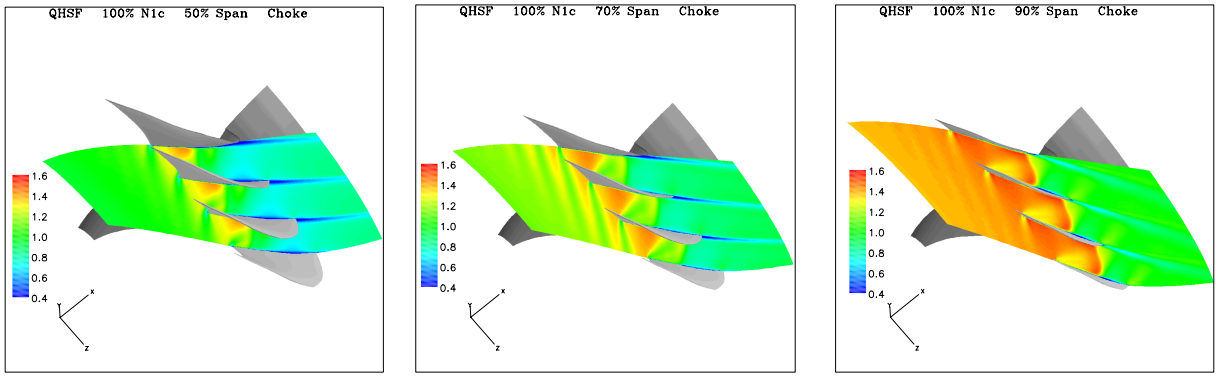

Figure 5.1.2-11. DAWES Calculated Blade-to-Blade Relative Mach Number Contours at 100% N1c Choke for 50, 70, and 90% Spans

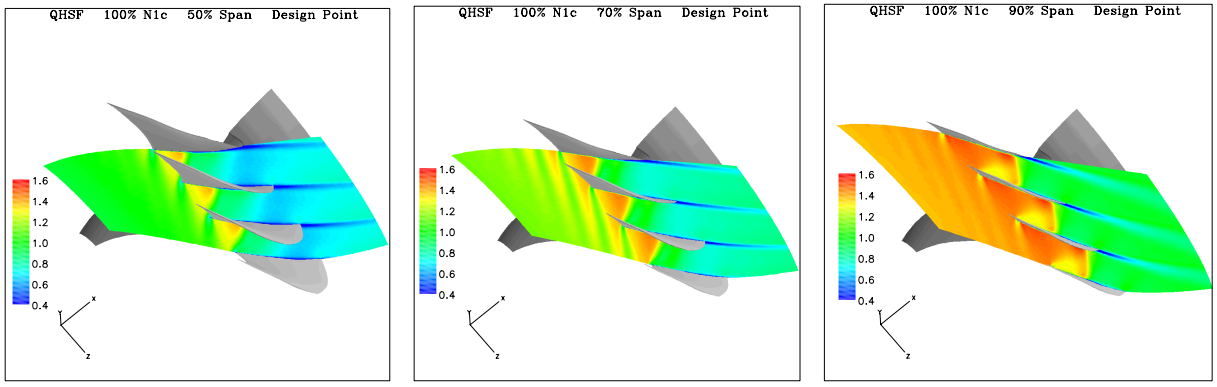

Figure 5.1.2-12. DAWES Calculated Blade-to-Blade Relative Mach Number Contours at 100% N1c Design Point for 50, 70, and 90% Spans

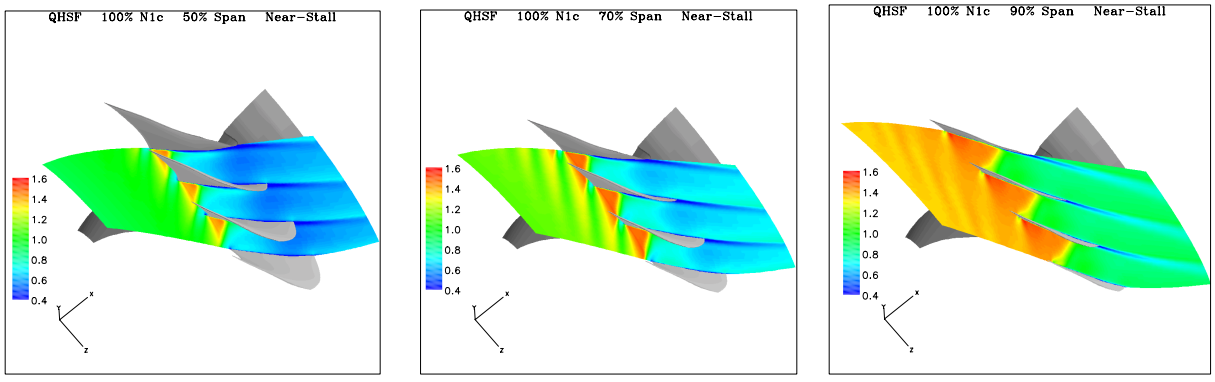

Figure 5.1.2-13. DAWES Calculated Blade-to-Blade Relative Mach Number Contours at 100% N1c Near Stall for 50, 70, and 90% Spans

A rotor-only predicted map for the QHSF is shown in Figures 5.1.2-14 through 5.1.2-16. DAWES analyses were completed at the points indicated. The map agrees very well with DAWES analyses completed with the baseline rotor. Relative to test data of the baseline rotor, flow and work agreed very well but the efficiency would be adjusted higher approximately 1.5 points.

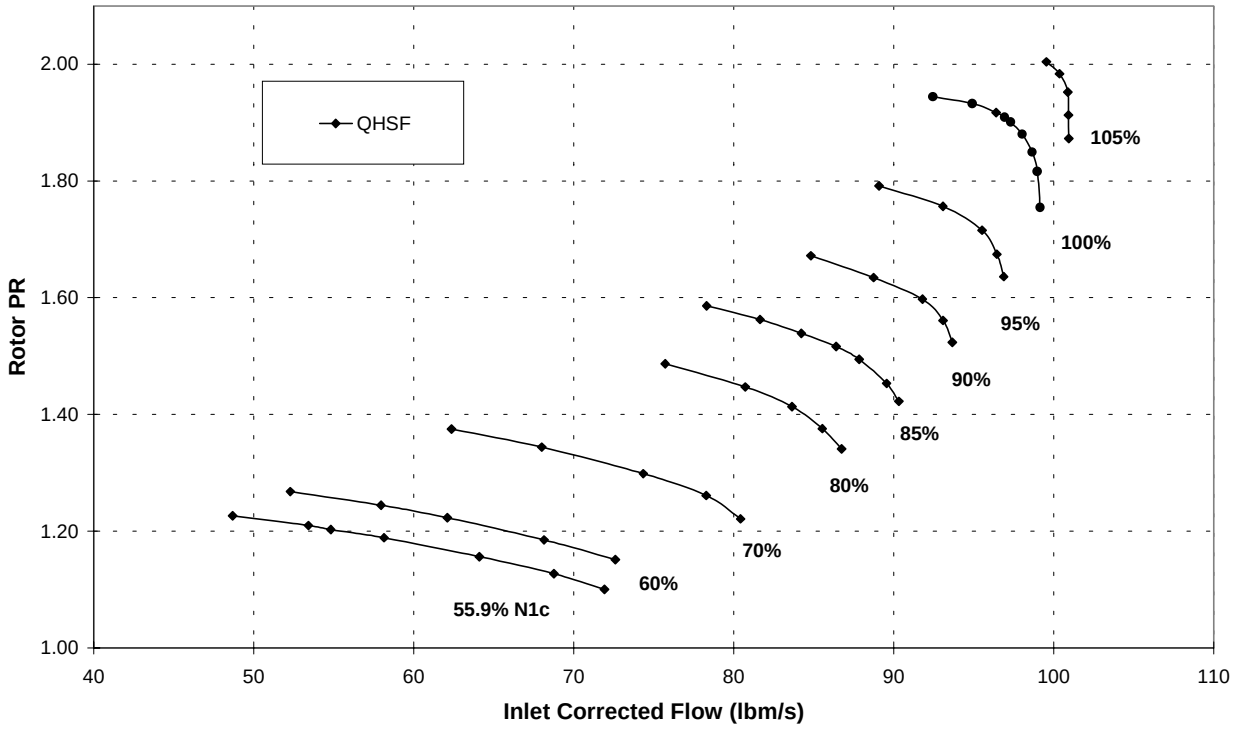

Figure 5.1.2-14. QHSF Predicted Map (Wc vs. PR) Based on DAWES Analyses

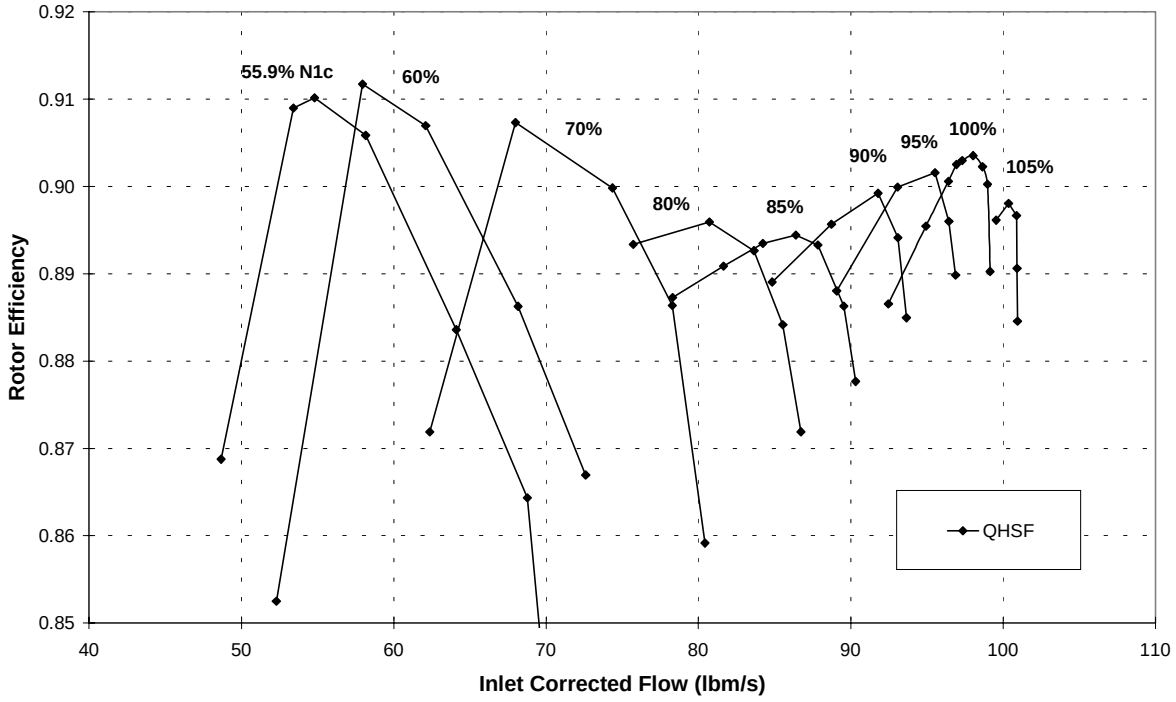

Figure 5.1.2-15. QHSF Predicted Map (Wc vs. Eff) Based on DAWES Analyses

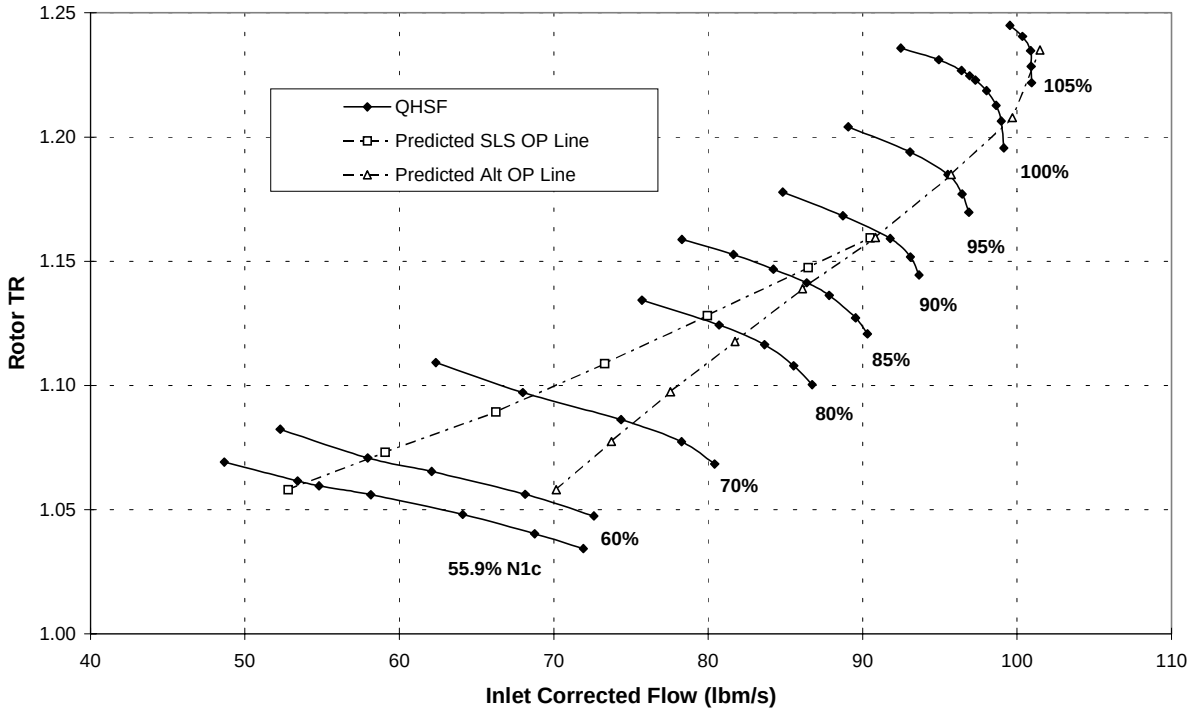

Figure 5.1.2-16. QHSF Predicted Map (Wc vs. TR) Based on DAWES Analyses with Predicted Operating Lines

5.1.3 Acoustic Results

5.1.3.1 Design Philosophy

The design philosophy employed in reducing multiple pure tone (MPT) noise below that of the baseline rotor was to use rotor forward sweep to control the strength and position of the passage shock emanating from the suction surface of the airfoil. It was assumed that use of forward sweep would delay the onset of strong shocks to higher fan speeds and allow the capture of shocks within the blade passages at lower fan speeds, thereby affecting buzzsaw noise as shown in Figure 5.1.3-1.

5.1.3.2 Baseline Fan

It became apparent that the geometry and operating conditions of the baseline were such that the dominant shock structure consisted of a normal shock emanating from the suction side of the rotor, herein called a "passage" shock. At all conditions except 100% corrected fan speed (see Figure 5.1.3-2), the presence of a propagating passage shock (not contained within the blade passage) precluded the need for a bow shock at the blade leading edge since the flow was subsonic at this location (see Figure 5.1.3-3). The volume of literature gathered to date seem only to discuss the effects of blade geometry and stagger angle variation on the strength and position of a bow shock (References 2 to 13). Evidently these studies were conducted on rotors which operated closer to choke where the passage shock was swallowed. For this effort it was assumed that the geometric variations classically deemed responsible for MPT noise generation, due to their effect on bow shocks, in a similar way cause variations in the strength and propagation direction of the expelled (propagating) passage shocks.

Using the 3-D thin-layer Navier-Stokes equation solver DAWES, the location of the passage shock relative to the leading edge of the following blade was predicted at a number of fan speeds for the baseline rotor. Figure 5.1.3-4 shows the linear relationship between shock location and wheel speed.

A correlation was developed between the predicted rotor passage shock position relative to the leading edge of the downstream blade and the measured buzzsaw noise in the 500 Hz, 1 kHz and 2 kHz octave bands which contain harmonics of shaft speed below the BPF. In an attempt to capture noise level differences due to buzzsaw cuton, inlet sound pressures (measured from 10-90° from the inlet engine centerline) were summed over the 3 octave bands mentioned above and normalized by the level at 75.3% corrected fan speed (the speed above which MPT noise was cuton). Reference 14 contains measured buzzsaw noise spectra for the baseline.

Figure 5.1.3-5 shows the normalized inlet noise versus passage shock position normalized by the rotor chord. As fan speed increases, the passage shock strength increases (see Figure 5.1.3-6) as it moves closer to the leading edge of the following blade, and buzzsaw noise levels increase. Between 75.3% and 86.5% speed the variation of measured sound pressure level is nearly linear with shock location following the equation

$$SPL = -45.6(x) + 13.0$$

where *SPL* is the increase in level after MPT noise is cuton, and *x* is the shock location divided by the rotor chord. From 86.5% to 90.0% speed, however, the correlation deviates from a linear behavior, showing little increase in noise level with increasing rotor speed and decreasing shock stand-off distance.

At 90.0% speed the shock location, predicted assuming symmetric rotor blades, is very near the leading edge of the downstream blade. It may be that in actuality, with asymmetric blade shapes and stagger angles, the leading edge of the following blade interferes with the propagation of the passage shock to the far-field. From Figure 5.1.3-4 it can be inferred that near 94% speed the passage shock is completely swallowed and buzzsaw noise is cutoff. This is confirmed by the fact that in cruise (100% corrected fan speed) the baseline engine generates no buzzsaw noise (see Figure 5.1.3-2). The transition between conditions of passage shock propagation and swallowing (as corrected speed is increased) may involve some hysterisis effects, but it appears to begin between 86.5% and 90.0% corrected fan speed for the baseline.

5.1.3.3 QHSF

As shown in Figure 5.1.3-7, the spanwise distribution of effective sweep causes the passage shock location to vary with span at 100% speed. A strong shock is swallowed at 90% span while a weaker shock is expelled at 70% span. As fan speed is reduced to near takeoff conditions (85% corrected speed, Figure 5.1.3-8), the strong tip shock dissipates leaving only a weak shock at 70% span.

Examination of the shock position at 2 radial locations along the rotor reveals that, at 100% speed and 90% span, the QHSF passage shock is severely swallowed (see Figure 5.1.3-9). The streamwise shock position at 90% span is not recorded for speeds below design because the computed pressure gradient at that location does not suggest the presence of a shock, but merely a gradual pressure rise (see Figure 5.1.3-8). At 70% span, the QHSF passage shock is expelled, but the strength of this shock is much less than that of the baseline at 75% speed where buzzsaw noise is nearly cutoff (see Figure 5.1.3-10). The shock at 90% span is relatively strong, but its position near the streamwise center of the rotor passage suggests buzzsaw noise cutoff.

The main objectives have been achieved to reduce buzzsaw noise: passage shock strength has been greatly reduced from that of the baseline rotor and strong shocks are swallowed within the rotor passage. Buzzsaw noise levels are predicted to be much lower for the QHSF than for the baseline, if not completely eliminated.

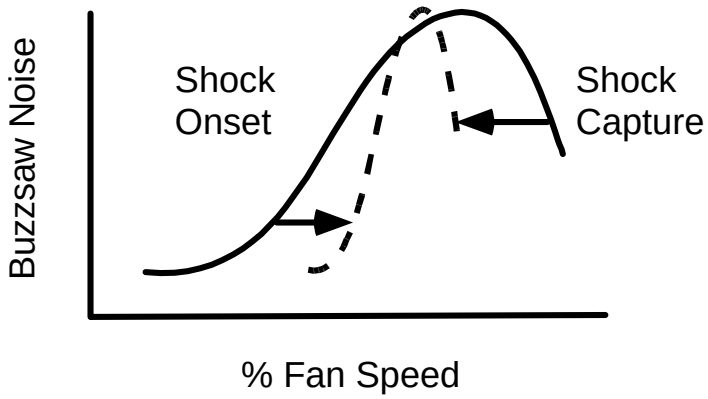

Figure 5.1.3-1. **Potential Buzzsaw Noise Control Accomplished Using Forward Sweep**

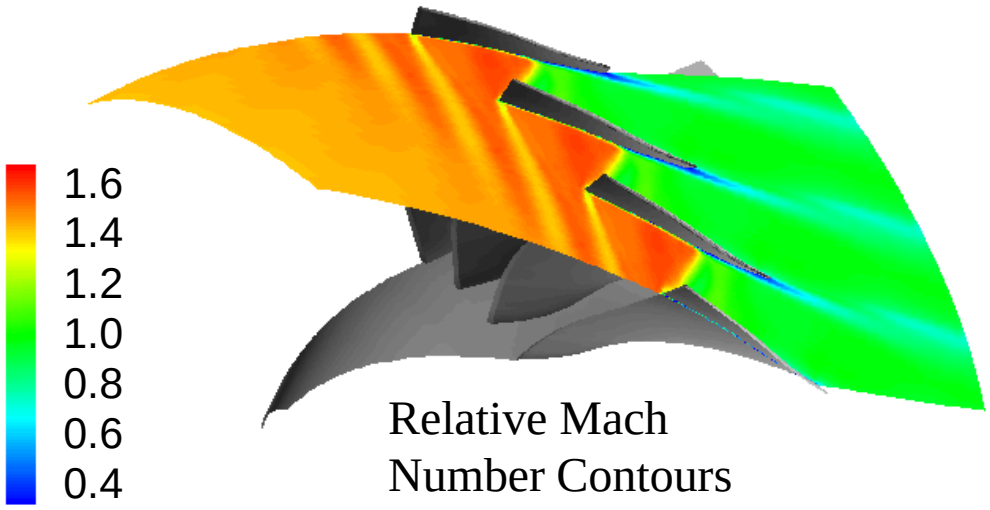

Figure 5.1.3-2. **Passage Shock Position for Baseline at Design Point Showing Swallowed Shock**

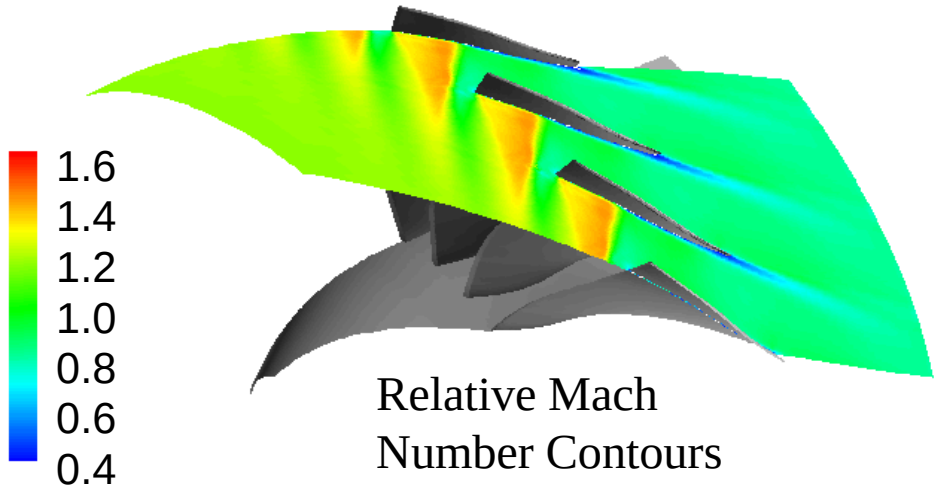

Figure 5.1.3-3. Passage Shock Position for Baseline at Take-Off (86.5% N1c)

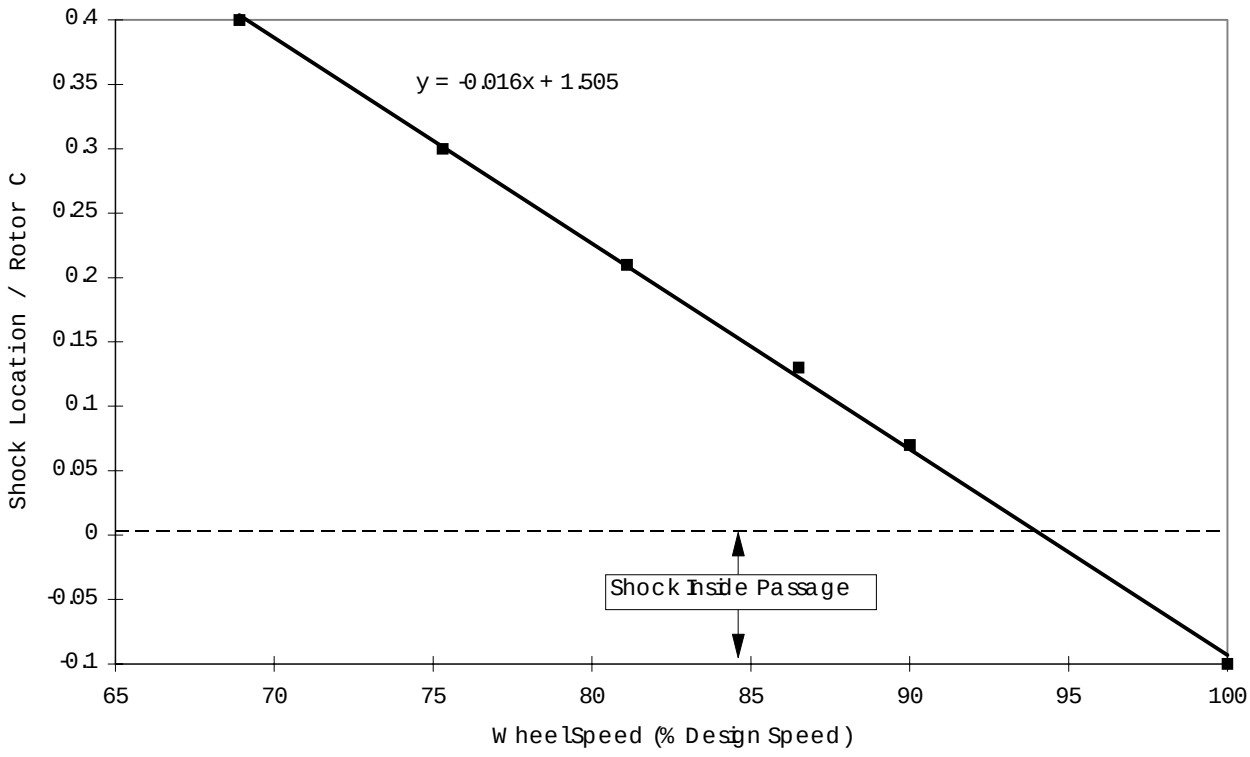

Figure 5.1.3-4. Relationship Between Shock Location and Fan Rotational Speed for Baseline

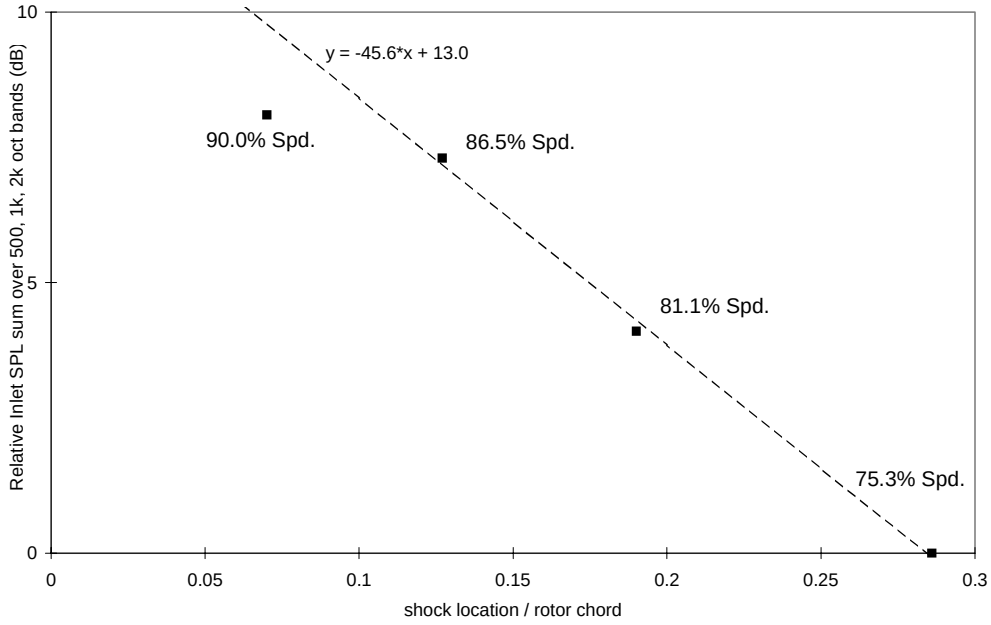

Figure 5.1.3-5. Correlation Between Passage Shock Position and Buzzsaw Noise For Baseline

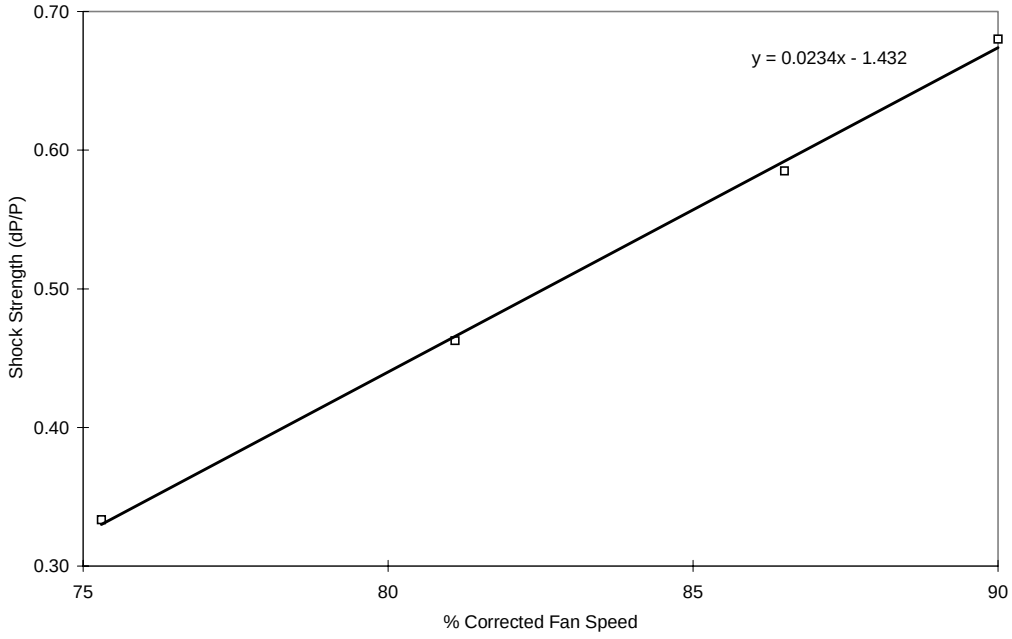

Figure 5.1.3-6. Predicted Strengths of Expelled Passage Shocks at the Rotor Corrected Speeds For Which Buzzsaw Noise Was Measured in the Baseline (strengths extracted from pressure distribution along stagnation streamline)

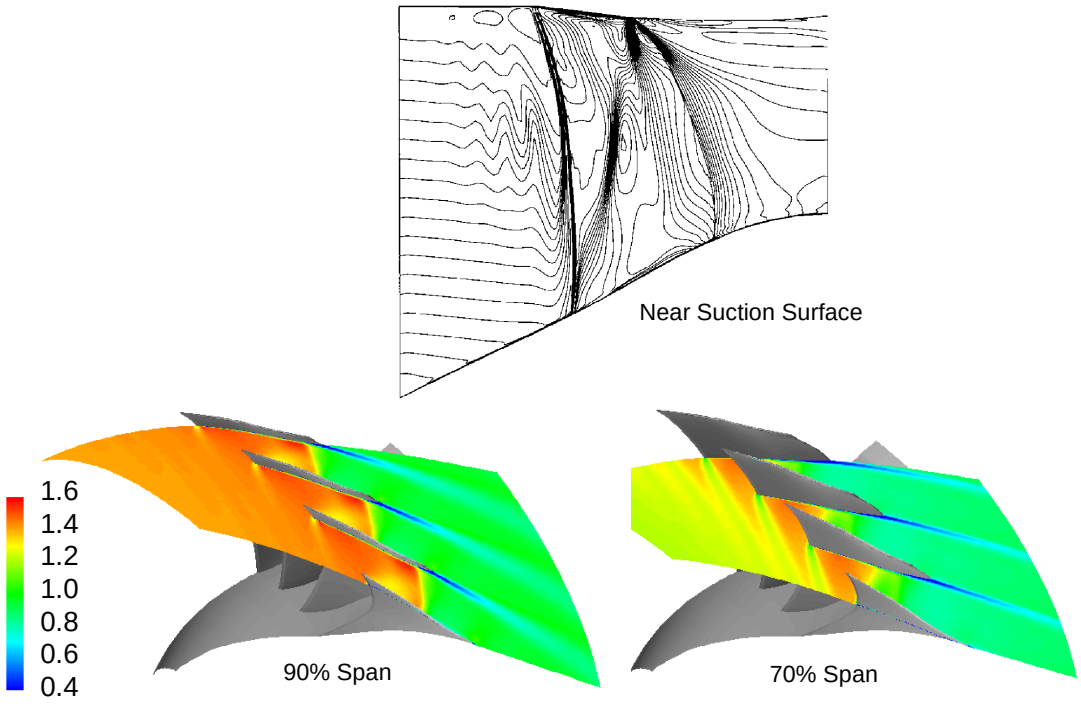

Figure 5.1.3-7. Mach Number Contours for QHSF at 100% Speed

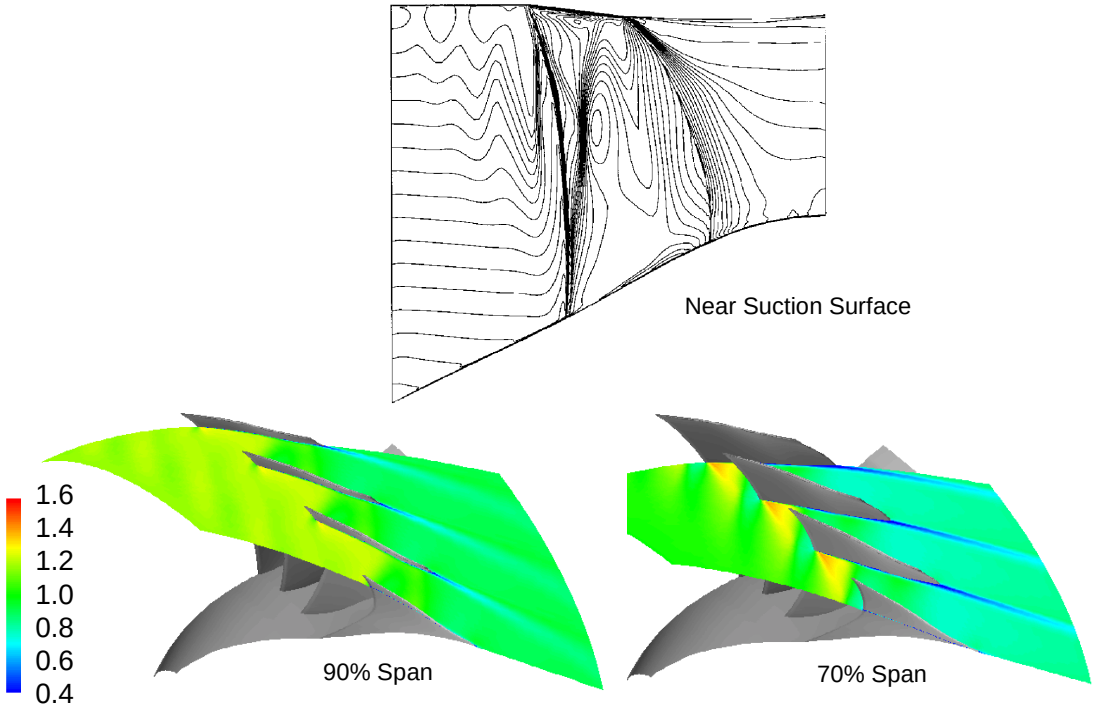

Figure 5.1.3-8. Mach Number Contours for QHSF at 85% Speed

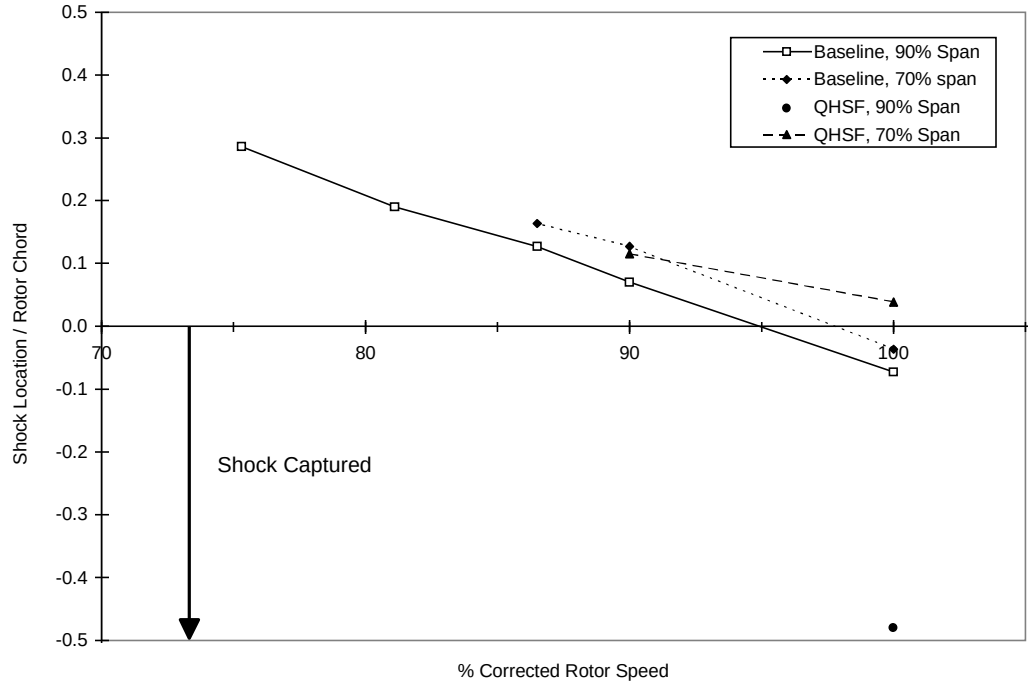

Figure 5.1.3-9. Comparison of Shock Locations for Baseline and QHSF

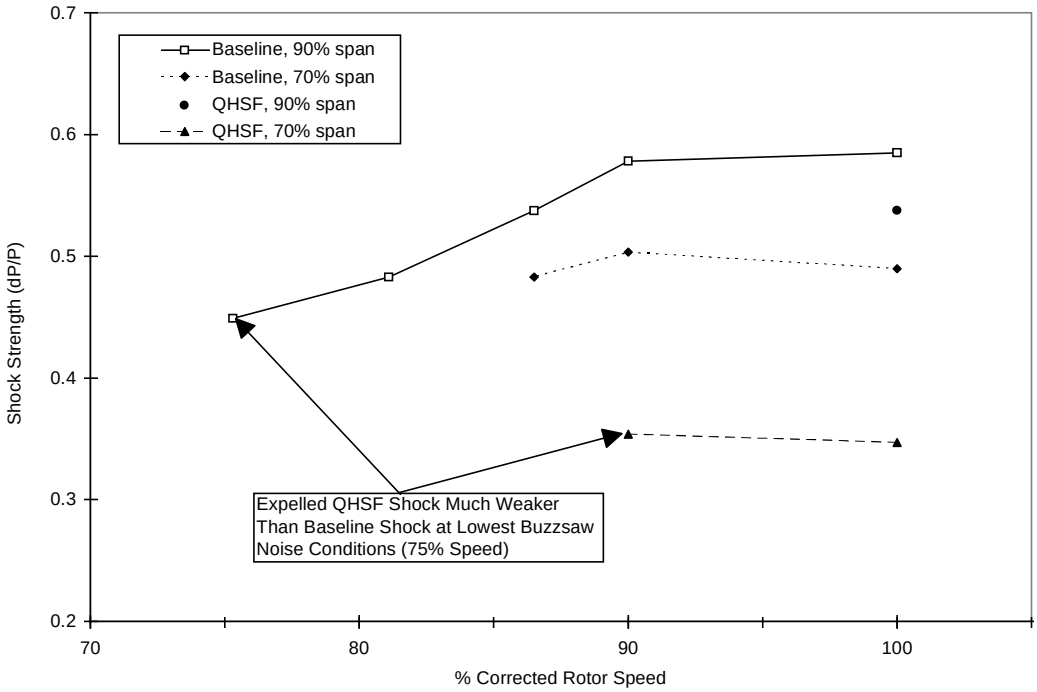

Figure 5.1.3-10. Comparison of Shock Strengths for Baseline and QHSF (strengths extracted from pressure distribution along 50% pitch streamline)

5.1.4 Mechanical Results

This section presents the results of the Mechanical Analysis of the QHSF Fan Rotor Blade.

5.1.4.1 Design Criteria

Mechanical design criteria were selected to satisfy both AE and NASA requirements. While the NASA criteria primarily addresses rig safety, the more stringent AE criteria is intended to ensure long-term field reliability. The QHSF blade was designed to achieve state-of-the-art noise reduction while maintaining commercial viability.

- Peak steady-state stresses in the blade and attachment are at levels providing unlimited Low-Cycle Fatigue (LCF) life.
- Adequate frequency margin exists to preclude resonant vibration at maximum power conditions.
- Leading edge thickness and stress levels are within range of successful AE experience.
- Flutter parameters involving reduced frequency and incidence are within AE experience.

5.1.4.2 Finite-Element Model Description

A fully 3D finite element model was constructed of the entire rig scale (22-inch diameter) fan rotor, including the airfoil, blade attachment, and disk. The complete model is shown in Figure 5.1.4-1. The airfoil and blade attachment were modeled separately and connected via an AE multi-point constraint equation technique. Due to cyclic symmetry, the disk model consisted of a single, slotted wedge. Figure 5.1.4-2 shows the detail of the blade model; the disk model will described in a later section.

The QHSF fan airfoil has roughly the same geometric parameters, such as chord, hub/tip ratio, etc., as an existing AE fan. To reduce design costs, the platform/ blade attachment from the AE fan was used for the QHSF rotor. Optimization of the circumferential position of the airfoil on the platform was done to minimize the peak stress in the attachment.

For computational efficiency, the disk and attachment were modeled as linear substructures. Blade to disk interaction at the dovetail was modeled using 3D contact surface elements.

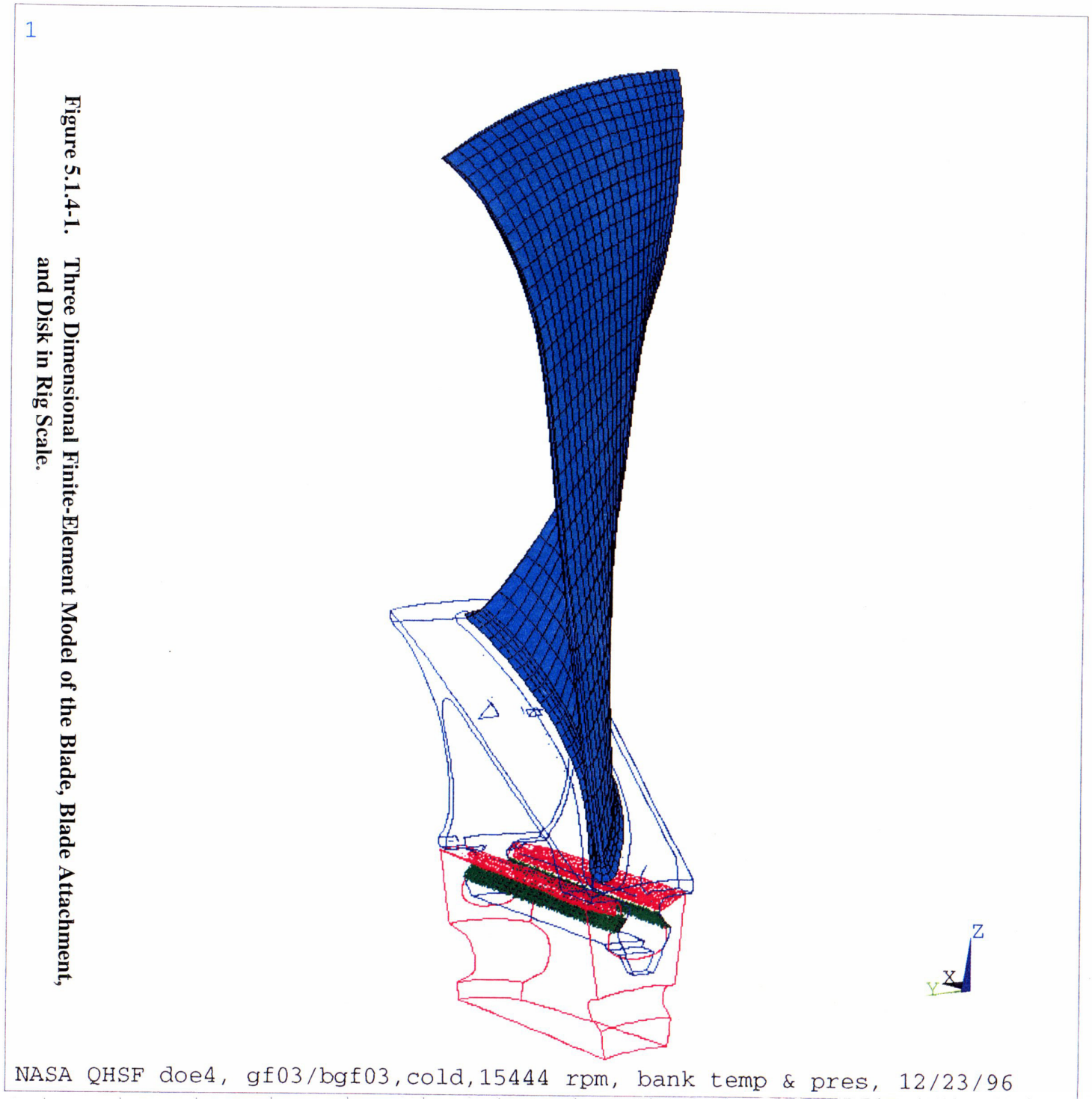

Figure 5.1.4-1. Three Dimensional Finite-Element Model of the Blade, Blade Attachment, and Disk in Rig Scale.

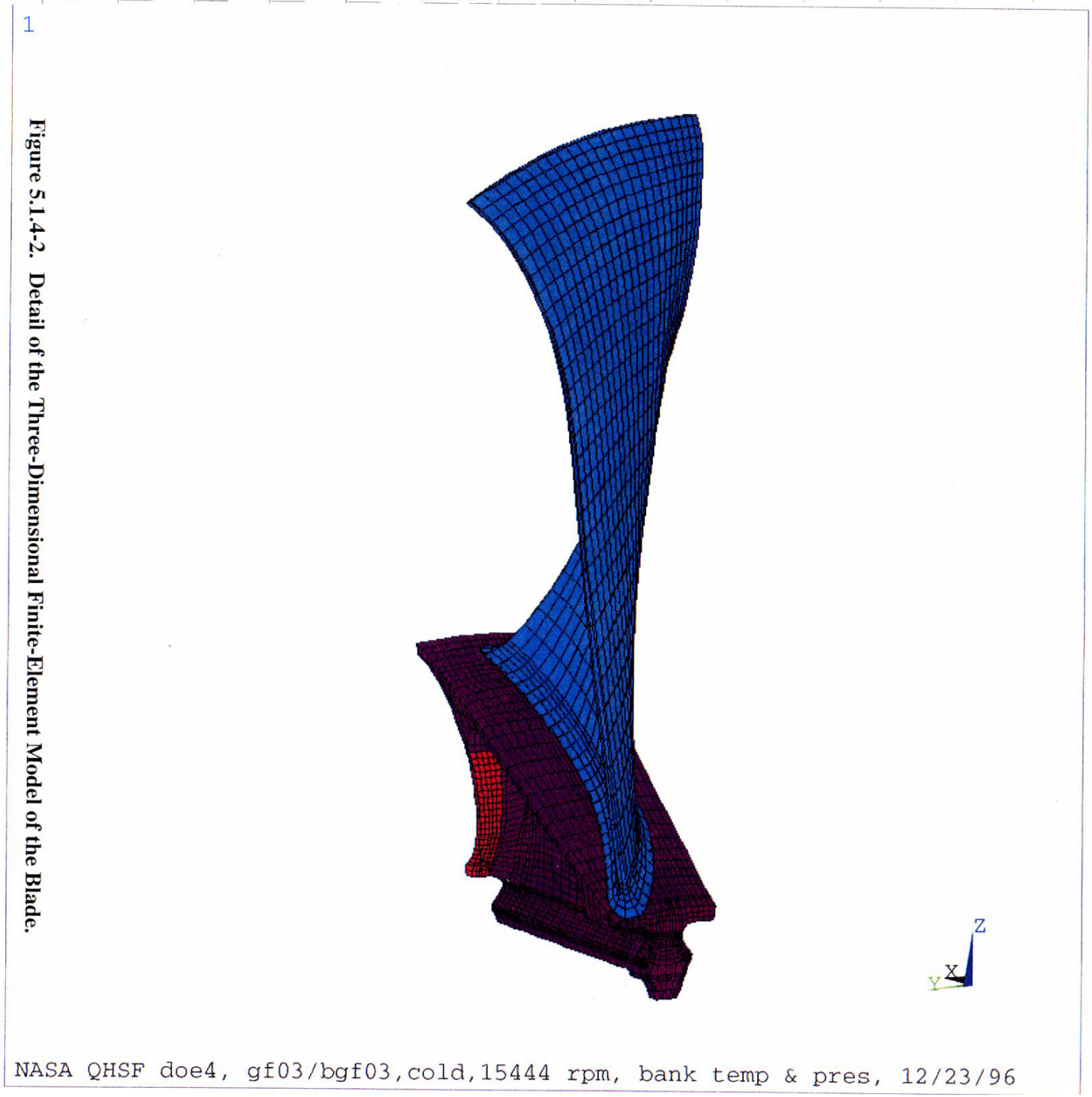

Figure 5.1.4-2. Detail of the Three-Dimensional Finite-Element Model of the Blade.

Material Selection and Properties

The blade material was chosen to be Ti-6Al-4V STOA with the nominal properties summarized in Table 5.4.1-1.

Table 5.1.4-1 Ti-6AL-4V STOA Mechanical Properties

Property	75F	250F
Modulus, Mpsi	17.5	17.1
Weight Density, lb/in^3	0.161	0.161
0.2% Yield Strength, ksi	137.7	111.4
Ultimate Strength, ksi	146.2	127.3

Boundary Conditions

A physical speed of 15444 rpm was applied to the rotor along the x-axis. The cut wedge faces were coupled together cylindrically to enforce cyclic symmetry. Axial (thrust) and tangential (torque) loads were reacted on the forward annular face representing the disk bolt flange.

Figure 5.1.4-3 shows metal temperatures corresponding to the aerodynamic design point as mapped to the airfoil model. A uniform metal temperature of 75 degrees F was applied to the platform/attachment and 85 degrees F was applied to the disk to simulate operating conditions. Design point suction and pressure-side static pressure distributions were mapped to the corresponding element faces on the airfoil (Figure 5.1.4-4).

5.1.4.3 Static Analysis Results

As constructed, the airfoil model represented the at-speed, design point geometry (“hot” shape). The first phase of the static analysis is to calculate the manufactured shape (“cold”), that will, under design point conditions of speed, temperature, and pressure, deflect the blade into the desired “hot” shape. This transformation was done using an iterative procedure within ANSYS where the maximum error between the deflected cold geometry and the desired hot geometry is reduced to less than 0.001 inch. For undampered fans of this type a non-linear, large-deflection analysis is required.

At the conclusion of the hot-to-cold analysis the nonlinear, steady-state stresses and deflections are available. Figure 5.1.4-5 shows the maximum principal stress distribution on the pressure and suction sides of the airfoil. Figure 5.1.4-6 shows the Equivalent (Von Mises) stress distribution.

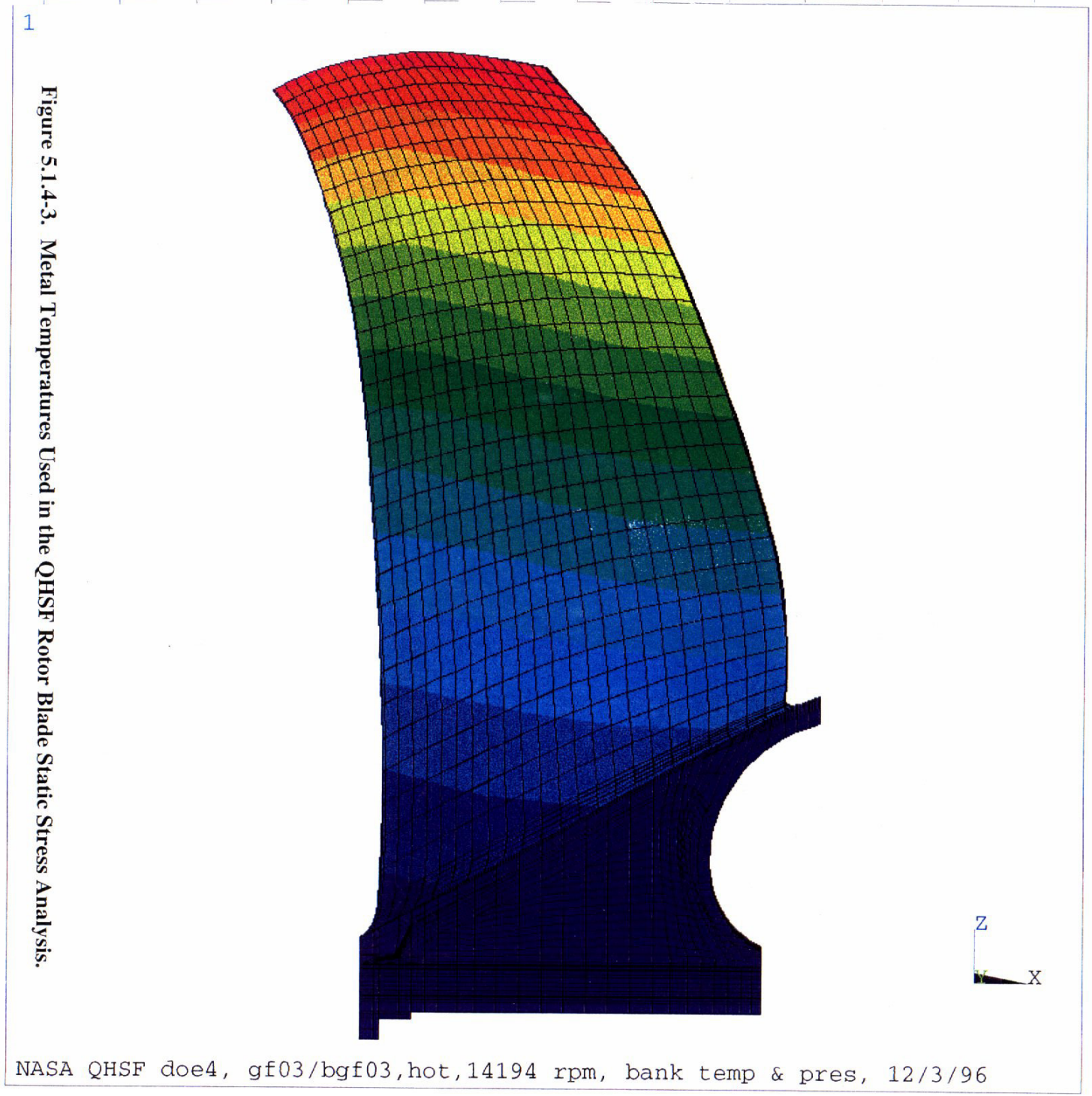

Figure 5.1.4-3. Metal Temperatures Used in the QHSF Rotor Blade Static Stress Analysis.

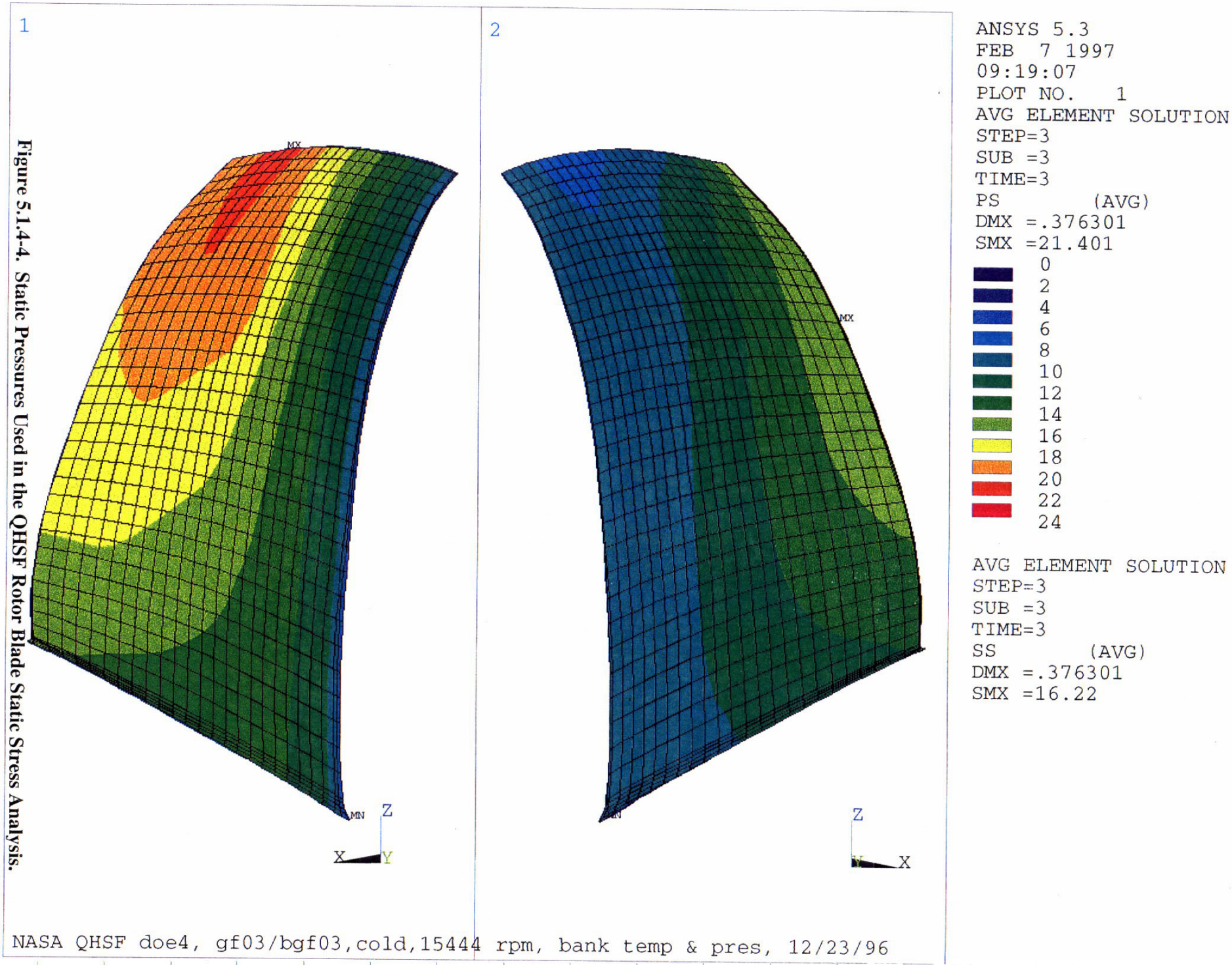

Figure 5.1.4-4. Static Pressures Used in the QHSF Rotor Blade Static Stress Analysis.

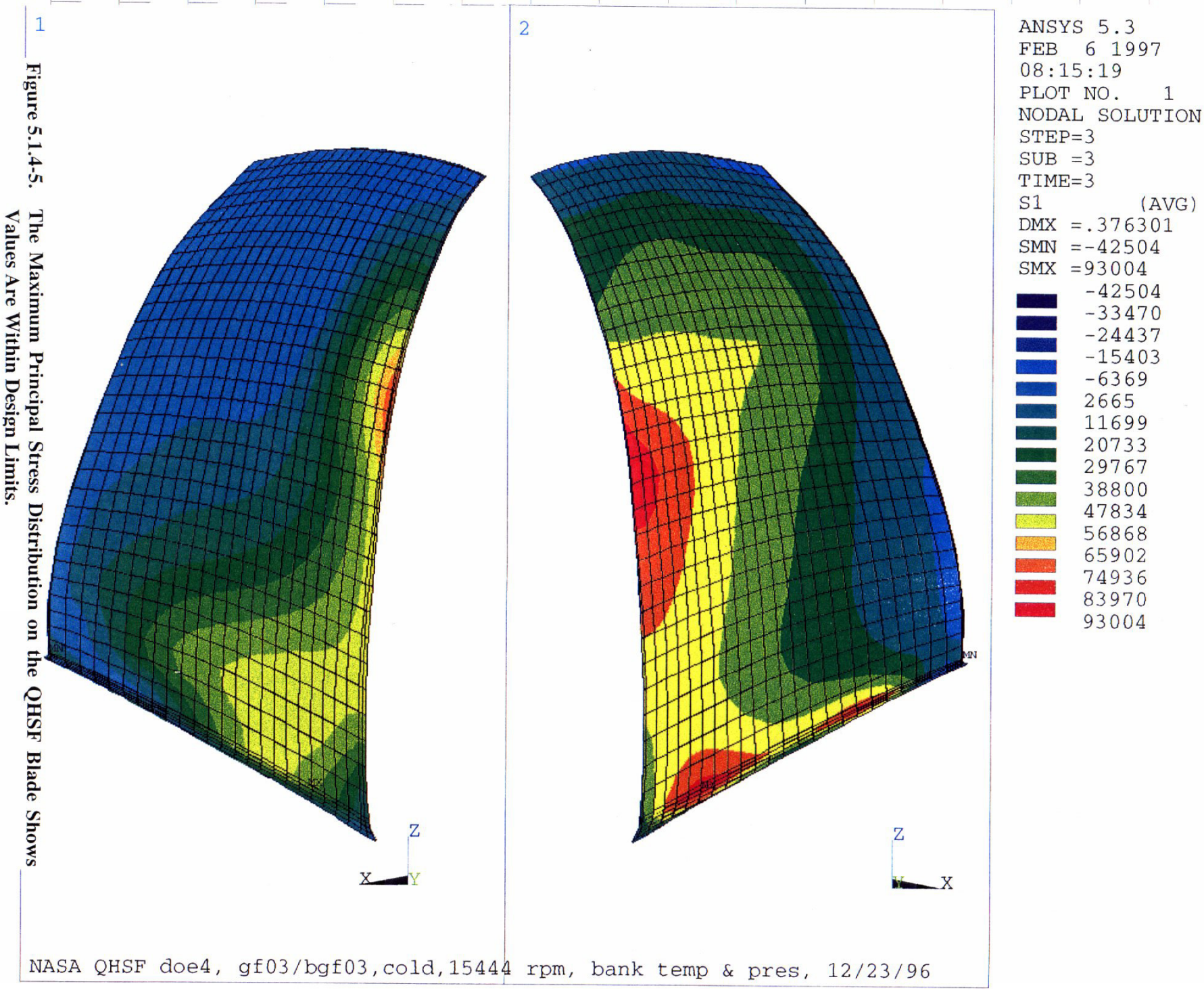

Figure 5.1.4-5. The Maximum Principal Stress Distribution on the QHSF Blade Shows Values Are Within Design Limits.

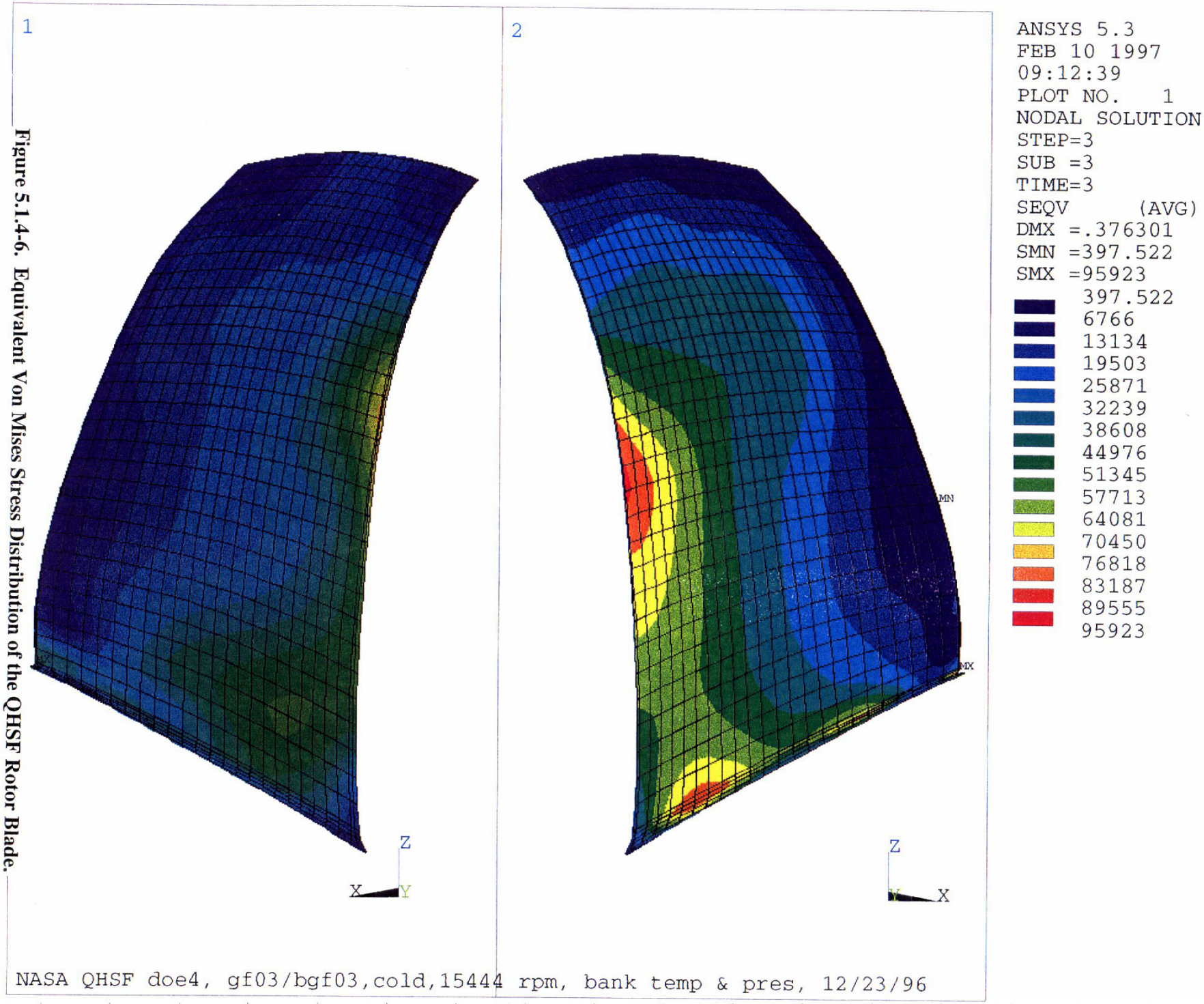

Figure 5.1.4-6. Equivalent Von Mises Stress Distribution of the QHSF Rotor Blade.

Airfoil deflections at the Design point are shown next. Figure 5.1.4-7 shows the true-scale displaced shape of the airfoil (shown as element grid) along with the undeformed, cold geometry (shown in outline) as viewed along the tip chord. Quantitative plots of airfoil deflection are presented in the next four figures. Figure 5.1.4-8 shows the vector sum (scalar) displacement of the airfoil. The maximum airfoil deflection was predicted to be 0.376 inch.

Radial displacements (positive outward from center) are shown in Figure 5.1.4-9. A maximum radial deflection of 0.051 inch occurred at the leading-edge. Figure 5.1.4-10 shows the airfoil tangential deflection (positive toward pressure-side) and Figure 5.1.4-11 shows the axial (positive forward) component.

The substructure displacements at the airfoil root and the disk contact faces were used to expand the attachment stress and displacement solutions. Pressure and suction side attachment principal and equivalent stress distributions are shown in Figures 5.1.4-12 & 5.1.4-13 respectively. Figure 5.1.4-14 shows the displacement contours for the attachment and platform.

Inspection of the principal stress plot (Figure 5.1.4-12) and the displacement plot (Figure 5.1.4-14) showed a significant amount of bending in the attachment due to the large tangential sweep of the blade. Stress levels, however, were well within acceptable range, and the effect of the bending displacement was accounted for in the cold blade geometry.

5.1.4.4 Modal Analysis Results

Modal analysis was performed on the QHSF blade using the same model as was used for the static analysis (Figure 5.1.4-2). The effect of the disk was ignored based on the relative rigidity of the disk combined with past experience with similar designs.

All nodes on the contact faces of the blade dovetail were fixed in the three translational degrees-of -freedom (DOF). To define the Campbell diagram two analyses were performed. The first was done assuming uniform room-temperature, with no pressure loading, and no rotational speed. The second analysis assumed ADP metal temperatures (Figure 5.1.4-3), static pressures (Figure 5.1.4-4), and a rotational speed of 15444 rpm. Natural frequencies for the first five modes are tabulated in Table 5.1.4-2. Also included are the frequencies for the fixed-root condition (attachment effects neglected) under identical conditions.

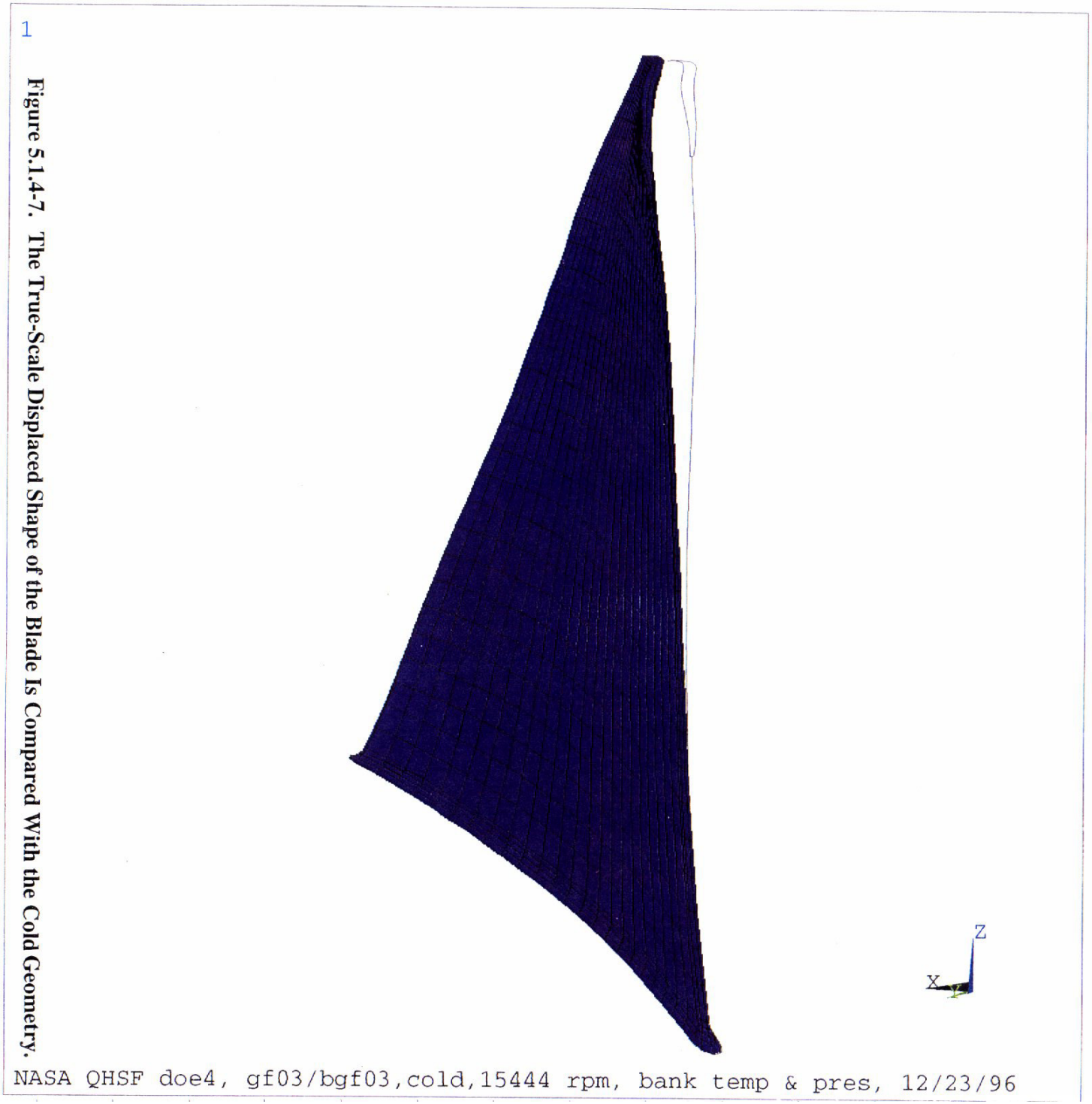

Figure 5.1.4-7. The True-Scale Displaced Shape of the Blade Is Compared With the Cold Geometry.

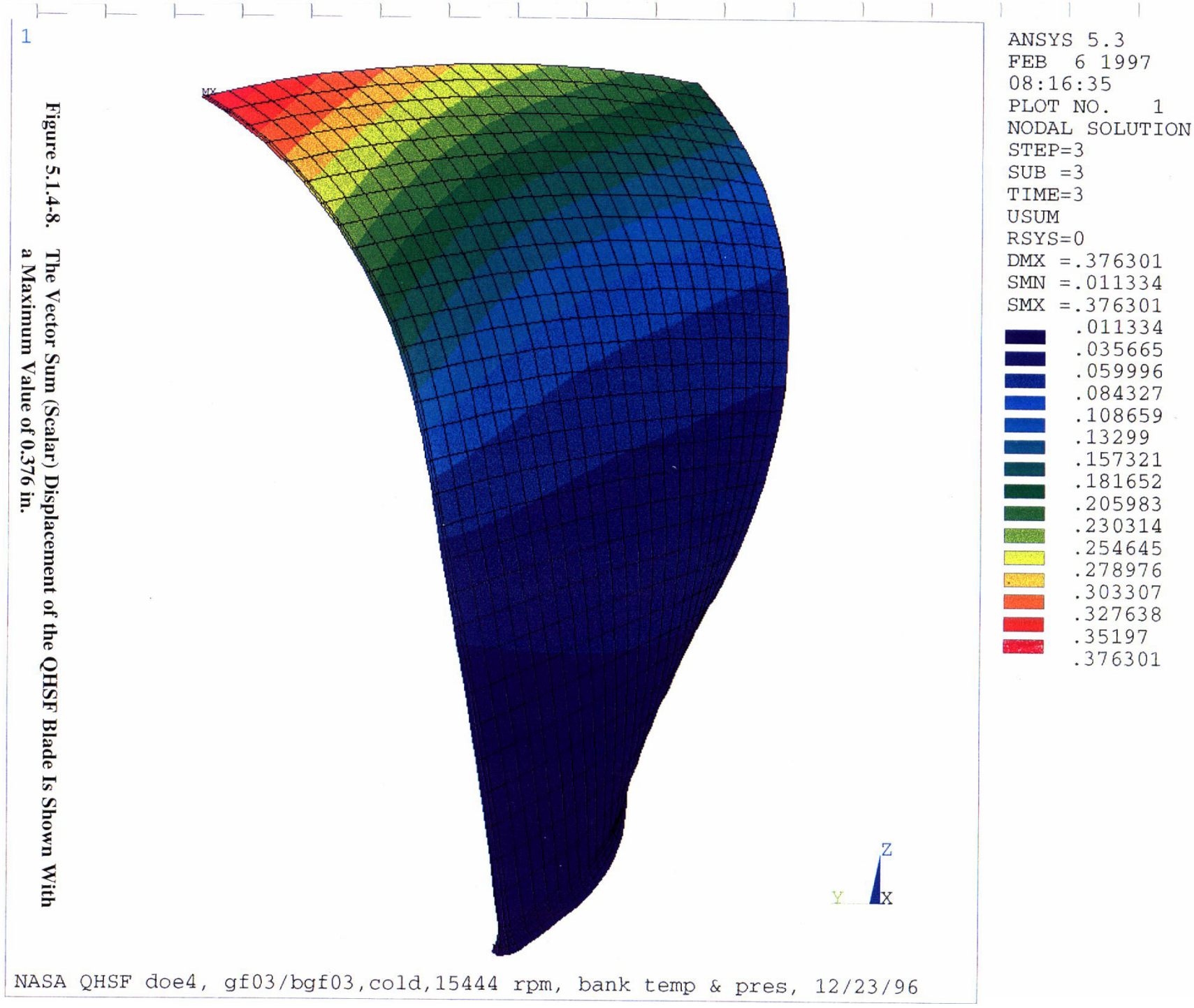

Figure 5.1.4-8. The Vector Sum (Scalar) Displacement of the QHSF Blade Is Shown With a Maximum Value of 0.376 in.

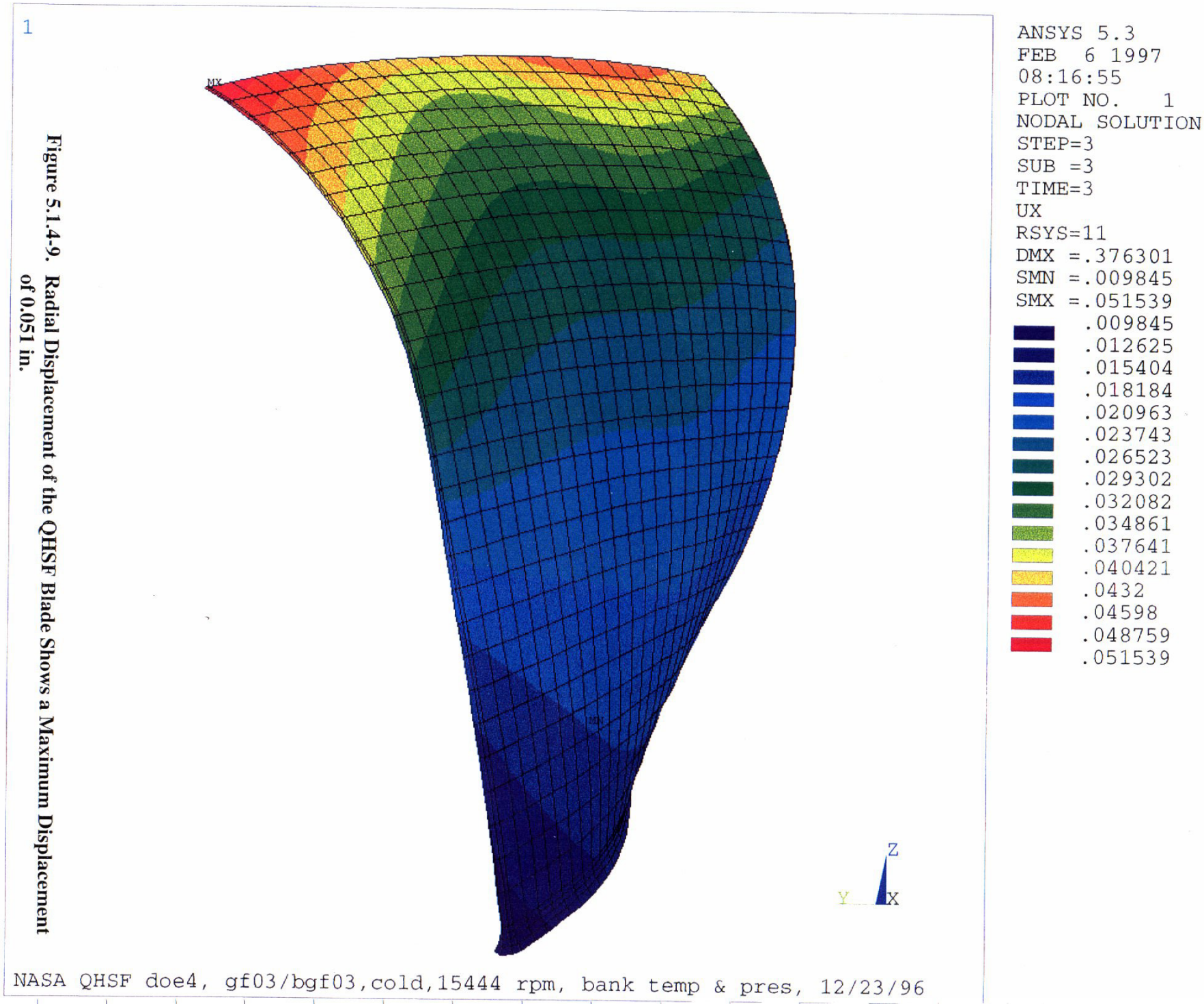

Figure 5.1.4-9. Radial Displacement of the QHSF Blade Shows a Maximum Displacement of 0.051 in.

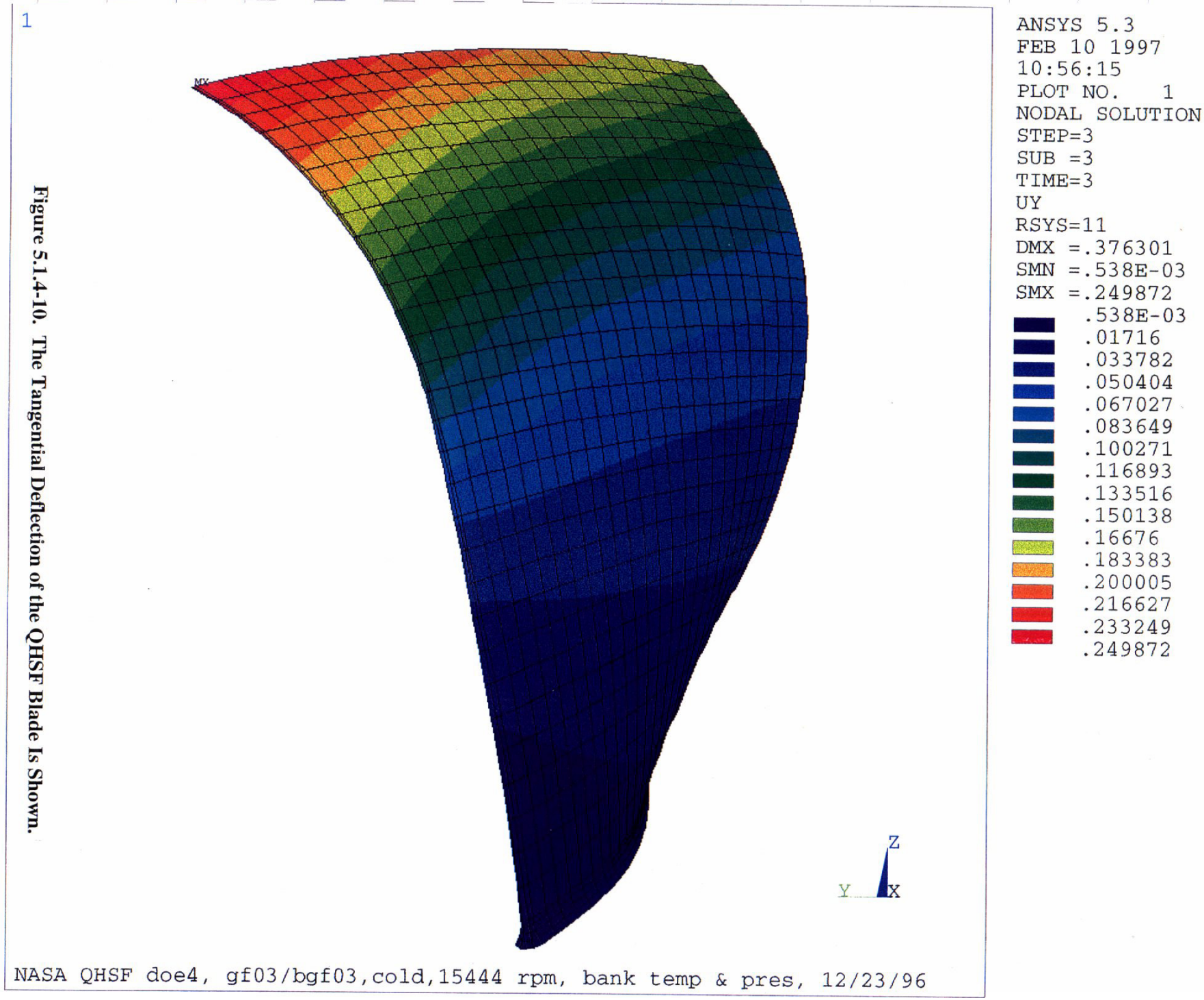

Figure 5.1.4-10. The Tangential Deflection of the QHSF Blade Is Shown.

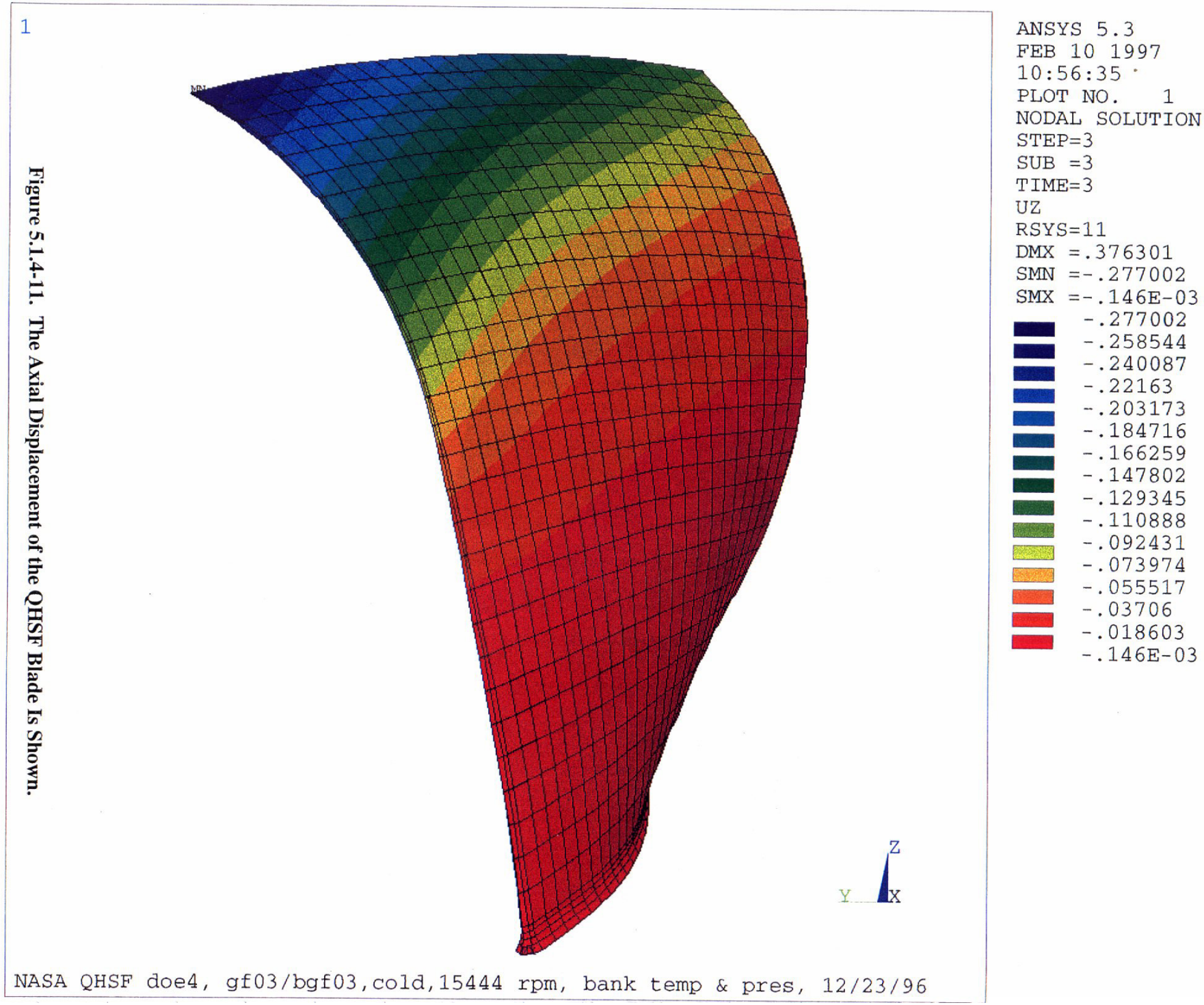

Figure 5.1.4-11. The Axial Displacement of the QHSF Blade Is Shown.

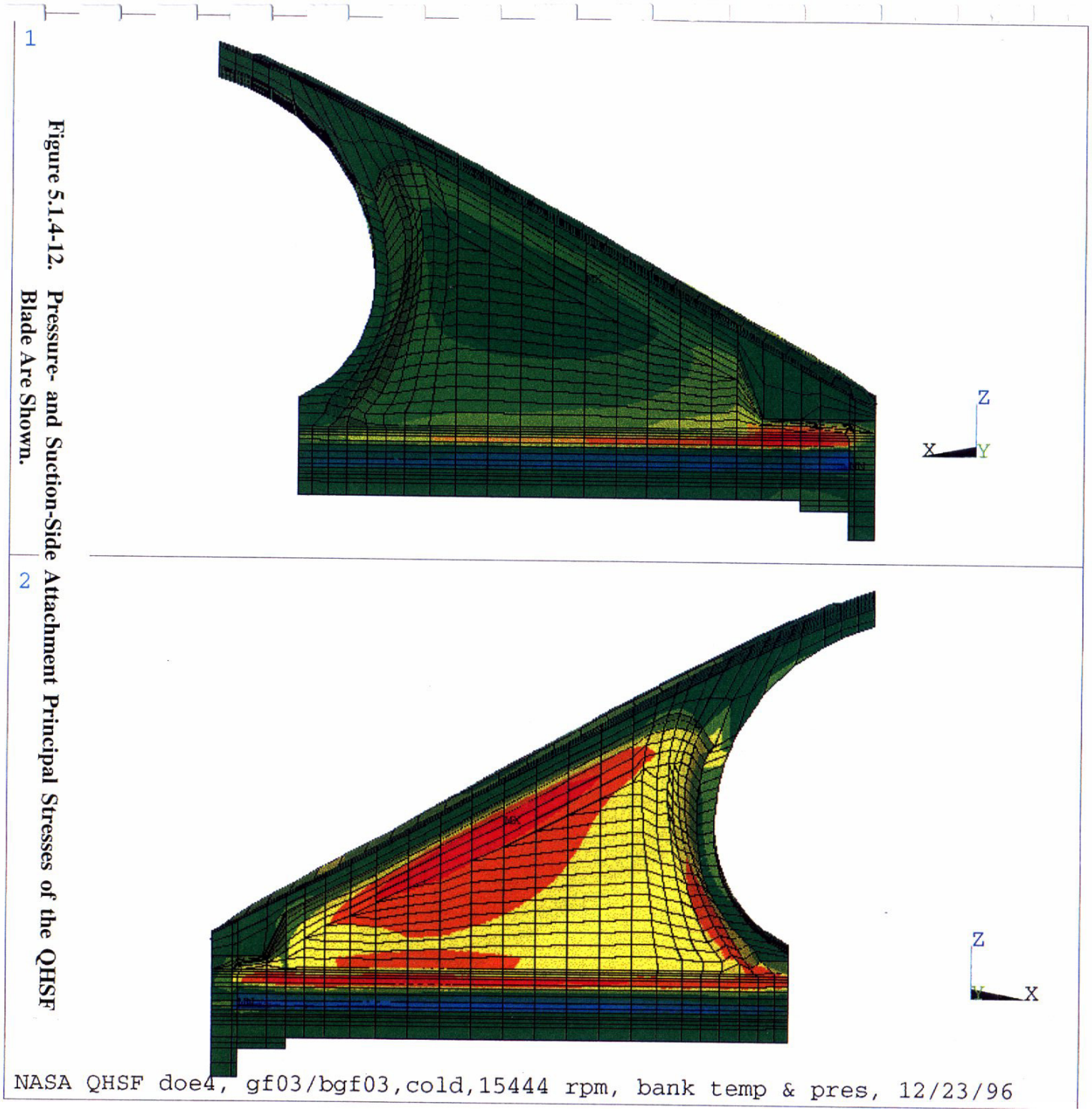

Figure 5.1.4-12. Pressure- and Suction-Side Attachment Principal Stresses of the QHSF Blade Are Shown.

Figure 5.1.4-13. Pressure- and Suction-Side Attachment Equivalent Stresses of the QHSF Blade Are Shown.

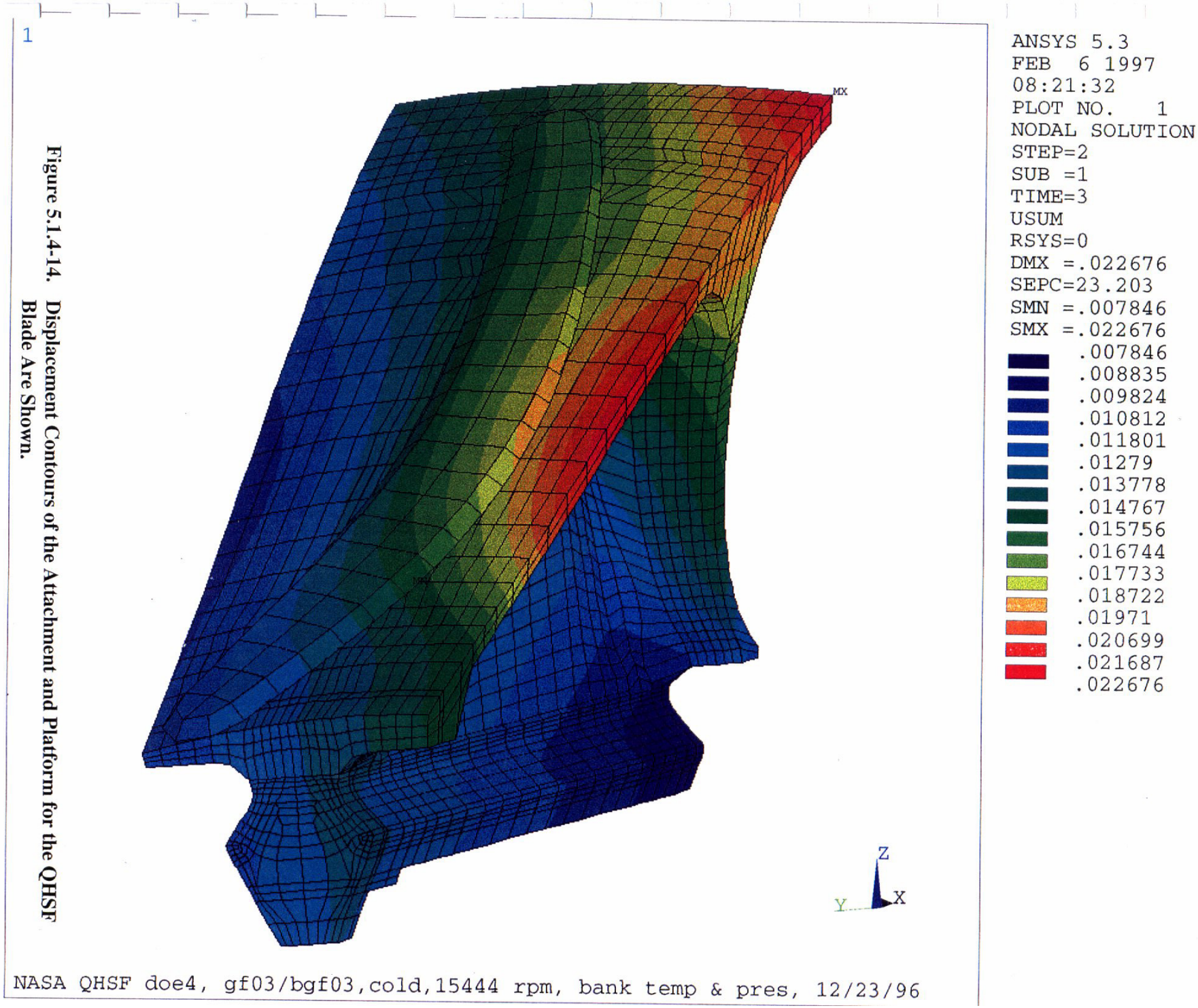

Figure 5.1.4-14. Displacement Contours of the Attachment and Platform for the QHSF Blade Are Shown.

Table 5.1.4-2 QHSF Vibration Results - Natural Frequencies

	Mode				
Conditions	1	2	3	4	5
Room temp., 0 rpm	172	520	879	1136	1521
ADP temp, 15444 rpm	349	704	984	1485	1568
Fixed-Root, 0 rpm	177	599	879	1333	1556
Fixed Root, 15444 rpm	373	791	1020	1600	1682

The resulting Campbell diagrams are shown in Figure 5.1.4-15 along with the first six excitation orders. Vertical lines highlight the design speed of 15444 rpm as well as the maximum test speed of 110 percent. Design speed frequency margin with respect to the nearest excitation order for the first five modes is shown in Table 5.1.4-3.

Table 5.1.4-3 QHSF Frequency Margin Summary

	Mode/Engine Order				
Conditions	1/2E	2/3E	3/4E	4/6E	5/6E
ADP temp, 15444 rpm	58%	15%	5%	6%	2%

As the Campbell diagrams illustrate, a significant frequency shift was experienced for modes 2 and 4 after adding the attachment to the model. The shift in mode 2 frequency of 11 percent was especially relevant as it moved the 3E crossing to within the operating range.

Figures 5.1.4-16 through 5.1.4-20 show contour plots of the first 5 modes at design point conditions with mode shapes normalized to unit generalized mass. Normalized vibratory stress (maximum absolute value principal stress) contours for each mode are shown in Figures 5.1.4-21 through 5.1.4-25.

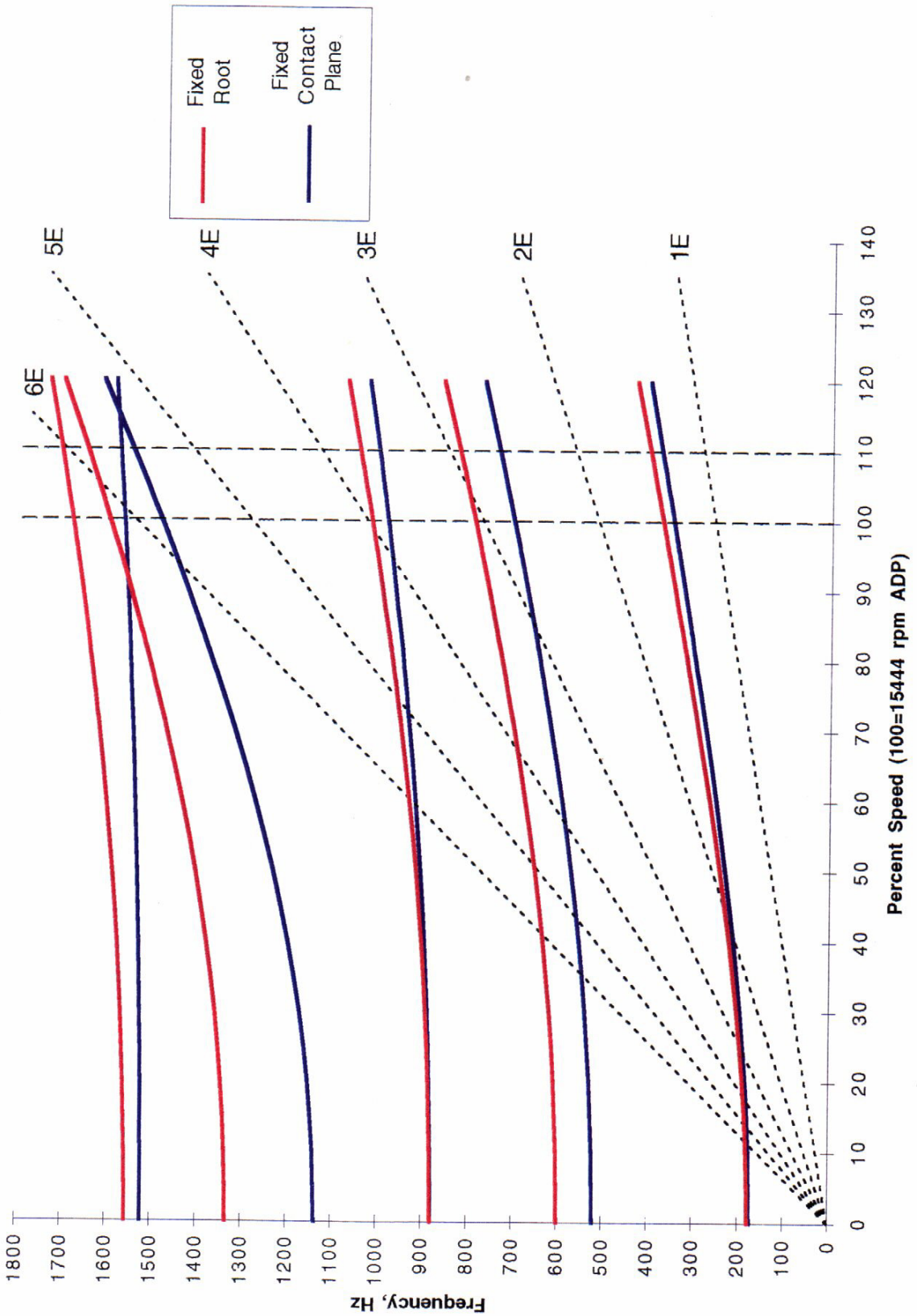

Figure 5.1.4-15. Cambell Diagram for the QHSF Rotor Blade Shows the Mode 3 Crossing in the Fan Operating Range.

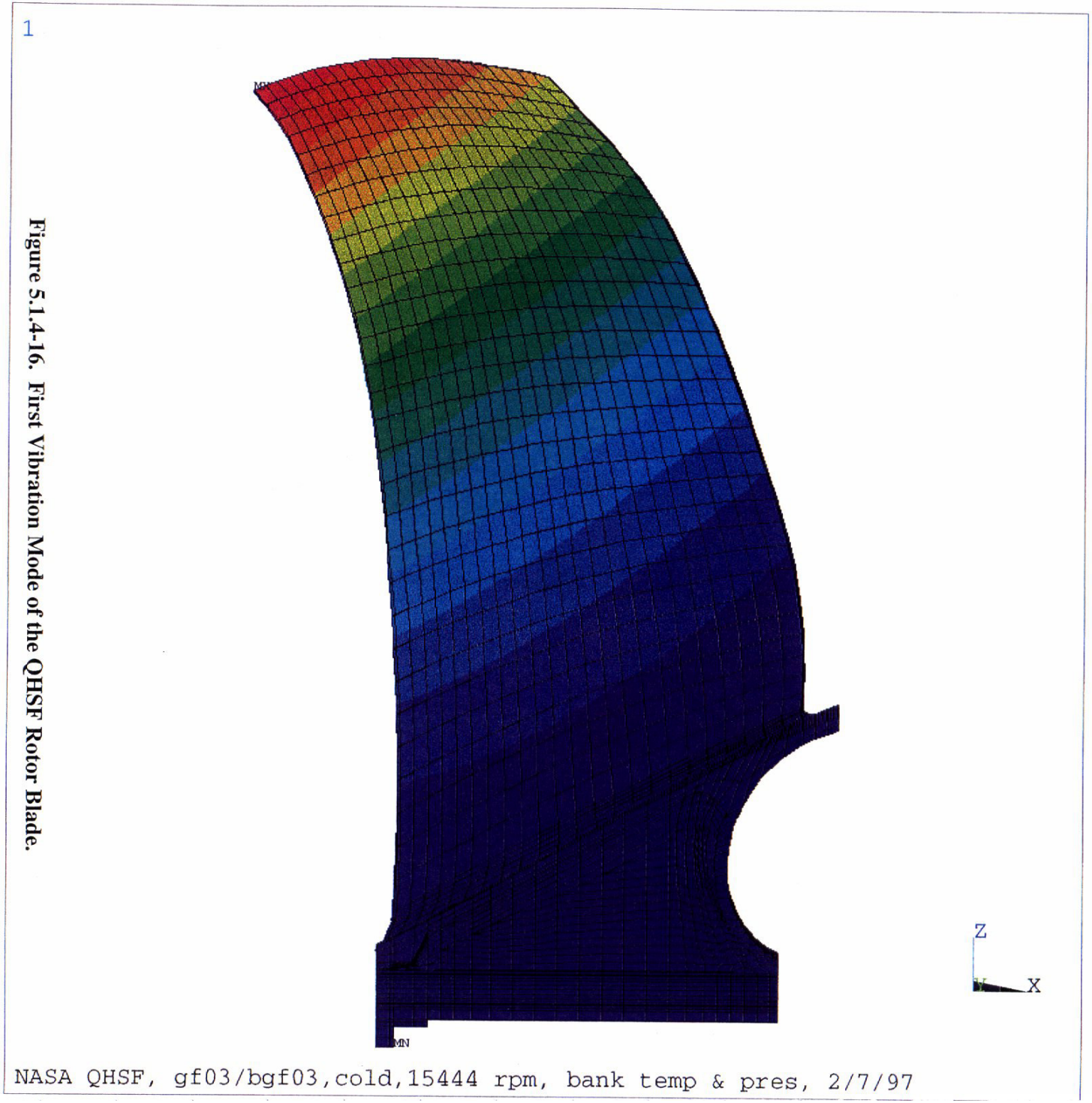

Figure 5.1.4-16. First Vibration Mode of the QHSF Rotor Blade.

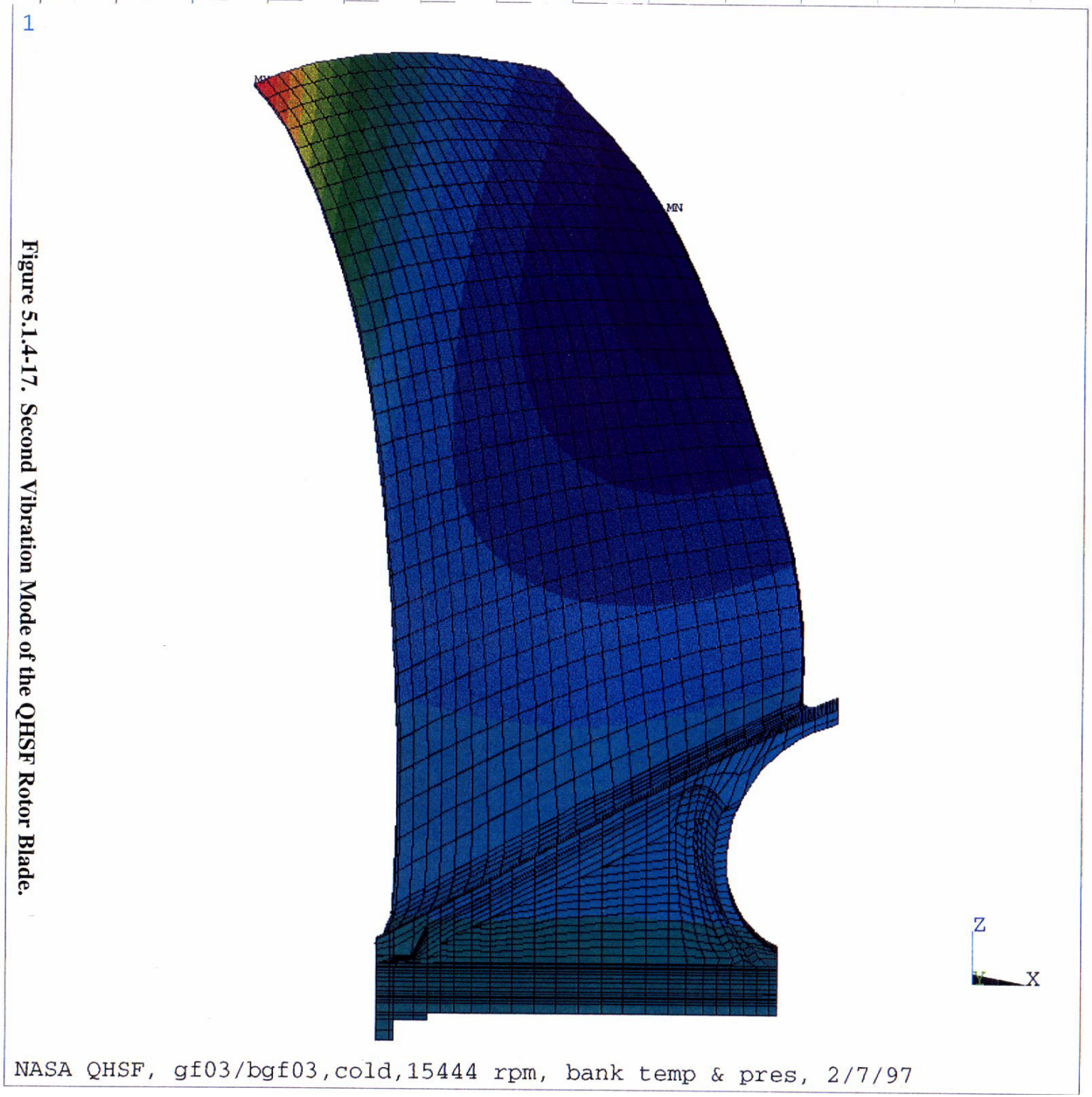

Figure 5.1.4-17. Second Vibration Mode of the QHSF Rotor Blade.

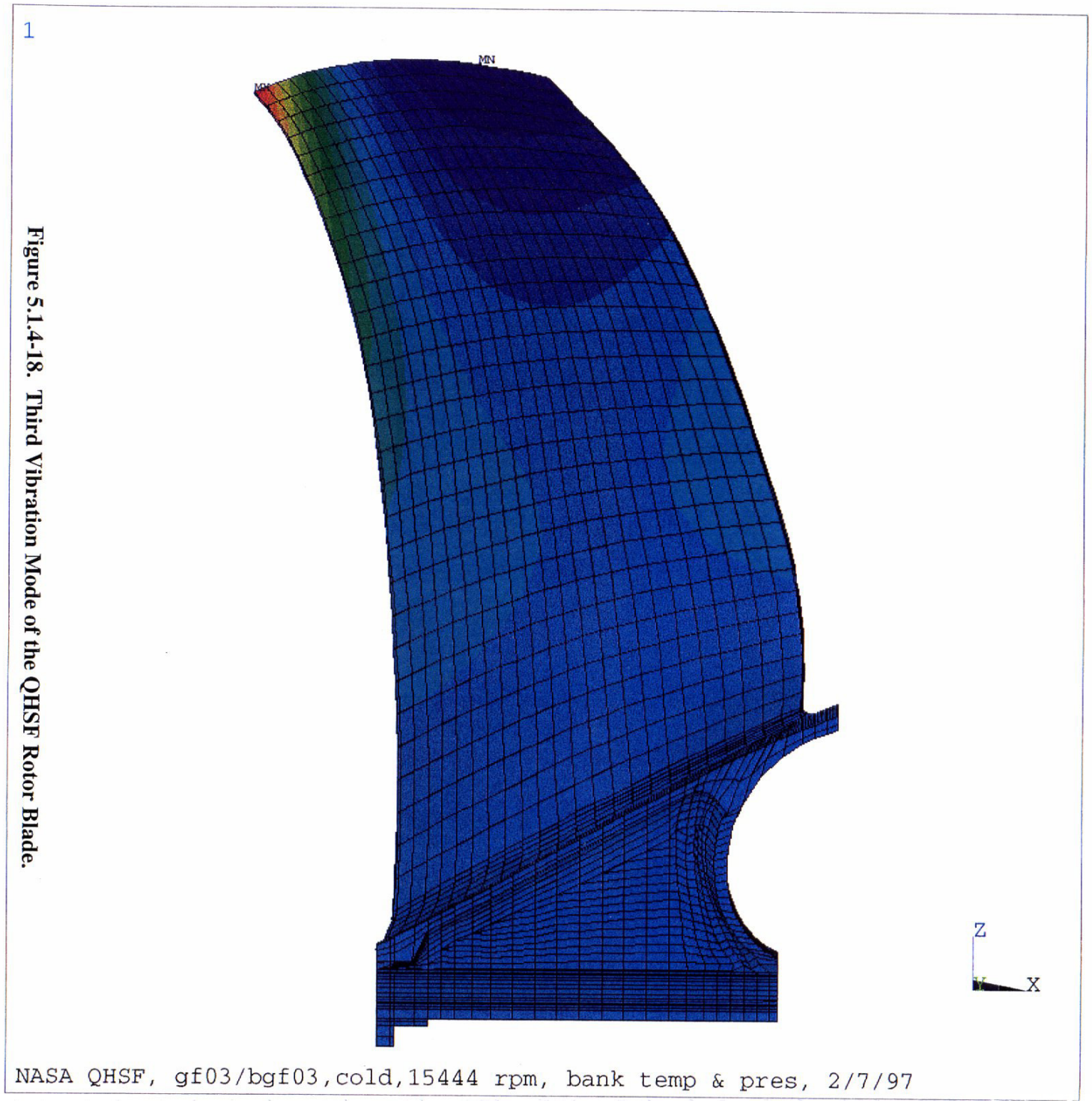

Figure 5.1.4-18. Third Vibration Mode of the QHSF Rotor Blade.

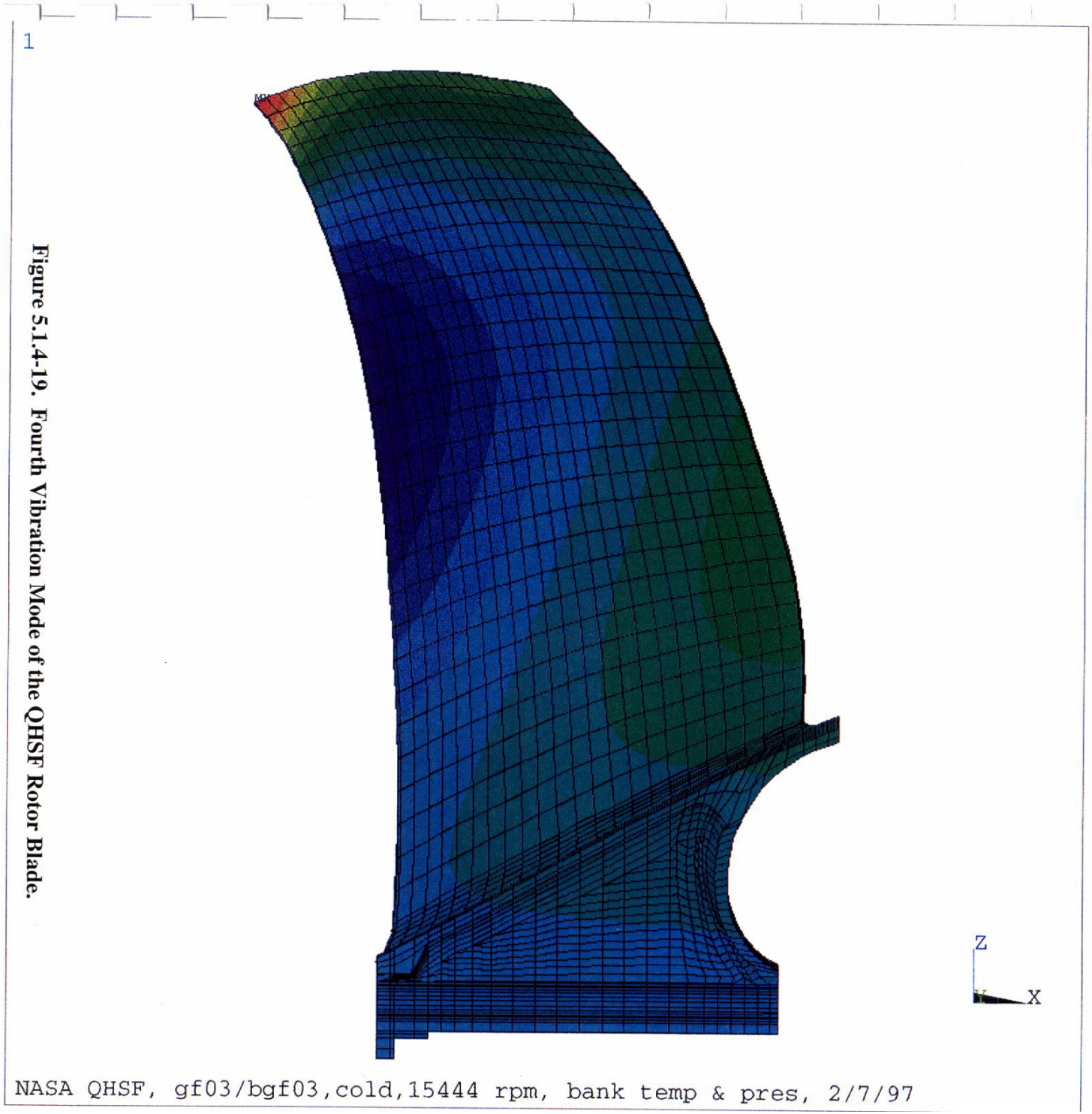

Figure 5.1.4-19. Fourth Vibration Mode of the QHSF Rotor Blade.

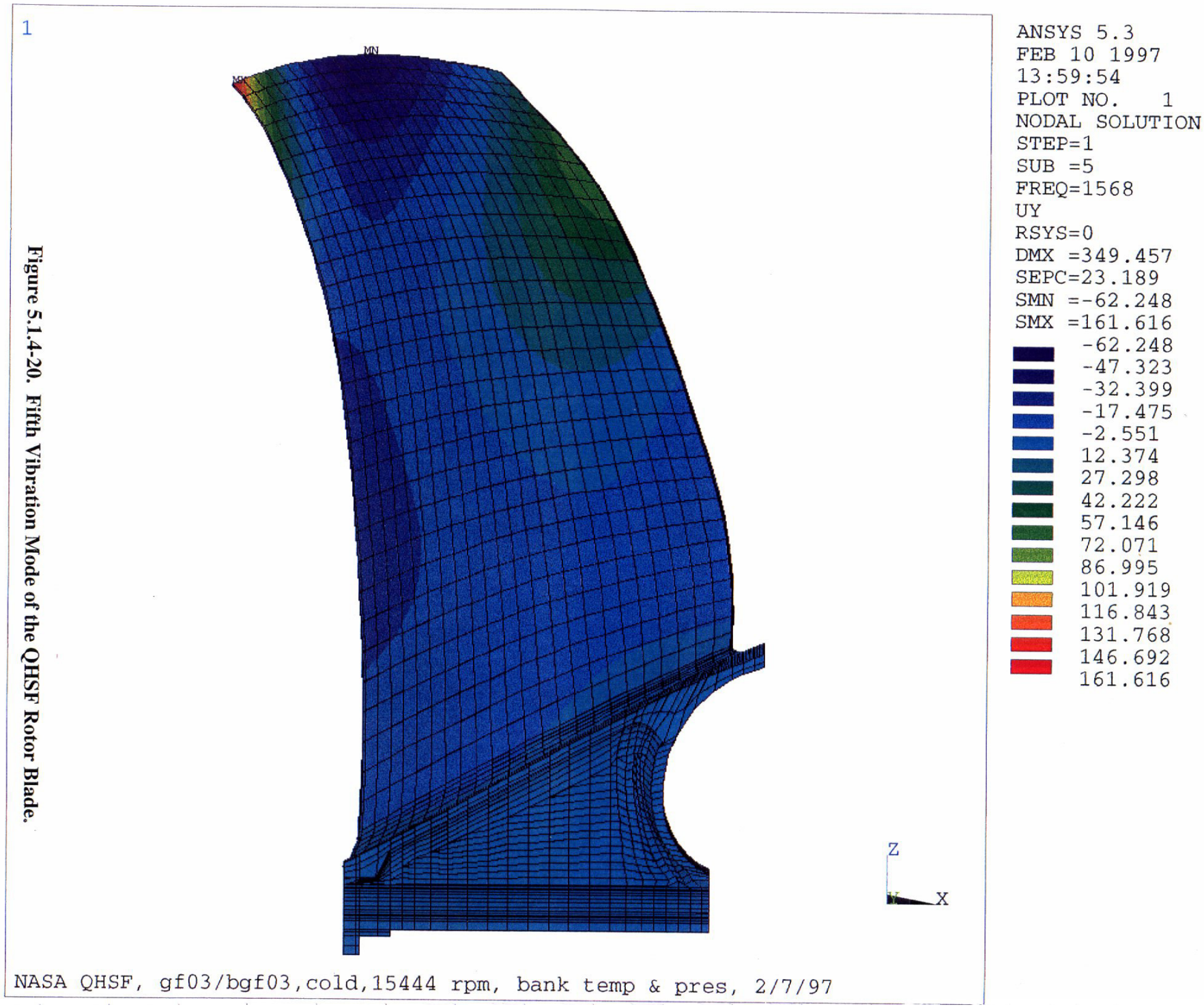

Figure 5.1.4-20. Fifth Vibration Mode of the QHSF Rotor Blade.

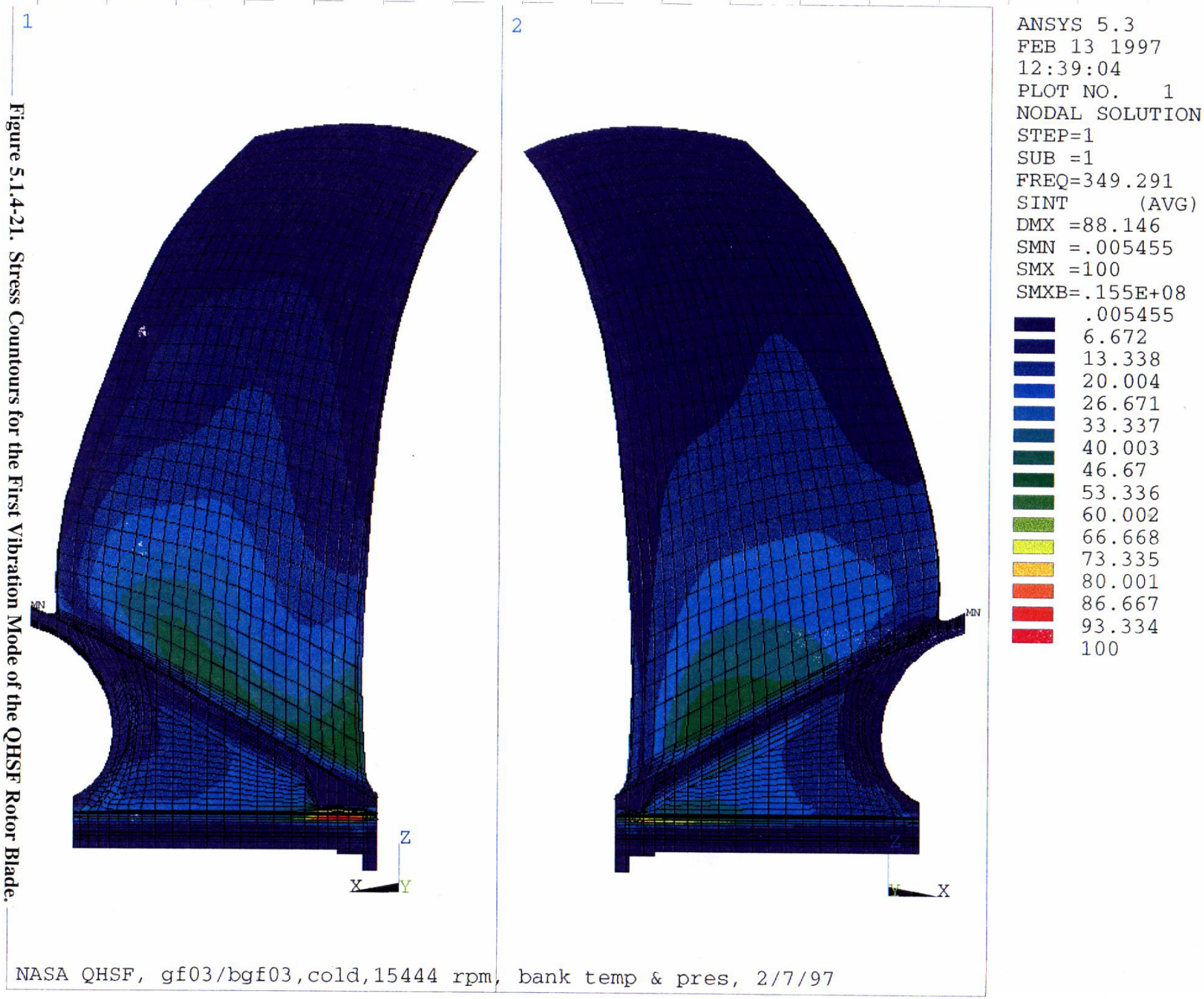

Figure 5.1.4-21. Stress Countours for the First Vibration Mode of the QHSF Rotor Blade.

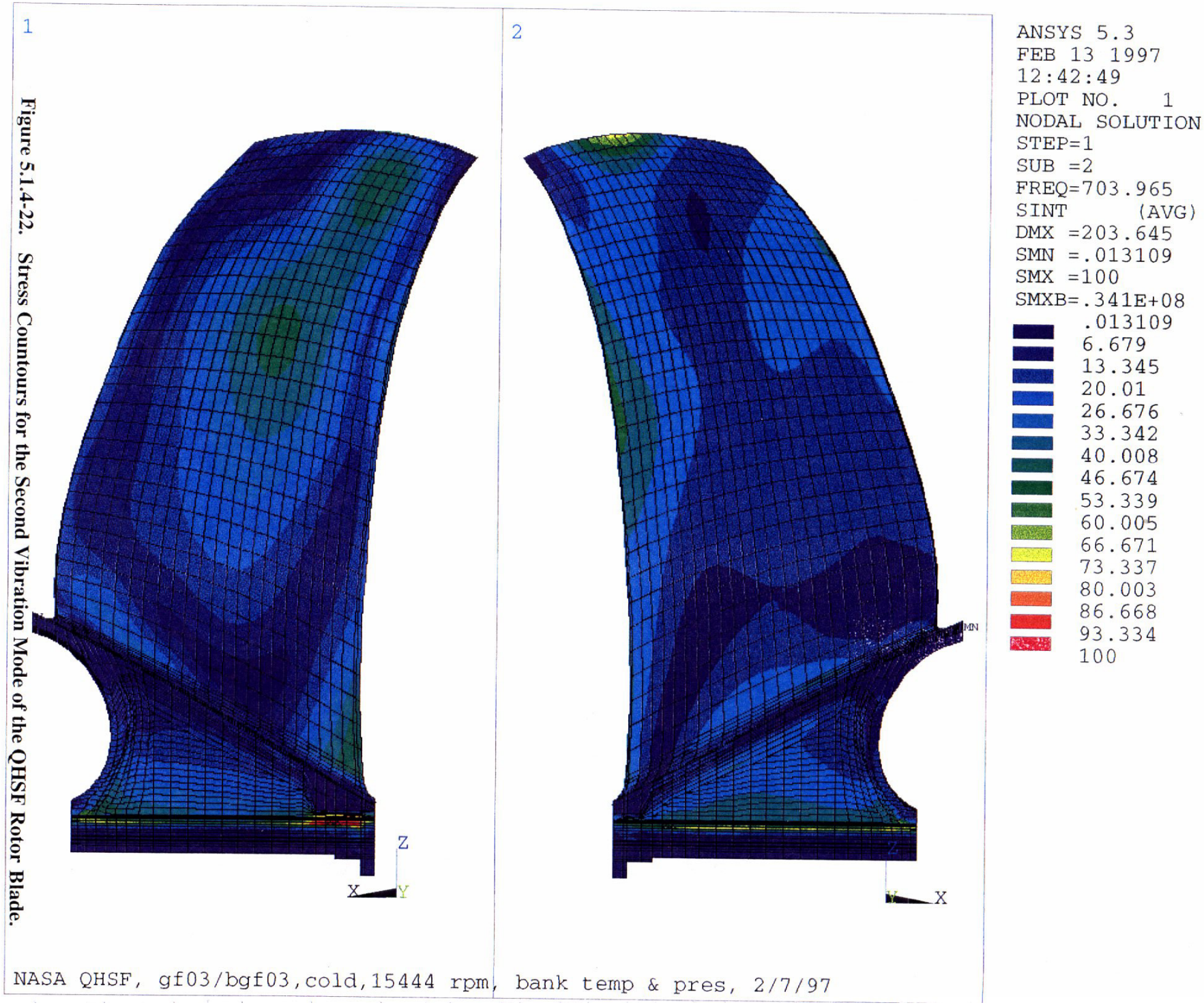

Figure 5.1.4-22. Stress Countours for the Second Vibration Mode of the QHSF Rotor Blade.

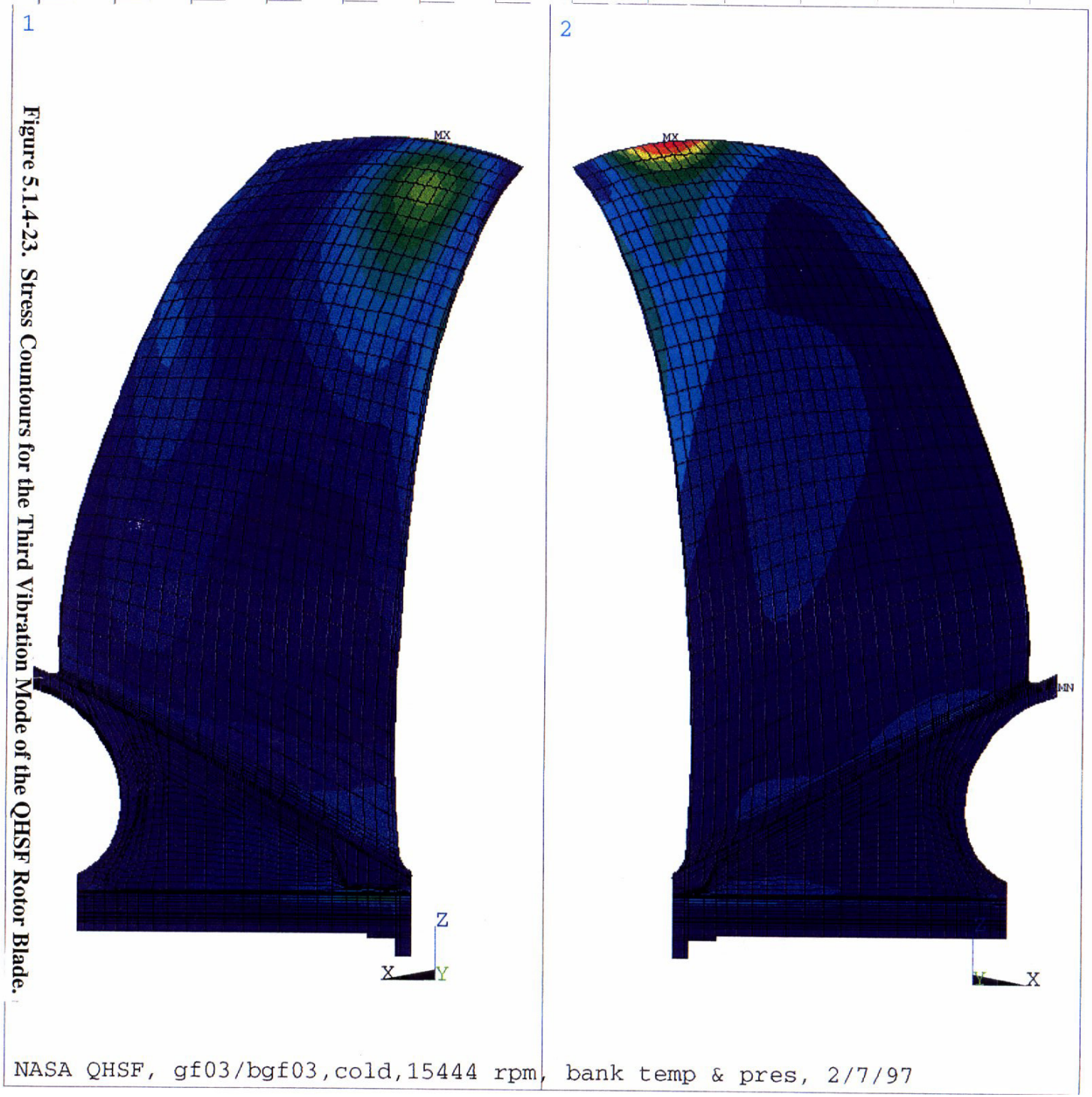

Figure 5.1.4-23. Stress Countours for the Third Vibration Mode of the QHSF Rotor Blade.

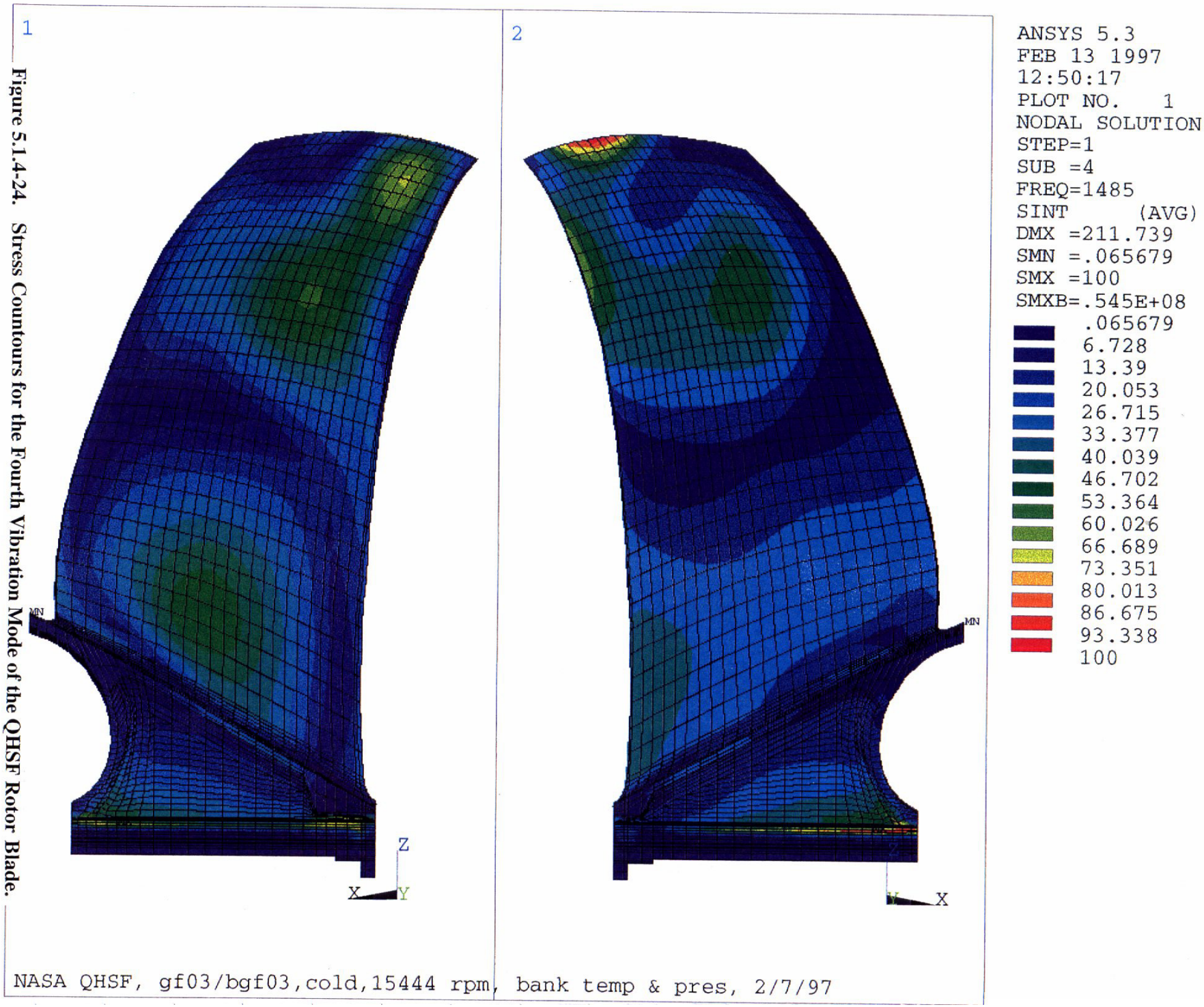

Figure 5.1.4-24. Stress Countours for the Fourth Vibration Mode of the QHSF Rotor Blade.

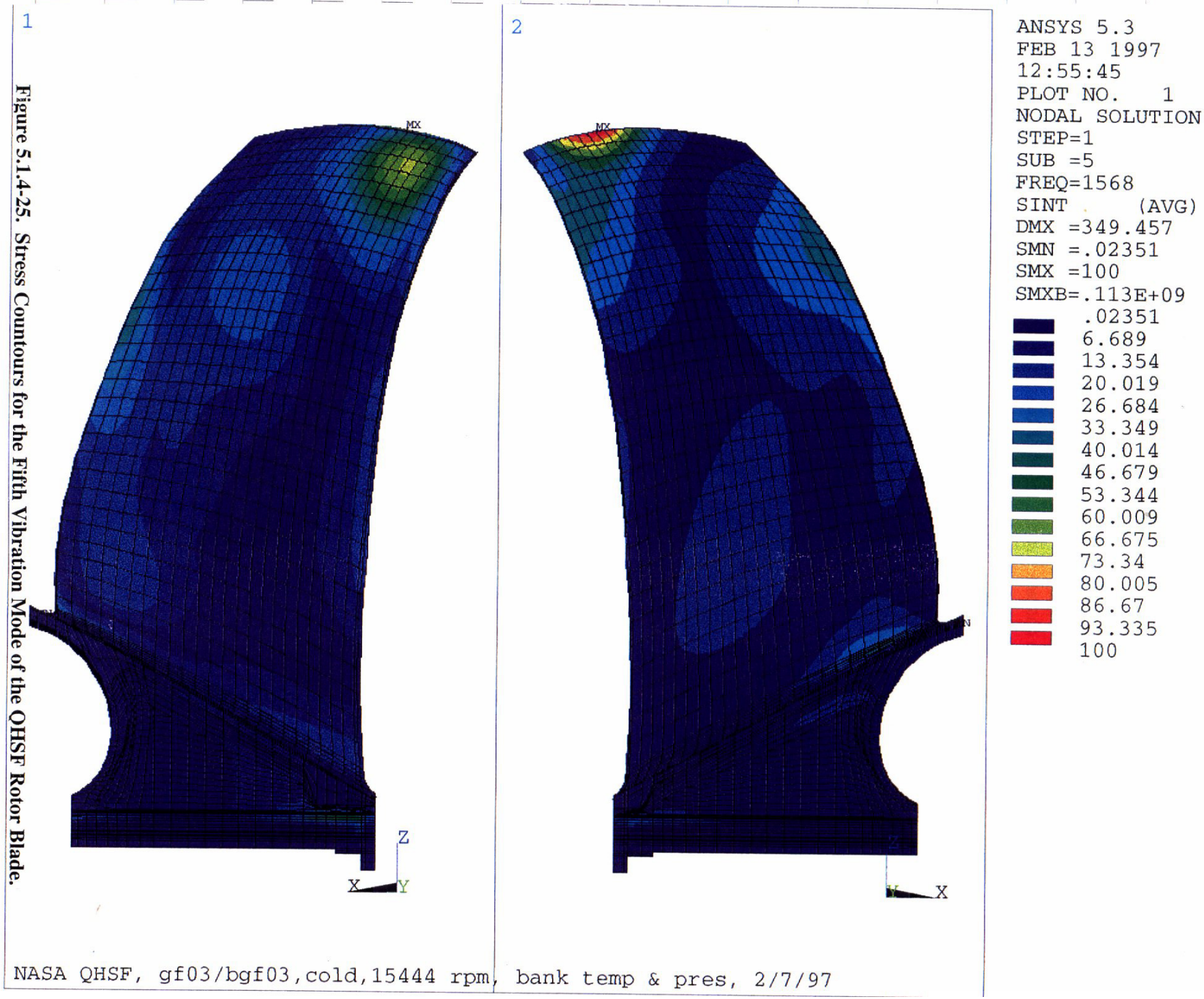

Figure 5.1.4-25. Stress Countours for the Fifth Vibration Mode of the QHSF Rotor Blade.

5.1.4.5 Flutter Parameters

AE criteria for flutter is based on reduced frequency (fc/V), where f is the blade natural frequency, c is the chord at 75 % span, and V is the design-point relative velocity at 75 % span. The twist-to-flex ratio is used to characterize the mode as being flexure-dominate (small ratio) or torsion-dominant (large ratio).

The reduced frequency flutter parameter calculations are shown in Table 5.1.4-4.

Table 5.1.4-4 QHSF Flutter Parameter Summary

Parameter						
					Twist/Flex	
Mode	f (Hz)	c (in)	V (ft/sec)	fc/V	75%	95%
1	349	4.31	1435	0.6	0.45	0.37
2	704	4.31	1435	1.1	4.8	1.1
3	984	4.31	1435	1.6	1.3	1.8
4	1485	4.31	1435	2.3	1.2	0.62
5	1568	4.31	1435	2.5	0.82	0.42

As can be seen in the above table, mode 1 was predominantly flexure, and the reduced frequency of 0.6 exceeded AE's minimum design criteria for bending mode. Modes 2 and 3 both displayed significant torsional activity hence AE's minimum design criteria for torsion mode was applied. Mode 2 appeared to be moderately aggressive, due in part to the frequency shift associated with the attachment.

Dynamic response measurements, either with strain-gages or by other means, are highly recommended to ensure flutter free operation.

5.1.4.6 Bird Ingestion

A preliminary Foreign-Object-Damage (FOD) assessment performed on the QHSF blade indicated leading-edge thickness parameters to be well within successful AE experience. This analysis is comparative in nature and considers only spanwise geometric characteristics, LE thickness distribution, blade count, metal angles, bird weight, as well as other parameters. The computed damage tolerance factors are compared with a database consisting of very successful, marginal, and poor designs. This preliminary analysis however, can not account for the high degree of forward sweep and tangential lean built into the QHSF, which will be accounted for using NOSAPM.

A more accurate prediction of ingestion damage was obtained using the NOSAPM code developed for the Air Force Wright Aeronautical Laboratories (Reference 15). NOSAPM can perform an inelastic, transient, impact response analysis on the rotating blade, and predict with good success, the resulting permanent deformations of the airfoil. A key characteristic of the code is a loading model which allows an interactive determination of the pressure distribution on the impacted blade based on the blade's instantaneous, deflected shape. With simple user input defining the geometry and initial conditions, i.e., rotor rpm, bird weight and trajectory, etc., the program solves for the blade transient response.

Figure 5.1.4-26 shows the impact model in detail. Since the impact analysis is nonlinear, the model was constructed using the "cold" geometry as described above. The shaded region represents the predefined set of impacted elements centered upon the designated impact radius.

As certification requirements vary with the inlet area of the fan, this analysis was performed at baseline fan scale. The bird weight, impact radius, as well as the rotor rotational speed were chosen to match conditions defined for a FAA certification test of the baseline fan. These conditions were defined as follows:

Rotor Speed	88.8%
Bird Weight	1.5 pounds
Aircraft Forward Speed	138 knots
Impact Radius	56% span

Transient response of the blade due to the bird impact is illustrated in Figure 5.1.4-27 with time histories of the tip leading and trailing edges. The maximum displacement of approximately 3.1 inches occurs at t=0.011 seconds at the tip trailing edge. The maximum displacement is overlayed on the undeformed blade in Figure 5.1.4-28. The undeformed blade shown includes the effects of rotational speed.

At the conclusion of the transient (t=0.053 seconds) the permanent deformations are readily visible. Figure 5.1.4-29 shows the deformation contours overlayed on the undeformed blade. Damage appears to be localized to the leading edge tip where the maximum deformation is 0.36 inches. The remainder of the blade appears to have been unaffected by the impact. Figure 5.1.4-30 presents another view of the deformation superimposed on the undeformed geometry.

An identical analysis performed on the baseline blade revealed contrasting results. Instead of localized deformation like the QHSF, the baseline blade exhibited an overall gross, albeit very small, torsional deformation (restagger).

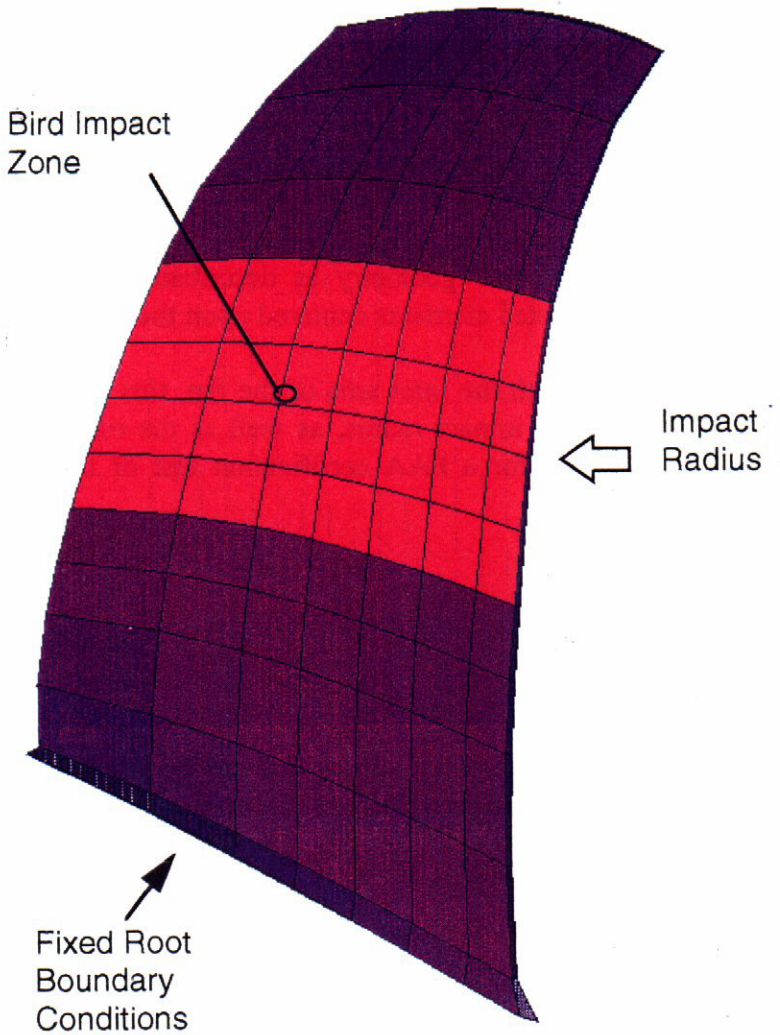

Figure 5.1.4-26. Impact Model for Assessing the Bird Strike Capability of the QHSF Rotor.

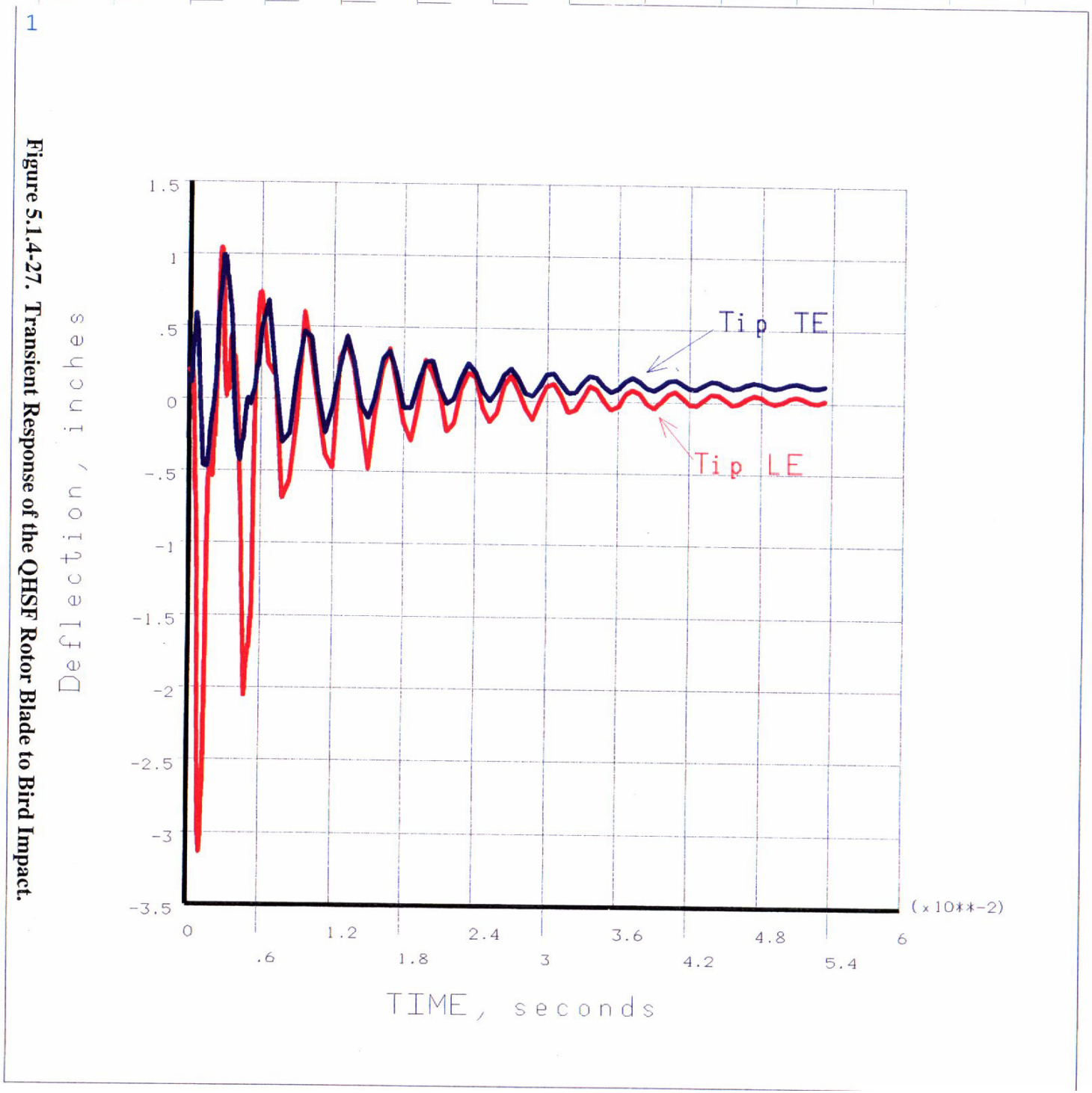

Figure 5.1.4-27. Transient Response of the QHSF Rotor Blade to Bird Impact.

Figure 5.1.4-28. Maximum Displacement of the QHSF Rotor Blade Due to Bird Impact.

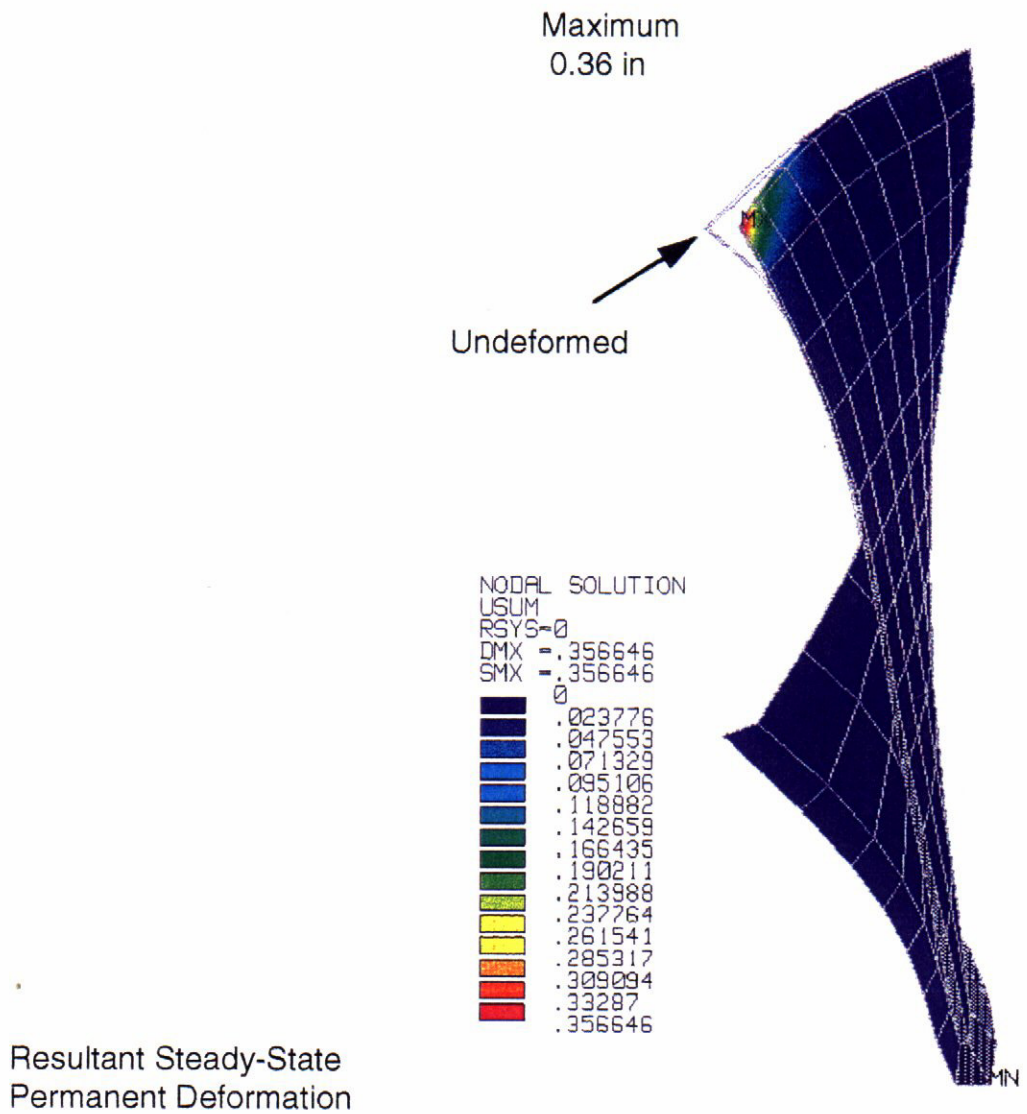

Figure 5.1.4-29. Permanent Deformation of the QHSF Rotor Blade After Bird Strike Compared to the Undeformed Blade.

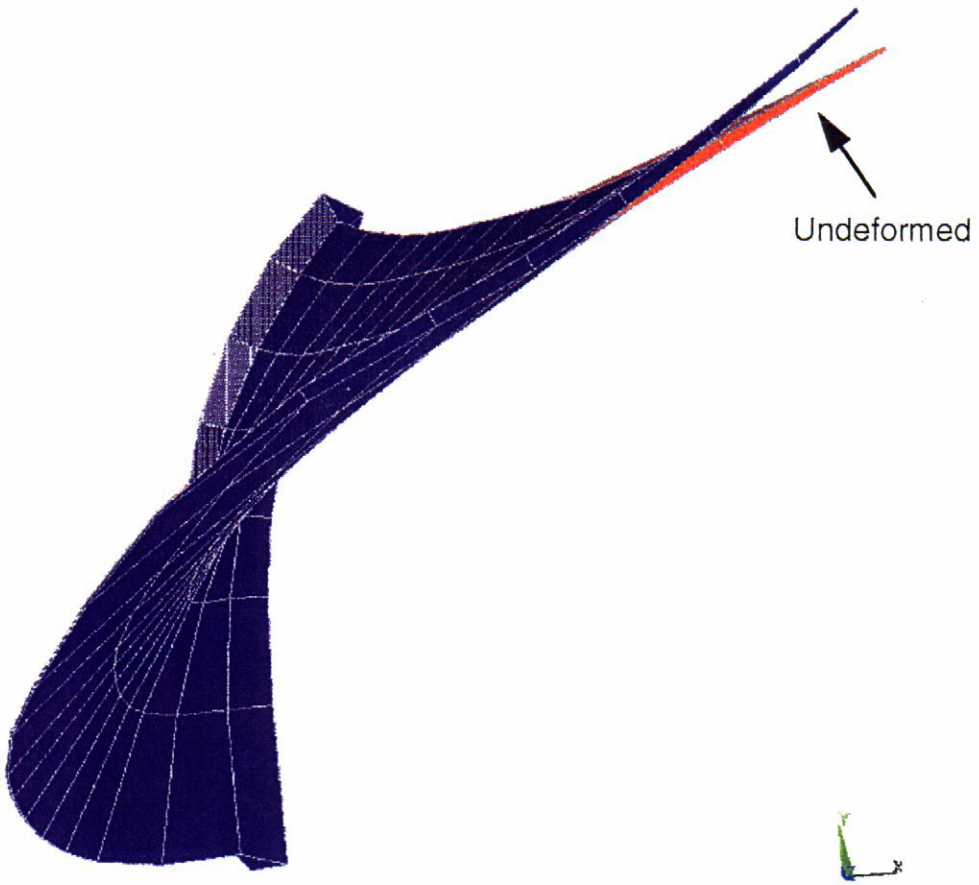

Figure 5.1.4-30. Tip View of Permanent Deformation of the QHSF Rotor Blade After Bird Strike Compared With the Undeformed Blade.

5.2 Stator

The analytical tools used in the stator aerodynamic design and analysis were the AXCAPS streamline curvature code and the DAWES 3D viscous CFD code. AXCAPS was used to perform a 2D streamline solution, calculating velocity triangles based on user-specified blade row performance profiles and generating airfoil section coordinates for use in mechanical and CFD analysis. These airfoil sections are generated according to user specifications of chord, leading and trailing edge angles (or incidence and deviation), mean camber line angles, stacking, and thickness. In this design, AXCAPS was used mainly as a geometry generator since the extreme vane stacking was felt to make some of the 2D calculations questionable. An example is the disagreement in leading edge swirl angle seen between AXCAPS and DAWES in the vane stacking FF 2.

The rotor used in the stator design AXCAPS model changed as the stator design proceeded. The stator stacking DOE was done using the "optc" rotor which was the most current available at the time. The rest of the design was done using the final "gf03" rotor. The rotor exit velocity triangles which set the stator inlet velocity triangles were taken from the rotor DAWES solution at the design point. Some profile smoothing and adjustment was needed near the endwalls since the AXCAPS streamline curvature code cannot impose a no-slip condition at flowpath and airfoil surfaces. The flow used in the stator design AXCAPS cases was the flow predicted by the rotor DAWES model.

The actual stator performance calculations used during the stator design were performed with the DAWES code. The DAWES calculation grid used for this stator was as similar as possible to the grid used in the baseline stator DAWES model, with 41 nodes pitchwise, 71 nodes spanwise, and 121 nodes streamwise.

The model was run through enough timesteps to reach acceptable convergence. One of the boundary conditions in the DAWES model is the exit static pressure which, if the inlet boundary conditions are held constant, sets the flow. For the design point runs in the latter part of the design the model exit static pressure was adjusted to match the flow predicted by DAWES in the stator model to the flow predicted by DAWES in the rotor model to within 0.5%.

5.2.1 Stator Geometry

The final vane geometry was reached when the composite vane thickness criteria were met. This geometry is tabulated in Appendix I.

The vane leading and trailing edge, stagger, and camber angles are shown in Figure 5.2.1-1. The stator solidity, which is the same as the baseline stator, is shown in Figure 5.2.1-2. Vane maximum thickness/chord, where maximum thickness is defined as tangential thickness, is shown in Figure 5.2.1-3. The increase in thickness around 90% span was needed to maintain a desired normal thickness with an increasing vane lean angle. The waves in the thickness were not completely understood, but they were necessary to meet the required normal thickness profile; and, similar waves were seen in the required tangential leading and trailing edge

thicknesses. They were at least partially due to the fact that the vane lean angle at the maximum thickness location and at the trailing edge was slightly wavy.

The maximum thickness location is shown in Figure 5.2.1-4. The maximum thickness was located at 60% of the mean camber line length as in the baseline vane. This was set by mechanical, aerodynamic, and producibility considerations. The leading and trailing edge radii (tangential), shown in Figure 5.2.1-5, are the radii of semicircles that form the vane section leading and trailing edges. They were scaled appropriately for the 22-inch rig. Edge thickness was approximately twice these radii. This was not exactly true for the leading edge since the vane leading edge was formed by a cubic generated using the semicircular leading edge as a starting point. The edge radii show some waviness similar to the maximum thickness. These were what was necessary to match the normal edge thicknesses required for composite producibility.

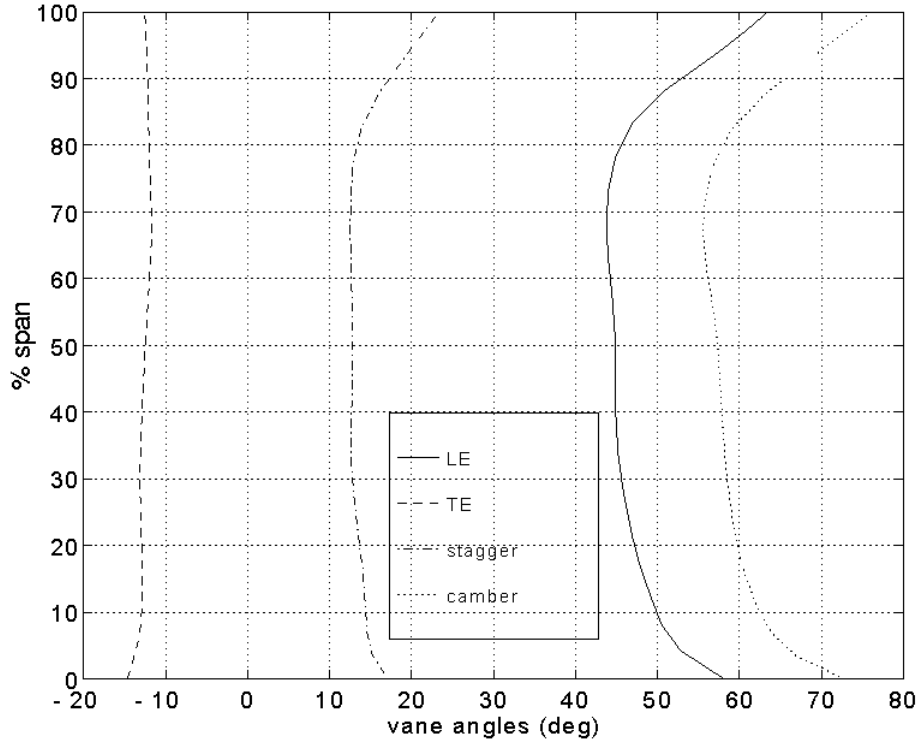

Figure 5.2.1-1. QHSF Stator Angles

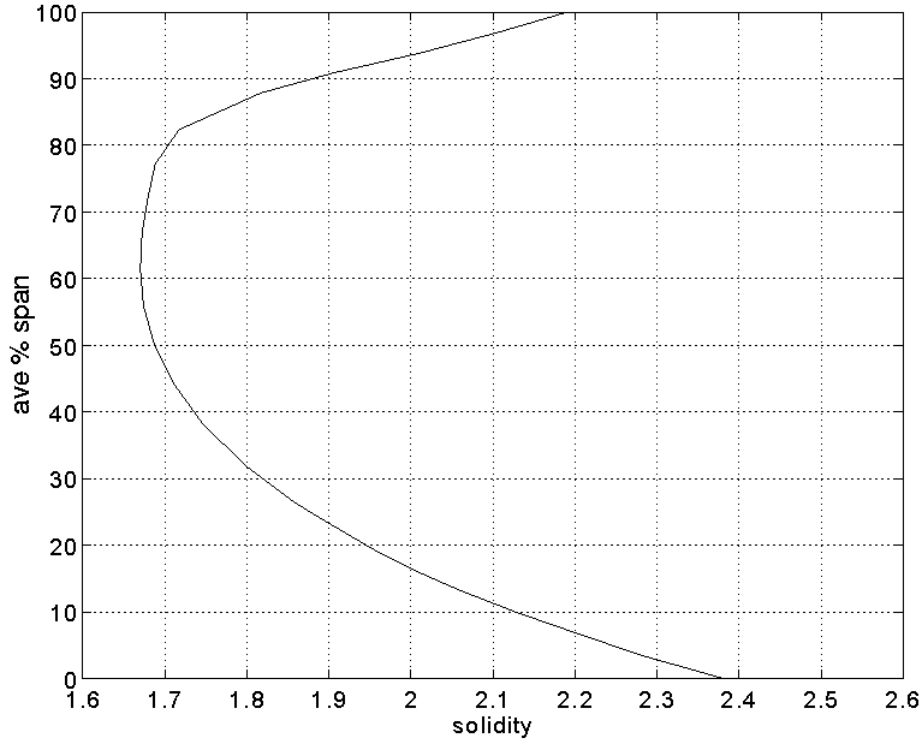

Figure 5.2.1-2. QHSF Stator Solidity

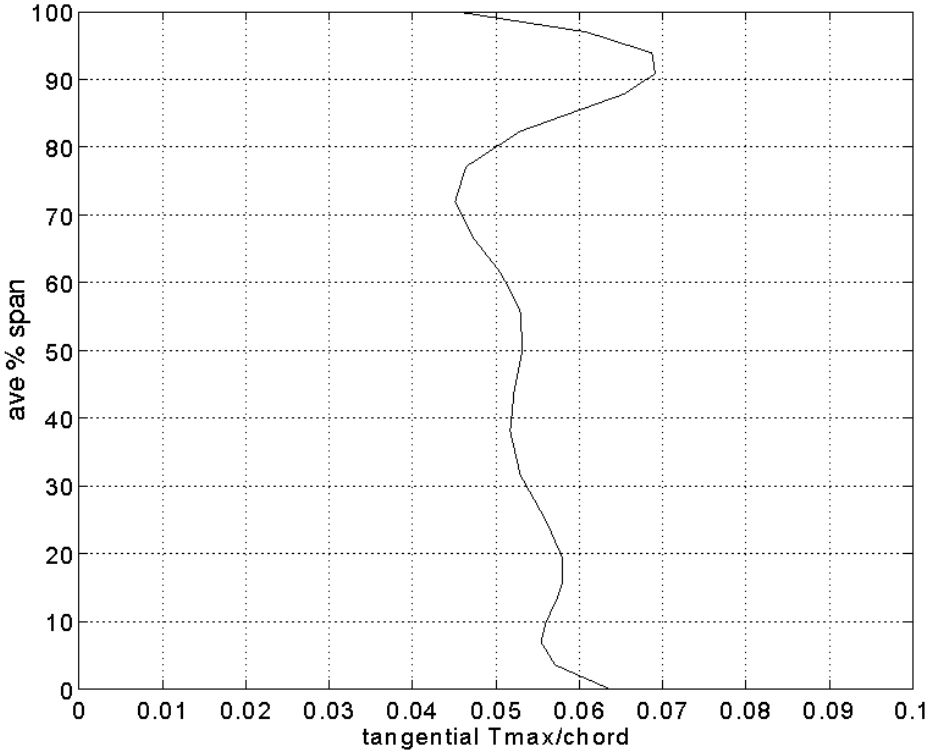

Figure 5.2.1-3. QHSF Stator Tmax/c

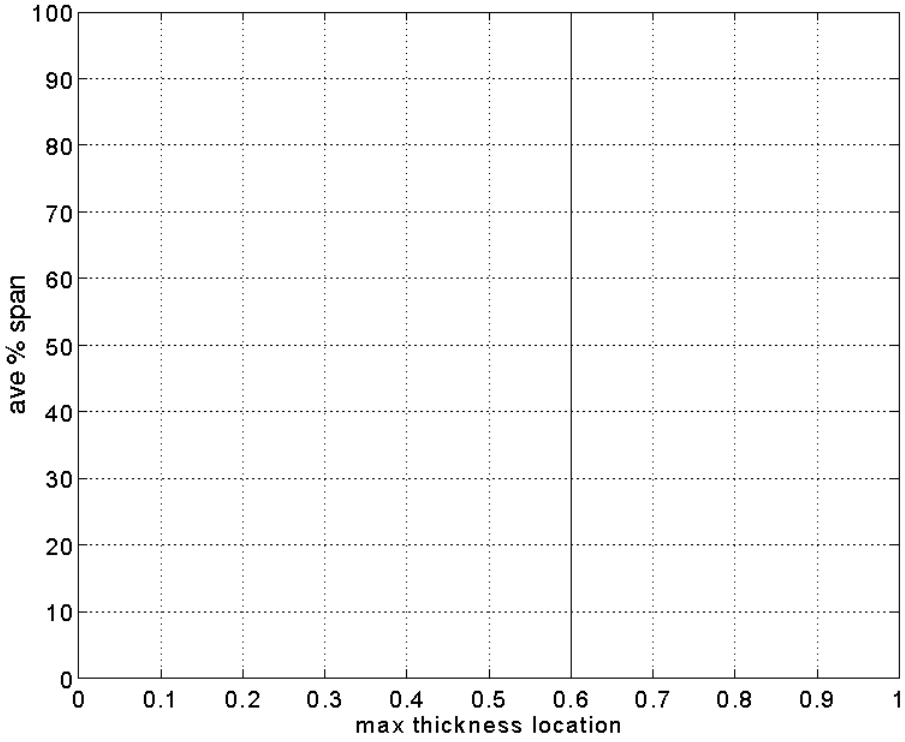

Figure 5.2.1-4. QHSF Stator Max Thickness Location

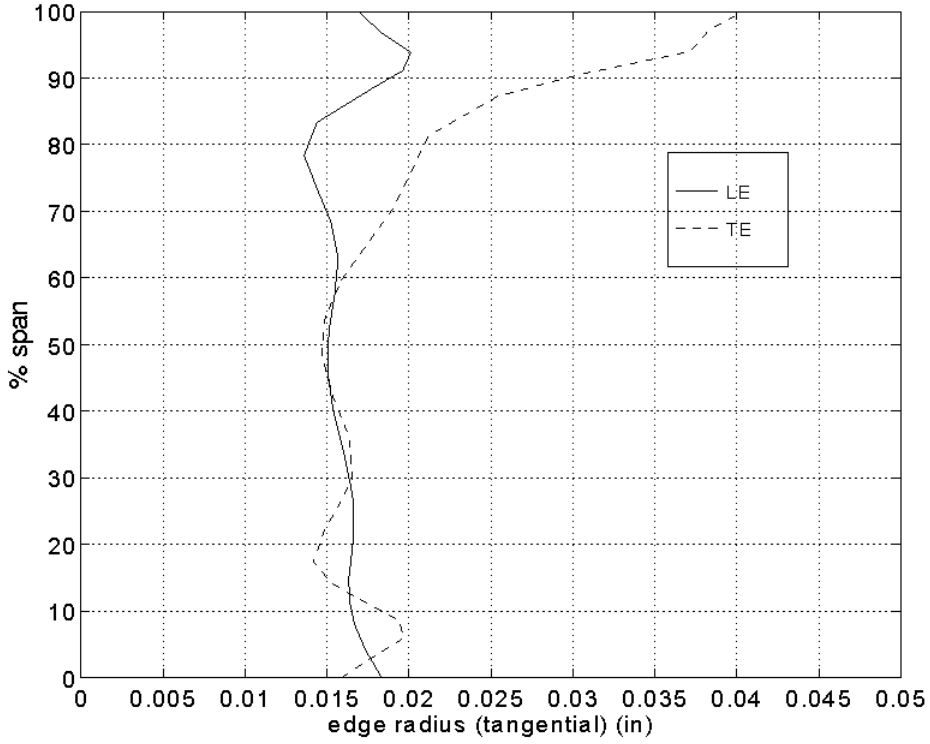

Figure 5.2.1-5. QHSF Stator Edge Radii (Rig Size)

The vane chord, scaled for the rig, is shown in Figure 5.2.1-6. The chord is determined from the solidity and vane count, which were maintained from the baseline stator. Figure 5.2.1-7 shows the vane section leading edge tangential shifts applied to produce the required vane tangential stack. Figures 5.2.1-8 and -9 show the chordwise distribution of mean camber line angle in dimensional (Fig. 5.2.1-8) and non-dimensional (Fig. 5.2.1-9) form.

These plots show how the vane camber was distributed from the leading edge (0) to the trailing edge (1). Figure 5.2.1-8 shows actual angles. At the leading and trailing edge, these are the hub, midspan, and tip angles from Figure 5.2.1-1. This figure provides a view of the actual curvature for different areas of the vane. Figure 5.2.1-9 shows the non-dimensionalized version which is how these curves are usually used in design. This allows the leading and trailing edge angles (or incidence and deviation) to be varied without the need to change these curves. The non-dimensional curves were retained from the baseline stator. The curves in Figure 5.2.1-8 were slightly different from the baseline stator since the leading and trailing edge vane angles were different.

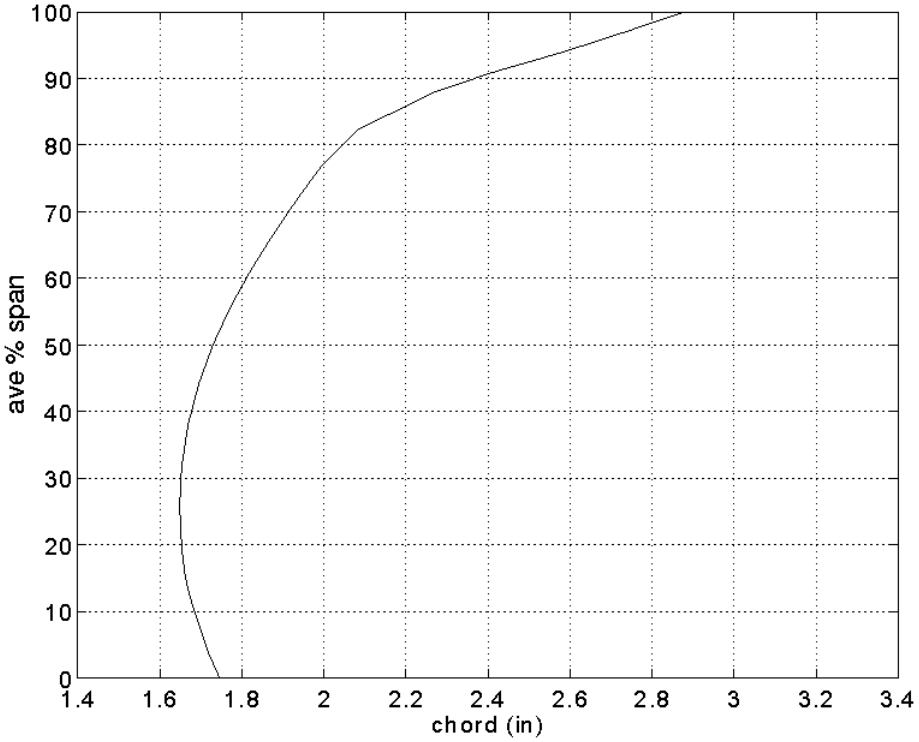

Figure 5.2.1-6. QHSF Stator Chord (Rig Size)

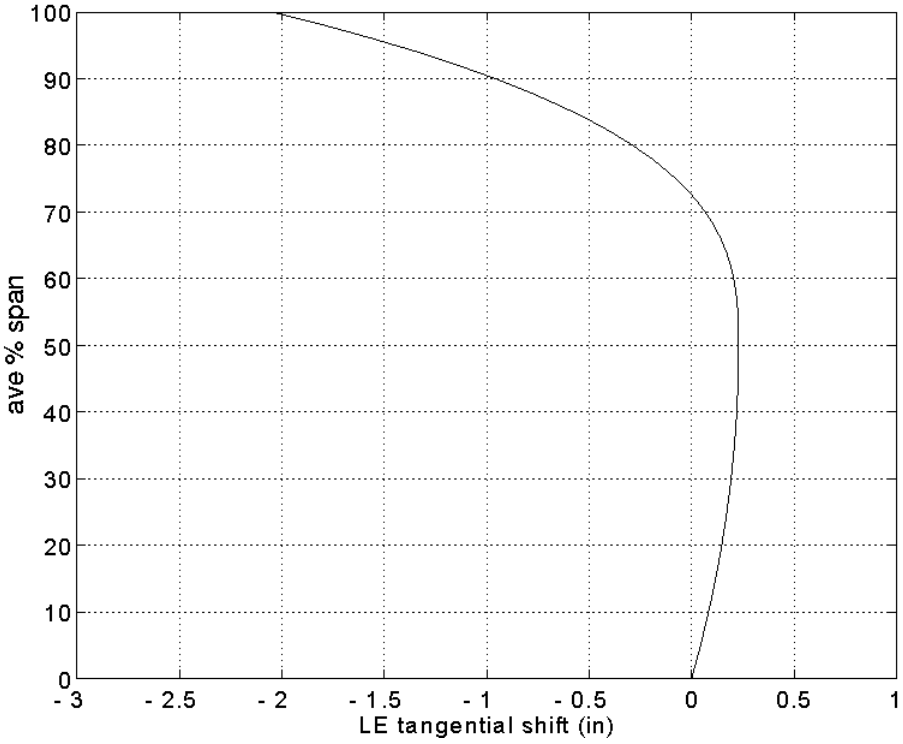

Figure 5.2.1-7. QHSF Stator LE Tangential Shifts (Rig Size)

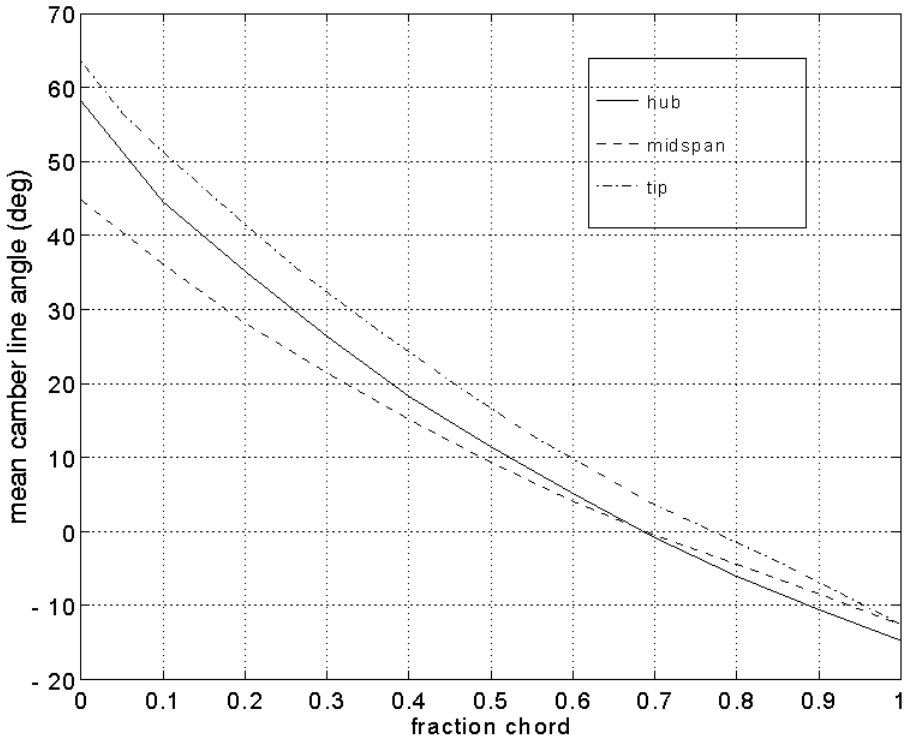

Figure 5.2.1-8. QHSF Stator Mean Camber Line Angles

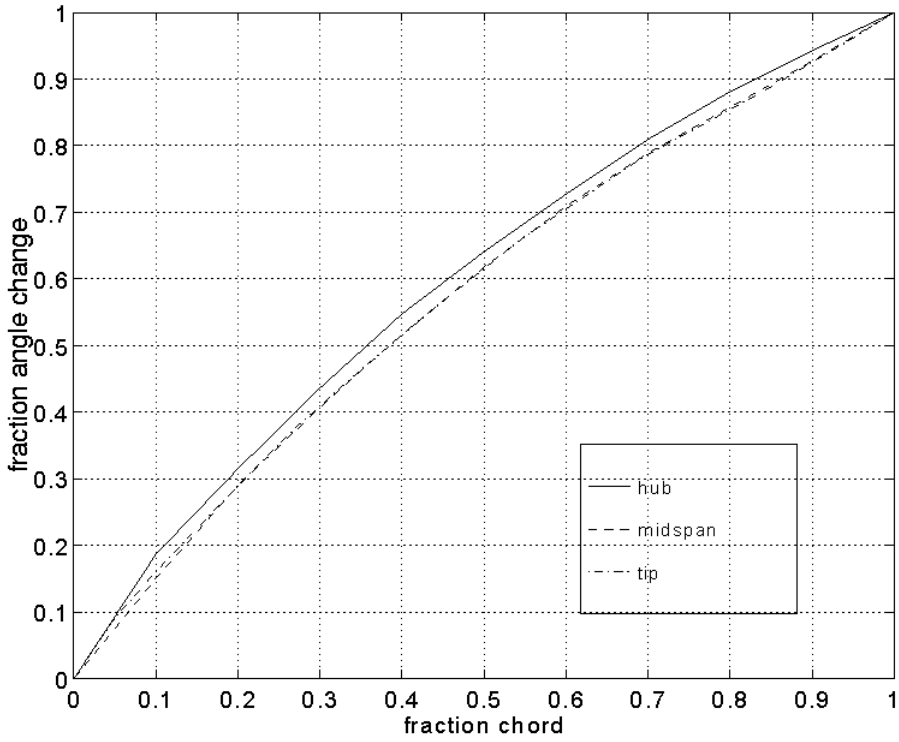

Figure 5.2.1-9. QHSF Stator Mean Camber Line Angles

5.2.2 Aerodynamic Results

Stator Streamline Curvature Velocity Triangles

After the final vane geometry was obtained, the design point loss estimated by DAWES was used in the AXCAPS model along with the design point rotor pressure ratio and temperature ratio profiles and flow predicted by DAWES. This procedure was done to calculate performance information that cannot be easily extracted from DAWES results.

Stator loss and D-factor are shown in Figures 5.2.2-1 and 5.2.2-2. This loss was the same as shown in Figure 4.3.6-1 except for some local modification at the endwalls necessary for AXCAPS convergence. The bump in D-factor around 25% span was caused by the flow splitter downstream of the vane trailing edge in AXCAPS. The splitter causes the streamtube area to increase as the flow moves radially inward and outward to get around the splitter, resulting in a local region of low stator exit velocity. The splitter was not modeled in DAWES. The D-factor peak at 90% span was caused by the bump in the loss profile from DAWES. Since this loss bump was due to radial migration of corner flow, the D-factor peak did not really indicate locally high stator loading. All D-factor values were in the acceptable range.

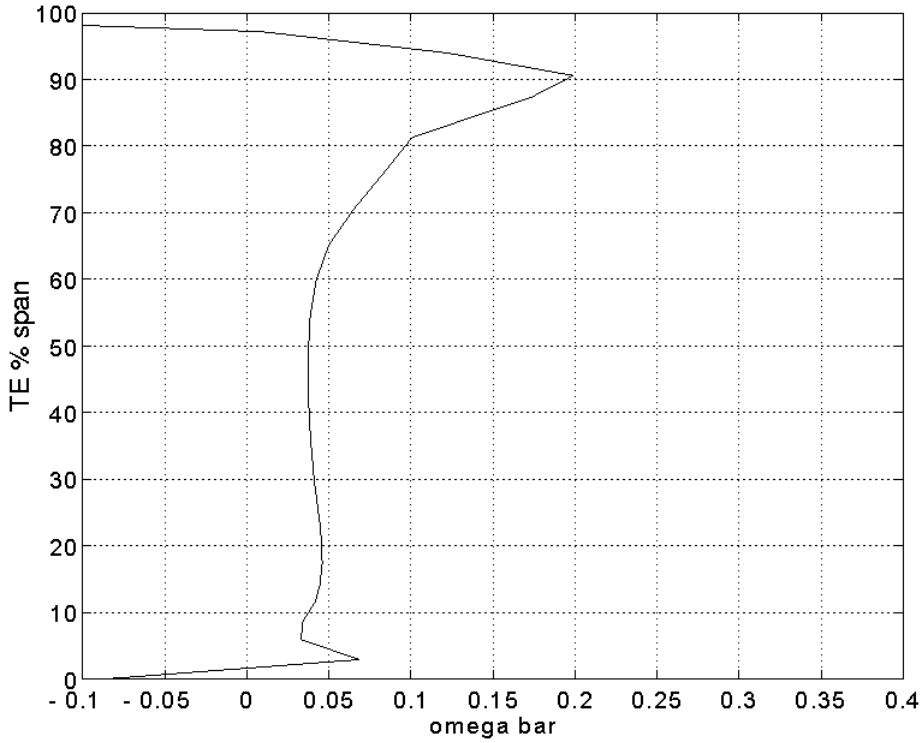

Figure 5.2.2-1. QHSF Stator Design Point Loss

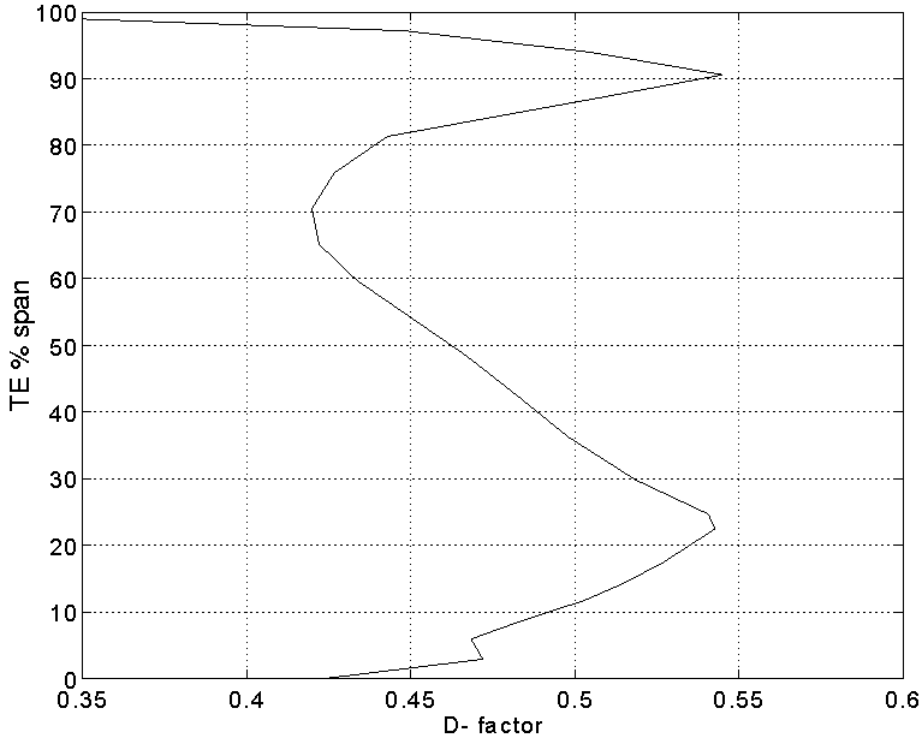

Figure 5.2.2-2. QHSF Stator design point D-factor

Figure 5.2.2-3 shows leading edge swirl from the AXCAPS calculation. Since AXCAPS distributes flow radially differently than DAWES, the swirl from DAWES was slightly different. In the AXCAPS model, the small amount of swirl at the stator exit was neglected and stator exit flow was assumed to be axial; therefore, Figure 5.2.2-3 also shows the flow turning.

Figure 5.2.2-4 shows the leading and trailing edge Mach number profiles from AXCAPS. These were slightly different than the DAWES profiles, particularly at the exit where DAWES does not include the effect of the splitter. These Mach numbers were within previous AE experience at the stator hub leading edge and at the core inlet region of the stator exit.

Figures 5.2.2-5, -6, and -7 show profiles of pressure ratio, temperature ratio, and efficiency at the stator trailing edge. These profiles combine the DAWES predictions of rotor performance and of stator loss and reflect the performance of the stage as a whole.

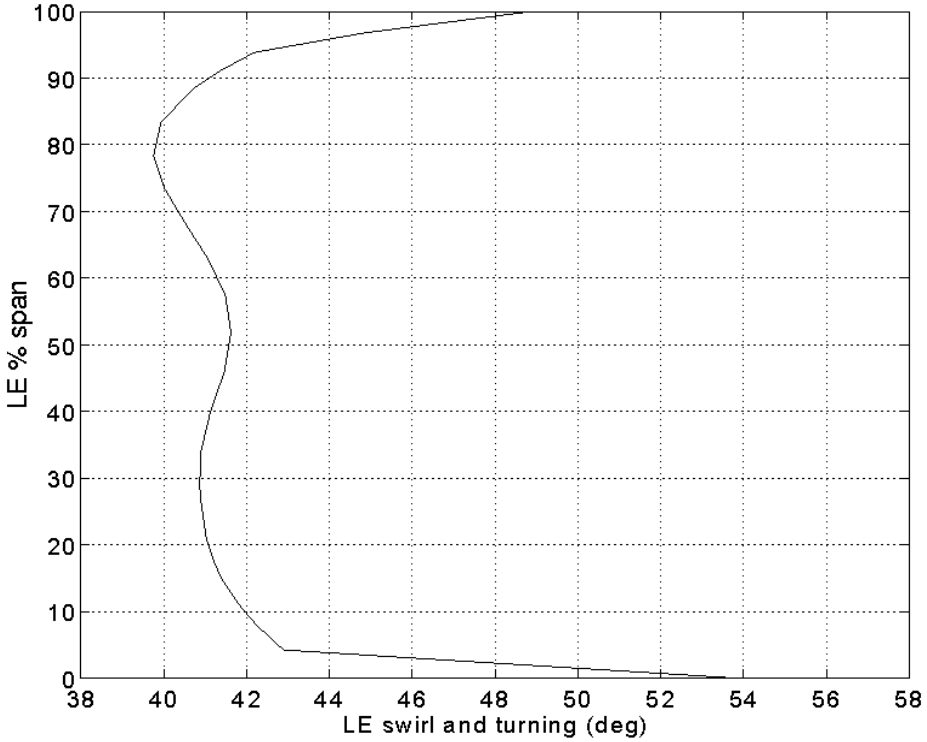

Figure 5.2.2-3. QHSF Stator Design Point LE Swirl and Turning

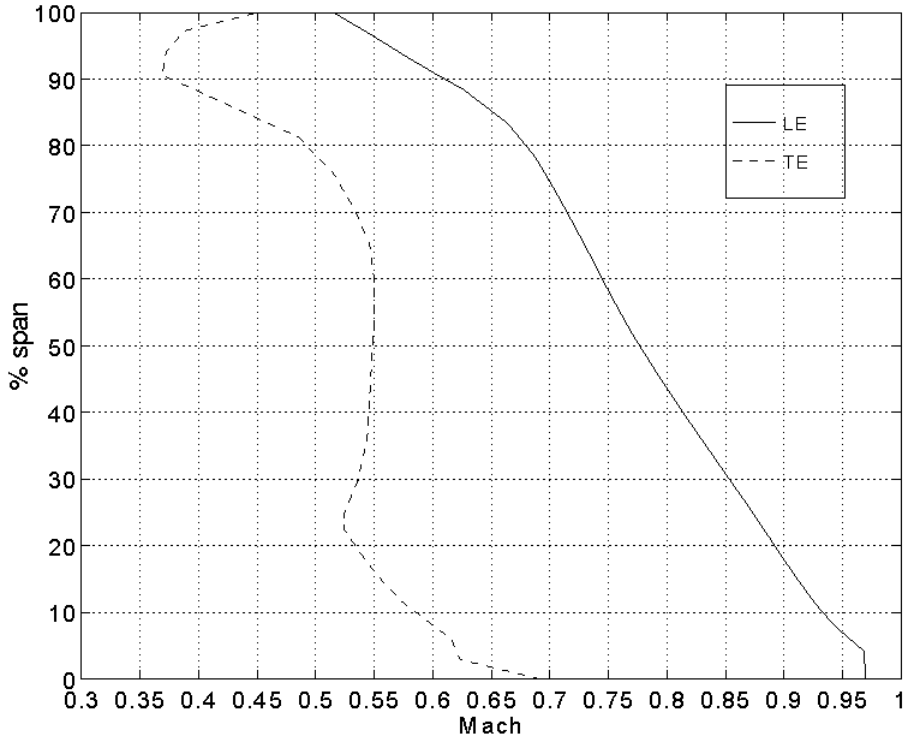

Figure 5.2.2-4. QHSF Stator Design Point LE and TE Mach

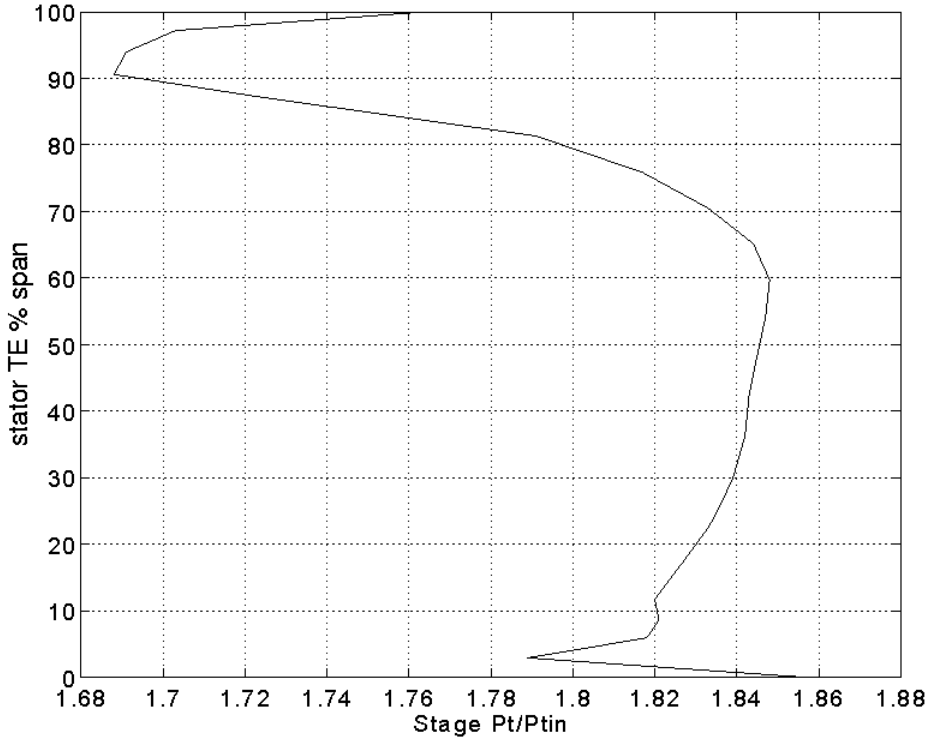

Figure 5.2.2-5. QHSF Stage Design Point Pt/Ptin

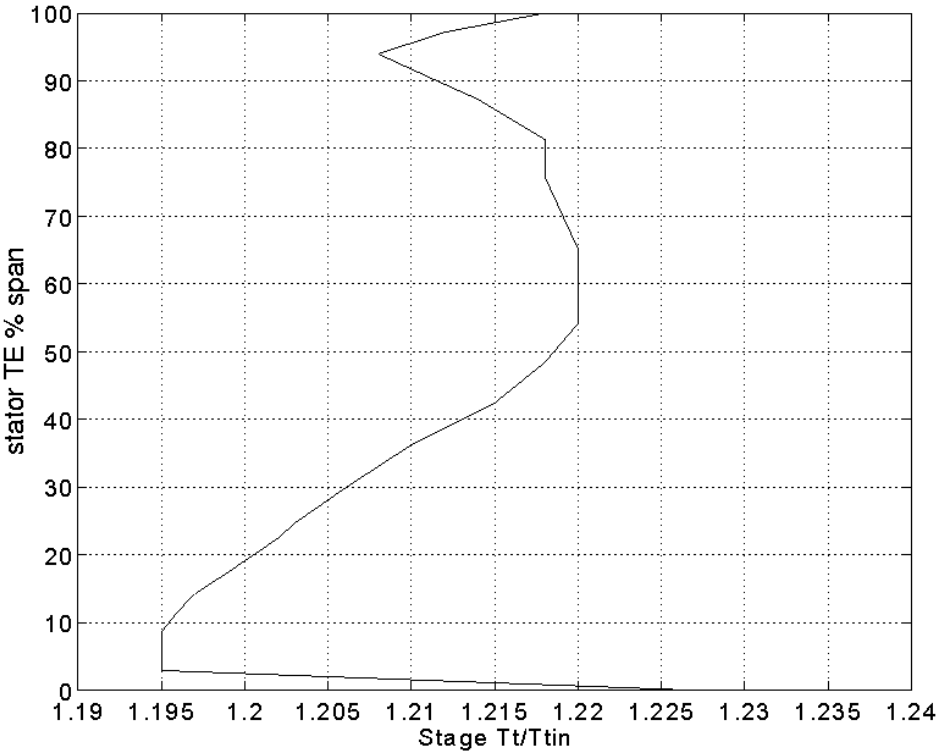

Figure 5.2.2-6. QHSF Stage Design Point Tt/Ttin

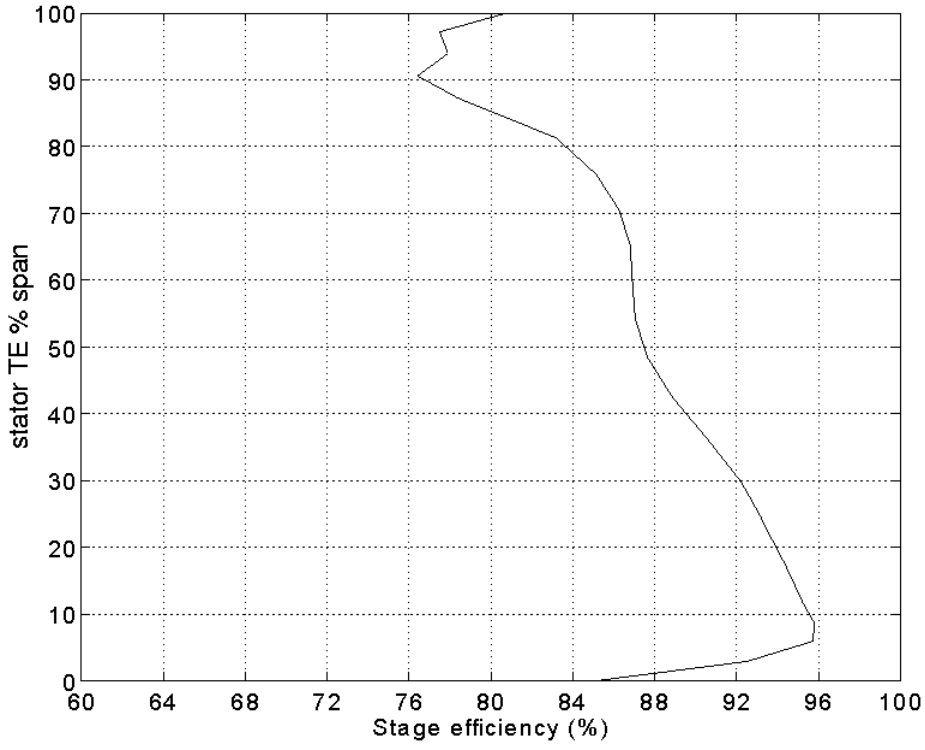

Figure 5.2.2-7. QHSF Stage Design Point Efficiency

Stator DAWES Analysis

Figures 5.2.2-8 through -12 show design point Mach number contours on the vane-to-vane surface at 10%, 30%, 50%, 70%, and 90% spans. Figures 5.2.2-13 through -17 show stator loadings as isentropically-calculated pressure and suction surface Mach numbers at 10%, 30%, 50%, 70%, and 90% span. There were two things considered when evaluating these loadings:

1.) Judging blade row quality by looking at suction and pressure surface Mach numbers on a grid surface assumes that flow mostly follows that grid surface. This is not strictly the case for highly three-dimensional blade rows.

2.) The isentropic Mach number is a convenient quantity to make it easier to compare the results of viscous CFD codes to past experience with inviscid analyses.

The loadings were biased towards choke near the hub which was a guideline used in setting the incidence, which past experience had shown to be a good strategy at the design point.

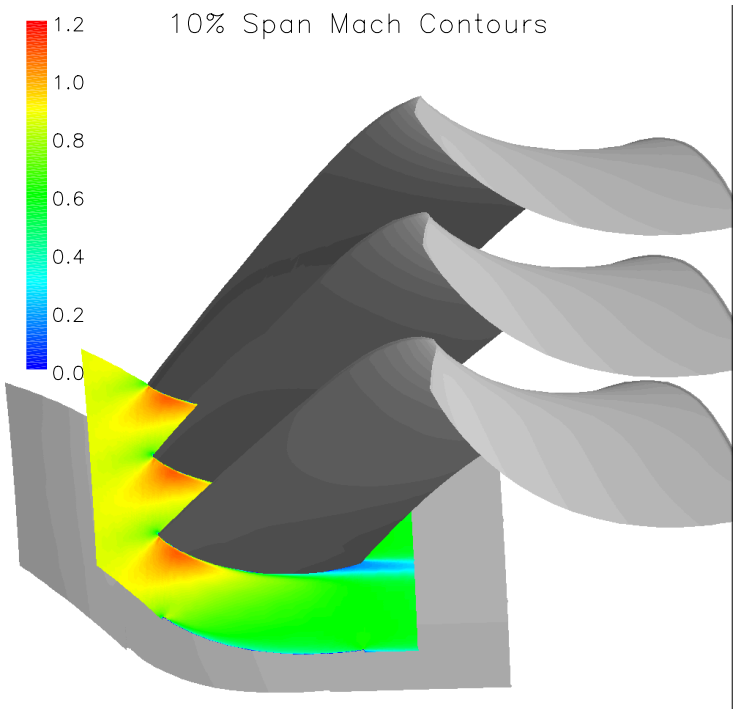

Figure 5.2.2-8. QHSF Stator Design Point Mach Contours 10% Span

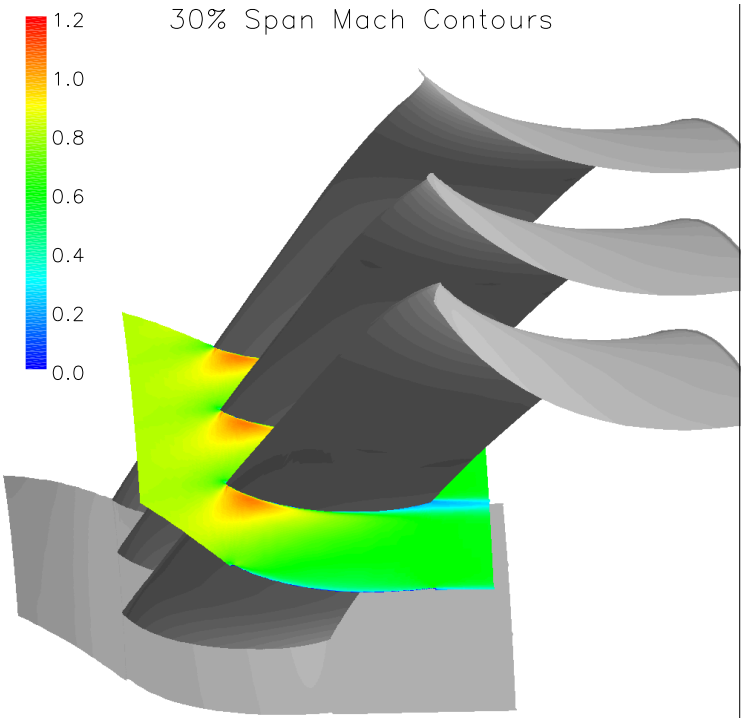

Figure 5.2.2-9. QHSF Stator Design Point Mach Contours 30% Span

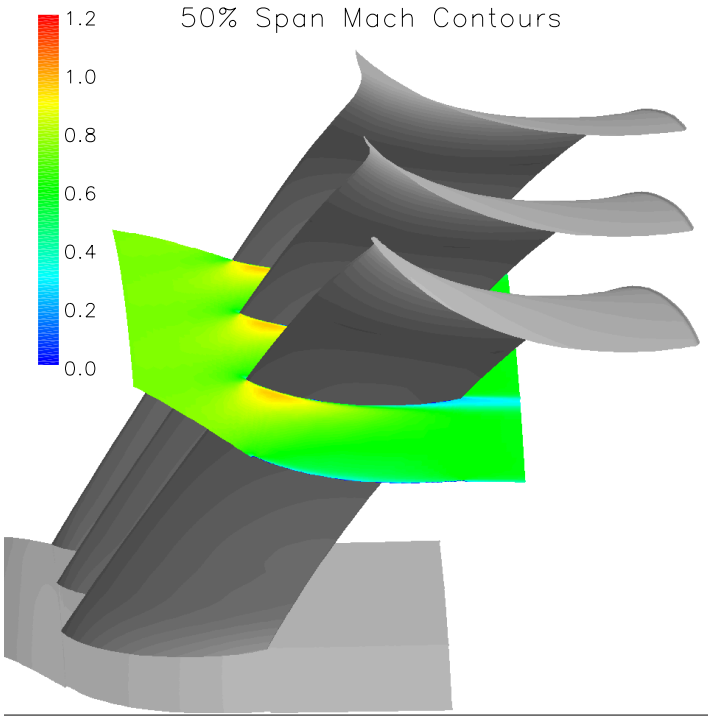

Figure 5.2.2-10. QHSF Stator Design Point Mach Contours 50% Span

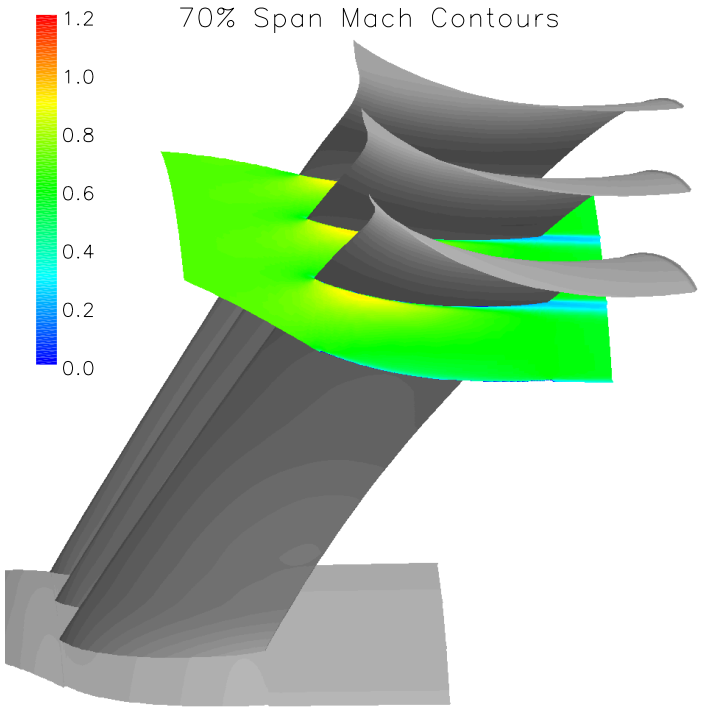

Figure 5.2.2-11. QHSF Stator Design Point Mach Contours 70% Span

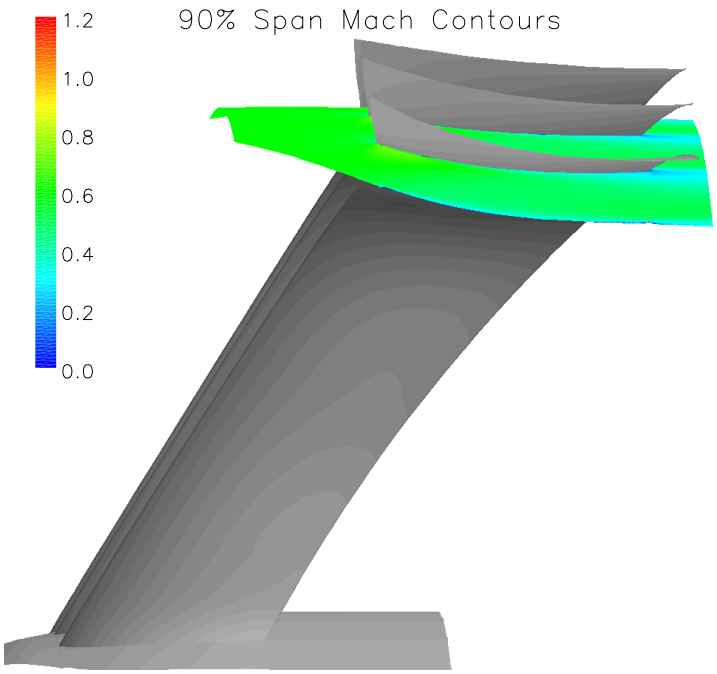

Figure 5.2.2-12. QHSF Stator Design Point Mach Contours 90% Span

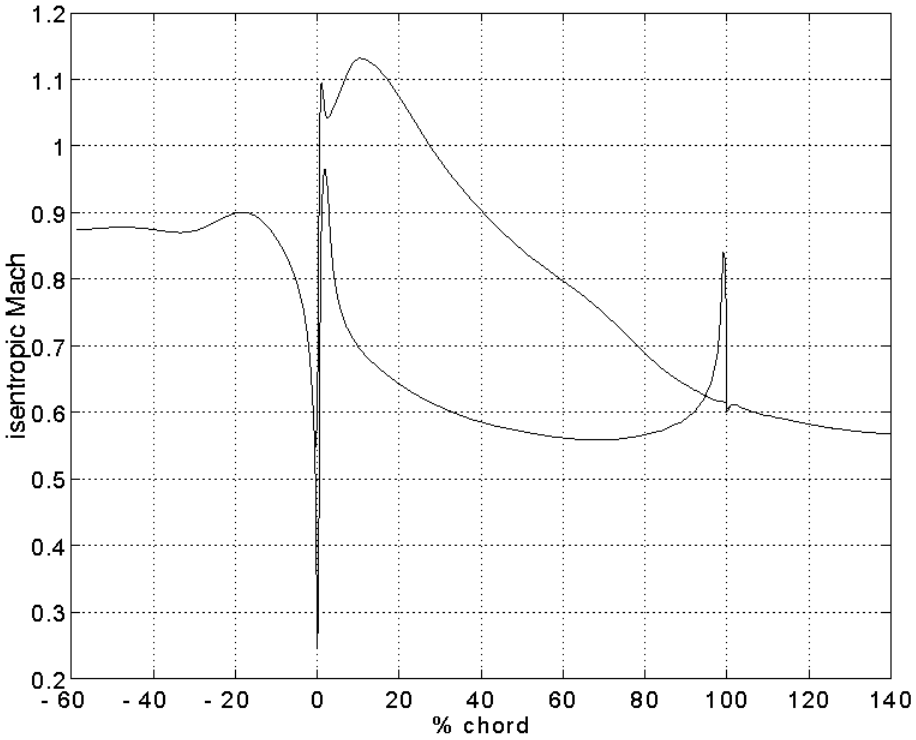

Figure 5.2.2-13. QHSF Stator Design Point Loading 10% Span

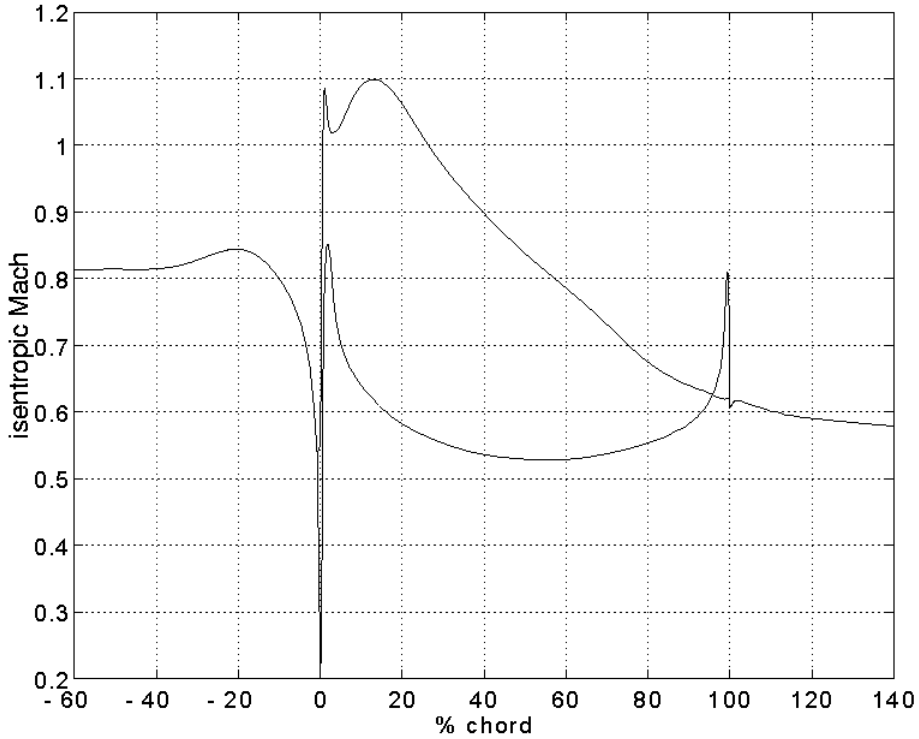

Figure 5.2.2-14. QHSF Stator Design Point Loading 30% Span

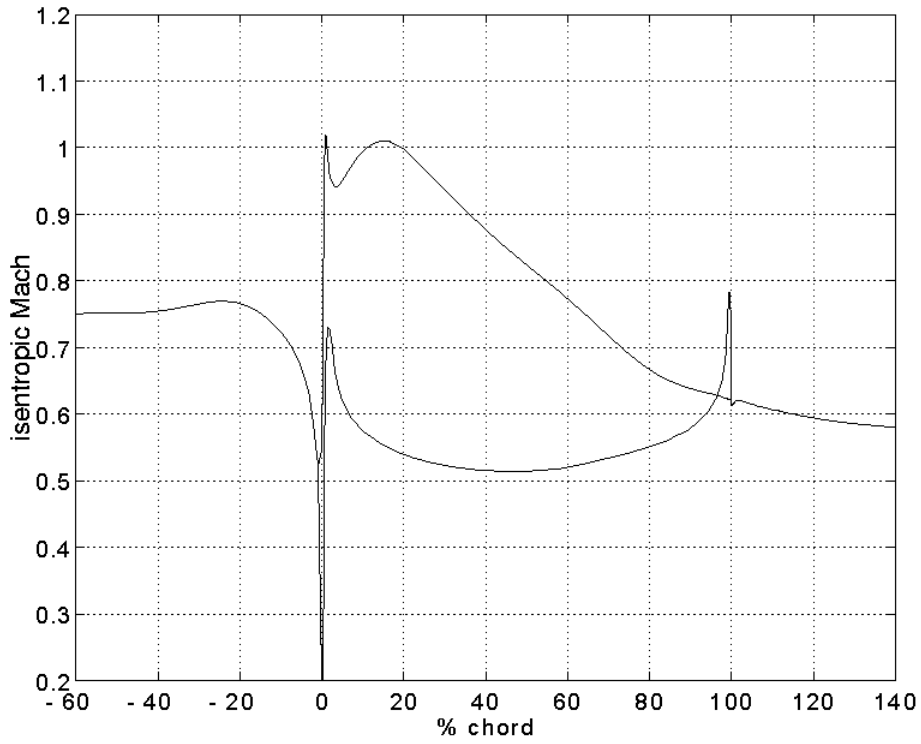

Figure 5.2.2-15. QHSF Stator Design Point Loading 50% Span

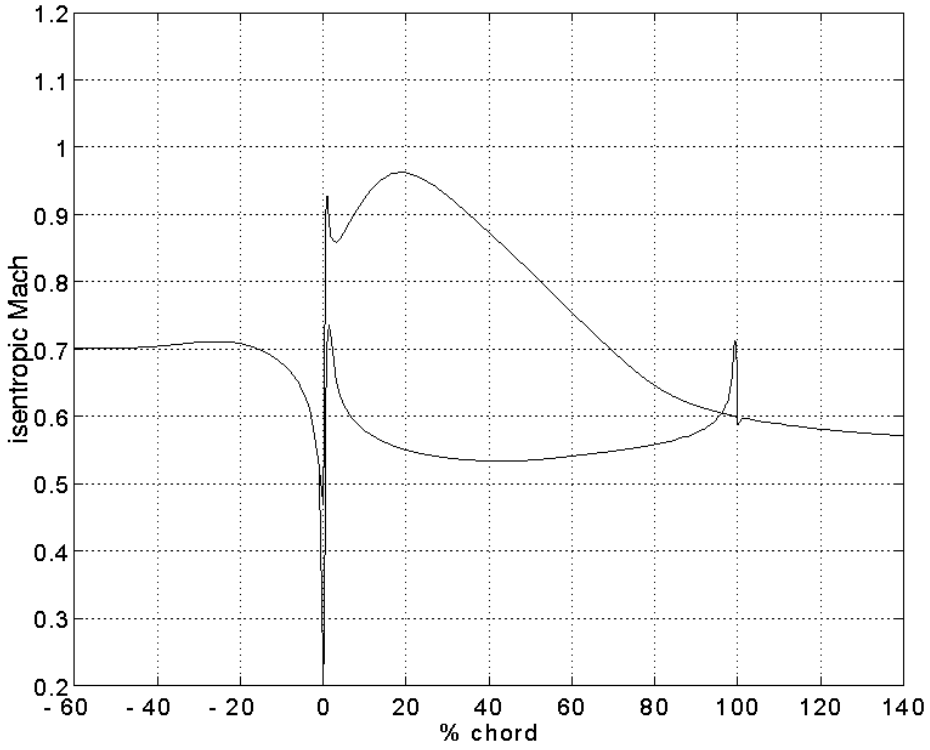

Figure 5.2.2-16. QHSF Stator Design Point Loading 70% Span

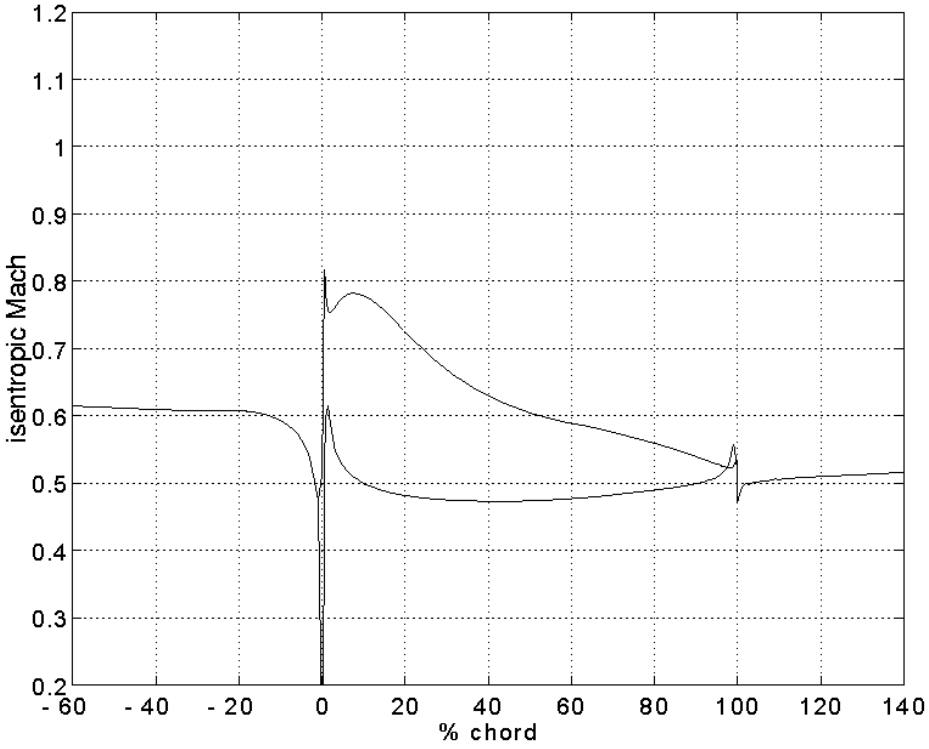

Figure 5.2.2-17. QHSF Stator Design Point Loading 90% Span

The stator performance at several off-design conditions was evaluated using DAWES. The points analyzed were on the sea level operating line at 55.9%, 70%, and 80% fan corrected design speed and on the altitude operating line at 90%, 100%, and 105% speed. The 55.9% speed point is a representative approach point where most of the acoustic V072 analysis had been performed. The 100% speed operating line point was slightly lower on the speed line than the design point so an additional run was completed. The stator inlet conditions for the stator DAWES model came from rotor exit velocity triangles predicted by the rotor DAWES model at these points. Figures 5.2.2-18 through -24 show stator profiles at these off-design conditions. Stator loss was well-behaved at part speed conditions. The loss bump increased between 100% and 105% speed and grew to affect more of the span. If efficiency at overspeed conditions (like max climb points) is important, this may need to be studied. The stator leading edge Mach numbers remained subsonic, even at 105% speed. The tip of the stator had an exceptionally large incidence swing throughout this speed range. The vane leading edge angle at the shroud was set as a compromise between design and part-speed shroud swirl. The stator exit swirl was adequately close to axial throughout. The importance of the locally high exit swirl accompanying the loss bump at 105% speed would have to be assessed considering the importance of overspeed performance.

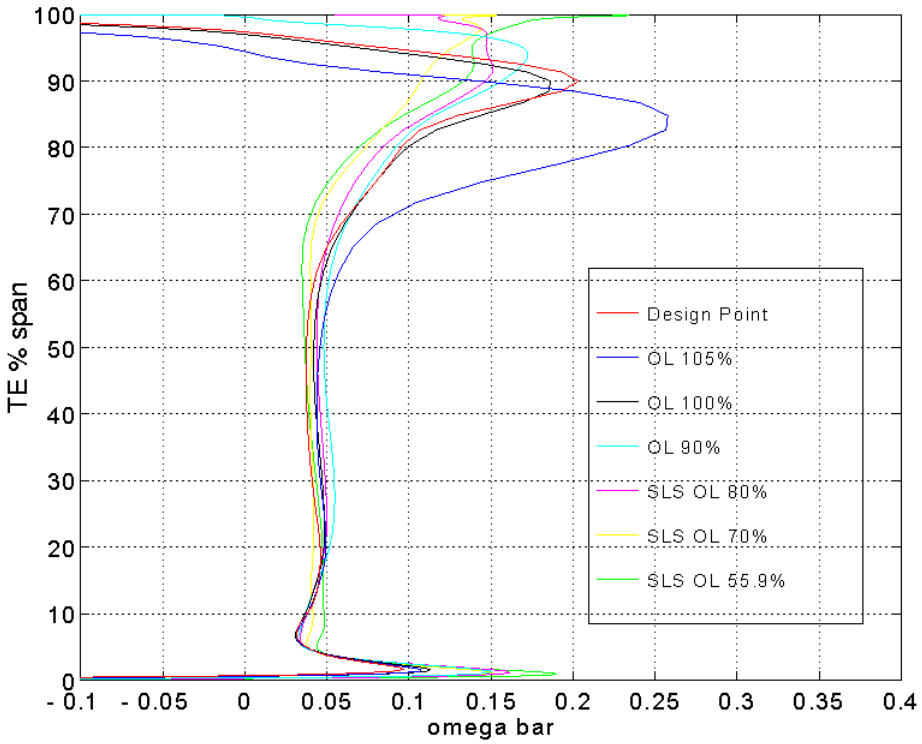

Figure 5.2.2-18. QHSF Stator Off-Design Loss

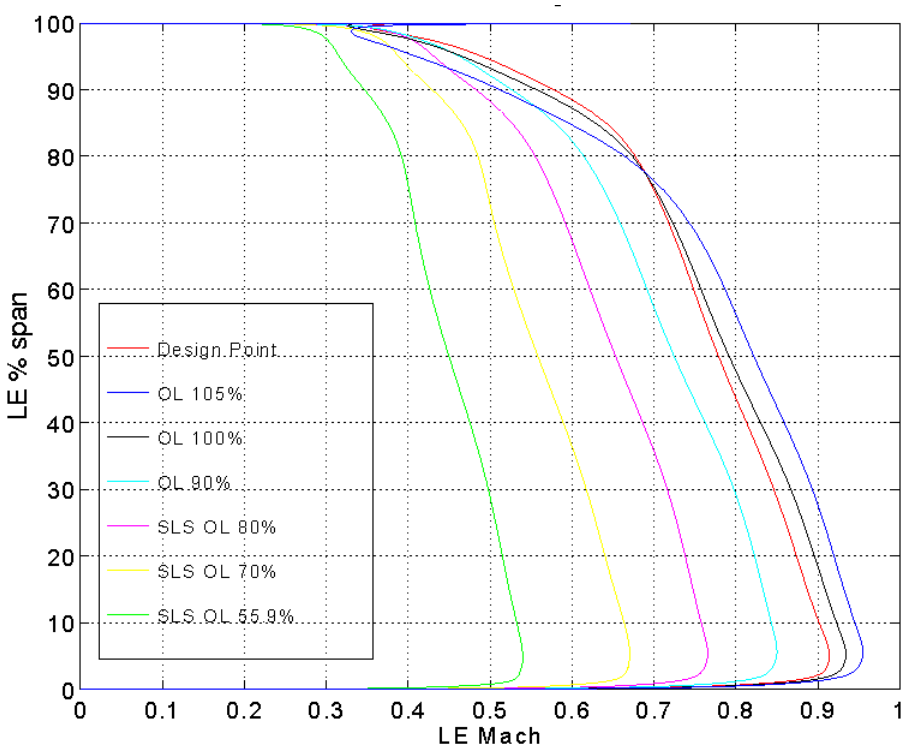

Figure 5.2.2-19. QHSF Stator Off-Design LE Mach

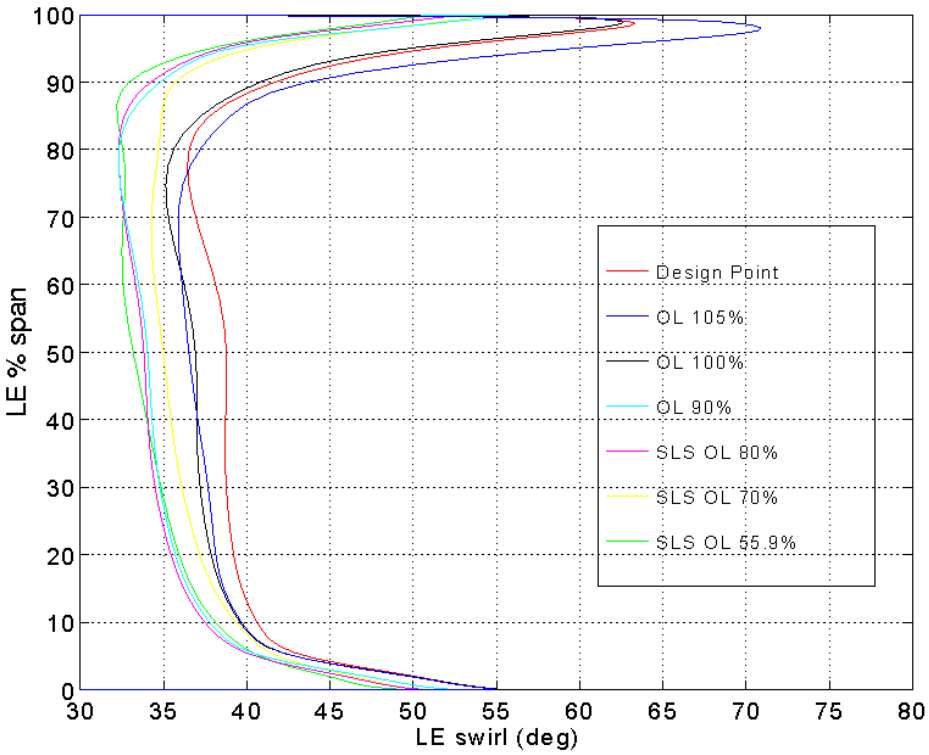

Figure 5.2.2-20. QHSF Stator Off-Design LE Swirl

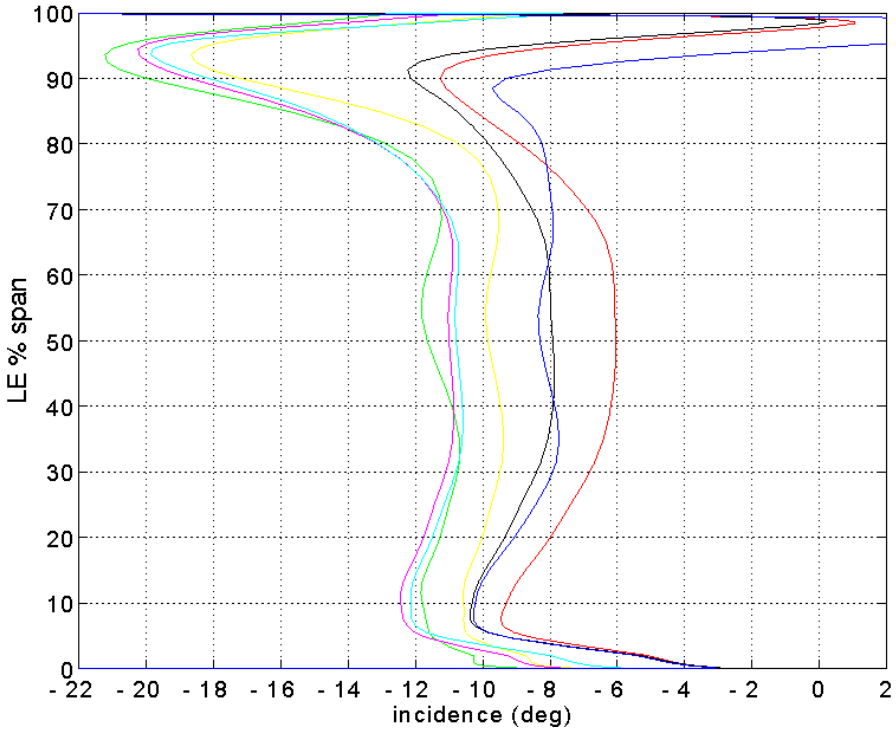

Figure 5.2.2-21. QHSF Stator Off-Design Incidence

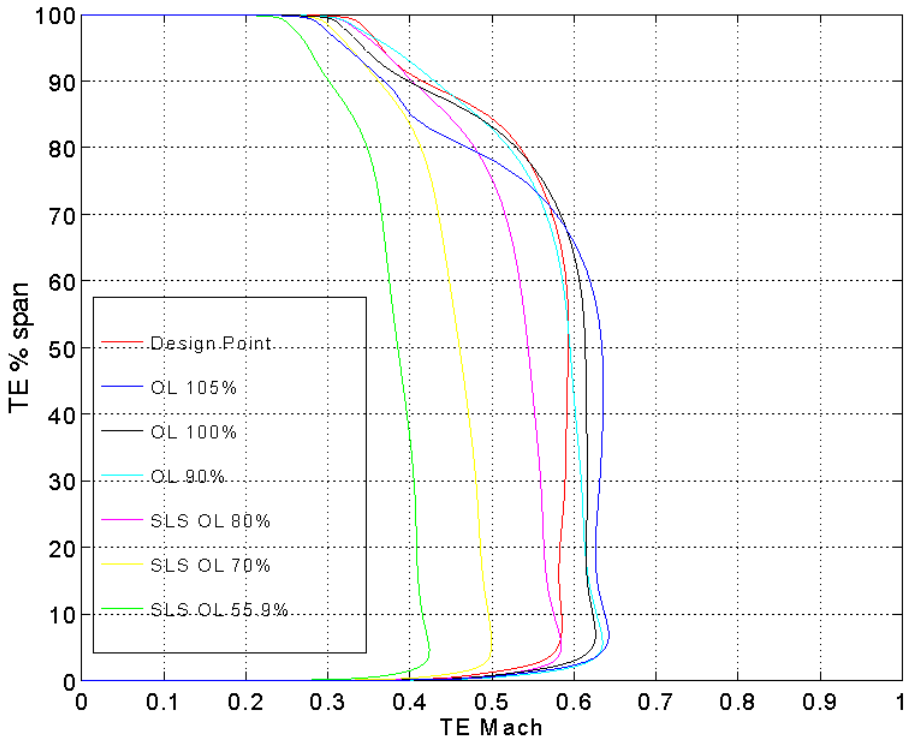

Figure 5.2.2-22. QHSF Stator Off-Design TE Mach

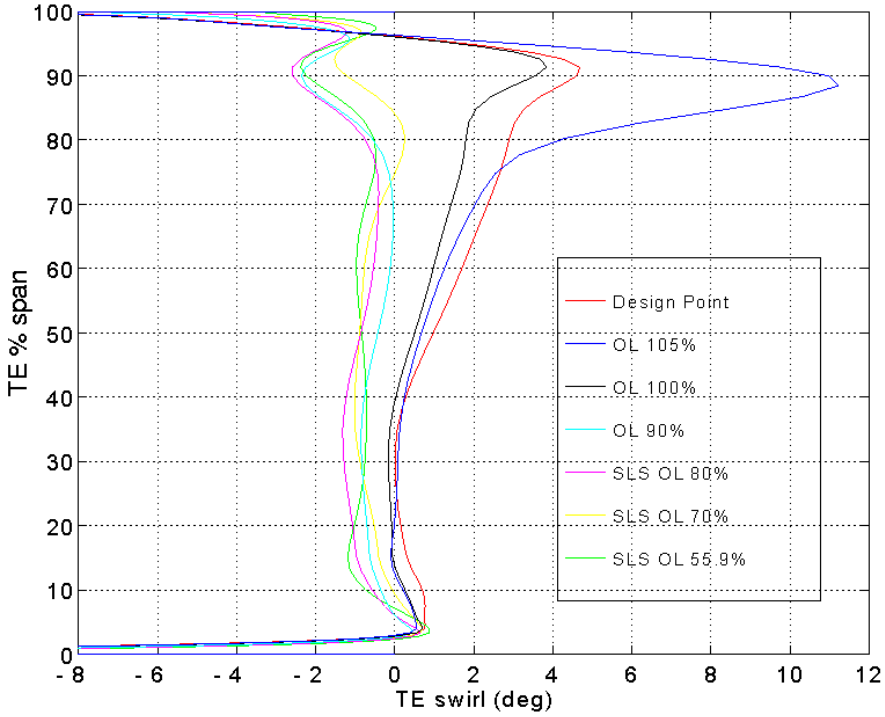

Figure 5.2.2-23. QHSF Stator Off-Design TE Swirl

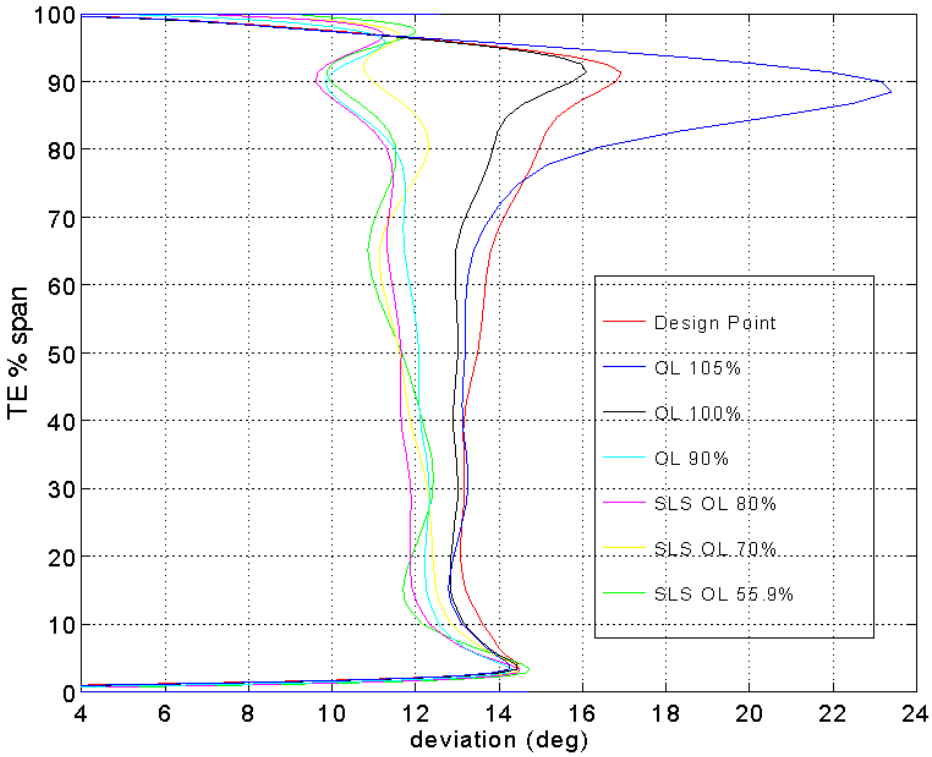

Figure 5.2.2-24. QHSF Stator Off-Design Deviation

5.2.3 Acoustic Results

Interaction of the fan rotor wake with the leading edge of the fan stator represents a significant source of noise at certain fan speeds. The noise associated with this interaction is most noticeable at approach conditions, when other noise sources are not dominant. Rotor-stator interaction tones are caused as the rotor wake impinges on the vane leading edge. The wakes emanating from the rotor are skewed and rotate circumferentially as they move downstream. Based on theory, the rotor wake/stator interaction noise occurs when the wake trace speed over the stator leading edge is supersonic. Thus, to minimize the interaction noise, the wake trace speed should be subsonic.

If the shape of the rotor wake is known, then the wake trace speed may be controlled during the design of the stator. This can be accomplished through vane axial and/or tangential lean. Increased axial lean (or sweep) increases the distance between the stator and rotor, causing a longer time increment for the circumferential wake pattern to impact the leading edge tip relative to the hub. Increased tangential lean (pressure side down) increases the delta in slope between the vane leading edge and wake trace, thereby reducing the amount of simultaneous impingement.

5.2.3.1 Objective

The objective was to use the QHSF fan rotor wake structure predicted by DAWES to help direct the design of the stator with the leading edge configured to minimize the acoustic effects of rotor wake/stator interaction, without appreciably degrading performance. The V072 acoustic prediction program was used to confirm the effect of the design on the interaction noise, and the stator design was evaluated with DAWES to determine the overall performance relative to the baseline stator.

5.2.3.2 Approach

Interaction of the fan rotor wake with the stator leading edge was assessed using a graphical technique. A contour plot of the rotor wake was produced on a surface formed by tangentially sweeping the stator leading edge curve (Figure 5.2.3-1). By superimposing the stator leading edge curve on the rotor wake plot, the time required for the wake to traverse a given distance along the leading edge was computed, thereby obtaining the wake trace speed.

5.2.3.3 Design Philosophy

The design philosophy employed in reducing interaction noise below that of the baseline was to use rotor forward sweep and stator aft sweep and tangential lean. The goal was to increase rotor/stator spacing to allow greater rotor wakes diffusion, and to increase the tangential lean of the rotor wakes relative to the stators thereby reducing wake trace speed and increasing phase variation along the stator span.

5.2.3.4 Stator DOE

Many stator configurations involving increased sweep and lean compared to the baseline were analyzed. It was found that leans of 30° and sweeps beyond the approximately 30° of the baseline stator did not provide significant acoustic benefit. In addition to the lack of acoustic benefit achieved by large leans and sweeps, DAWES results showed large flow separations near the hub for these cases. Consequently, more conservative leans were investigated.

For stator DOE1 involving variations on a 15° leaned vane, interaction noise predictions showed that the compound bow (leaning with the rotation direction at the midspan and against rotation at the tip) of case 5 produced high levels while the straight and compound leans with rotation of cases 1, 6 and 8 produced benefits in some harmonics (Figure 5.2.3-2). The aero results showed that separation and high hub losses resulted from leaning the suction surface towards the endwall. Case 6 was selected as a go forward case.

5.2.3.5 Final Configuration

The final QHSF stage was predicted to be 3 to 5 dB quieter than the baseline in all but the forward-propagating 3*BPF harmonic (Figure 5.2.3-1). Recall that the 1*BPF tone was cut-off at this speed. Although the predicted wake velocity deficit was greater for the quiet fan, the wake width was also greater and may at least partially offset the effect of the increased deficit. Reduced interaction noise was likely due to increased phase variation across the stator leading edge as shown in the wake traces. The pressure contours were extracted from a DAWES solution and revealed that the 2-D kinematic analysis of V072 may predict greater wake leans than exist in a 3-D flow. However, variation between the V072 and DAWES predictions appeared to be the same for both the baseline and the QHSF.

The objective of reducing interaction noise using rotor forward sweep and stator aft sweep and tangential lean was accomplished. Large reductions in the 2*BPF harmonic will translate into significantly lower flyover effective perceived noise levels.

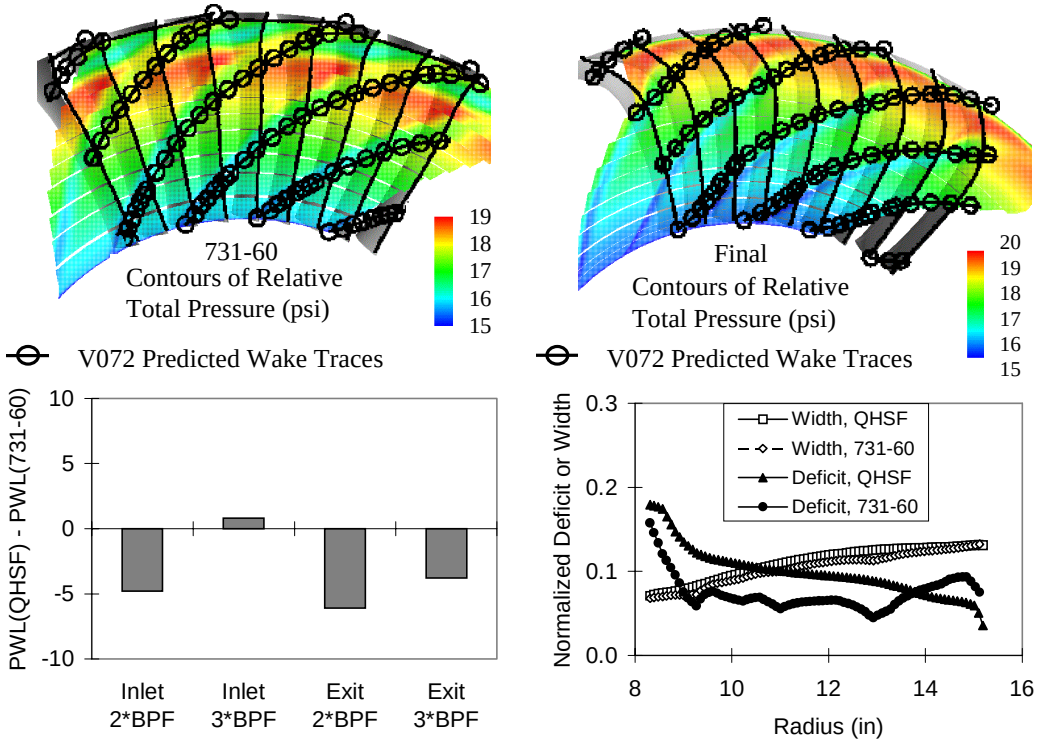

Figure 5.2.3-1. V072 Predictions for Final QHSF Rotor and Stator at 55.9% Speed

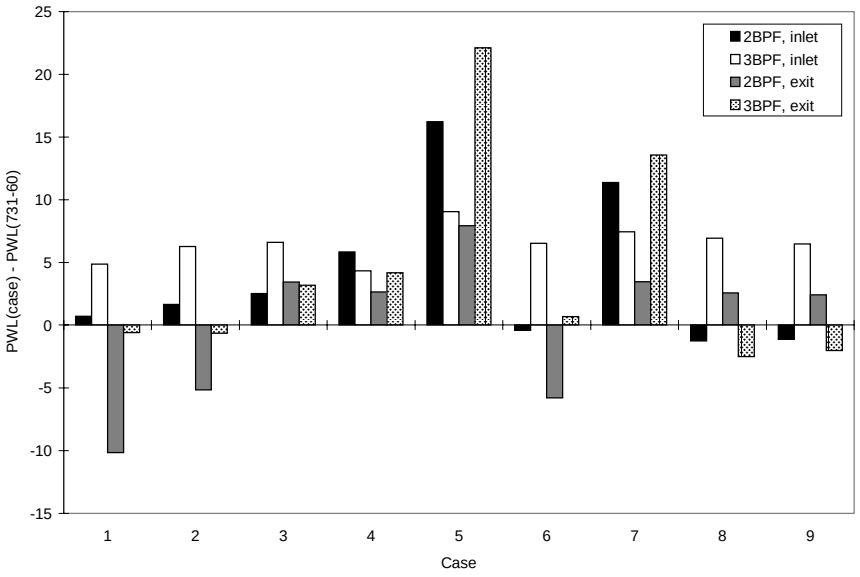

Figure 5.2.3-2. V072 Results for Stators with Moderate Leans, all with Baseline Sweep (30°)

5.2.4 Mechanical Results

The static and vibration results for the final QHSF stator design are discussed in this section. As mentioned in section 4.3.3, two different retention schemes were recommended — the conventional single-band scheme and a two-band scheme as a backup in case flutter is observed in the rig. The two configurations have no aerodynamic impact; however, they have different mechanical behavior due to the change in the boundary conditions.

Table 5.2.4-1 Effect of Retention Scheme on Modal Frequencies

Mode	Frequency (Hz) One-Band Scheme	Two-Band Scheme	% Change in Frequency
1	505.52	579.66	14.67
2	764.19	740.23	-3.14
3	861.4	867.59	0.72
4	997.33	1086.7	8.96
5	1296.1	1381.7	6.60

Table 5.2.4-1 shows the frequency predictions for the two retention schemes. The mode shapes for the first five modes are presented in Figures 5.2.4-1 and 5.2.4-2, respectively, for one-band and two-band schemes. In both schemes, the first mode was a torsion mode with frequency for the two-band scheme about 14% higher than the one-band scheme. However, second mode frequency was lower by about 3%. The flutter parameter for one-band scheme was 0.85, and 0.98 for the two-band scheme. The flutter parameter for baseline vane was 1.03 with taped construction and 0.96 with the braided construction. The Campbell diagram for two-band case is shown in Figure 5.2.4.3. Stress analyses completed for the two schemes, Figures 5.2.4-4 to 5.2.4-7, showed all design criteria was achieved.

Figure 5.2.4-1. Vibration Modes for One-Band Scheme, Mode 4.

Figure 5.2.4-1. Vibration Modes for One-Band Scheme, Mode 2.

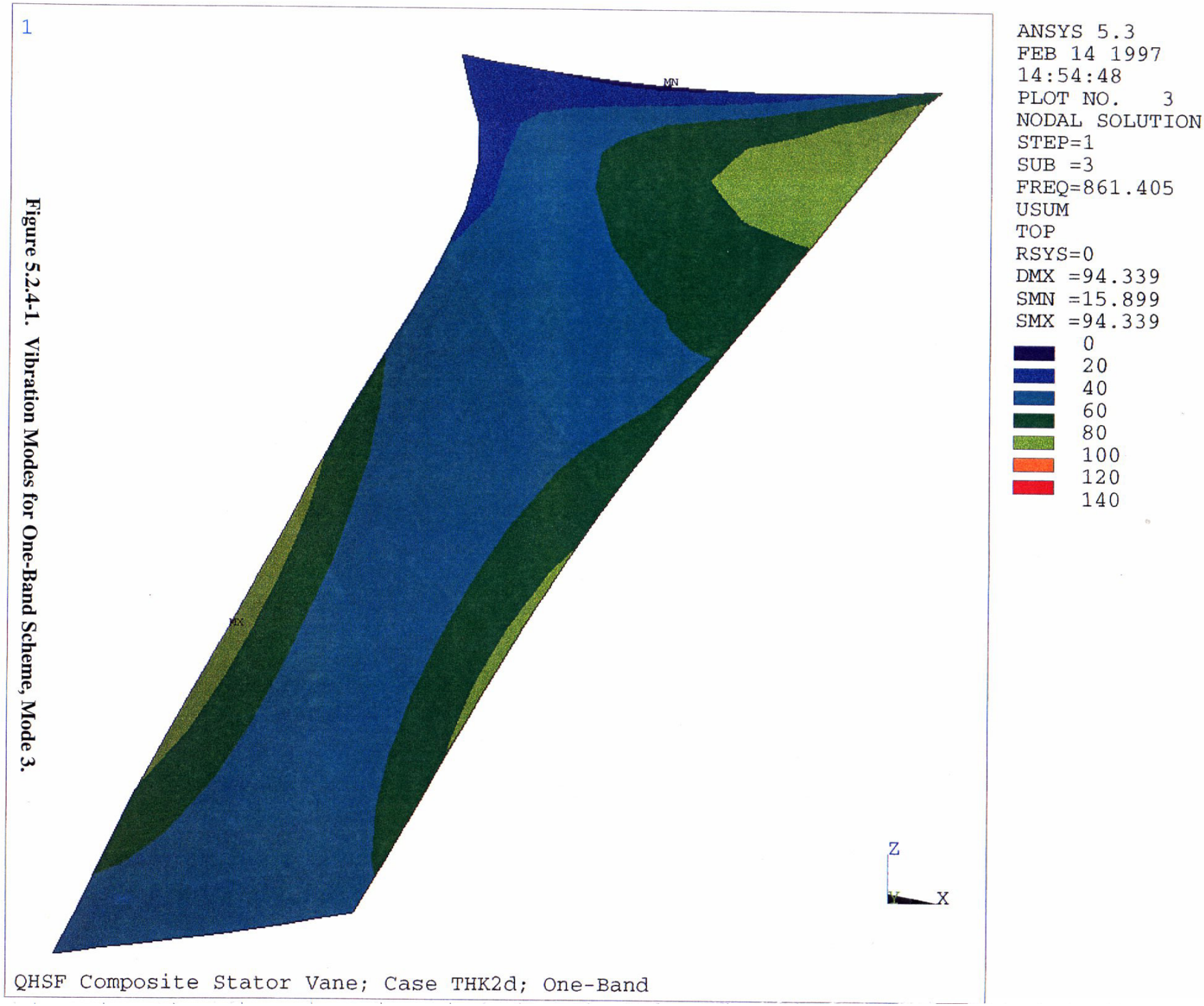

Figure 5.2.4-1. Vibration Modes for One-Band Scheme, Mode 3.

Figure 5.2.4-1. Vibration Modes for One-Band Scheme, Mode 1.

Figure 5.2.4-1. Vibration Modes for One-Band Scheme, Mode 5.

Figure 5.2.4-2. Vibration Modes for Two-Band Scheme, Mode 1.

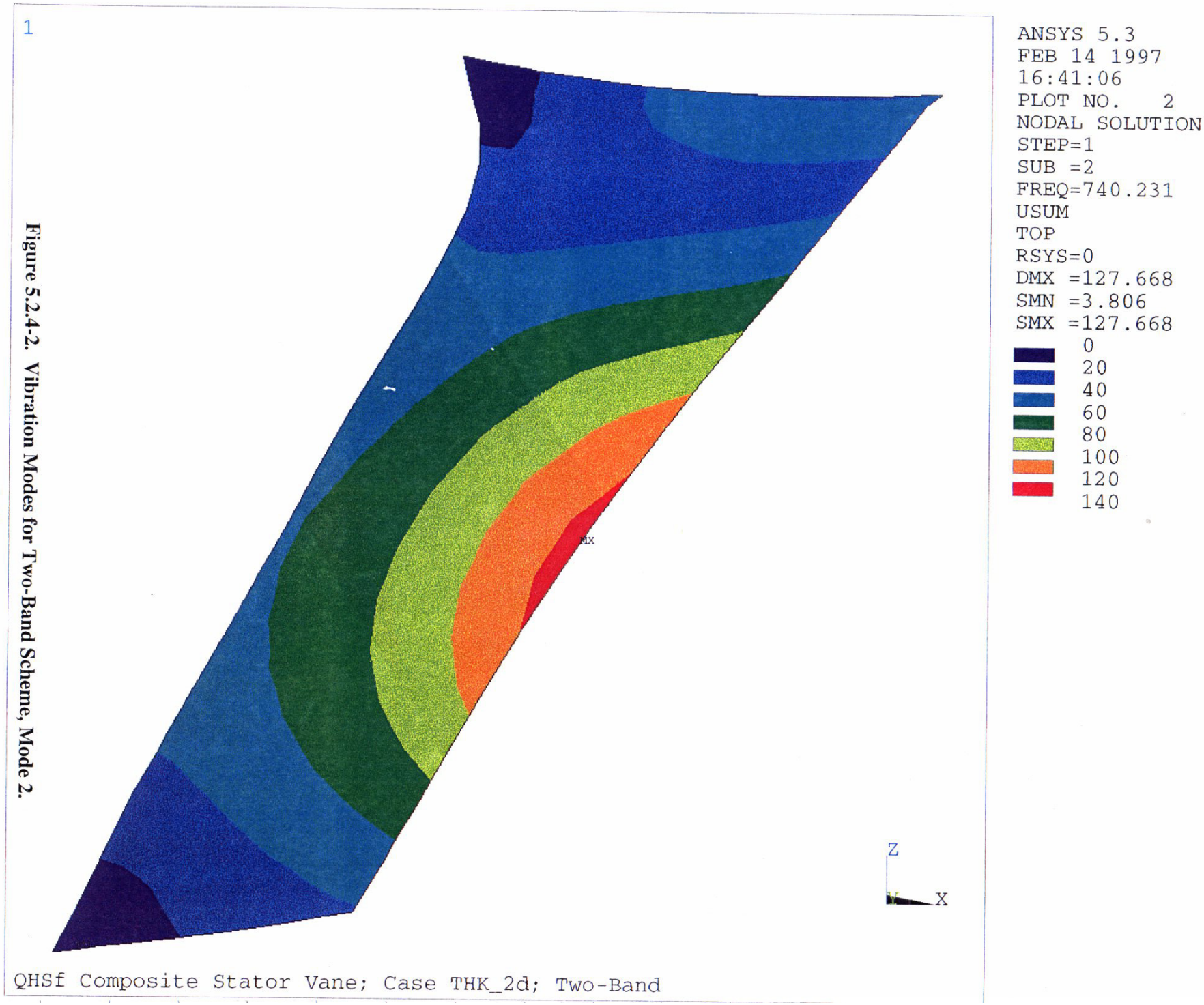

Figure 5.2.4-2. Vibration Modes for Two-Band Scheme, Mode 2.

Figure 5.2.4-2. Vibration Modes for Two-Band Scheme, Mode 3.

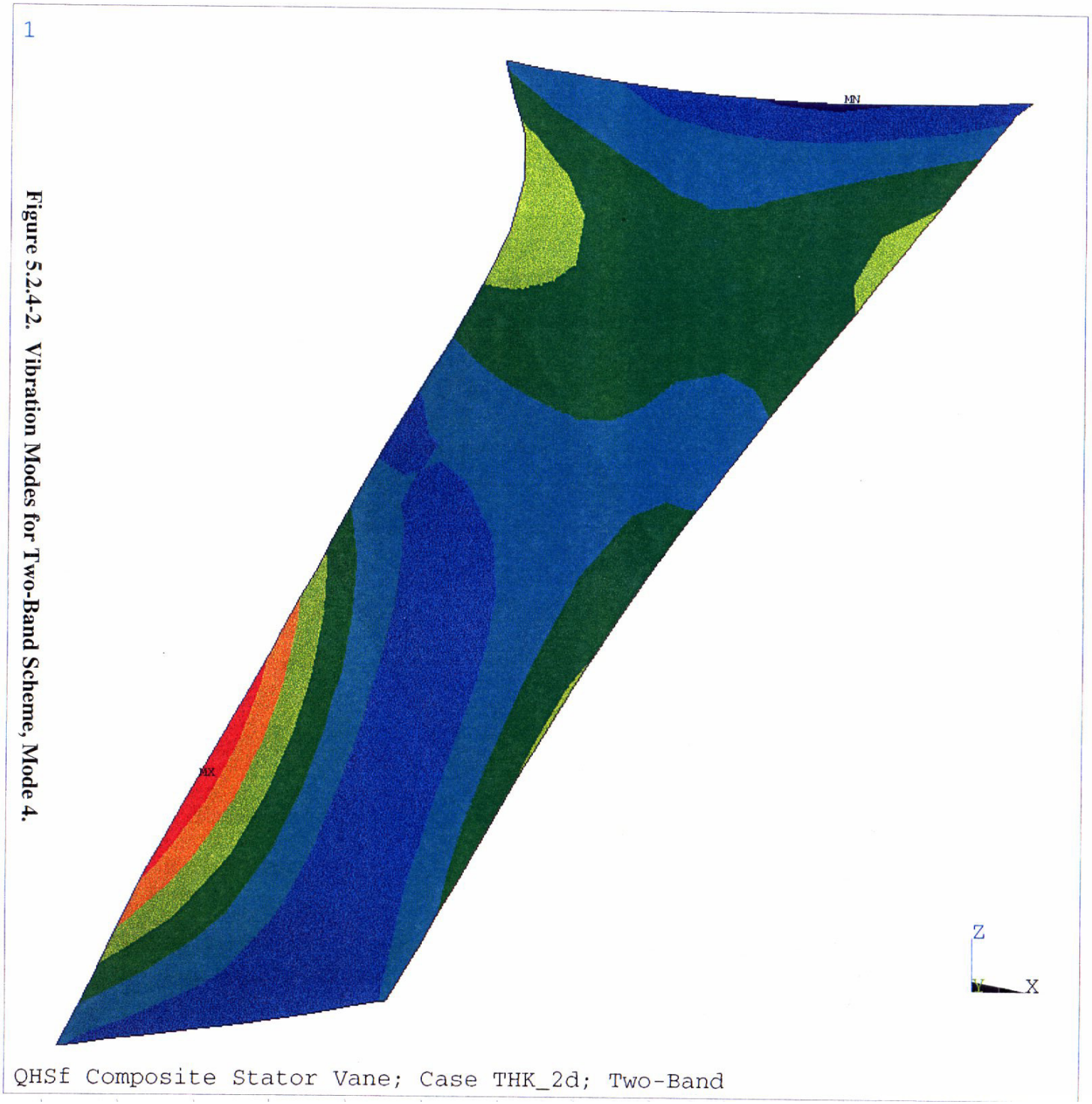

Figure 5.2.4-2. Vibration Modes for Two-Band Scheme, Mode 4.

Figure 5.2.4-2. Vibration Modes for Two-Band Scheme, Mode 5.

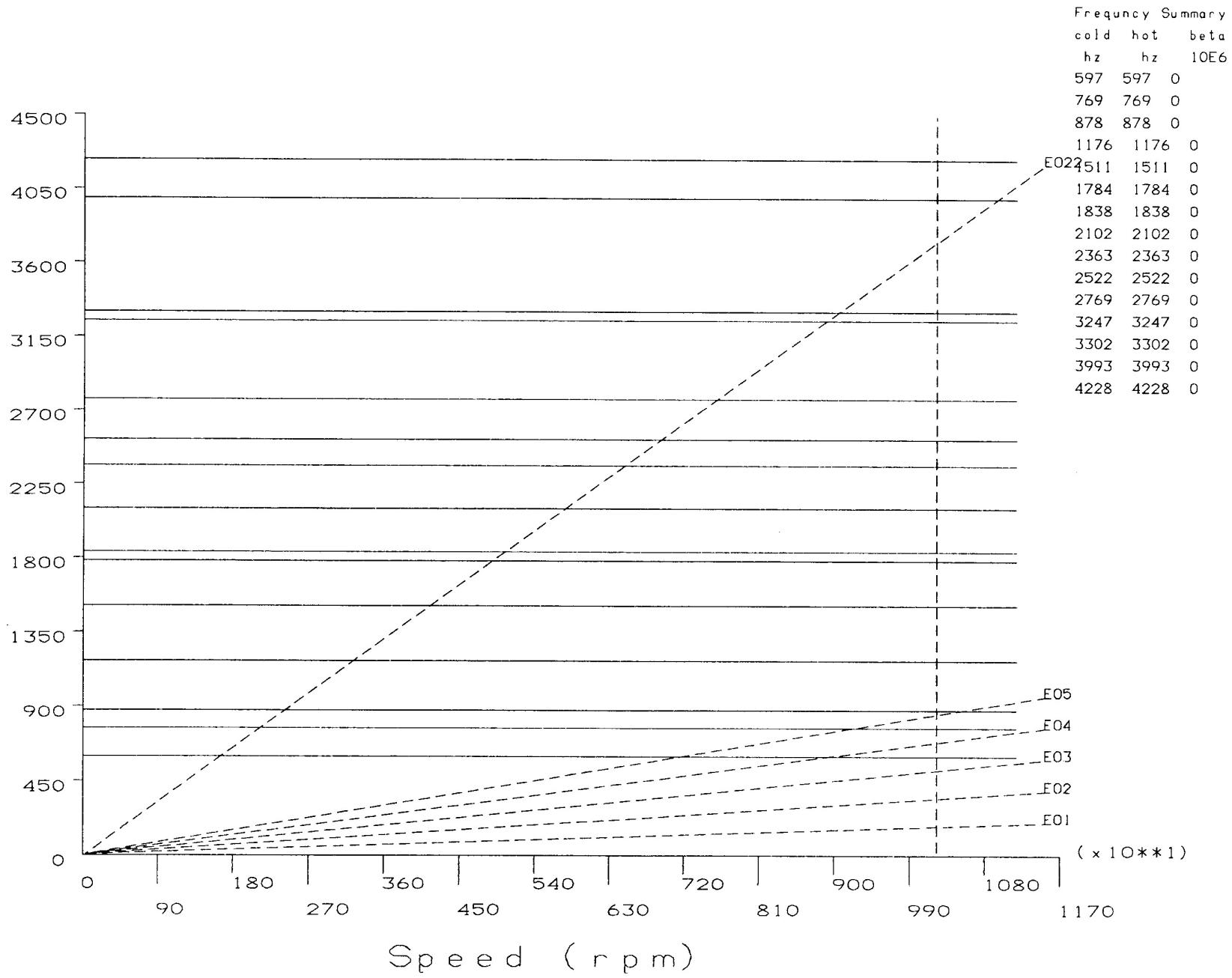

Figure 5.2.4-3. Campbell Diagram for Two-Band Scheme

QHSF COMPOSITE STATOR VANE; CASE THK_2D; TWO-BAND

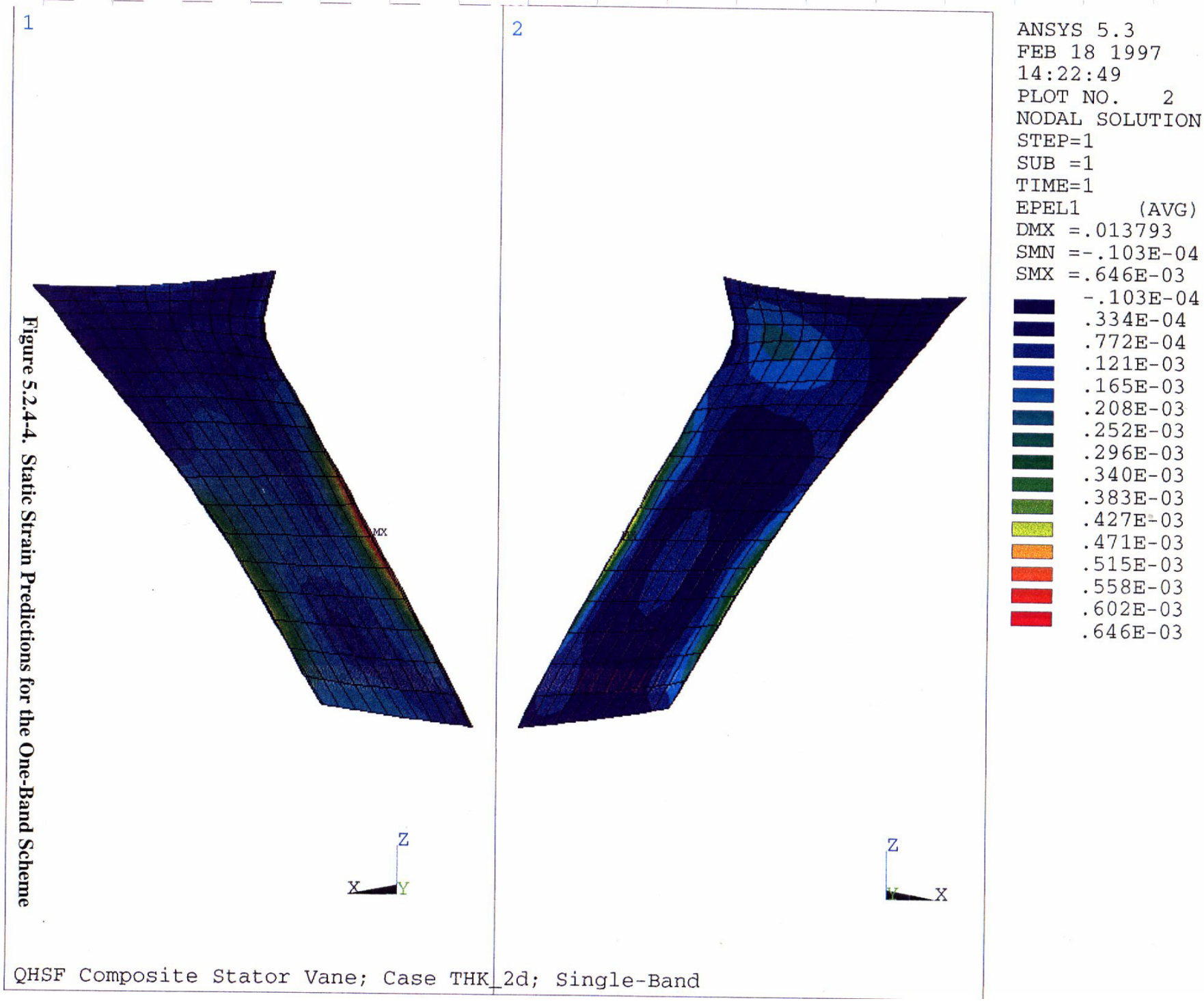

Figure 5.2.4-4. Static Strain Predictions for the One-Band Scheme

Figure 5.2.4-5. Static Displacement Predictions for the One-Band Scheme

Figure 5.2.4-6. Static Strain Predictions for the Two -Band Scheme

Figure 5.2.4-7. Static Displacement Predictions for the Two-Band Scheme

5.3 Disk

5.3.1 2-D Analysis

The preliminary design (PD) of the rig disk was reexamined with the optm3 airfoil loads. The results from the 2-D wedge model showed adequate burst margins and acceptable stresses in the disk. However, a 2-D axisymmetric analysis of the disk showed excessive roll at the rim with both baseline rotor and optm3 airfoil loads. It may be recalled that the PD of the disk was assumed to have rectangular cross section; i.e., no undercuts.

The rim roll and the tangential stress distribution along the rim (slot bottom) were balanced by providing undercuts in the disk. Also, the disk width was reduced to 3.08″ to conform with the blade attachment width. The bore radius was increased to 2.3″ to accommodate a 0.25″ thick torque sleeve. Figure 5.3.1-1 shows the layout of the disk with undercuts and the torque sleeve mounted on the NASA balance. The tangential stress distribution in the disk hub at design speed is shown in Figure 5.3.1-2 for the two airfoil load cases. Figures 5.3.1-3 and 5.3.1-4, respectively, show the variation of tangential stress and radial displacement at the slot bottom.

5.3.2 3-D Analysis

A solid model of the 3D disk was constructed in ANSYS using Boolean operators. The 2D disk profile was swept about the centerline by an angle of 360/22= 16.36°. A solid defined by the slot contour was then subtracted from the swept disk wedge, resulting in the final slotted disk sector; as shown in Figure 5.3.2-1. The finite element mesh of the final model consisted almost entirely of brick elements, with tetrahedra only in regions of low stress. Figures 5.3.2-2 and 5.3.2-3 show the maximum principal stresses and the tangential stresses in the disk at design speed for QHSF airfoil loads.

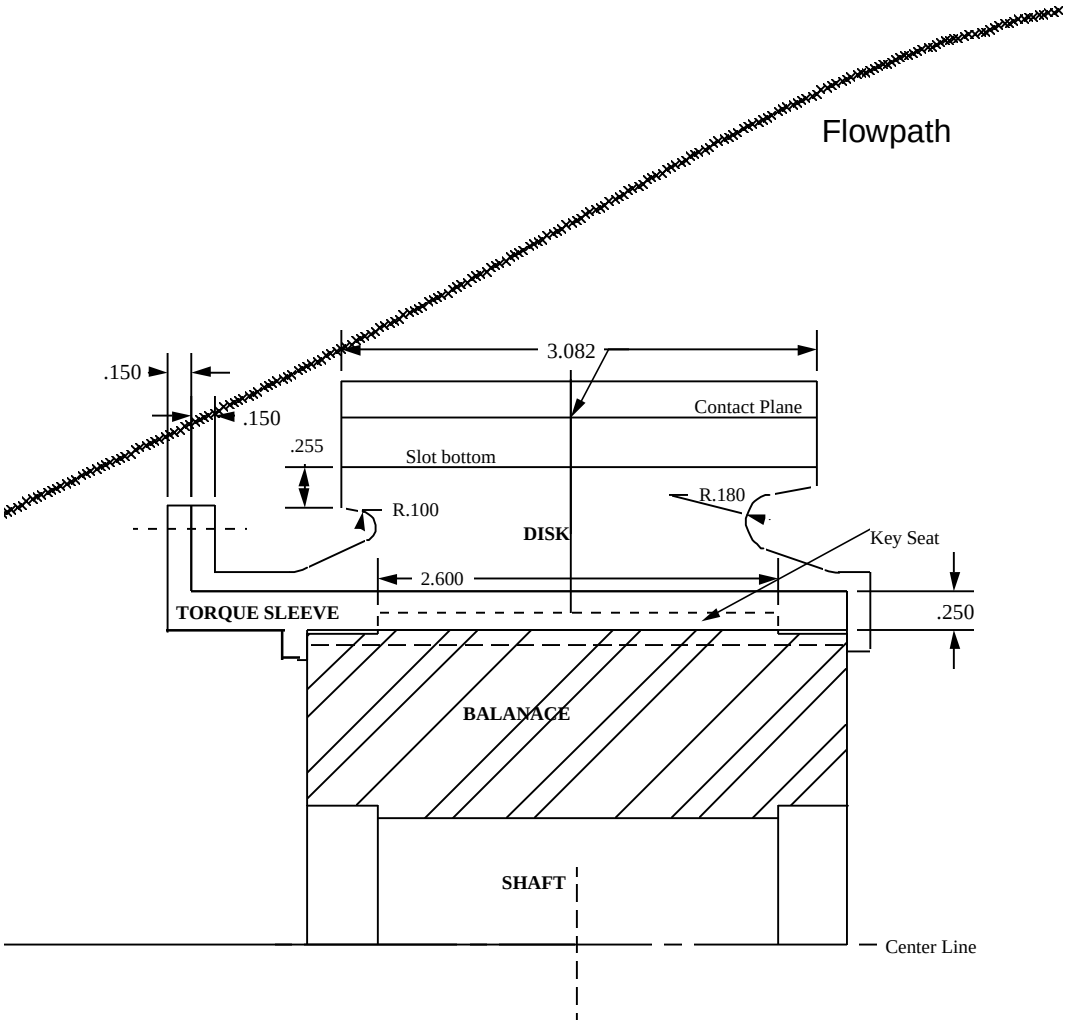

Figure 5.3.1-1. QHSF Disk Layout with Torque Sleeve Mounted on NASA Balance

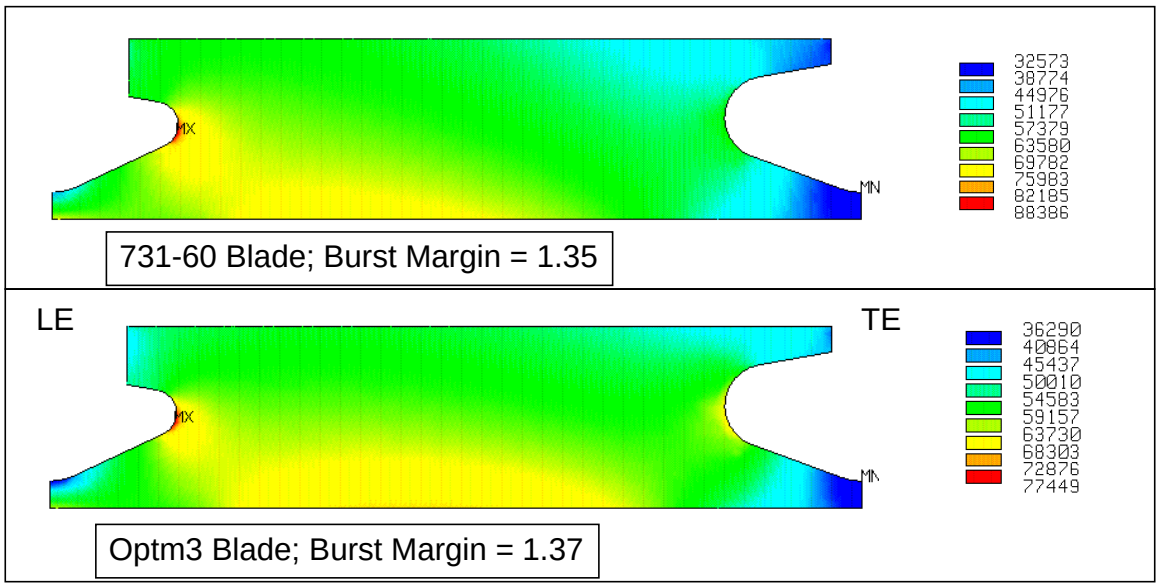

Figure 5.3.1-2. Tangential Stresses in Disk Hub from 2-D Axisymmetric Analysis

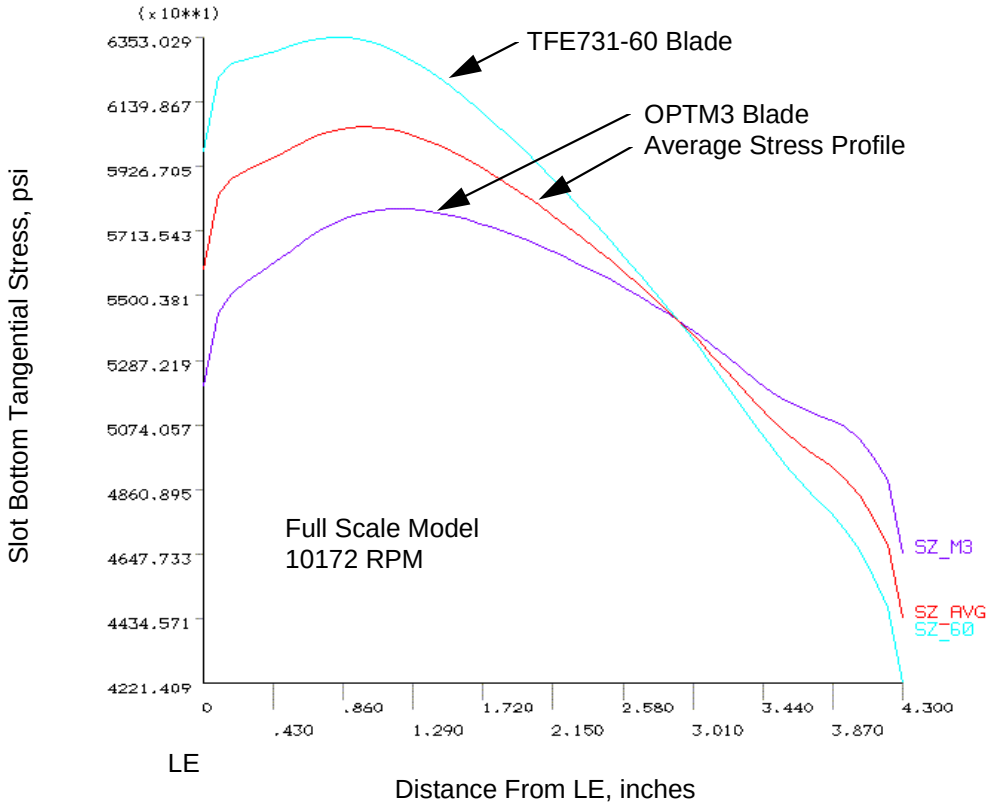

Figure 5.3.1-3. Rig Disk Optimized to Perform Well With Both Blades

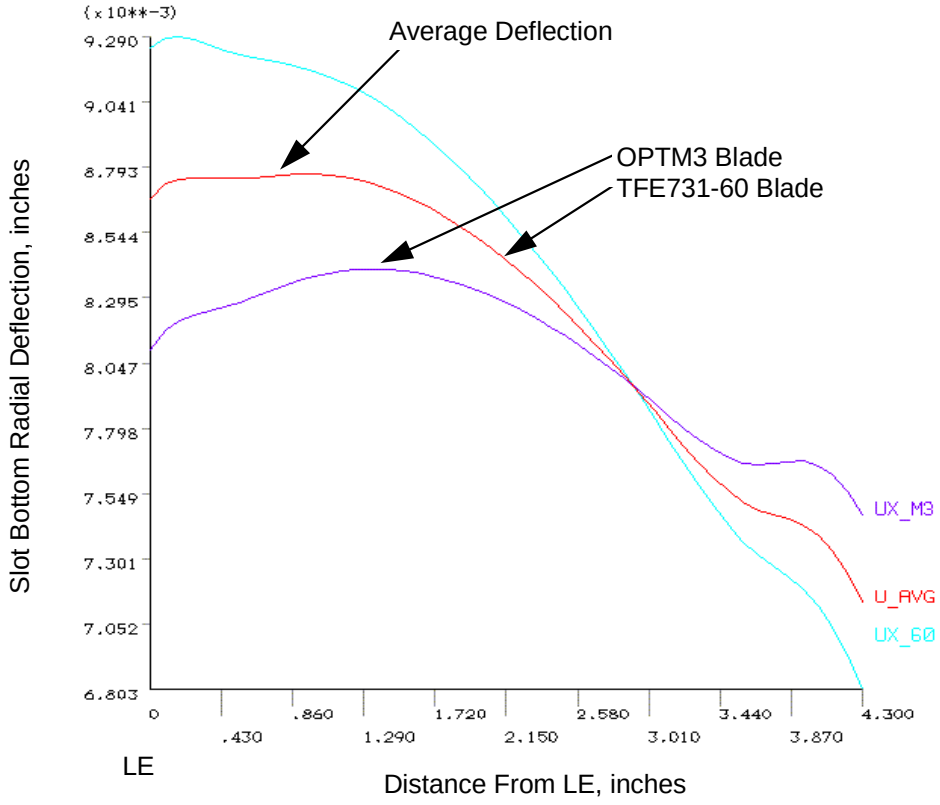

Figure 5.3.1-4. Rim Rolling Well Balanced for Both Blades

Figure 5.3.2-1. Solid Geometry of the Disk

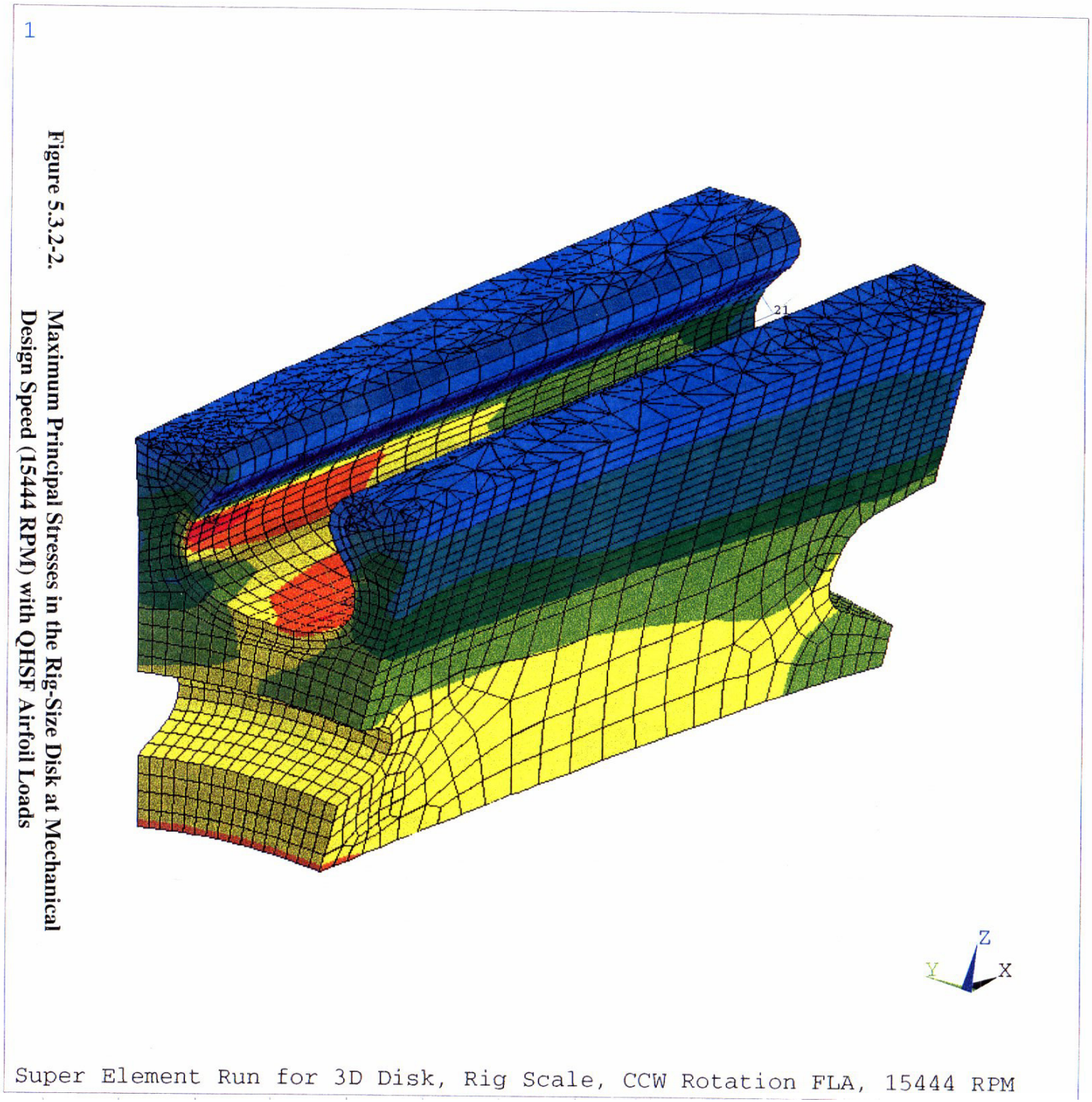

Figure 5.3.2-2. Maximum Principal Stresses in the Rig-Size Disk at Mechanical Design Speed (15444 RPM) with QHSF Airfoil Loads

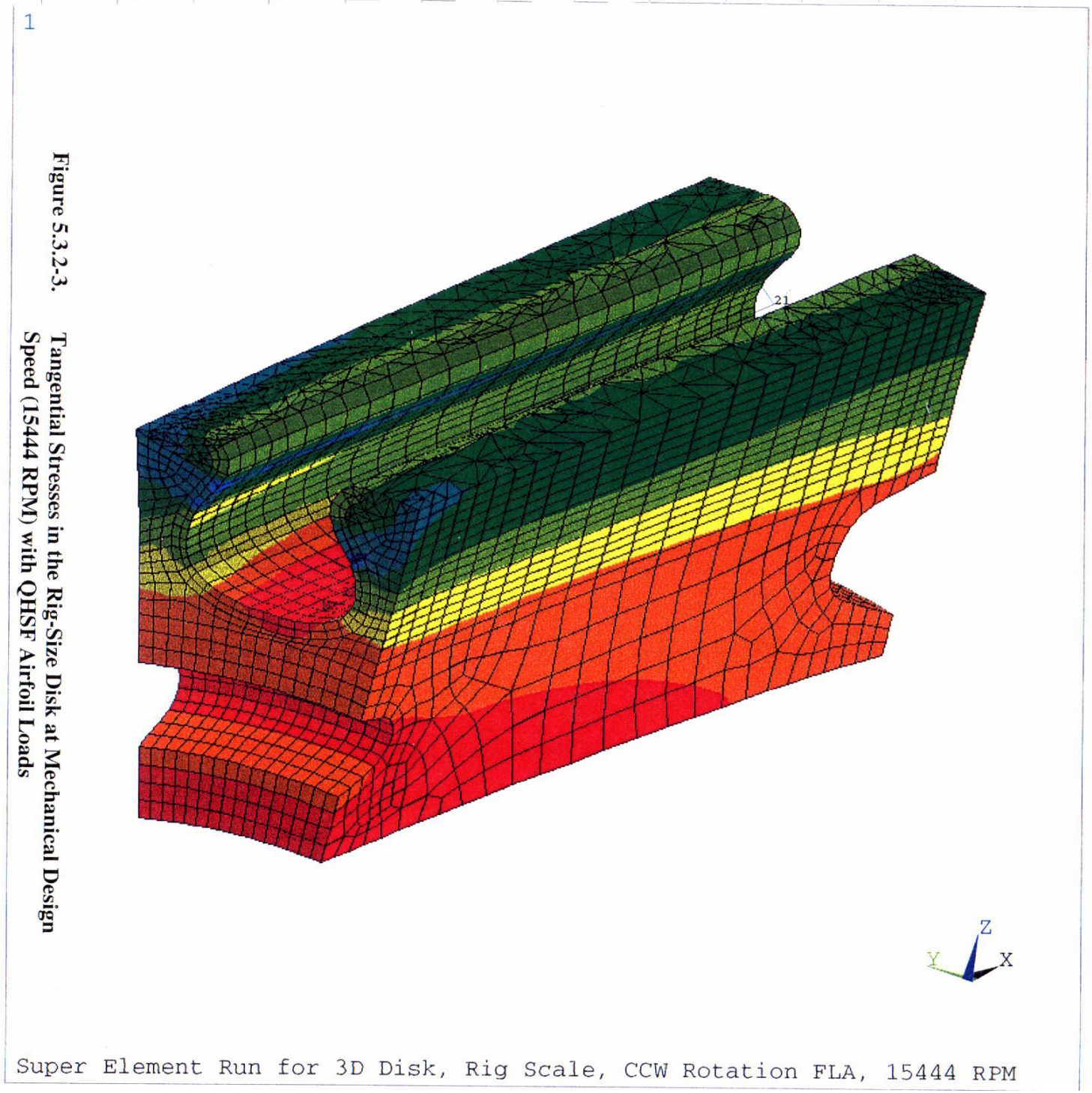

Figure 5.3.2-3. Tangential Stresses in the Rig-Size Disk at Mechanical Design Speed (15444 RPM) with QHSF Airfoil Loads

Highlights of QHSF Disk are summarized below:

- Disk Material is C250 steel
- Disk/dovetail profile is a derivative of the baseline disk design
- Dimensions modified to fit into the NASA balance and to accommodate .25″ thick torque sleeve
- Meets both NASA and AE design criteria
- Disk has adequate burst margins, unzip capability and factors of safety
- Optimized to perform well with both QHSF and baseline rotors
- Well balanced to minimize rim roll by providing undercuts
- 3-D stress analysis performed to qualify design

6.0 CONCLUSIONS

The QHSF has been designed to meet aggressive acoustic goals while maintaining performance and mechanical qualities equal to or better than the baseline fan. The design was achieved through innovative use of advanced design techniques and close cooperation between the different disciplines on the team. Validation of this technology in the upcoming rig test will allow it to be used to meet the stringent acoustic requirements of the next generation of turbofan engines.

7.0 REFERENCES

1 R.E. Hayden, D.B. Bliss, B.S. Murray, K.L. Chandiramani, J.I. Smullin, P.G. Schwaar, "Analysis and Design of a High Speed, Low Noise Aircraft Fan Incorporating Swept Leading Edge Rotor and Stator Blades", NASA CR-135092, December 1977.

2 Kester, J. D., "Generation and Suppression of Combination Tone Noise from Turbofan Engines", *Proceedings AGARD Fluid Dynamics Panel*, Saint-Louis, France, May 1969.

3 Sofrin, T. G., Pickett, G. F., "Multiple Pure Tone Noise Generated by Fans at Supersonic Tip Speeds," *Fluid Mechanics, Acoustics, and Design of Turbomachinery Symposium*, Penn State, 1970.

4 Morfey, C. L., Fisher, M. J., "Shock Wave Radiation from a Supersonic Ducted Rotor," *The Aeronautical Journal of the Royal Aeronautical Society*, **74**, July 1970, pp. 579-585.

5 Hawkings, D., "Multiple Tone Generation by Transonic Compressors," Journal of Sound and Vibration, Vol. 17 (2), 1971, pp. 241-250.

6 Kurosaka, M., "A Note on Multiple Pure Tone Noise," *Journal of Sound and Vibration*, Vol. 19 (4), 1971, pp. 453-462.

7 Pickett, G. F., "The Prediction of the Spectral Content of Combination Tone Noise," *AIAA Paper 71-730*, 1971.

8 Fink, M. R., "Shock Wave Behavior in Transonic Compressor Noise Generation," *ASME Paper 71-GT-7*, 1971.

9 Kantola, R. A., and Kurosaka, M., "The Theoretical and Experimental Investigations on Multiple Pure Tone Noise," *AIAA Paper 72-127*, 1972.

10 Stratford, B. S., Newby, D. R., A New Look at the Generation of Buzz-Saw Noise, AIAA Paper 77-1343, 1977.

11 Cargill, A. M., "Shock Waves Ahead of a Fan With Nonuniform Blades," AIAA Journal, Vol. 21, No. 4, April 1983, pp. 572-578.

12 Kantola, R. A., Kurosaka, M., "The Theoretical and Experimental Investigations on Multiple Pure Tone Noise, Part 1," *NASA-CR-1831*, 1971.

13 Goldstein, A. W., Glaser, F. W., Coats, J. W., *Acoustic Properties of a Supersonic Fan*, NASA Lewis Research Center, 1972.

14 Lieber, L., Repp, R., Weir, D. S., “Quiet High Speed Fan Final Report,” Contract NAS3-27483, AlliedSignal Engines, NASA CR-1996-198518, November 1996.

15 Storace, AF, “Foreign Object Damage Criteria”, AFAPL -TR-78-81 Volume IV Aero Propulsion Laboratory (AFWAL/POTA), Air Force Wright Aeronautical Laboratories, January, 1985

APPENDIX I

COMPUTER LISTING OF AEROTHERMODYNAMIC PARAMETERS FOR QHSF ROTOR, STATOR, AND FLOWPATH DESIGN

This appendix contains a computer listing of the aerothermodynamic output data for the QHSF fan stage design. All units are in the English system and headings on the columns are self-explanatory. Rotor and stator geometry and loss parameters are included in Tables A-1 to A-3, respectively. Tables A-4 to A-6 contain rotor and stator performance and vector output from spinner leading edge (station 7) to stator trailing edge (station 22).

Table A1. Summary of Quiet High Speed Fan Design

*SUMMARY NASA/AE QHSF Fan. Design Point. 22-in rotor LE tip diameter. 97/03/07
Design report geometry. Final core duct flowpath w/ -60 duct loss. 15:44:24
Rotor and stator performance from DAWES models.

		-------STAGE-------			-----OVERALL-----			--MACH NO--			INLET					
		INLET CORR. FLOW	PRESS. RATIO	EFFI- CIENCY	TEMP RISE	PRESS. RATIO	EFFI- CIENCY	TEMP RISE	ROTOR TIP REL.	VANE HUB ABS.	CORRECTED TIP SPEED	SPEC. FLOW	RPM PHYS.	RPM CORR.	FLOW COEF	PRESS COEF	WORK COEF
ROTOR	1	98.65	1.844	90.15	.212	1.844	90.16	.212	1.423		1474.	42.35	15444.	15357.	.631	.907	1.006
VANE	1		1.813	87.43	.212	1.813	87.43	.212		.968					.631	.880	1.006

		----------CORE----------						----------BYPASS----------						BYPASS RATIO 3.783
		-------STAGE-------			-----OVERALL-----			-------STAGE-------			-----OVERALL-----			
		INLET CORR. FLOW	PRESS. RATIO	EFFI- CIENCY	TEMP RISE	PRESS. RATIO	EFFI- CIENCY	TEMP RISE	INLET CORR. FLOW	PRESS. RATIO	EFFI- CIENCY	TEMP RISE	PRESS. RATIO	EFFI- CIENCY	TEMP RISE
ROTOR	1	20.57	1.845	95.96	.199	1.850	96.41	.199	78.11	1.839	88.31	.215	1.837	88.15	.215
VANE	1		1.817	93.40	.199	1.822	93.85	.199		1.813	85.99	.215	1.811	85.83	.215

		D-FACTOR			TURNING			SOLIDITY			VM RATIO		
		HUB	MEAN	TIP	HUB	MEAN	TIP	HUB	MEAN	TIP	HUB	MEAN	TIP
ROTOR	1	.504	.498	.399	60.1	21.5	8.8	2.849	1.848	1.490	.924	.931	1.008
VANE	1	.434	.479	.291	54.0	41.4	48.7	2.381	1.709	2.191	1.246	.953	1.334

		TWO THETA	TWO THETA FREE	DELTA P OVER Q	DELTA P OVER Q FREE	LOAD COEF.	ASPECT RATIO	MEAN SOLID -ITY	MID SPAN BETA	DODGE SURGE MARGIN	DODGE STALL MARGIN	HORSE POWER
ROTOR	1	6.9	5.8	.470	.418	.589	1.35	1.872	57.41	20.4	14.8	3149.
VANE	1	8.7	8.7	.403	.403	.509	2.42	1.879	41.39	17.2	17.2	

Table A2. Quiet High Speed Fan Rotor Blade Airfoil Geometry

1*AIRFOIL GEOMETRY NASA/AE QHSF Fan. Design Point. 22-in rotor LE tip diameter. 97/03/07
Design report geometry. Final core duct flowpath w/ -60 duct loss. 15:44:24
Rotor and stator performance from DAWES models.

ROTOR 1 AT STATION 16 HAS 22 AXIARB AIRFOILS
INCIDENCE RULE --METAL AN DEVIATION RULE --METAL A

STL NO.	STAG -GER	CAMBER	SOLID -ITY	TMAX/ CHORD	THROAT /SPACE	CHORD	INLET METAL ANGLE	EXIT METAL ANGLE	--------INCIDENCE--------- MEAN LINE	SUCTION SURFACE	FCMW	DELTA	INLET REL. MACH	PASSAGE ANGLE	MIN. A/A* NS	PASSAGE ANGLE LOCATION	MAXIMUM THICKNESS LOCATION	CRP
24	61.55	13.30	1.490	.0203	.4270	4.626	65.69	52.39	5.52	4.36	3.81	.00	1.425	59.04	1.018	.600	.601	.834
23	60.47	11.63	1.509	.0207	.4438	4.609	64.21	52.58	2.35	1.14	.92	.00	1.463	58.38	1.042	.587	.602	.854
22	59.48	10.74	1.526	.0210	.4580	4.594	63.01	52.28	1.90	.66	.25	.00	1.466	57.59	1.053	.574	.604	.880
21	58.42	10.67	1.543	.0213	.4720	4.577	62.00	51.34	2.03	.75	.62	.00	1.459	56.64	1.060	.561	.604	.896
20	57.42	10.70	1.559	.0215	.4846	4.559	61.09	50.39	2.39	1.08	.77	.00	1.445	55.72	1.058	.551	.604	.910
19	55.56	10.82	1.587	.0220	.5092	4.507	59.42	48.60	3.12	1.77	1.63	.00	1.415	54.03	1.057	.531	.604	.938
18	53.88	10.63	1.607	.0225	.5321	4.431	57.82	47.19	3.74	2.35	2.40	.00	1.383	52.54	1.052	.510	.601	.973
17	52.23	10.60	1.626	.0230	.5542	4.347	56.30	45.69	4.29	2.88	3.12	.00	1.351	51.05	1.048	.494	.597	1.000
16	50.50	11.16	1.649	.0237	.5745	4.269	54.88	43.73	4.71	3.29	3.48	.00	1.316	49.40	1.043	.473	.591	1.038
15	48.64	12.26	1.683	.0250	.5935	4.208	53.55	41.29	5.01	3.52	3.74	.00	1.280	47.56	1.036	.449	.583	1.087
14	46.66	13.87	1.727	.0273	.6109	4.161	52.28	38.41	5.14	3.12	3.87	.00	1.242	45.51	1.054	.428	.573	1.139
13	44.50	15.93	1.782	.0309	.6266	4.122	51.01	35.08	5.15	2.81	3.65	.00	1.202	43.23	1.057	.400	.560	1.220
12	42.12	18.61	1.848	.0353	.6405	4.089	49.76	31.15	4.97	2.22	3.25	.00	1.160	40.65	1.053	.372	.544	1.314
11	39.32	22.06	1.925	.0397	.6549	4.056	48.66	26.60	4.46	1.34	2.62	.00	1.117	37.81	1.050	.341	.525	1.440
10	36.27	25.99	2.012	.0430	.6682	4.017	47.59	21.60	3.69	.35	2.04	.00	1.071	34.75	1.041	.310	.501	1.595
9	33.72	28.98	2.088	.0447	.6787	3.979	46.69	17.71	3.01	-.39	1.56	.00	1.033	32.32	1.025	.283	.479	1.752
8	32.21	30.28	2.123	.0452	.6840	3.961	46.26	15.97	2.71	-.68	1.34	.00	1.015	31.23	1.017	.272	.469	1.822
7	29.25	33.12	2.214	.0462	.6959	3.919	45.07	11.96	2.14	-1.22	.84	.00	.973	28.60	1.006	.245	.443	2.027
6	27.10	34.54	2.282	.0468	.7045	3.893	44.12	9.58	1.86	-3.08	.50	.00	.944	26.92	1.000	.230	.424	2.165
5	25.09	35.54	2.345	.0474	.7118	3.876	43.22	7.68	1.71	-3.32	.20	.00	.919	25.51	.996	.214	.407	2.326
4	22.50	36.71	2.437	.0483	.7211	3.858	41.93	5.21	1.61	-3.41	.15	.00	.886	23.62	.991	.193	.385	2.588
3	19.60	38.05	2.533	.0494	.7304	3.846	40.59	2.55	1.61	-3.86	.14	.00	.854	21.62	.991	.175	.363	2.846
2	15.91	39.12	2.667	.0509	.7404	3.842	38.83	-.29	1.70	-4.50	-.60	.00	.814	19.31	.992	.156	.335	3.205
1	10.21	41.15	2.849	.0530	.7485	3.841	36.66	-4.49	3.96	-3.47	.19	.00	.732	16.08	1.052	.132	.302	3.788

Table A2. Quiet High Speed Fan Rotor Blade Airfoil Geometry (cont.)

STL NO.	-DEVIATION- MEAN LINE	DELTA	LEAD -ING RADIUS	TRAIL -ING RADIUS	STACK RADIUS	CONE ANGLE	X-CG	Y-CG	EDGE COORDINATES---------- FRONT------- AXIAL	RADIAL	REAR-------- AXIAL	RADIAL	SHOCK LOSS	DELTA S	MAX CAMBER LOC	SUCTION SURFACE MACH NO	INCI- DENTAL ANGLE
24	10.06	.00	.0142	.0087	10.732	-7.00	-1.225	-1.221	-12.402	11.013	-10.199	10.743	.0000	.2491	.709	1.289	64.80
23	7.91	.00	.0142	.0091	10.592	-6.02	-1.098	-1.029	-12.314	10.824	-10.042	10.585	.0000	.2285	.697	1.315	63.65
22	6.42	.00	.0142	.0093	10.455	-5.55	-.986	-.861	-12.235	10.661	-9.903	10.435	.0000	.2442	.689	1.341	62.76
21	5.50	.00	.0143	.0096	10.321	-5.08	-.895	-.728	-12.175	10.504	-9.779	10.291	.0002	.2634	.683	1.354	61.94
20	4.55	.00	.0143	.0098	10.188	-4.60	-.806	-.598	-12.114	10.349	-9.661	10.152	.0020	.2875	.678	1.369	61.19
19	3.28	.00	.0143	.0103	9.922	-3.41	-.659	-.391	-12.014	10.035	-9.466	9.883	.0093	.3338	.672	1.394	59.73
18	2.39	.00	.0145	.0108	9.651	-2.08	-.537	-.228	-11.924	9.717	-9.313	9.622	.0187	.3783	.666	1.418	58.33
17	1.77	.00	.0152	.0113	9.372	-.70	-.433	-.098	-11.841	9.393	-9.181	9.360	.0299	.4220	.660	1.440	56.96
16	1.42	.00	.0163	.0117	9.079	.75	-.344	.005	-11.770	9.057	-9.057	9.093	.0421	.4625	.657	1.456	55.64
15	1.33	.00	.0176	.0122	8.772	2.26	-.268	.085	-11.713	8.709	-8.938	8.818	.0478	.5014	.654	1.468	54.40
14	1.41	.00	.0187	.0130	8.448	3.85	-.201	.144	-11.670	8.343	-8.825	8.534	.0431	.5336	.653	1.454	53.30
13	1.60	.00	.0199	.0136	8.107	5.53	-.143	.187	-11.636	7.959	-8.715	8.242	.0350	.5666	.653	1.440	52.28
12	2.05	.00	.0213	.0142	7.746	7.37	-.094	.213	-11.609	7.552	-8.608	7.940	.0268	.6005	.654	1.422	51.31
11	2.78	.00	.0237	.0151	7.365	9.43	-.050	.228	-11.587	7.119	-8.500	7.632	.0213	.6388	.649	1.417	50.36
10	3.60	.00	.0274	.0161	6.960	11.76	-.012	.233	-11.560	6.658	-8.399	7.316	.0158	.6763	.643	1.403	49.27
9	3.93	.00	.0305	.0169	6.627	13.76	.014	.229	-11.537	6.278	-8.335	7.062	.0116	.7031	.630	1.386	48.26
8	4.04	.00	.0318	.0172	6.480	14.69	.024	.226	-11.531	6.107	-8.304	6.953	.0102	.7147	.608	1.382	47.76
7	4.12	.00	.0351	.0182	6.127	16.98	.042	.212	-11.510	5.699	-8.260	6.692	.0026	.7321	.583	1.336	46.63
6	3.77	.00	.0374	.0189	5.888	18.59	.051	.198	-11.499	5.421	-8.238	6.518	.0004	.7384	.551	1.291	45.68
5	3.35	.00	.0392	.0194	5.692	19.96	.054	.181	-11.497	5.188	-8.224	6.377	.0000	.7407	.523	1.250	45.03
4	2.61	.00	.0408	.0200	5.438	21.78	.054	.155	-11.494	4.885	-8.217	6.194	.0002	.7400	.500	1.198	43.74
3	2.07	.00	.0420	.0204	5.202	23.53	.049	.125	-11.500	4.597	-8.215	6.028	.0000	.7340	.480	1.147	42.50
2	.62	.00	.0431	.0204	4.923	25.69	.033	.077	-11.512	4.249	-8.226	5.830	.0000	.7168	.463	1.083	41.50
1	-14.99	.00	.0442	.0204	4.608	27.88	.000	.000	-11.543	3.850	-8.252	5.591	.0000	.7384	.447	1.014	40.91

THE STACKING AXIS COORDINATE IS -10.1104

Table A2. Quiet High Speed Fan Rotor Blade Airfoil Geometry (concluded)

	INLET					SHOCK IMPINGEMENT POINT							
STL NO	STA SWEEP ANGLE	STL ANGLE	REL FLOW ANGLE	BLADE LEAN ANGLE	OBLQ SHOCK ANGLE	STA SWEEP ANGLE	STL ANGLE	REL FLOW ANGLE	BLADE LEAN ANGLE	OBLQ SHOCK ANGLE	MACH NO INLET	S.S	SHOCK OMEGA BAR
1	4.55	27.32	40.62	-6.94	71.38	13.27	27.62	33.33	1.87	55.63	.732	1.014	.000
2	3.28	25.19	40.53	-6.90	73.65	12.00	25.64	34.63	2.08	58.48	.814	1.083	.000
3	1.55	23.51	42.20	-7.60	77.17	10.40	23.98	35.85	2.13	61.38	.854	1.147	.000
4	.37	22.23	43.54	-9.28	80.57	9.44	22.68	36.89	2.04	63.48	.886	1.198	.000
5	-.52	20.95	44.93	-9.96	83.03	9.00	21.37	37.95	2.28	64.99	.919	1.250	.000
6	-1.43	20.01	45.98	-9.18	84.04	8.66	20.40	38.68	2.39	66.11	.944	1.291	.000
7	-2.58	18.86	47.21	-9.67	86.31	7.37	19.20	39.59	2.58	68.10	.973	1.336	.003
8	-2.43	17.21	48.97	-11.14	88.94	7.05	17.49	40.93	1.92	70.39	1.015	1.382	.010
9	-2.72	16.57	49.69	-11.61	90.11	7.04	16.81	41.72	2.36	70.80	1.033	1.386	.012
10	-3.51	15.14	51.28	-11.20	91.60	6.62	15.27	43.05	3.38	71.81	1.071	1.403	.016
11	-3.18	13.48	53.12	-11.59	93.19	6.59	13.44	44.82	3.79	73.21	1.117	1.417	.021
12	-3.37	11.93	54.73	-12.08	94.99	6.03	11.69	46.67	4.17	74.85	1.160	1.422	.027
13	-4.38	10.48	56.15	-13.61	97.93	4.56	9.98	48.17	3.78	77.52	1.202	1.440	.035
14	-5.82	9.10	57.41	-16.12	101.79	1.77	8.21	49.74	1.50	82.42	1.242	1.454	.043
15	-8.01	7.79	58.56	-20.23	107.28	-1.93	6.36	51.37	-1.97	88.78	1.280	1.468	.048
16	-10.71	6.45	59.60	-25.57	113.96	-5.61	4.47	53.02	-5.85	95.35	1.316	1.456	.042
17	-13.16	5.02	60.58	-29.99	119.71	-10.52	2.69	54.68	-11.73	104.06	1.351	1.440	.030
18	-15.02	3.49	61.56	-33.68	124.53	-13.86	1.03	56.39	-15.64	110.06	1.383	1.418	.019
19	-16.76	1.95	62.54	-37.27	129.14	-17.01	-.65	58.13	-19.28	115.57	1.415	1.394	.009
20	-19.56	.39	63.48	-40.38	133.74	-21.30	-2.32	59.96	-24.33	122.64	1.445	1.369	.002
21	-21.13	-.39	64.04	-43.35	137.21	-24.46	-3.14	60.96	-27.11	126.77	1.459	1.354	.000
22	-23.34	-1.16	64.92	-45.42	140.22	-27.17	-4.01	62.03	-29.12	129.94	1.466	1.341	.000
23	-25.33	-1.97	66.56	-46.86	142.58	-31.14	-5.03	63.10	-32.54	134.81	1.463	1.315	.000
24	-24.94	-3.26	71.21	-46.86	142.64	-32.22	-7.00	64.37	-33.18	136.25	1.425	1.289	.000

Table A3. Quiet High Speed Fan Stator Vane Airfoil Geometry

1*AIRFOIL GEOMETRY NASA/AE QHSF Fan. Design Point. 22-in rotor LE tip diameter. 97/03/07
Design report geometry. Final core duct flowpath w/ -60 duct loss. 15:44:24
Rotor and stator performance from DAWES models.

VANE 1 AT STATION 22 HAS 52 AXIARB AIRFOILS
INCIDENCE RULE --METAL AN DEVIATION RULE --METAL A

STL NO.	STAG -GER	CAMBER	SOLID -ITY	TMAX/ CHORD	THROAT /SPACE	CHORD	INLET METAL ANGLE	EXIT METAL ANGLE	--------INCIDENCE--------- MEAN LINE	SUCTION SURFACE	FCMW	DELTA	INLET REL. MACH	PASSAGE ANGLE	MIN. A/A* NS	PASSAGE ANGLE LOCATION	MAXIMUM THICKNESS LOCATION	CRP
24	23.34	76.05	2.191	.0453	.5802	2.883	63.49	-12.56	-14.77	-17.08	-7.90	.00	.516	25.46	1.092	.302	.600	1.658
23	21.51	72.89	2.107	.0609	.6073	2.738	60.42	-12.46	-15.71	-19.22	-8.60	.00	.547	23.98	1.077	.297	.600	1.684
22	19.61	69.70	2.014	.0687	.6408	2.583	57.35	-12.35	-15.26	-19.10	-11.61	.00	.574	22.50	1.076	.293	.600	1.705
21	17.81	66.45	1.905	.0691	.6794	2.413	54.24	-12.22	-12.96	-16.73	-9.54	.00	.600	21.01	1.100	.288	.600	1.734
20	16.07	63.34	1.818	.0654	.7166	2.270	51.18	-12.16	-10.55	-14.10	-6.82	.00	.627	19.53	1.112	.285	.600	1.756
19	13.81	59.02	1.717	.0531	.7674	2.087	46.94	-12.08	-7.10	-9.86	-6.03	.00	.665	17.44	1.121	.273	.600	1.834
18	12.84	56.86	1.689	.0464	.7881	2.001	44.93	-11.93	-5.27	-7.49	-3.72	.00	.689	16.50	1.123	.263	.600	1.900
17	12.57	55.82	1.679	.0452	.7943	1.939	44.04	-11.78	-4.12	-6.01	-2.62	.00	.706	16.13	1.121	.259	.600	1.934
16	12.52	55.53	1.673	.0471	.7940	1.881	43.76	-11.77	-3.35	-5.20	-2.84	.00	.722	16.00	1.117	.260	.600	1.925
15	12.60	55.97	1.670	.0505	.7896	1.826	43.98	-11.98	-3.03	-5.05	-2.69	.00	.737	16.01	1.110	.259	.600	1.927
14	12.75	56.73	1.674	.0529	.7843	1.776	44.45	-12.28	-3.06	-5.26	-2.44	.00	.753	16.10	1.101	.262	.600	1.905
13	12.82	57.34	1.686	.0532	.7808	1.733	44.78	-12.56	-3.22	-5.45	-2.25	.00	.771	16.11	1.090	.263	.600	1.903
12	12.79	57.63	1.709	.0523	.7790	1.698	44.85	-12.78	-3.43	-5.53	-2.20	.00	.791	16.05	1.076	.260	.600	1.925
11	12.63	57.93	1.745	.0517	.7775	1.671	44.90	-13.03	-3.79	-5.67	-2.39	.00	.814	15.95	1.060	.256	.600	1.952
10	12.67	58.36	1.799	.0529	.7714	1.655	45.19	-13.17	-4.30	-7.86	-2.47	.00	.839	16.02	1.040	.253	.600	1.972
9	13.02	58.83	1.854	.0551	.7623	1.650	45.77	-13.06	-4.87	-8.52	-3.94	.00	.858	16.35	1.021	.251	.600	1.994
8	13.22	59.12	1.882	.0562	.7578	1.651	46.11	-13.00	-5.18	-8.88	-3.85	.00	.867	16.54	1.013	.248	.600	2.014
7	13.73	59.88	1.954	.0579	.7461	1.656	46.98	-12.90	-5.91	-9.75	-3.39	.00	.887	17.04	.993	.246	.600	2.029
6	14.10	60.59	2.008	.0580	.7379	1.662	47.70	-12.89	-6.44	-10.31	-4.94	.00	.900	17.41	.980	.244	.600	2.047
5	14.21	61.36	2.057	.0574	.7313	1.670	48.46	-12.90	-6.99	-10.78	-4.80	.00	.911	17.78	.971	.242	.600	2.067
4	14.43	62.52	2.127	.0560	.7214	1.686	49.52	-13.01	-7.66	-11.29	-4.58	.00	.926	18.27	.957	.237	.600	2.111
3	14.57	63.86	2.197	.0554	.7112	1.703	50.57	-13.29	-8.26	-11.77	-4.48	.00	.942	18.67	.946	.234	.600	2.130
2	15.20	66.80	2.279	.0571	.6871	1.721	52.82	-13.97	-9.86	-13.35	-5.84	.00	.966	19.46	.923	.233	.600	2.142
1	17.14	72.84	2.381	.0637	.6256	1.748	58.14	-14.70	-4.15	-8.05	-1.43	.00	.968	21.72	.977	.245	.600	2.039

Table A3. Quiet High Speed Fan Stator Vane Airfoil Geometry (cont.)

STL NO.	-DEVIATION- MEAN LINE	DELTA	LEAD -ING RADIUS	TRAIL -ING RADIUS	STACK RADIUS	CONE ANGLE	X-CG	Y-CG	EDGE COORDINATES---------- FRONT------- AXIAL	RADIAL	REAR-------- AXIAL	RADIAL	SHOCK LOSS	DELTA S	MAX CAMBER LOC	SUCTION SURFACE MACH NO	INCI- DENTAL ANGLE
24	12.56	.00	.0169	.0404	10.889	.00	3.468	2.136	-5.075	10.889	-2.443	10.889	.0000	.8688	.480	1.303	55.57
23	12.46	.00	.0183	.0383	10.707	.59	3.448	1.816	-5.046	10.730	-2.513	10.757	.0000	.6322	.475	.687	53.32
22	12.35	.00	.0201	.0372	10.568	.48	3.430	1.514	-5.016	10.586	-2.600	10.607	.0000	.6244	.471	.735	53.96
21	12.22	.00	.0196	.0306	10.454	-.07	3.408	1.244	-4.978	10.451	-2.698	10.448	.0000	.6342	.468	.812	51.15
20	12.16	.00	.0178	.0254	10.349	-.72	3.380	1.015	-4.957	10.320	-2.792	10.293	.0000	.6346	.465	.884	47.68
19	12.08	.00	.0144	.0212	10.130	-1.53	3.279	.699	-4.999	10.069	-2.986	10.015	.0000	.6271	.463	.980	45.86
18	11.93	.00	.0136	.0201	9.897	-1.92	3.122	.508	-5.124	9.825	-3.187	9.760	.0000	.6250	.461	1.035	43.33
17	11.78	.00	.0144	.0191	9.652	-2.09	2.945	.382	-5.268	9.579	-3.390	9.511	.0000	.6282	.461	1.077	42.48
16	11.77	.00	.0153	.0175	9.393	-2.03	2.765	.303	-5.413	9.327	-3.592	9.262	.0000	.6366	.461	1.120	43.20
15	11.98	.00	.0157	.0160	9.120	-1.78	2.585	.256	-5.560	9.067	-3.793	9.012	.0000	.6441	.461	1.150	43.60
14	12.28	.00	.0155	.0149	8.834	-1.40	2.406	.235	-5.713	8.796	-3.994	8.754	.0000	.6537	.461	1.178	43.77
13	12.56	.00	.0151	.0147	8.539	-.95	2.227	.225	-5.870	8.516	-4.194	8.488	.0000	.6621	.462	1.202	43.75
12	12.78	.00	.0150	.0153	8.235	-.50	2.047	.220	-6.034	8.225	-4.392	8.210	.0000	.6748	.462	1.225	43.58
11	13.03	.00	.0154	.0163	7.926	-.13	1.865	.218	-6.205	7.924	-4.588	7.920	.0001	.6931	.462	1.252	43.47
10	13.17	.00	.0161	.0165	7.610	.15	1.677	.226	-6.382	7.612	-4.782	7.616	.0005	.7039	.462	1.270	43.30
9	13.06	.00	.0165	.0155	7.357	.36	1.527	.242	-6.525	7.362	-4.931	7.372	.0010	.7116	.462	1.280	44.79
8	13.00	.00	.0166	.0150	7.246	.53	1.463	.251	-6.587	7.252	-4.994	7.267	.0012	.7101	.463	1.281	44.74
7	12.90	.00	.0166	.0143	6.982	1.26	1.318	.276	-6.730	6.994	-5.136	7.029	.0017	.6937	.464	1.285	44.35
6	12.89	.00	.0165	.0152	6.808	1.91	1.227	.296	-6.824	6.823	-5.226	6.877	.0022	.6819	.464	1.287	46.08
5	12.90	.00	.0164	.0169	6.668	2.57	1.159	.312	-6.899	6.685	-5.294	6.756	.0026	.6719	.463	1.290	46.13
4	13.01	.00	.0164	.0193	6.490	3.59	1.074	.335	-6.993	6.508	-5.377	6.609	.0031	.6553	.461	1.289	46.16
3	13.29	.00	.0167	.0197	6.331	4.71	.997	.358	-7.076	6.347	-5.447	6.482	.0001	.6413	.460	1.303	46.47
2	13.97	.00	.0173	.0177	6.151	6.14	.897	.395	-7.172	6.162	-5.533	6.338	.0018	.6178	.459	1.308	48.53
1	14.70	.00	.0183	.0159	5.952	8.60	.783	.469	-7.272	5.952	-5.631	6.200	.0292	.6731	.460	1.497	54.80

THE STACKING AXIS COORDINATE IS -7.2723

Table A3. Quiet High Speed Fan Stator Vane Airfoil Geometry (concluded)

	INLET					SHOCK IMPINGEMENT POINT							
STL NO	STA SWEEP ANGLE	STL ANGLE	REL FLOW ANGLE	BLADE LEAN ANGLE	OBLQ SHOCK ANGLE	STA SWEEP ANGLE	STL ANGLE	REL FLOW ANGLE	BLADE LEAN ANGLE	OBLQ SHOCK ANGLE	MACH NO INLET	S.S	SHOCK OMEGA BAR
1	25.36	13.29	53.99	-5.40	73.18	29.02	12.82	38.14	-15.68	70.24	.968	1.497	.029
2	26.25	11.68	42.96	-5.18	67.26	29.63	10.95	34.65	-12.09	66.16	.966	1.308	.002
3	27.31	10.51	42.30	-4.72	66.63	29.94	9.69	33.06	-6.99	62.34	.942	1.303	.000
4	27.72	9.55	41.86	-4.27	66.42	30.18	8.65	32.47	-5.02	61.31	.926	1.289	.003
5	28.15	8.55	41.47	-3.95	66.36	30.59	7.58	31.55	-4.30	60.92	.911	1.290	.003
6	28.50	7.82	41.26	-3.59	66.23	30.47	6.83	31.07	-4.13	61.27	.900	1.287	.002
7	28.83	6.99	41.07	-3.18	66.17	30.53	5.98	30.40	-3.84	61.43	.887	1.285	.002
8	29.22	5.86	40.93	-2.91	66.40	30.84	4.86	29.48	-3.37	61.43	.867	1.281	.001
9	29.57	5.42	40.90	-2.45	66.10	31.25	4.42	29.04	-2.51	60.79	.858	1.280	.001
10	29.69	4.49	40.89	-1.66	66.07	31.32	3.53	28.36	-1.54	60.67	.839	1.270	.001
11	29.61	3.46	41.11	-1.06	66.49	31.31	2.57	27.88	-.23	60.61	.814	1.252	.000
12	29.47	2.58	41.42	-.65	67.02	31.26	1.78	27.88	.73	60.80	.791	1.225	.000
13	29.36	1.82	41.55	.18	67.07	31.34	1.09	27.65	1.33	60.94	.771	1.202	.000
14	29.35	1.14	41.39	1.88	66.29	31.16	.46	27.33	2.46	60.98	.753	1.178	.000
15	29.46	.52	40.95	5.13	64.25	31.52	-.11	27.00	5.71	59.52	.737	1.150	.000
16	29.71	-.06	40.41	9.87	61.17	31.64	-.64	26.65	10.97	57.50	.722	1.120	.000
17	30.09	-.57	39.92	16.20	57.19	31.98	-1.06	26.91	18.34	54.74	.706	1.077	.000
18	28.80	-.96	39.66	24.17	53.89	31.75	-1.35	27.40	28.27	52.15	.689	1.035	.000
19	18.90	-1.08	39.84	35.07	55.91	23.32	-1.36	28.70	42.13	55.56	.665	.980	.000
20	.64	-.50	40.63	43.84	63.10	8.72	-.71	31.89	52.31	60.63	.627	.884	.000
21	-12.01	.12	41.28	49.61	66.29	-7.42	-.07	34.44	58.31	64.86	.600	.812	.000
22	-13.56	.79	42.09	52.06	64.67	-10.21	.61	37.07	60.01	62.90	.574	.735	.000
23	-10.98	1.23	44.72	53.48	60.41	-8.49	1.01	39.73	60.68	59.45	.547	.687	.000
24	-10.44	.96	48.72	53.67	57.25	-7.15	.68	41.89	60.85	57.16	.516	.653	.000

Table A4. Quiet High Speed Fan Rotor Blade Performance

1*LOSS AND DEV. NASA/AE QHSF Fan. Design Point. 22-in rotor LE tip diameter. 97/03/07
Design report geometry. Final core duct flowpath w/ -60 duct loss. 15:44:24
Rotor and stator performance from DAWES models.

ROTOR 1 AT STATION 16 HAS 22 AXIARB AIRFOILS THE SHIFT IS .00 THE FLOW AND SPEED ARE 83.38
15444.

* * * * * * * AIRFOIL PROPERTIES * * * * * * * * * * * INCIDENCE SUMMARY * * * * * * *																	
STL NO.	PCT SPAN	STAGGER ANG	CAMBER ANG	SOLID -ITY	TMAX /C	THROAT /S	CHORD	MACH INLET	NUMBER CRITICAL	2-D D-FAC	INLET ANGLES METAL	AIR	CHOKE INC	MIN LOSS INC	STALL INC	NORM INC	MEAN INC	INCID DENTAL
24	100.00	61.55	13.30	1.490	.020	.427	4.626	1.425	.814	.399	65.69	71.21	-999.00	2.73	999.00	.003	5.52	6.41
23	95.96	60.47	11.63	1.509	.021	.444	4.610	1.463	.830	.404	64.21	66.56	-999.00	3.33	999.00	-.001	2.35	2.91
22	92.44	59.48	10.74	1.526	.021	.458	4.596	1.466	.839	.401	63.01	64.92	-999.00	3.69	999.00	-.002	1.90	2.16
21	89.22	58.42	10.67	1.543	.021	.472	4.580	1.459	.842	.410	62.00	64.04	-999.00	4.10	999.00	-.002	2.03	2.10
20	86.12	57.42	10.70	1.559	.021	.485	4.563	1.445	.845	.416	61.09	63.48	-999.00	4.49	999.00	-.002	2.39	2.29
19	80.42	55.56	10.82	1.587	.022	.509	4.513	1.415	.848	.425	59.42	62.54	-999.00	5.25	999.00	-.002	3.12	2.81
18	75.13	53.88	10.63	1.607	.022	.532	4.438	1.383	.852	.435	57.82	61.56	-999.00	6.07	999.00	-.002	3.74	3.23
17	69.97	52.23	10.60	1.626	.023	.554	4.354	1.351	.855	.449	56.30	60.58	-999.00	6.48	999.00	-.002	4.29	3.62
16	64.80	50.50	11.16	1.649	.024	.575	4.275	1.316	.854	.464	54.88	59.60	-999.00	6.59	999.00	-.002	4.71	3.96
15	59.54	48.64	12.26	1.683	.025	.594	4.212	1.280	.850	.479	53.55	58.56	-999.00	6.86	999.00	-.002	5.01	4.15
14	54.15	46.66	13.87	1.727	.027	.611	4.164	1.242	.844	.491	52.28	57.41	-999.00	7.26	999.00	-.002	5.14	4.11
13	48.63	44.50	15.93	1.782	.031	.627	4.124	1.202	.835	.498	51.01	56.15	-999.00	7.82	999.00	-.003	5.15	3.87
12	42.98	42.12	18.61	1.848	.035	.640	4.090	1.160	.823	.498	49.76	54.73	-999.00	8.42	999.00	-.003	4.97	3.42
11	37.22	39.32	22.06	1.925	.040	.655	4.057	1.117	.811	.491	48.66	53.12	-999.00	8.46	999.00	-.004	4.46	2.76
10	31.35	36.27	25.99	2.012	.043	.668	4.018	1.071	.800	.481	47.59	51.28	-999.00	8.04	999.00	-.004	3.69	2.02
9	26.71	33.72	28.98	2.088	.045	.679	3.980	1.033	.794	.471	46.69	49.69	-999.00	7.61	999.00	-.005	3.01	1.43
8	24.69	32.21	30.28	2.123	.045	.684	3.962	1.015	.792	.466	46.26	48.97	-999.00	7.17	999.00	-.004	2.71	1.21
7	19.96	29.25	33.12	2.214	.046	.696	3.919	.973	.789	.448	45.07	47.21	-999.00	6.80	999.00	-.005	2.14	.58
6	16.86	27.10	34.54	2.282	.047	.705	3.893	.944	.788	.434	44.12	45.98	-999.00	6.30	999.00	-.004	1.86	.30
5	14.34	25.09	35.54	2.345	.047	.712	3.876	.919	.788	.420	43.22	44.93	-999.00	6.06	999.00	-.004	1.71	-.10
4	11.10	22.50	36.71	2.437	.048	.721	3.858	.886	.789	.400	41.93	43.54	-999.00	5.67	999.00	-.004	1.61	-.21
3	8.13	19.60	38.05	2.533	.049	.730	3.846	.854	.789	.378	40.59	42.20	-999.00	5.93	999.00	-.004	1.61	-.29
2	4.59	15.91	39.12	2.667	.051	.740	3.842	.814	.791	.345	38.83	40.53	-999.00	6.17	999.00	-.004	1.70	-.97
1	.00	10.21	41.15	2.849	.053	.749	3.841	.732	.791	.504	36.66	40.62	-999.00	5.83	999.00	-.002	3.96	-.30

Table A4. Quiet High Speed Fan Rotor Blade Performance (cont.)

* * * * L O S S	C O M P O N E N T	S U M M A R Y * * * *	* * * * * * D E V I A T I O N	S U M M A R Y * * * * * * * * * * * * *
STL NUM. NO.	PROFILE LOSS	DRAG RISE	INC. LOSS	SHOCK LOSS	REY NO LOSS	MIG. LOSS	TOTAL LOSS	APPLIED LOSS	INPUT TABLE	EXIT ANGLES METAL	AIR	APPLIED OVER-DEV	LORD	CARTER RULE	SP 36 (DELTA DEVIATION) (MACH NO	INPUT)	REY X 10**-5
24	.0479	.0023	.0000	.0000	.0000	.0960	.1462	.0819	.0000	52.39	62.45	10.06	4.14	4.46	5.06	.00	.00	26.74
23	.0463	.0022	.0000	.0000	.0000	.0714	.1199	.1321	.0000	52.58	60.49	7.91	5.14	5.44	5.31	.00	.00	28.01
22	.0440	.0020	.0000	.0000	.0000	.0502	.0962	.1279	.0000	52.28	58.70	6.42	5.36	5.13	4.92	.00	.00	28.12
21	.0437	.0020	.0000	.0002	.0000	.0324	.0783	.1300	.0000	51.34	56.84	5.50	5.45	4.94	4.73	.00	.00	27.87
20	.0431	.0019	.0000	.0020	.0000	.0158	.0629	.1245	.0000	50.39	54.94	4.55	5.54	4.66	4.52	.00	.00	27.48
19	.0423	.0019	.0000	.0093	.0000	.0000	.0534	.1121	.0000	48.60	51.88	3.28	5.65	4.34	4.24	.00	.00	26.57
18	.0423	.0018	.0000	.0187	.0000	.0000	.0628	.1057	.0000	47.19	49.59	2.39	5.78	4.19	4.06	.00	.00	25.51
17	.0430	.0018	.0000	.0299	.0000	.0000	.0747	.1061	.0000	45.69	47.46	1.77	5.97	4.23	4.03	.00	.00	24.39
16	.0440	.0019	.0000	.0421	.0000	.0000	.0880	.1110	.0000	43.73	45.15	1.42	6.27	4.48	4.18	.00	.00	23.31
15	.0451	.0020	.0000	.0478	.0000	.0000	.0948	.1175	.0000	41.29	42.61	1.33	6.73	4.93	4.52	.00	.00	22.31
14	.0460	.0021	.0000	.0431	.0000	.0000	.0912	.1221	.0000	38.41	39.81	1.41	7.27	5.54	4.99	.00	.00	21.39
13	.0464	.0021	.0000	.0350	.0000	.0000	.0835	.1205	.0000	35.08	36.67	1.60	7.90	6.26	5.57	.00	.00	20.50
12	.0461	.0022	.0000	.0268	.0000	.0000	.0751	.1110	.0000	31.15	33.19	2.05	8.63	7.15	6.29	.00	.00	19.62
11	.0452	.0022	.0000	.0213	.0000	.0000	.0687	.0941	.0000	26.60	29.38	2.78	9.48	8.21	7.04	.00	.00	18.73
10	.0441	.0022	.0000	.0158	.0000	.0000	.0621	.0752	.0000	21.60	25.21	3.60	10.32	9.46	7.86	.00	.00	17.79
9	.0432	.0022	.0000	.0116	.0000	.0000	.0570	.0628	.0000	17.71	21.63	3.93	10.80	10.33	8.41	.00	.00	17.01
8	.0427	.0021	.0000	.0102	.0000	.0000	.0550	.0578	.0000	15.97	20.01	4.04	10.87	10.41	8.48	.00	.00	16.67
7	.0411	.0020	.0000	.0026	.0000	.0000	.0457	.0464	.0000	11.96	16.08	4.12	10.57	10.90	8.89	.00	.00	15.85
6	.0398	.0018	.0000	.0004	.0000	.0000	.0420	.0414	.0000	9.58	13.35	3.77	9.94	10.74	8.96	.00	.00	15.31
5	.0386	.0015	.0000	.0000	.0000	.0000	.0401	.0393	.0000	7.68	11.03	3.35	9.19	10.44	8.89	.00	.00	14.89
4	.0367	.0011	.0000	.0002	.0000	.0034	.0414	.0408	.0000	5.21	7.82	2.61	7.90	10.26	8.83	.00	.00	14.35
3	.0366	.0007	.0000	.0000	.0000	.0151	.0524	.0451	.0000	2.55	4.62	2.07	6.41	10.62	8.67	.00	.00	13.86
2	.0364	.0002	.0000	.0000	.0000	.0307	.0673	.0550	.0000	-.29	.33	.62	5.45	10.95	8.17	.00	.00	13.30
1	.0640	.0000	.0000	.0000	.0000	.0593	.1234	.3923	.0000	-4.49	-19.48	-14.99	6.99	11.69	7.60	.00	.00	11.88

Table A4. Quiet High Speed Fan Rotor Blade Performance (concluded)

STL NO.	UMCRP	ST2CRP	DELTA IMIN
24	.1505	1.9589	3.12
23	.1580	1.9789	3.19
22	.1662	2.0371	3.23
21	.1872	2.0625	3.50
20	.2095	2.0837	3.78
19	.2561	2.1360	4.36
18	.3066	2.1740	5.02
17	.3576	2.3450	5.29
16	.4096	2.5929	5.33
15	.4606	2.7098	5.49
14	.5038	2.6331	5.71
13	.5374	2.4325	5.95
12	.5551	2.2589	6.12
11	.6290	2.1739	5.73
10	.6843	2.3101	4.87
9	.7180	2.4456	4.08
8	.7447	2.5336	3.47
7	.7644	2.8341	2.68
6	.7878	3.1395	1.81
5	.8117	3.2698	1.20
4	.8459	3.4993	.25
3	.8809	3.3139	-.10
2	.9501	2.9198	-.75
1	1.0834	2.3826	-2.34

NOTE.... THE LETTER (X) TO THE RIGHT OF A NUMBER IN THE ABOVE COLUMNS INDICATES A PROGRAM DEFAULT IS IN EFFECT

Table A5. Quiet High Speed Fan Stator Vane Performance

1*LOSS AND DEV. NASA/AE QHSF Fan. Design Point. 22-in rotor LE tip diameter. 97/03/07
Design report geometry. Final core duct flowpath w/ -60 duct loss. 15:44:24
Rotor and stator performance from DAWES models.

VANE 1 AT STATION 22 HAS 52 AXIARB AIRFOILS THE SHIFT IS .00

STL NO.	PCT SPAN	STAGGER ANG	CAMBER ANG	SOLID -ITY	TMAX /C	THROAT /S	CHORD	MACH NUMBER INLET	CRITICAL	2-D D-FAC	INLET METAL ANGLES	AIR	CHOKE INC	MIN LOSS INC	STALL INC	NORM INC	MEAN INC	INCID DENTAL
24	100.00	23.34	76.05	2.191	.045	.464	2.883	.516	.707	.291	63.49	48.72	-8.30	-4.41	-.75	-2.668	-14.77	-6.86
23	97.19	21.51	72.89	2.107	.061	.486	2.735	.547	.690	.449	60.42	44.72	-8.29	-3.73	.27	-2.627	-15.71	-8.61
22	93.98	19.61	69.70	2.014	.069	.513	2.579	.574	.679	.506	57.35	42.09	-9.82	-4.27	.54	-1.982	-15.26	-11.87
21	90.60	17.81	66.45	1.905	.069	.544	2.406	.600	.675	.546	54.24	41.28	-11.67	-5.34	.10	-1.203	-12.96	-9.87
20	87.29	16.07	63.34	1.818	.065	.573	2.264	.627	.674	.510	51.18	40.63	-13.28	-6.31	-.37	-.608	-10.55	-7.05
19	81.37	13.81	59.02	1.717	.053	.614	2.084	.665	.682	.442	46.94	39.84	-16.15	-8.38	-1.69	.191	-7.10	-6.02
18	75.91	12.84	56.86	1.689	.046	.630	1.998	.689	.688	.425	44.93	39.66	-17.60	-9.39	-2.06	.562	-5.27	-3.68
17	70.57	12.57	55.82	1.679	.045	.635	1.936	.706	.690	.417	44.04	39.92	-18.20	-9.98	-2.18	.751	-4.12	-2.56
16	65.25	12.52	55.53	1.673	.047	.635	1.878	.722	.689	.418	43.76	40.41	-17.90	-10.09	-2.45	.882	-3.35	-2.79
15	59.89	12.60	55.97	1.670	.051	.632	1.824	.737	.685	.427	43.98	40.95	-16.58	-9.56	-2.79	.965	-3.03	-2.65
14	54.40	12.75	56.73	1.674	.053	.627	1.775	.753	.681	.442	44.45	41.39	-15.10	-8.97	-3.20	1.023	-3.06	-2.38
13	48.74	12.82	57.34	1.686	.053	.625	1.732	.771	.681	.457	44.78	41.55	-14.04	-8.64	-3.58	1.070	-3.22	-2.20
12	42.85	12.79	57.63	1.709	.052	.623	1.697	.791	.683	.479	44.85	41.42	-13.29	-8.56	-4.02	1.129	-3.43	-2.15
11	36.68	12.63	57.93	1.745	.052	.622	1.671	.814	.686	.507	44.90	41.11	-13.02	-9.06	-5.09	1.330	-3.79	-2.35
10	30.21	12.67	58.36	1.799	.053	.617	1.655	.839	.689	.529	45.19	40.89	-12.04	-9.07	-6.03	1.568	-4.30	-2.41
9	25.01	13.02	58.83	1.854	.055	.610	1.650	.858	.691	.546	45.77	40.90	-11.01	-8.51	-6.01	1.454	-4.87	-3.90
8	22.78	13.22	59.12	1.882	.056	.606	1.651	.867	.693	.548	46.11	40.93	-10.74	-8.24	-5.74	1.224	-5.18	-3.81
7	17.72	13.73	59.88	1.954	.058	.597	1.656	.887	.696	.534	46.98	41.07	-9.80	-7.30	-4.80	.556	-5.91	-3.28
6	14.48	14.10	60.59	2.008	.058	.590	1.662	.900	.699	.523	47.70	41.26	-9.31	-6.81	-4.31	.149	-6.44	-4.82
5	11.91	14.21	61.36	2.057	.057	.585	1.671	.911	.702	.512	48.46	41.47	-9.43	-6.93	-4.43	-.022	-6.99	-4.66
4	8.77	14.43	62.52	2.127	.056	.577	1.686	.926	.706	.494	49.52	41.86	-9.60	-7.10	-4.60	-.223	-7.66	-4.30
3	6.03	14.57	63.86	2.197	.055	.569	1.703	.942	.710	.480	50.57	42.30	-9.48	-6.98	-4.48	-.513	-8.26	-4.17
2	2.94	15.20	66.80	2.279	.057	.550	1.721	.966	.710	.484	52.82	42.96	-9.09	-6.59	-4.09	-1.311	-9.86	-5.57
1	.00	17.14	72.84	2.381	.064	.500	1.748	.968	.704	.434	58.14	53.99	-8.37	-5.87	-3.37	.685	-4.15	-.81

Table A5. Quiet High Speed Fan Stator Vane Performance (cont.)

* * * * L O S S C O M P O N E N T S U M M A R Y * * * *									* * * * * * D E V I A T I O N S U M M A R Y * * * * * * * * * * * *								
STL NUM. NO.	PROFILE LOSS	DRAG RISE	INC. SHOCK LOSS	REY NO LOSS	MIG. TOTAL LOSS	APPLIED LOSS	INPUT LOSS	EXIT TABLE	ANGLES METAL	AIR	APPLIED DEV	OVER- LORD	CARTER RULE	SP 36	(DELTA (MACH NO	DEVIATION INPUT)	REY X 10**-5
24	.0273	.0000	.1731	.0000	.0641	.2645	-.3218	.0000	-12.56	.00	12.56	24.86	12.92	11.58	.00	.00	8.62
23	.0377	.0000	.2338	.0000	.0379	.3094	.0085	.0000	-12.46	.00	12.46	21.63	12.46	10.82	.00	.00	8.76
22	.0428	.0000	.1774	.0000	.0227	.2429	.1222	.0000	-12.35	.00	12.35	18.75	11.99	10.26	.00	.00	8.72
21	.0442	.0000	.0730	.0000	.0099	.1271	.1988	.0000	-12.22	.00	12.22	16.19	11.60	9.95	.00	.00	8.53
20	.0390	.0000	.0079	.0000	.0005	.0475	.1730	.0000	-12.16	.00	12.16	14.00	11.18	9.61	.00	.00	8.38
19	.0300	.0000	.0021	.0000	.0000	.0322	.1010	.0000	-12.08	.00	12.08	11.47	10.55	9.06	.00	.00	8.19
18	.0278	.0000	.0110	.0000	.0000	.0388	.0832	.0000	-11.93	.00	11.93	10.43	10.18	8.72	.00	.00	8.10
17	.0268	.0001	.0162	.0000	.0000	.0431	.0654	.0000	-11.78	.00	11.78	10.01	10.01	8.65	.00	.00	8.00
16	.0267	.0002	.0197	.0000	.0000	.0467	.0503	.0000	-11.77	.00	11.77	9.87	9.98	8.75	.00	.00	7.87
15	.0277	.0004	.0221	.0000	.0000	.0502	.0423	.0000	-11.98	.00	11.98	9.98	10.07	8.96	.00	.00	7.74
14	.0292	.0006	.0240	.0000	.0000	.0538	.0386	.0000	-12.28	.00	12.28	10.20	10.20	9.18	.00	.00	7.61
13	.0310	.0009	.0255	.0000	.0000	.0573	.0373	.0000	-12.56	.00	12.56	10.36	10.27	9.26	.00	.00	7.53
12	.0337	.0011	.0277	.0000	.0000	.0625	.0374	.0000	-12.78	.00	12.78	10.40	10.24	9.17	.00	.00	7.50
11	.0372	.0014	.0350	.0001	.0000	.0738	.0386	.0000	-13.03	.00	13.03	10.42	10.14	8.95	.00	.00	7.52
10	.0402	.0018	.0416	.0005	.0000	.0841	.0409	.0000	-13.17	.00	13.17	10.56	10.04	8.72	.00	.00	7.59
9	.0430	.0020	.0356	.0010	.0000	.0816	.0435	.0000	-13.06	.00	13.06	10.85	9.99	8.57	.00	.00	7.66
8	.0438	.0021	.0270	.0012	.0000	.0740	.0447	.0000	-13.00	.00	13.00	11.03	9.97	8.51	.00	.00	7.70
7	.0442	.0022	.0068	.0017	.0000	.0548	.0459	.0000	-12.90	.00	12.90	11.49	9.96	8.41	.00	.00	7.80
6	.0443	.0022	.0007	.0022	.0000	.0494	.0446	.0000	-12.89	.00	12.89	11.89	9.98	8.34	.00	.00	7.87
5	.0444	.0022	.0000	.0026	.0000	.0492	.0421	.0000	-12.90	.00	12.90	12.32	10.00	8.16	.00	.00	7.94
4	.0438	.0022	.0001	.0031	.0000	.0492	.0343	.0000	-13.01	.00	13.01	12.95	10.05	8.00	.00	.00	8.05
3	.0434	.0022	.0011	.0001	.0000	.0100	.0567	.0328	.0000	-13.29	.00	13.29	13.61	10.12	7.89	.00	.00	8.17
2	.0456	.0023	.0111	.0018	.0000	.0321	.0930	.0677	.0000	-13.97	.00	13.97	15.14	10.44	8.06	.00	.00	8.32
1	.0404	.0020	.0025	.0292	.0000	.0580	.1320	-.0876	.0000	-14.70	.00	14.70	19.45	11.49	10.53	.00	.00	7.91

Table A5. Quiet High Speed Fan Stator Vane Performance (concluded)

STL NO.	UMCRP	ST2CRP	DELTA IMIN
24	1.1262	2.1466	-2.81
23	1.1752	1.9934	-3.52
22	1.2244	2.1143	-4.53
21	1.2704	2.2988	-5.54
20	1.3080	2.4723	-6.46
19	1.3641	2.8457	-8.01
18	1.3840	3.2441	-8.85
17	1.3797	3.7102	-9.49
16	1.3690	3.9523	-9.72
15	1.3546	3.8331	-9.29
14	1.3390	3.6424	-8.73
13	1.3263	3.5871	-8.43
12	1.3169	3.6985	-8.42
11	1.3380	3.9166	-9.12
10	1.3561	3.9633	-9.51
9	1.3679	3.7359	-9.39
8	1.3822	3.5870	-9.34
7	1.3901	3.2550	-8.94
6	1.3987	3.0982	-8.80
5	1.4354	3.0295	-9.11
4	1.4735	2.9971	-9.48
3	1.5114	2.9716	-9.62
2	1.5259	2.8270	-9.45
1	1.5018	2.3887	-8.73

NOTE.... THE LETTER (X) TO THE RIGHT OF A NUMBER IN THE ABOVE COLUMNS INDICATES A PROGRAM DEFAULT IS IN EFFECT

Table A6. AXCAPS Design Point Data for Quiet High Speed Fan (30 pages)

1*VECTORS NASA/AE QHSF Fan. Design Point. 22-in rotor LE tip diameter. 97/03/07
Design report geometry. Final core duct flowpath w/ -60 duct loss. 15:44:24
Rotor and stator performance from DAWES models.

STATION 7 FLOW 83.38 CORR. FLOW 98.65 TOTAL PRESSURE 12.49
AREA 378.9 SPEC. FLOW 37.49 TOTAL TEMPERATURE 524.6 GAMMA 1.40083

STL NO.	RADIUS CORD.	VELOCITIES -*-*-*-*-*-*-*-*-* AXIAL	RADIAL	TANG.	MERID.	ABS.	PRESSURE TOTAL	STATIC	TEMPERATURE TOTAL	STATIC	ABSOLUTE MACH NO.	MERIDINAL DISTANCE	R*VU	PERCENT S P A N	PERCENT F L O W	Q
24	11.001-19.617	571.	0.	0.	571.	571.	12.49	10.38	524.6	497.5	.522	12.900	.0	100.00	100.00	1.0000
23	10.833-19.617	571.	1.	0.	571.	571.	12.49	10.38	524.6	497.5	.522	12.900	.0	98.48	96.94	1.0000
22	10.663-19.617	571.	1.	0.	571.	571.	12.49	10.38	524.6	497.4	.522	12.900	.0	96.93	93.88	1.0000
21	10.491-19.617	571.	2.	0.	571.	571.	12.49	10.38	524.6	497.4	.522	12.900	.0	95.37	90.83	1.0000
20	10.316-19.617	571.	2.	0.	571.	571.	12.49	10.37	524.6	497.4	.522	12.900	.0	93.77	87.77	1.0000
19	9.955-19.617	571.	3.	0.	571.	571.	12.49	10.37	524.6	497.4	.522	12.900	.0	90.50	81.65	1.0000
18	9.582-19.617	571.	5.	0.	571.	571.	12.49	10.37	524.6	497.4	.522	12.900	.0	87.10	75.54	1.0000
17	9.193-19.617	571.	6.	0.	571.	571.	12.49	10.37	524.6	497.4	.522	12.900	.0	83.57	69.42	1.0000
16	8.787-19.617	570.	8.	0.	570.	570.	12.49	10.38	524.6	497.5	.522	12.900	.0	79.87	63.30	1.0000
15	8.361-19.617	570.	10.	0.	570.	570.	12.49	10.38	524.6	497.5	.521	12.900	.0	76.01	57.19	1.0000
14	7.911-19.617	568.	11.	0.	569.	569.	12.49	10.39	524.6	497.7	.520	12.900	.0	71.92	51.07	1.0000
13	7.435-19.617	567.	14.	0.	567.	567.	12.49	10.40	524.6	497.8	.518	12.900	.0	67.58	44.96	1.0000
12	6.923-19.617	564.	16.	0.	565.	565.	12.49	10.42	524.6	498.0	.516	12.900	.0	62.93	38.84	1.0000
11	6.368-19.617	561.	18.	0.	562.	562.	12.49	10.44	524.6	498.3	.513	12.900	.0	57.89	32.72	1.0000
10	5.759-19.617	557.	21.	0.	558.	558.	12.49	10.46	524.6	498.7	.509	12.901	.0	52.35	26.61	1.0000
9	5.239-19.617	553.	23.	0.	554.	554.	12.49	10.49	524.6	499.0	.506	12.901	.0	47.62	21.91	1.0000
8	5.000-19.617	551.	24.	0.	552.	552.	12.49	10.50	524.6	499.2	.504	12.901	.0	45.45	19.91	1.0000
7	4.408-19.617	546.	27.	0.	546.	546.	12.49	10.54	524.6	499.7	.498	12.901	.0	40.07	15.37	1.0000
6	3.986-19.617	541.	29.	0.	542.	542.	12.49	10.57	524.6	500.1	.494	12.901	.0	36.23	12.50	1.0000
5	3.618-19.617	537.	30.	0.	537.	537.	12.49	10.60	524.6	500.5	.490	12.901	.0	32.88	10.25	1.0000
4	3.105-19.617	530.	33.	0.	531.	531.	12.49	10.65	524.6	501.1	.484	12.901	.0	28.22	7.50	1.0000
3	2.574-19.617	522.	35.	0.	523.	523.	12.49	10.70	524.6	501.8	.476	12.901	.0	23.40	5.12	1.0000
2	1.805-19.617	507.	40.	0.	509.	509.	12.49	10.79	524.6	503.0	.463	12.900	.0	16.40	2.50	1.0000
1	.000-19.617	442.	90.	0.	451.	451.	12.49	11.14	524.6	507.6	.409	12.900	.0	.00	.00	1.0000

STATION 8 FLOW 83.38 CORR. FLOW 98.65 TOTAL PRESSURE 12.49
AREA 374.8 SPEC. FLOW 37.90 TOTAL TEMPERATURE 524.6 GAMMA 1.40083

24	11.001-17.464	584.	0.	0.	584.	584.	12.49	10.28	524.6	496.2	.535	15.053	.0	100.00	100.00	1.0000
23	10.836-17.464	584.	-5.	0.	584.	584.	12.49	10.28	524.6	496.2	.535	15.053	.0	98.36	96.94	1.0000
22	10.669-17.464	584.	-5.	0.	584.	584.	12.49	10.28	524.6	496.2	.535	15.053	.0	96.70	93.88	1.0000
21	10.500-17.464	584.	-5.	0.	584.	584.	12.49	10.28	524.6	496.2	.535	15.053	.0	95.01	90.83	1.0000
20	10.327-17.464	584.	-3.	0.	584.	584.	12.49	10.28	524.6	496.2	.535	15.053	.0	93.29	87.77	1.0000
19	9.973-17.464	584.	-1.	0.	584.	584.	12.49	10.28	524.6	496.2	.535	15.053	.0	89.77	81.65	1.0000
18	9.607-17.464	584.	3.	0.	584.	584.	12.49	10.28	524.6	496.2	.535	15.053	.0	86.12	75.54	1.0000
17	9.225-17.464	584.	6.	0.	584.	584.	12.49	10.28	524.6	496.2	.535	15.053	.0	82.31	69.42	1.0000
16	8.827-17.464	583.	10.	0.	583.	583.	12.49	10.29	524.6	496.2	.534	15.053	.0	78.35	63.30	1.0000
15	8.411-17.464	582.	14.	0.	582.	582.	12.49	10.29	524.6	496.3	.533	15.054	.0	74.20	57.19	1.0000
14	7.971-17.464	581.	19.	0.	581.	581.	12.49	10.31	524.6	496.5	.532	15.054	.0	69.82	51.07	1.0000
13	7.505-17.464	578.	23.	0.	579.	579.	12.49	10.32	524.6	496.7	.529	15.054	.0	65.18	44.96	1.0000
12	7.006-17.464	575.	29.	0.	576.	576.	12.49	10.34	524.6	497.0	.526	15.055	.0	60.20	38.84	1.0000
11	6.465-17.464	570.	35.	0.	571.	571.	12.49	10.37	524.6	497.4	.523	15.056	.0	54.82	32.72	1.0000
10	5.872-17.464	564.	42.	0.	566.	566.	12.49	10.41	524.6	497.9	.517	15.057	.0	48.91	26.61	1.0000
9	5.367-17.464	558.	48.	0.	560.	560.	12.49	10.45	524.6	498.4	.512	15.058	.0	43.88	21.91	1.0000
8	5.136-17.464	555.	51.	0.	557.	557.	12.49	10.47	524.6	498.7	.509	15.058	.0	41.57	19.91	1.0000
7	4.563-17.464	546.	59.	0.	550.	550.	12.49	10.52	524.6	499.4	.501	15.059	.0	35.87	15.37	1.0000
6	4.155-17.464	539.	64.	0.	543.	543.	12.49	10.56	524.6	500.0	.495	15.061	.0	31.81	12.50	1.0000
5	3.802-17.464	532.	70.	0.	537.	537.	12.49	10.61	524.6	500.6	.489	15.062	.0	28.28	10.25	1.0000
4	3.312-17.464	521.	79.	0.	527.	527.	12.49	10.67	524.6	501.4	.480	15.064	.0	23.40	7.50	1.0000
3	2.810-17.464	508.	89.	0.	516.	516.	12.49	10.74	524.6	502.4	.469	15.067	.0	18.41	5.12	1.0000
2	2.103-17.464	485.	108.	0.	497.	497.	12.49	10.86	524.6	504.0	.451	15.074	.0	11.36	2.50	1.0000
1	.963-17.464	435.	203.	0.	480.	480.	12.49	10.97	524.6	505.4	.435	15.258	.0	.00	.00	1.0000

STATION 9 FLOW 83.38 CORR. FLOW 98.64 TOTAL PRESSURE 12.49
AREA 364.9 SPEC. FLOW 38.92 TOTAL TEMPERATURE 524.6 GAMMA 1.40083

24	11.001-15.490	434.	0.	0.	434.	434.	11.15	10.03	524.6	508.9	.392	17.026	.0	100.00	100.00	.9680
23	10.801-15.490	567.	-3.	0.	567.	567.	12.04	10.03	524.6	497.8	.518	17.027	.0	97.79	96.94	.9896
22	10.629-15.490	602.	-3.	0.	602.	602.	12.34	10.03	524.6	494.4	.552	17.027	.0	95.90	93.88	.9965
21	10.462-15.490	614.	-2.	0.	614.	614.	12.45	10.04	524.6	493.2	.564	17.027	.0	94.07	90.83	.9991
20	10.295-15.490	617.	-1.	0.	617.	617.	12.48	10.04	524.6	492.9	.566	17.027	.0	92.22	87.77	.9997
19	9.954-15.490	619.	3.	0.	619.	619.	12.51	10.05	524.6	492.7	.569	17.027	.0	88.46	81.65	1.0004
18	9.602-15.490	620.	7.	0.	620.	620.	12.54	10.06	524.6	492.5	.570	17.027	.0	84.59	75.54	1.0010
17	9.238-15.490	619.	12.	0.	619.	619.	12.54	10.07	524.6	492.6	.569	17.027	.0	80.58	69.42	1.0011
16	8.858-15.490	618.	17.	0.	618.	618.	12.55	10.08	524.6	492.8	.568	17.027	.0	76.39	63.30	1.0012
15	8.461-15.490	615.	23.	0.	615.	615.	12.55	10.10	524.6	493.0	.565	17.028	.0	72.02	57.19	1.0012
14	8.042-15.490	612.	29.	0.	612.	612.	12.55	10.12	524.6	493.3	.562	17.029	.0	67.40	51.07	1.0013
13	7.599-15.490	608.	36.	0.	609.	609.	12.55	10.15	524.6	493.7	.559	17.030	.0	62.52	44.96	1.0013
12	7.126-15.490	602.	44.	0.	604.	604.	12.55	10.19	524.6	494.2	.554	17.032	.0	57.31	38.84	1.0013
11	6.615-15.490	596.	53.	0.	598.	598.	12.55	10.23	524.6	494.8	.548	17.035	.0	51.67	32.72	1.0013
10	6.057-15.490	587.	63.	0.	591.	591.	12.55	10.28	524.6	495.5	.541	17.039	.0	45.52	26.61	1.0013
9	5.584-15.490	579.	72.	0.	583.	583.	12.55	10.33	524.6	496.2	.534	17.043	.0	40.32	21.91	1.0013
8	5.369-15.490	575.	77.	0.	580.	580.	12.55	10.36	524.6	496.6	.531	17.045	.0	37.94	19.91	1.0013
7	4.839-15.490	563.	89.	0.	570.	570.	12.55	10.43	524.6	497.5	.521	17.052	.0	32.10	15.37	1.0013
6	4.466-15.490	554.	99.	0.	563.	563.	12.55	10.48	524.6	498.2	.514	17.058	.0	28.00	12.50	1.0014
5	4.147-15.490	546.	108.	0.	556.	556.	12.55	10.53	524.6	498.8	.508	17.065	.0	24.48	10.25	1.0014
4	3.712-15.490	533.	121.	0.	546.	546.	12.55	10.59	524.6	499.7	.498	17.077	.0	19.69	7.50	1.0014
3	3.280-15.490	518.	137.	0.	536.	536.	12.55	10.66	524.6	500.7	.488	17.095	.0	14.93	5.12	1.0014
2	2.708-15.490	495.	164.	0.	522.	522.	12.56	10.76	524.6	501.9	.475	17.138	.0	8.63	2.50	1.0014
1	1.925-15.490	401.	196.	0.	446.	446.	12.11	10.82	524.6	508.0	.404	17.454	.0	.00	.00	.9911

1*VECTORS NASA/AE QHSF Fan. Design Point. 22-in rotor LE tip diameter. 97/03/07
Design report geometry. Final core duct flowpath w/ -60 duct loss. 15:44:24
Rotor and stator performance from DAWES models.

STATION 10 FLOW 83.38 CORR. FLOW 98.64 TOTAL PRESSURE 12.49
AREA 349.5 SPEC. FLOW 40.65 TOTAL TEMPERATURE 524.6 GAMMA 1.40083

STL NO.	RADIUS CORD.	VELOCITIES -*-*-*-*-*-*-*-*-* AXIAL	RADIAL	TANG.	MERID.	ABS.	PRESSURE TOTAL	STATIC	TEMPERATURE TOTAL	STATIC	ABSOLUTE MACH NO.	MERIDINAL DISTANCE	R*VU	PERCENT S P A N	PERCENT F L O W	Q
24	11.001-13.818	462.	0.	0.	462.	462.	11.15	9.89	524.6	506.8	.418	18.699	.0	100.00	100.00	.9680
23	10.808-13.799	588.	5.	0.	588.	588.	12.04	9.89	524.6	495.8	.539	18.718	.0	97.62	96.94	.9896
22	10.641-13.782	623.	8.	0.	623.	623.	12.34	9.88	524.6	492.3	.572	18.735	.0	95.55	93.88	.9965
21	10.479-13.766	635.	11.	0.	635.	635.	12.45	9.88	524.6	491.0	.585	18.751	.0	93.55	90.83	.9991
20	10.316-13.749	639.	14.	0.	639.	639.	12.48	9.87	524.6	490.6	.588	18.768	.0	91.54	87.77	.9997
19	9.985-13.716	643.	20.	0.	643.	643.	12.51	9.86	524.6	490.1	.593	18.801	.0	87.45	81.65	1.0004
18	9.645-13.683	647.	27.	0.	647.	647.	12.54	9.85	524.6	489.7	.596	18.835	.0	83.26	75.54	1.0010
17	9.294-13.648	648.	34.	0.	649.	649.	12.54	9.84	524.6	489.5	.598	18.871	.0	78.93	69.42	1.0011
16	8.930-13.613	649.	41.	0.	650.	650.	12.55	9.84	524.6	489.3	.600	18.906	.0	74.44	63.30	1.0012
15	8.552-13.585	649.	49.	0.	650.	650.	12.55	9.84	524.6	489.3	.600	18.935	.0	69.77	57.19	1.0012
14	8.154-13.565	647.	59.	0.	649.	649.	12.55	9.85	524.6	489.4	.599	18.958	.0	64.87	51.07	1.0013
13	7.735-13.551	644.	69.	0.	647.	647.	12.55	9.86	524.6	489.7	.597	18.975	.0	59.71	44.96	1.0013
12	7.290-13.541	639.	80.	0.	644.	644.	12.55	9.89	524.6	490.0	.594	18.988	.0	54.22	38.84	1.0013
11	6.811-13.535	634.	92.	0.	640.	640.	12.55	9.92	524.6	490.4	.590	19.000	.0	48.33	32.72	1.0013
10	6.293-13.532	626.	107.	0.	635.	635.	12.55	9.96	524.6	491.0	.584	19.012	.0	41.95	26.61	1.0013
9	5.860-13.530	618.	119.	0.	629.	629.	12.55	10.00	524.6	491.6	.579	19.023	.0	36.61	21.91	1.0013
8	5.663-13.529	614.	125.	0.	627.	627.	12.55	10.02	524.6	491.8	.576	19.029	.0	34.19	19.91	1.0013
7	5.187-13.527	603.	140.	0.	620.	620.	12.55	10.07	524.6	492.6	.569	19.046	.0	28.32	15.37	1.0013
6	4.857-13.524	595.	152.	0.	614.	614.	12.55	10.11	524.6	493.2	.564	19.063	.0	24.26	12.50	1.0014
5	4.580-13.523	587.	162.	0.	609.	609.	12.55	10.15	524.6	493.7	.559	19.080	.0	20.84	10.25	1.0014
4	4.210-13.521	576.	176.	0.	602.	602.	12.55	10.20	524.6	494.4	.552	19.109	.0	16.29	7.50	1.0014
3	3.856-13.520	564.	191.	0.	596.	596.	12.55	10.25	524.6	495.0	.546	19.149	.0	11.93	5.12	1.0014
2	3.415-13.518	548.	214.	0.	588.	588.	12.56	10.30	524.6	495.7	.539	19.234	.0	6.49	2.50	1.0014
1	2.888-13.517	474.	228.	0.	526.	526.	12.11	10.35	524.6	501.5	.479	19.650	.0	.00	.00	.9911

STATION 11 FLOW 83.38 CORR. FLOW 98.65 TOTAL PRESSURE 12.49
AREA 338.1 SPEC. FLOW 42.02 TOTAL TEMPERATURE 524.6 GAMMA 1.40083

24	11.001-12.732	511.	-1.	0.	511.	511.	11.15	9.61	524.6	502.8	.465	19.785	.0	100.00	100.00	.9680
23	10.820-12.704	628.	-2.	0.	628.	628.	12.04	9.60	524.6	491.7	.578	19.813	.0	97.61	96.94	.9896
22	10.659-12.680	663.	-1.	0.	663.	663.	12.34	9.58	524.6	488.0	.612	19.837	.0	95.49	93.88	.9965
21	10.504-12.656	676.	1.	0.	676.	676.	12.45	9.56	524.6	486.4	.625	19.862	.0	93.43	90.83	.9991
20	10.348-12.631	681.	4.	0.	681.	681.	12.48	9.55	524.6	485.9	.630	19.887	.0	91.37	87.77	.9997
19	10.030-12.583	685.	12.	0.	685.	685.	12.51	9.54	524.6	485.5	.634	19.935	.0	87.18	81.65	1.0004
18	9.705-12.534	687.	21.	0.	688.	688.	12.54	9.54	524.6	485.2	.637	19.985	.0	82.89	75.54	1.0010
17	9.370-12.484	689.	31.	0.	689.	689.	12.54	9.53	524.6	485.0	.638	20.036	.0	78.47	69.42	1.0011
16	9.023-12.437	689.	41.	0.	690.	690.	12.55	9.53	524.6	484.9	.639	20.085	.0	73.91	63.30	1.0012
15	8.663-12.402	688.	52.	0.	690.	690.	12.55	9.53	524.6	484.9	.639	20.124	.0	69.18	57.19	1.0012
14	8.286-12.379	686.	63.	0.	689.	689.	12.55	9.54	524.6	485.1	.638	20.151	.0	64.21	51.07	1.0013
13	7.889-12.367	681.	74.	0.	685.	685.	12.55	9.57	524.6	485.5	.634	20.169	.0	58.99	44.96	1.0013
12	7.466-12.363	675.	87.	0.	680.	680.	12.55	9.61	524.6	486.0	.629	20.180	.0	53.44	38.84	1.0013
11	7.015-12.365	666.	101.	0.	674.	674.	12.55	9.66	524.6	486.8	.623	20.187	.0	47.49	32.72	1.0013
10	6.526-12.373	654.	117.	0.	665.	665.	12.55	9.73	524.6	487.7	.614	20.194	.0	41.07	26.61	1.0013
9	6.118-12.380	643.	132.	0.	656.	656.	12.55	9.79	524.6	488.7	.606	20.201	.0	35.70	21.91	1.0013
8	5.935-12.384	637.	139.	0.	652.	652.	12.55	9.83	524.6	489.1	.601	20.205	.0	33.28	19.91	1.0013
7	5.489-12.391	622.	156.	0.	641.	641.	12.55	9.91	524.6	490.3	.591	20.221	.0	27.42	15.37	1.0013
6	5.183-12.395	611.	169.	0.	633.	633.	12.55	9.97	524.6	491.2	.583	20.238	.0	23.39	12.50	1.0014
5	4.926-12.399	600.	179.	0.	626.	626.	12.55	10.02	524.6	491.9	.576	20.256	.0	20.01	10.25	1.0014
4	4.585-12.405	586.	194.	0.	617.	617.	12.55	10.09	524.6	492.9	.567	20.286	.0	15.53	7.50	1.0014
3	4.262-12.412	571.	210.	0.	608.	608.	12.55	10.16	524.6	493.8	.558	20.328	.0	11.28	5.12	1.0014
2	3.865-12.420	552.	230.	0.	598.	598.	12.56	10.23	524.6	494.8	.549	20.420	.0	6.05	2.50	1.0014
1	3.405-12.431	481.	236.	0.	535.	535.	12.11	10.29	524.6	500.7	.488	20.853	.0	.00	.00	.9911

STATION 12 FLOW 83.38 CORR. FLOW 98.65 TOTAL PRESSURE 12.49
AREA 327.0 SPEC. FLOW 43.45 TOTAL TEMPERATURE 524.6 GAMMA 1.40083

24	11.000-12.293	504.	-29.	0.	504.	504.	11.15	9.65	524.6	503.4	.459	20.224	.0	100.00	100.00	.9680
23	10.815-12.229	632.	-22.	0.	632.	632.	12.04	9.58	524.6	491.3	.582	20.288	.0	97.36	96.94	.9896
22	10.654-12.166	672.	-14.	0.	672.	672.	12.34	9.51	524.6	486.9	.621	20.352	.0	95.04	93.88	.9965
21	10.500-12.121	689.	-5.	0.	689.	689.	12.45	9.47	524.6	485.0	.638	20.397	.0	92.84	90.83	.9991
20	10.345-12.067	696.	5.	0.	696.	696.	12.48	9.44	524.6	484.3	.645	20.451	.0	90.64	87.77	.9997
19	10.033-11.982	702.	24.	0.	703.	703.	12.51	9.40	524.6	483.4	.652	20.537	.0	86.22	81.65	1.0004
18	9.716-11.896	708.	43.	0.	709.	709.	12.54	9.37	524.6	482.7	.658	20.623	.0	81.75	75.54	1.0010
17	9.392-11.808	711.	63.	0.	714.	714.	12.54	9.34	524.6	482.1	.663	20.713	.0	77.18	69.42	1.0011
16	9.058-11.732	712.	80.	0.	716.	716.	12.55	9.32	524.6	481.8	.666	20.791	.0	72.49	63.30	1.0012
15	8.710-11.671	711.	97.	0.	718.	718.	12.55	9.31	524.6	481.6	.667	20.856	.0	67.63	57.19	1.0012
14	8.346-11.627	710.	114.	0.	719.	719.	12.55	9.30	524.6	481.5	.668	20.905	.0	62.55	51.07	1.0013
13	7.963-11.596	708.	131.	0.	720.	720.	12.55	9.29	524.6	481.4	.669	20.942	.0	57.21	44.96	1.0013
12	7.557-11.574	705.	149.	0.	720.	720.	12.55	9.29	524.6	481.4	.669	20.973	.0	51.56	38.84	1.0013
11	7.125-11.555	700.	168.	0.	720.	720.	12.55	9.29	524.6	481.3	.670	21.005	.0	45.55	32.72	1.0013
10	6.663-11.537	695.	188.	0.	720.	720.	12.55	9.29	524.6	481.4	.669	21.041	.0	39.13	26.61	1.0013
9	6.282-11.520	688.	205.	0.	718.	718.	12.55	9.31	524.6	481.6	.667	21.077	.0	33.83	21.91	1.0013
8	6.111-11.514	685.	212.	0.	717.	717.	12.55	9.32	524.6	481.8	.666	21.093	.0	31.46	19.91	1.0013
7	5.702-11.500	673.	230.	0.	711.	711.	12.55	9.36	524.6	482.4	.660	21.138	.0	25.77	15.37	1.0013
6	5.424-11.492	664.	242.	0.	706.	706.	12.55	9.41	524.6	483.0	.655	21.173	.0	21.90	12.50	1.0014
5	5.190-11.493	655.	251.	0.	701.	701.	12.55	9.45	524.6	483.6	.650	21.200	.0	18.65	10.25	1.0014
4	4.884-11.496	641.	262.	0.	693.	693.	12.55	9.51	524.6	484.6	.642	21.243	.0	14.40	7.50	1.0014
3	4.596-11.503	626.	272.	0.	683.	683.	12.55	9.59	524.6	485.7	.632	21.297	.0	10.39	5.12	1.0014
2	4.247-11.516	606.	285.	0.	669.	669.	12.56	9.70	524.6	487.3	.618	21.401	.0	5.53	2.50	1.0014
1	3.850-11.543	537.	278.	0.	605.	605.	12.11	9.82	524.6	494.1	.555	21.846	.0	.00	.00	.9911

1*VECTORS NASA/AE QHSF Fan. Design Point. 22-in rotor LE tip diameter. 97/03/07
Design report geometry. Final core duct flowpath w/ -60 duct loss. 15:44:24
Rotor and stator performance from DAWES models.

INSIDE ROTOR 1 AT STATION 13 FLOW 83.38 CORR. FLOW 85.46 TOTAL PRESSURE 14.80
AREA 286.7 SPEC. FLOW 42.93 TOTAL TEMPERATURE 552.7 GAMMA 1.40029

STL NO.	RADIUS CORD.	VELOCITIES -*-*-*-*-*-*-*-*-* AXIAL	RADIAL	TANG.	MERID.	ABS.	PRESSURE TOTAL	STATIC	TEMPERATURE TOTAL	STATIC	ABSOLUTE MACH NO.	MERIDINAL DISTANCE	R*VU	PERCENT S P A N	PERCENT F L O W	Q
24	10.937-11.780	711.	-87.	108.	716.	724.	13.06	9.78	551.1	507.4	.656	20.741	1179.7	100.00	100.00	.9641
23	10.783-11.705	761.	-65.	103.	763.	770.	13.85	9.96	549.5	500.1	.703	20.813	1108.1	97.57	96.94	.9832
22	10.638-11.635	767.	-50.	100.	769.	776.	14.13	10.11	548.6	498.5	.709	20.883	1068.6	95.29	93.88	.9905
21	10.497-11.579	768.	-38.	102.	769.	776.	14.27	10.21	548.7	498.7	.708	20.939	1075.5	93.10	90.83	.9930
20	10.355-11.527	761.	-25.	103.	762.	768.	14.31	10.30	548.5	499.3	.701	20.991	1064.9	90.91	87.77	.9942
19	10.067-11.427	749.	-2.	106.	749.	756.	14.38	10.47	548.6	500.9	.689	21.093	1067.2	86.48	81.65	.9956
18	9.773-11.329	736.	18.	110.	737.	745.	14.45	10.62	548.7	502.5	.678	21.193	1074.5	81.98	75.54	.9966
17	9.470-11.234	723.	38.	115.	724.	733.	14.48	10.76	548.9	504.2	.666	21.292	1084.4	77.36	69.42	.9969
16	9.156-11.148	712.	57.	121.	714.	724.	14.53	10.87	549.4	505.7	.657	21.384	1106.5	72.60	63.30	.9968
15	8.829-11.073	703.	78.	128.	707.	719.	14.57	10.96	550.0	507.0	.651	21.466	1131.3	67.67	57.19	.9967
14	8.487-11.010	702.	100.	141.	709.	723.	14.71	11.03	551.5	508.0	.654	21.538	1198.2	62.55	51.07	.9966
13	8.130-10.958	702.	122.	155.	712.	729.	14.85	11.09	552.9	508.6	.659	21.602	1259.2	57.21	44.96	.9968
12	7.754-10.915	701.	144.	169.	715.	735.	14.97	11.14	554.0	509.0	.664	21.662	1308.4	51.59	38.84	.9973
11	7.351-10.877	695.	166.	182.	714.	737.	15.08	11.20	554.7	509.4	.666	21.720	1341.1	45.60	32.72	.9980
10	6.918-10.844	686.	188.	197.	712.	738.	15.18	11.26	555.3	509.9	.667	21.779	1365.5	39.15	26.61	.9988
9	6.559-10.820	678.	207.	212.	709.	740.	15.26	11.31	555.8	510.2	.668	21.830	1389.3	33.80	21.91	.9993
8	6.397-10.810	676.	216.	223.	710.	744.	15.35	11.34	556.7	510.6	.672	21.853	1428.3	31.41	19.91	.9995
7	6.012-10.787	666.	237.	242.	706.	747.	15.44	11.38	557.3	510.8	.674	21.915	1456.0	25.67	15.37	1.0000
6	5.749-10.772	657.	251.	256.	703.	748.	15.48	11.41	557.6	511.0	.675	21.963	1470.8	21.76	12.50	1.0002
5	5.530-10.762	649.	262.	269.	700.	750.	15.53	11.42	558.0	511.2	.677	22.006	1489.9	18.51	10.25	1.0003
4	5.244-10.749	640.	278.	290.	698.	756.	15.59	11.42	558.7	511.1	.682	22.072	1519.8	14.26	7.50	1.0003
3	4.976-10.740	631.	294.	312.	696.	763.	15.66	11.41	559.4	511.0	.688	22.149	1552.1	10.28	5.12	1.0003
2	4.652-10.730	620.	313.	345.	694.	775.	15.77	11.37	560.6	510.6	.700	22.286	1604.4	5.47	2.50	1.0001
1	4.283-10.727	555.	303.	451.	632.	776.	15.54	11.24	568.0	517.8	.696	22.770	1931.9	.00	.00	.9830

STL NO.	D-FACTOR	OMEGA BAR	SOLID-ITY	RHO*V RATIO	REL. ANGLES INLET	REL. ANGLES EXIT	TURN-ING	REL MACH NO INLET	REL MACH NO EXIT	PRESS-URE RATIO	EFFIC IENCY	TEMP RISE	REL VELCITY INLET	REL VELCITY EXIT	PS RISE	MERID VEL RATIO	WHEEL SPEED INLET	WHEEL SPEED EXIT	FREE PS RISE
24	.0394	.0202	1.400	1.428	71.21	62.33	8.88	1.424	1.397	1.171	91.49	.051	1566.	1543.	.006	1.420	1483.	1474.	.0121
23	.0467	.0313	1.400	1.234	66.56	60.52	6.03	1.462	1.415	1.150	85.75	.047	1589.	1551.	.016	1.208	1458.	1453.	.0192
22	.0518	.0294	1.400	1.188	64.92	60.02	4.90	1.465	1.406	1.145	86.14	.046	1585.	1539.	.025	1.144	1436.	1434.	.0265
21	.0570	.0294	1.400	1.171	64.04	59.63	4.40	1.458	1.389	1.146	86.35	.046	1574.	1521.	.032	1.116	1415.	1415.	.0322
20	.0607	.0272	1.400	1.159	63.48	59.50	3.98	1.444	1.369	1.146	87.36	.046	1558.	1500.	.038	1.095	1394.	1396.	.0374
19	.0683	.0240	1.400	1.145	62.54	59.09	3.45	1.414	1.329	1.150	89.13	.046	1524.	1458.	.051	1.066	1352.	1357.	.0471
18	.0768	.0226	1.400	1.131	61.56	58.61	2.95	1.383	1.287	1.153	90.09	.046	1489.	1414.	.063	1.039	1310.	1317.	.0575
17	.0863	.0226	1.400	1.117	60.58	58.08	2.50	1.350	1.243	1.155	90.41	.046	1453.	1369.	.077	1.014	1266.	1276.	.0687
16	.0962	.0238	1.400	1.108	59.60	57.31	2.28	1.315	1.200	1.158	90.36	.047	1415.	1323.	.091	.997	1221.	1234.	.0796
15	.1063	.0254	1.400	1.102	58.56	56.33	2.22	1.279	1.156	1.161	90.23	.048	1376.	1276.	.105	.985	1174.	1190.	.0904
14	.1181	.0267	1.400	1.109	57.41	54.73	2.68	1.241	1.111	1.172	90.59	.051	1335.	1228.	.119	.986	1125.	1144.	.1015
13	.1300	.0268	1.400	1.117	56.15	52.88	3.27	1.201	1.067	1.183	91.36	.054	1292.	1180.	.135	.989	1073.	1096.	.1130
12	.1422	.0249	1.400	1.126	54.73	50.78	3.96	1.160	1.023	1.193	92.56	.056	1247.	1131.	.153	.993	1018.	1045.	.1253
11	.1564	.0213	1.400	1.130	53.12	48.53	4.59	1.116	.975	1.202	94.09	.057	1200.	1079.	.174	.992	960.	991.	.1416
10	.1735	.0170	1.400	1.131	51.28	45.93	5.35	1.070	.924	1.209	95.60	.058	1151.	1023.	.200	.988	898.	932.	.1614
9	.1897	.0141	1.400	1.132	49.69	43.47	6.22	1.032	.882	1.216	96.56	.059	1110.	977.	.223	.987	847.	884.	.1792
8	.2000	.0130	1.400	1.138	48.97	41.99	6.98	1.015	.862	1.223	96.99	.061	1092.	955.	.235	.990	824.	862.	.1889
7	.2192	.0105	1.400	1.140	47.21	38.80	8.41	.972	.818	1.230	97.75	.062	1047.	906.	.259	.993	769.	810.	.2074
6	.2329	.0094	1.400	1.141	45.98	36.43	9.55	.943	.788	1.233	98.09	.063	1017.	874.	.275	.995	731.	775.	.2195
5	.2455	.0089	1.400	1.142	44.93	34.20	10.73	.919	.764	1.237	98.27	.064	990.	847.	.288	.999	699.	745.	.2291
4	.2612	.0094	1.400	1.147	43.54	30.84	12.69	.885	.734	1.242	98.30	.065	956.	813.	.301	1.008	658.	707.	.2370
3	.2766	.0106	1.400	1.152	42.20	27.27	14.94	.853	.706	1.247	98.23	.066	922.	783.	.311	1.019	619.	671.	.2415
2	.2952	.0131	1.400	1.160	40.53	22.11	18.43	.814	.677	1.256	98.01	.069	881.	749.	.315	1.037	572.	627.	.2390
1	.4042	.0973	1.400	1.141	40.62	11.30	29.32	.731	.578	1.283	89.36	.083	797.	645.	.338	1.045	519.	577.	.2455

STL NO.	CUM.PT RATIO	CUM.TT RATIO	CUM. EFF. ADIA.	EFF. POLY.	ABS. ANGLES INLET	ABS. ANGLES EXIT	REL. PRESS. INLET	REL. PRESS. EXIT	REL. TEMP. INLET	REL. TEMP. EXIT
24	1.045	1.051	25.32	25.78	.00	8.56	31.77	31.00	707.6	705.5
23	1.108	1.047	62.92	63.43	.00	7.67	33.29	32.37	701.5	700.5
22	1.131	1.046	78.22	78.56	.00	7.44	33.23	32.44	696.3	695.8
21	1.142	1.046	84.23	84.47	.00	7.59	32.70	32.00	691.3	691.3
20	1.145	1.046	86.72	86.93	.00	7.69	31.98	31.41	686.5	686.8
19	1.151	1.046	90.03	90.18	.00	8.06	30.51	30.16	676.9	677.9
18	1.156	1.046	92.28	92.38	.00	8.49	29.10	28.91	667.4	669.1
17	1.159	1.046	92.97	93.06	.00	8.99	27.71	27.63	658.0	660.3
16	1.163	1.047	93.01	93.10	.00	9.60	26.37	26.35	648.7	651.4
15	1.166	1.048	92.88	92.99	.00	10.27	25.07	25.10	639.4	642.5
14	1.177	1.051	93.16	93.26	.00	11.26	23.80	23.89	629.9	633.6
13	1.188	1.054	93.83	93.93	.00	12.27	22.58	22.75	620.5	624.6
12	1.199	1.056	94.96	95.04	.00	13.28	21.39	21.65	611.0	615.5
11	1.207	1.057	96.46	96.50	.00	14.33	20.24	20.59	601.4	606.4
10	1.215	1.058	97.92	97.93	.00	15.50	19.13	19.56	591.7	597.0
9	1.221	1.059	98.87	98.86	.00	16.64	18.30	18.76	584.3	589.7
8	1.229	1.061	99.26	99.24	.00	17.46	17.95	18.43	581.1	586.5
7	1.236	1.062	100.04	99.99	.00	18.92	17.17	17.67	573.8	579.3
6	1.239	1.063	100.38	100.33	.00	20.00	16.69	17.19	569.1	574.6
5	1.243	1.064	100.54	100.48	.00	21.05	16.31	16.81	565.3	570.9
4	1.248	1.065	100.57	100.51	.00	22.54	15.84	16.33	560.7	566.2
3	1.254	1.066	100.49	100.43	.00	24.14	15.44	15.92	556.5	562.1
2	1.262	1.069	100.24	100.20	.00	26.42	14.99	15.45	551.9	557.3
1	1.244	1.083	77.82	78.48	.00	35.51	14.02	14.09	547.0	552.4

1*VECTORS NASA/AE QHSF Fan. Design Point. 22-in rotor LE tip diameter. 97/03/07
Design report geometry. Final core duct flowpath w/ -60 duct loss. 15:44:24
Rotor and stator performance from DAWES models.

INSIDE ROTOR 1 AT STATION 14 FLOW 83.38 CORR. FLOW 71.06 TOTAL PRESSURE 18.40
AREA 265.3 SPEC. FLOW 38.57 TOTAL TEMPERATURE 590.6 GAMMA 1.39934

STL NO.	RADIUS CORD.	VELOCITIES -*-*-*-*-*-*-*-*-* AXIAL	RADIAL	TANG.	MERID.	ABS.	PRESSURE TOTAL	STATIC	TEMPERATURE TOTAL	STATIC	ABSOLUTE MACH NO.	MERIDINAL DISTANCE	R*VU	PERCENT S P A N	PERCENT F L O W	Q
24	10.874-11.267	692.	-85.	244.	697.	738.	15.77	11.88	584.1	538.7	.649	21.258	2649.4	100.00	100.00	.9599
23	10.725-11.175	715.	-76.	235.	719.	756.	16.46	12.20	581.3	533.7	.668	21.347	2525.0	97.38	96.94	.9764
22	10.583-11.087	709.	-70.	236.	713.	751.	16.85	12.55	580.7	533.9	.663	21.434	2501.3	94.86	93.88	.9838
21	10.443-11.013	705.	-65.	247.	708.	750.	17.19	12.82	582.6	535.8	.661	21.507	2582.8	92.45	90.83	.9864
20	10.303-10.941	697.	-59.	259.	699.	746.	17.47	13.09	584.4	538.2	.656	21.579	2664.7	90.04	87.77	.9879
19	10.020-10.804	677.	-46.	277.	679.	733.	17.88	13.55	587.0	542.3	.643	21.717	2779.9	85.22	81.65	.9900
18	9.733-10.677	665.	-31.	298.	665.	729.	18.26	13.90	589.7	545.5	.637	21.846	2901.2	80.38	75.54	.9913
17	9.441-10.563	655.	-14.	320.	656.	729.	18.57	14.15	592.4	548.1	.636	21.964	3020.1	75.49	69.42	.9917
16	9.142-10.461	652.	4.	344.	652.	737.	18.86	14.31	595.1	549.9	.641	22.071	3140.8	70.56	63.30	.9915
15	8.838-10.371	653.	25.	368.	653.	750.	19.12	14.37	597.6	550.8	.652	22.168	3252.8	65.57	57.19	.9913
14	8.521-10.291	644.	45.	381.	646.	750.	19.10	14.35	597.4	550.6	.652	22.258	3243.0	60.41	51.07	.9912
13	8.188-10.220	642.	64.	392.	645.	755.	19.05	14.25	596.7	549.3	.658	22.343	3213.4	55.01	44.96	.9917
12	7.834-10.156	644.	84.	403.	650.	765.	18.99	14.09	595.5	546.9	.667	22.425	3158.3	49.31	38.84	.9928
11	7.459-10.099	649.	107.	413.	658.	776.	18.89	13.87	593.6	543.6	.679	22.505	3077.2	43.27	32.72	.9944
10	7.059-10.047	654.	133.	424.	667.	790.	18.79	13.62	591.8	539.8	.694	22.589	2993.1	36.85	26.61	.9961
9	6.731-10.009	655.	157.	434.	674.	801.	18.68	13.40	590.1	536.8	.706	22.658	2920.2	31.60	21.91	.9971
8	6.585 -9.994	654.	168.	437.	675.	805.	18.61	13.30	589.2	535.4	.709	22.690	2878.6	29.27	19.91	.9975
7	6.238 -9.961	655.	196.	451.	684.	819.	18.51	13.05	587.8	532.0	.724	22.772	2814.2	23.72	15.37	.9984
6	6.005 -9.942	654.	216.	462.	689.	830.	18.44	12.87	586.9	529.7	.736	22.831	2776.6	19.99	12.50	.9989
5	5.813 -9.928	654.	234.	474.	694.	841.	18.40	12.71	586.4	527.7	.747	22.886	2755.1	16.93	10.25	.9991
4	5.566 -9.913	652.	260.	492.	702.	857.	18.37	12.49	586.1	525.0	.763	22.968	2740.4	12.99	7.50	.9991
3	5.337 -9.902	649.	285.	513.	709.	875.	18.36	12.27	586.1	522.4	.781	23.062	2738.9	9.34	5.12	.9990
2	5.066 -9.892	644.	318.	545.	718.	902.	18.39	11.98	586.5	519.0	.807	23.221	2759.7	5.01	2.50	.9987
1	4.751 -9.894	552.	306.	682.	631.	929.	18.02	11.50	597.3	525.5	.827	23.725	3238.4	.00	.00	.9751

STL NO.	D-FACTOR	OMEGA BAR	SOLID-ITY	RHO*V RATIO	REL. ANGLES INLET	REL. ANGLES EXIT	TURN-ING	REL MACH NO INLET	REL MACH NO EXIT	PRESS-URE RATIO	EFFIC IENCY	TEMP RISE	REL VELCITY INLET	REL VELCITY EXIT	PS RISE	MERID VEL RATIO	WHEEL SPEED INLET	WHEEL SPEED EXIT	FREE PS RISE
24	.1570	.0407	1.400	1.589	71.21	60.30	10.91	1.424	1.237	1.414	91.83	.113	1566.	1407.	.101	1.382	1483.	1466.	.1143
23	.1669	.0632	1.400	1.334	66.56	59.30	7.26	1.462	1.243	1.366	86.41	.108	1589.	1407.	.111	1.137	1458.	1446.	.1200
22	.1782	.0601	1.400	1.276	64.92	59.08	5.84	1.466	1.225	1.365	87.00	.107	1585.	1387.	.128	1.061	1436.	1426.	.1352
21	.1925	.0603	1.400	1.260	64.04	58.61	5.43	1.458	1.198	1.381	87.41	.111	1574.	1359.	.144	1.027	1415.	1407.	.1503
20	.2063	.0571	1.400	1.255	63.48	58.24	5.24	1.445	1.169	1.400	88.56	.114	1558.	1329.	.162	1.005	1394.	1389.	.1666
19	.2317	.0511	1.400	1.241	62.54	57.68	4.86	1.414	1.113	1.429	90.37	.119	1524.	1270.	.196	.966	1352.	1350.	.1977
18	.2574	.0486	1.400	1.231	61.56	56.72	4.84	1.383	1.059	1.457	91.42	.124	1489.	1213.	.229	.938	1310.	1312.	.2274
17	.2831	.0490	1.400	1.224	60.58	55.46	5.12	1.350	1.008	1.481	91.87	.129	1453.	1156.	.262	.918	1266.	1272.	.2557
16	.3085	.0516	1.400	1.224	59.60	53.74	5.86	1.316	.959	1.503	91.98	.134	1415.	1102.	.292	.910	1221.	1232.	.2815
15	.3325	.0548	1.400	1.230	58.56	51.55	7.01	1.279	.914	1.524	92.01	.139	1376.	1051.	.321	.910	1174.	1191.	.3042
14	.3512	.0573	1.400	1.213	57.41	49.92	7.49	1.241	.873	1.522	91.93	.139	1335.	1003.	.348	.899	1125.	1148.	.3237
13	.3668	.0569	1.400	1.206	56.15	47.77	8.38	1.202	.836	1.518	92.24	.137	1292.	960.	.373	.897	1073.	1103.	.3403
12	.3792	.0528	1.400	1.205	54.73	45.13	9.60	1.160	.804	1.513	93.04	.135	1247.	921.	.397	.902	1018.	1056.	.3542
11	.3881	.0448	1.400	1.207	53.12	42.03	11.09	1.116	.775	1.506	94.26	.132	1200.	885.	.419	.913	960.	1005.	.3655
10	.3966	.0359	1.400	1.211	51.28	38.33	12.95	1.070	.747	1.498	95.56	.128	1151.	850.	.440	.927	898.	951.	.3746
9	.4029	.0299	1.400	1.212	49.69	35.09	14.60	1.032	.725	1.489	96.41	.125	1110.	823.	.455	.938	847.	907.	.3788
8	.4049	.0276	1.400	1.210	48.97	33.69	15.28	1.015	.716	1.483	96.72	.123	1092.	812.	.461	.942	824.	887.	.3795
7	.4095	.0222	1.400	1.214	47.21	29.68	17.53	.973	.696	1.474	97.47	.120	1047.	787.	.472	.961	769.	841.	.3762
6	.4117	.0198	1.400	1.218	45.98	26.72	19.26	.944	.684	1.469	97.81	.119	1017.	772.	.475	.976	731.	809.	.3694
5	.4129	.0189	1.400	1.221	44.93	24.02	20.91	.919	.675	1.466	97.99	.118	990.	760.	.475	.990	699.	783.	.3596
4	.4137	.0197	1.400	1.227	43.54	20.17	23.36	.886	.666	1.463	97.99	.117	956.	748.	.470	1.013	658.	750.	.3401
3	.4132	.0220	1.400	1.234	42.20	16.22	25.98	.854	.659	1.462	97.88	.117	922.	738.	.458	1.038	619.	719.	.3135
2	.4098	.0272	1.400	1.244	40.53	10.87	29.66	.814	.655	1.464	97.59	.118	881.	731.	.430	1.073	572.	683.	.2655
1	.5435	.1979	1.400	1.150	40.62	-3.74	44.36	.732	.563	1.488	86.82	.139	797.	633.	.401	1.044	519.	640.	.1966

STL NO.	CUM.PT RATIO	CUM.TT RATIO	CUM. ADIA.	EFF. POLY.	ABS. ANGLES INLET	ABS. ANGLES EXIT	REL. PRESS. INLET	REL. PRESS. EXIT	REL. TEMP. INLET	REL. TEMP. EXIT
24	1.262	1.113	60.73	61.90	.00	19.27	31.78	30.23	707.3	703.2
23	1.317	1.108	75.89	76.68	.00	18.14	33.30	31.31	701.2	698.4
22	1.349	1.107	83.44	83.99	.00	18.34	33.24	31.43	696.0	693.8
21	1.376	1.111	86.48	86.93	.00	19.26	32.71	31.01	691.1	689.4
20	1.399	1.114	88.29	88.68	.00	20.29	31.98	30.48	686.2	685.0
19	1.431	1.119	90.74	91.06	.00	22.23	30.51	29.37	676.6	676.3
18	1.461	1.124	92.29	92.55	.00	24.13	29.10	28.22	667.1	667.7
17	1.486	1.129	92.86	93.10	.00	26.01	27.72	27.02	657.8	659.3
16	1.510	1.134	92.99	93.25	.00	27.79	26.37	25.82	648.5	650.9
15	1.531	1.139	93.01	93.28	.00	29.39	25.07	24.67	639.2	642.6
14	1.529	1.139	92.95	93.23	.00	30.50	23.80	23.57	629.8	634.3
13	1.525	1.137	93.29	93.54	.00	31.30	22.58	22.53	620.3	625.9
12	1.520	1.135	94.10	94.31	.00	31.82	21.39	21.55	610.8	617.4
11	1.512	1.132	95.36	95.48	.00	32.11	20.24	20.63	601.2	608.7
10	1.504	1.128	96.69	96.73	.00	32.45	19.13	19.72	591.6	599.9
9	1.495	1.125	97.57	97.55	.00	32.78	18.30	19.01	584.2	593.1
8	1.489	1.123	97.92	97.88	.00	32.91	17.95	18.71	581.0	590.2
7	1.481	1.120	98.72	98.63	.00	33.43	17.17	18.03	573.7	583.4
6	1.476	1.119	99.09	98.98	.00	33.86	16.69	17.60	569.0	579.1
5	1.473	1.118	99.28	99.16	.00	34.31	16.31	17.25	565.3	575.7
4	1.470	1.117	99.31	99.19	.00	35.06	15.84	16.81	560.6	571.5
3	1.469	1.117	99.22	99.10	.00	35.91	15.44	16.42	556.5	567.7
2	1.472	1.118	98.94	98.84	.00	37.18	14.99	15.97	551.8	563.4
1	1.442	1.139	79.64	80.55	.00	47.19	14.02	14.27	547.0	558.8

1*VECTORS NASA/AE QHSF Fan. Design Point. 22-in rotor LE tip diameter. 97/03/07
Design report geometry. Final core duct flowpath w/ -60 duct loss. 15:44:24
Rotor and stator performance from DAWES models.

INSIDE ROTOR 1 AT STATION 15 FLOW 83.38 CORR. FLOW 61.36 TOTAL PRESSURE 21.90
AREA 250.7 SPEC. FLOW 35.25 TOTAL TEMPERATURE 623.4 GAMMA 1.39848

STL NO.	RADIUS CORD.	VELOCITIES -*-*-*-*-*-*-*-*-* AXIAL	RADIAL	TANG.	MERID.	ABS.	PRESSURE TOTAL	STATIC	TEMPERATURE TOTAL	STATIC	ABSOLUTE MACH NO.	MERIDINAL DISTANCE	R*VU	PERCENT S P A N	PERCENT F L O W	Q
24	10.811-10.753	644.	-79.	414.	649.	770.	19.70	14.77	625.1	575.9	.655	21.775	4481.0	100.00	100.00	.9555
23	10.669-10.641	651.	-79.	399.	655.	767.	20.12	15.08	620.0	571.1	.655	21.883	4253.0	97.11	96.94	.9691
22	10.529-10.531	648.	-78.	396.	653.	763.	20.47	15.38	618.2	569.8	.653	21.992	4171.5	94.28	93.88	.9768
21	10.391-10.434	649.	-76.	410.	654.	772.	20.89	15.60	620.2	570.7	.659	22.088	4261.4	91.55	90.83	.9793
20	10.254-10.337	652.	-73.	426.	656.	782.	21.29	15.80	622.4	571.7	.667	22.185	4363.4	88.85	87.77	.9811
19	9.982-10.160	654.	-62.	450.	657.	796.	21.87	16.07	625.4	572.8	.679	22.362	4495.4	83.59	81.65	.9840
18	9.713-10.006	655.	-48.	472.	656.	808.	22.26	16.20	627.4	573.1	.689	22.517	4583.3	78.49	75.54	.9857
17	9.442 -9.873	654.	-33.	494.	654.	820.	22.52	16.25	629.1	573.4	.699	22.654	4662.8	73.47	69.42	.9862
16	9.166 -9.754	653.	-19.	518.	653.	833.	22.73	16.24	631.0	573.3	.710	22.778	4744.1	68.45	63.30	.9860
15	8.885 -9.644	653.	-5.	542.	654.	849.	22.90	16.16	632.5	572.7	.724	22.896	4813.8	63.36	57.19	.9856
14	8.592 -9.542	644.	8.	554.	644.	849.	22.73	16.02	631.3	571.4	.725	23.011	4756.8	58.12	51.07	.9856
13	8.284 -9.447	638.	24.	564.	638.	852.	22.55	15.84	629.3	569.1	.729	23.122	4669.7	52.66	44.96	.9864
12	7.959 -9.360	635.	43.	572.	637.	856.	22.36	15.63	626.7	565.9	.734	23.230	4553.0	46.95	38.84	.9881
11	7.616 -9.280	636.	68.	580.	640.	863.	22.18	15.37	623.6	561.8	.743	23.339	4416.8	40.96	32.72	.9906
10	7.255 -9.204	637.	97.	590.	645.	874.	22.01	15.07	620.7	557.2	.756	23.454	4283.4	34.67	26.61	.9932
9	6.961 -9.152	637.	124.	599.	649.	883.	21.82	14.80	618.2	553.4	.766	23.546	4171.9	29.57	21.91	.9948
8	6.831 -9.131	636.	136.	600.	650.	885.	21.67	14.65	616.5	551.5	.769	23.588	4097.9	27.32	19.91	.9954
7	6.523 -9.087	637.	167.	612.	659.	899.	21.48	14.31	614.2	547.0	.785	23.691	3992.8	21.99	15.37	.9968
6	6.317 -9.061	639.	190.	623.	667.	912.	21.36	14.04	612.8	543.7	.798	23.766	3933.2	18.45	12.50	.9974
5	6.149 -9.042	642.	210.	633.	675.	926.	21.28	13.79	611.9	540.8	.812	23.834	3893.5	15.56	10.25	.9977
4	5.934 -9.022	646.	236.	650.	688.	946.	21.19	13.44	611.2	536.8	.834	23.933	3859.0	11.87	7.50	.9978
3	5.738 -9.007	652.	264.	670.	703.	972.	21.14	13.06	610.9	532.5	.859	24.042	3845.5	8.51	5.12	.9977
2	5.510 -8.995	662.	300.	702.	727.	1010.	21.17	12.54	611.3	526.6	.898	24.221	3865.9	4.60	2.50	.9972
1	5.241 -8.998	548.	276.	863.	613.	1059.	20.66	11.75	626.0	533.0	.936	24.746	4523.7	.00	.00	.9672

STL NO.	D-FACTOR	OMEGA BAR	SOLID-ITY	RHO*V RATIO	REL. ANGLES INLET	REL. ANGLES EXIT	TURN-ING	REL MACH NO INLET	REL MACH NO EXIT	PRESS-URE RATIO	EFFIC IENCY	TEMP RISE	REL VELCITY INLET	REL VELCITY EXIT	PS RISE	MERID VEL RATIO	WHEEL SPEED INLET	WHEEL SPEED EXIT	FREE PS RISE
24	.3095	.0613	1.400	1.721	71.21	58.09	13.12	1.424	1.045	1.766	92.10	.192	1566.	1228.	.231	1.287	1483.	1457.	.2535
23	.3157	.0955	1.400	1.405	66.56	57.76	8.79	1.463	1.049	1.670	86.78	.182	1589.	1229.	.232	1.037	1458.	1438.	.2483
22	.3235	.0913	1.400	1.342	64.92	57.46	7.45	1.466	1.037	1.659	87.19	.178	1585.	1213.	.247	.971	1436.	1419.	.2611
21	.3386	.0922	1.400	1.329	64.04	56.57	7.47	1.458	1.014	1.677	87.39	.182	1574.	1187.	.264	.949	1415.	1400.	.2763
20	.3528	.0879	1.400	1.337	63.48	55.56	7.92	1.445	.990	1.706	88.36	.187	1558.	1160.	.282	.943	1394.	1382.	.2927
19	.3768	.0793	1.400	1.348	62.54	53.73	8.81	1.414	.947	1.748	90.04	.192	1524.	1110.	.316	.935	1352.	1345.	.3217
18	.3988	.0755	1.400	1.348	61.56	51.90	9.66	1.383	.907	1.776	90.94	.196	1489.	1064.	.346	.926	1310.	1309.	.3467
17	.4218	.0763	1.400	1.342	60.58	49.95	10.63	1.351	.867	1.795	91.25	.199	1453.	1017.	.376	.917	1266.	1272.	.3698
16	.4457	.0803	1.400	1.336	59.60	47.70	11.90	1.316	.827	1.812	91.22	.203	1415.	970.	.406	.912	1221.	1235.	.3909
15	.4693	.0855	1.400	1.329	58.56	45.09	13.47	1.279	.790	1.825	91.09	.206	1376.	926.	.434	.910	1174.	1197.	.4096
14	.4886	.0894	1.400	1.301	57.41	43.17	14.25	1.241	.754	1.812	90.96	.203	1335.	883.	.463	.896	1125.	1158.	.4267
13	.5054	.0888	1.400	1.280	56.15	40.88	15.27	1.202	.723	1.797	91.29	.200	1292.	844.	.493	.887	1073.	1116.	.4432
12	.5188	.0822	1.400	1.265	54.73	38.17	16.56	1.160	.695	1.782	92.17	.195	1247.	810.	.524	.884	1018.	1073.	.4589
11	.5285	.0699	1.400	1.259	53.12	34.92	18.20	1.117	.672	1.767	93.55	.189	1200.	780.	.555	.888	960.	1026.	.4726
10	.5374	.0561	1.400	1.255	51.28	31.00	20.28	1.070	.650	1.754	95.03	.183	1151.	752.	.588	.896	898.	978.	.4837
9	.5434	.0468	1.400	1.250	49.69	27.58	22.11	1.032	.635	1.739	95.98	.178	1110.	732.	.611	.903	847.	938.	.4876
8	.5429	.0432	1.400	1.247	48.97	26.25	22.72	1.015	.630	1.726	96.33	.175	1092.	725.	.618	.908	824.	921.	.4857
7	.5439	.0348	1.400	1.248	47.21	22.05	25.16	.973	.620	1.711	97.17	.171	1047.	711.	.633	.926	769.	879.	.4768
6	.5421	.0311	1.400	1.252	45.98	18.93	27.05	.944	.617	1.702	97.56	.168	1017.	705.	.637	.944	731.	851.	.4626
5	.5378	.0296	1.400	1.258	44.93	16.15	28.78	.919	.617	1.695	97.75	.166	990.	703.	.633	.963	699.	829.	.4430
4	.5302	.0309	1.400	1.266	43.54	12.27	31.27	.886	.620	1.688	97.76	.165	956.	704.	.620	.993	658.	800.	.4068
3	.5172	.0343	1.400	1.279	42.20	8.35	33.85	.854	.629	1.684	97.65	.164	922.	711.	.593	1.030	619.	773.	.3555
2	.4949	.0421	1.400	1.299	40.53	3.22	37.31	.814	.647	1.686	97.33	.165	881.	728.	.537	1.086	572.	743.	.2664
1	.6517	.3054	1.400	1.124	40.62	-14.33	54.95	.732	.560	1.707	85.28	.193	797.	633.	.459	1.014	519.	706.	.1241

STL NO.	CUM.PT RATIO	CUM.TT RATIO	CUM. ADIA.	EFF. POLY.	ABS. ANGLES INLET	ABS. ANGLES EXIT	REL. PRESS. INLET	REL. PRESS. EXIT	REL. TEMP. INLET	REL. TEMP. EXIT
24	1.577	1.192	72.51	74.03	.00	32.56	31.79	29.46	707.0	701.0
23	1.610	1.182	80.16	81.24	.00	31.31	33.30	30.25	701.0	696.4
22	1.638	1.178	84.93	85.73	.00	31.27	33.24	30.41	695.7	692.0
21	1.672	1.182	86.79	87.49	.00	32.10	32.71	30.01	690.8	687.6
20	1.704	1.187	88.19	88.82	.00	32.98	31.99	29.55	685.9	683.3
19	1.751	1.192	90.28	90.80	.00	34.44	30.52	28.60	676.4	675.1
18	1.782	1.196	91.52	91.97	.00	35.71	29.11	27.60	666.9	667.1
17	1.802	1.199	91.92	92.35	.00	37.04	27.72	26.53	657.6	659.2
16	1.819	1.203	91.92	92.36	.00	38.39	26.37	25.43	648.3	651.5
15	1.833	1.206	91.80	92.26	.00	39.66	25.07	24.37	639.0	643.8
14	1.820	1.203	91.69	92.15	.00	40.67	23.81	23.35	629.6	636.1
13	1.805	1.200	92.04	92.46	.00	41.44	22.58	22.42	620.2	628.3
12	1.790	1.195	92.95	93.28	.00	41.94	21.39	21.57	610.7	620.3
11	1.775	1.189	94.35	94.56	.00	42.20	20.24	20.79	601.1	612.3
10	1.761	1.183	95.85	95.93	.00	42.48	19.13	20.02	591.5	604.2
9	1.747	1.178	96.83	96.83	.00	42.73	18.30	19.41	584.1	597.9
8	1.734	1.175	97.21	97.17	.00	42.68	17.95	19.15	580.9	595.2
7	1.719	1.171	98.09	97.97	.00	42.89	17.17	18.54	573.6	589.0
6	1.710	1.168	98.49	98.34	.00	43.05	16.69	18.15	568.9	585.0
5	1.703	1.166	98.70	98.54	.00	43.16	16.31	17.83	565.2	581.8
4	1.696	1.165	98.74	98.57	.00	43.40	15.84	17.41	560.6	577.9
3	1.692	1.164	98.64	98.47	.00	43.61	15.44	17.04	556.4	574.5
2	1.694	1.165	98.34	98.19	.00	44.00	14.99	16.62	551.8	570.6
1	1.654	1.193	79.93	81.11	.00	54.60	14.02	14.53	546.9	566.2

1*VECTORS NASA/AE QHSF Fan. Design Point. 22-in rotor LE tip diameter. 97/03/07
Design report geometry. Final core duct flowpath w/ -60 duct loss. 15:44:24
Rotor and stator performance from DAWES models.

ROTOR 1 AT STATION 16 FLOW 83.38 CORR. FLOW 58.90 TOTAL PRESSURE 23.03 RPM 15444.
AREA 247.5 SPEC. FLOW 34.27 TOTAL TEMPERATURE 635.7 GAMMA 1.39816

STL NO.	RADIUS CORD.	VELOCITIES -*-*-*-*-*-*-*-*-* AXIAL	RADIAL	TANG.	MERID.	ABS.	PRESSURE TOTAL	STATIC	TEMPERATURE TOTAL	STATIC	ABSOLUTE MACH NO.	MERIDINAL DISTANCE	R*VU	PERCENT S P A N	PERCENT F L O W	Q
24	10.748-10.240	506.	-52.	474.	508.	695.	20.92	16.66	638.8	598.8	.580	22.293	5096.5	100.00	100.00	.9510
23	10.584-10.038	539.	-58.	468.	542.	716.	21.30	16.70	635.7	593.1	.601	22.492	4955.3	95.96	96.94	.9607
22	10.433 -9.883	568.	-61.	466.	572.	738.	21.65	16.70	633.6	588.5	.621	22.647	4862.6	92.44	93.88	.9683
21	10.289 -9.750	589.	-61.	480.	592.	762.	22.03	16.70	635.3	587.1	.642	22.780	4938.0	89.22	90.83	.9705
20	10.149 -9.625	610.	-59.	494.	613.	787.	22.42	16.68	637.1	585.6	.664	22.905	5016.6	86.12	87.77	.9726
19	9.880 -9.416	638.	-51.	516.	640.	822.	22.97	16.63	638.8	582.7	.695	23.113	5095.1	80.42	81.65	.9767
18	9.620 -9.256	650.	-42.	531.	652.	841.	23.22	16.56	639.2	580.5	.712	23.274	5110.9	75.13	75.54	.9792
17	9.360 -9.121	654.	-31.	548.	655.	854.	23.33	16.46	639.5	579.0	.724	23.410	5124.9	69.97	69.42	.9800
16	9.094 -8.999	656.	-21.	566.	656.	867.	23.38	16.32	640.0	577.7	.736	23.536	5146.7	64.80	63.30	.9798
15	8.820 -8.885	656.	-11.	585.	656.	879.	23.38	16.14	640.2	576.1	.748	23.658	5158.9	59.54	57.19	.9795
14	8.538 -8.775	657.	1.	603.	657.	892.	23.35	15.94	640.0	574.0	.760	23.779	5146.1	54.15	51.07	.9796
13	8.246 -8.672	662.	17.	618.	662.	906.	23.33	15.70	638.9	570.8	.774	23.898	5099.4	48.63	44.96	.9809
12	7.945 -8.572	670.	37.	632.	671.	922.	23.31	15.45	637.2	566.7	.790	24.019	5020.8	42.98	38.84	.9834
11	7.636 -8.475	680.	62.	645.	683.	939.	23.32	15.17	634.9	561.8	.809	24.144	4921.9	37.22	32.72	.9870
10	7.319 -8.384	689.	92.	659.	695.	958.	23.33	14.87	632.7	556.6	.829	24.276	4823.5	31.35	26.61	.9905
9	7.066 -8.319	694.	118.	673.	704.	974.	23.32	14.61	631.2	552.5	.846	24.386	4755.5	26.71	21.91	.9927
8	6.955 -8.297	696.	130.	679.	708.	981.	23.30	14.48	630.5	550.6	.854	24.431	4725.4	24.69	19.91	.9936
7	6.695 -8.250	700.	159.	695.	718.	1000.	23.25	14.15	629.0	546.1	.873	24.545	4654.8	19.96	15.37	.9954
6	6.523 -8.224	702.	180.	707.	724.	1012.	23.20	13.92	628.0	543.0	.887	24.628	4613.2	16.86	12.50	.9963
5	6.383 -8.208	702.	197.	718.	729.	1023.	23.15	13.71	627.4	540.5	.899	24.700	4583.5	14.34	10.25	.9967
4	6.202 -8.197	701.	220.	735.	735.	1039.	23.08	13.43	626.8	537.2	.915	24.800	4558.3	11.10	7.50	.9968
3	6.037 -8.195	699.	242.	754.	740.	1057.	23.05	13.15	626.6	534.0	.933	24.908	4550.6	8.13	5.12	.9967
2	5.840 -8.204	696.	271.	783.	747.	1082.	23.07	12.78	627.1	530.0	.959	25.079	4572.2	4.59	2.50	.9961
1	5.591 -8.252	510.	229.	951.	559.	1104.	22.32	12.26	643.8	542.8	.967	25.571	5319.7	.00	.00	.9612

STL NO.	D-FACTOR	OMEGA BAR	SOLID-ITY	RHO*V RATIO	REL. ANGLES INLET	REL. ANGLES EXIT	TURN-ING	REL MACH NO INLET	REL MACH NO EXIT	PRESS-URE RATIO	EFFIC IENCY	TEMP RISE	REL VELCITY INLET	REL VELCITY EXIT	PS RISE	MERID VEL RATIO	WHEEL SPEED INLET	WHEEL SPEED EXIT	FREE PS RISE
24	.3987	.0819	1.490	1.463	71.21	62.45	8.76	1.425	.917	1.876	90.36	.218	1566.	1099.	.317	1.008	1483.	1449.	.3480
23	.4035	.1321	1.509	1.240	66.56	60.49	6.06	1.463	.923	1.769	83.50	.212	1589.	1101.	.300	.858	1458.	1427.	.3268
22	.4014	.1279	1.526	1.236	64.92	58.70	6.22	1.466	.926	1.754	83.79	.208	1585.	1100.	.303	.850	1436.	1406.	.3284
21	.4097	.1300	1.543	1.253	64.04	56.84	7.19	1.459	.912	1.769	83.83	.211	1574.	1083.	.311	.860	1415.	1387.	.3353
20	.4159	.1245	1.559	1.288	63.48	54.94	8.54	1.445	.900	1.796	84.90	.214	1558.	1067.	.321	.881	1394.	1368.	.3442
19	.4252	.1121	1.587	1.338	62.54	51.88	10.66	1.415	.877	1.836	86.99	.218	1524.	1037.	.342	.911	1352.	1332.	.3610
18	.4355	.1057	1.607	1.351	61.56	49.59	11.97	1.383	.852	1.853	88.14	.218	1489.	1005.	.364	.919	1310.	1297.	.3766
17	.4490	.1061	1.626	1.347	60.58	47.46	13.12	1.351	.822	1.860	88.51	.219	1453.	969.	.387	.918	1266.	1261.	.3916
16	.4641	.1110	1.649	1.338	59.60	45.15	14.45	1.316	.790	1.863	88.43	.220	1415.	930.	.410	.916	1221.	1226.	.4053
15	.4789	.1175	1.683	1.326	58.56	42.61	15.94	1.280	.759	1.864	88.23	.220	1376.	892.	.433	.914	1174.	1189.	.4178
14	.4912	.1221	1.727	1.315	57.41	39.81	17.60	1.242	.729	1.861	88.25	.220	1335.	856.	.457	.914	1125.	1151.	.4292
13	.4980	.1205	1.782	1.311	56.15	36.67	19.48	1.202	.705	1.859	88.87	.218	1292.	825.	.482	.920	1073.	1111.	.4390
12	.4979	.1110	1.848	1.316	54.73	33.19	21.54	1.160	.687	1.858	90.17	.215	1247.	802.	.509	.931	1018.	1071.	.4469
11	.4913	.0941	1.925	1.328	53.12	29.38	23.74	1.117	.675	1.859	92.05	.210	1200.	784.	.537	.948	960.	1029.	.4518
10	.4811	.0752	2.012	1.338	51.28	25.21	26.08	1.071	.665	1.859	93.99	.206	1151.	769.	.567	.966	898.	986.	.4525
9	.4713	.0628	2.088	1.342	49.69	21.63	28.06	1.033	.658	1.858	95.22	.203	1110.	758.	.589	.981	847.	952.	.4470
8	.4657	.0578	2.123	1.344	48.97	20.01	28.96	1.015	.656	1.857	95.70	.202	1092.	754.	.598	.988	824.	937.	.4421
7	.4483	.0464	2.214	1.348	47.21	16.08	31.14	.973	.653	1.852	96.74	.199	1047.	747.	.613	1.010	769.	902.	.4228
6	.4341	.0414	2.282	1.350	45.98	13.35	32.63	.944	.652	1.848	97.22	.197	1017.	744.	.620	1.025	731.	879.	.4029
5	.4204	.0393	2.345	1.351	44.93	11.03	33.90	.919	.652	1.844	97.46	.196	990.	743.	.622	1.040	699.	860.	.3811
4	.4004	.0408	2.437	1.351	43.54	7.82	35.71	.886	.653	1.839	97.50	.195	956.	742.	.618	1.061	658.	836.	.3441
3	.3778	.0451	2.533	1.351	42.20	4.62	37.59	.854	.656	1.836	97.40	.195	922.	743.	.608	1.084	619.	814.	.2986
2	.3450	.0550	2.667	1.352	40.53	.33	40.21	.814	.662	1.837	97.08	.195	881.	747.	.582	1.116	572.	787.	.2265
1	.5039	.3923	2.849	1.050	40.62	-19.48	60.10	.732	.520	1.843	83.92	.227	797.	593.	.580	.924	519.	754.	.1390

STL NO.	CUM.PT RATIO	CUM.TT RATIO	CUM. ADIA.	EFF. POLY.	ABS. ANGLES INLET	ABS. ANGLES EXIT	REL. PRESS. INLET	REL. PRESS. EXIT	REL. TEMP. INLET	REL. TEMP. EXIT
24	1.675	1.218	72.84	74.53	.00	43.01	31.79	28.69	706.9	699.0
23	1.705	1.212	77.73	79.11	.00	40.80	33.31	28.95	700.9	693.7
22	1.733	1.208	81.82	82.94	.00	39.19	33.25	29.04	695.6	688.9
21	1.763	1.211	83.31	84.35	.00	39.02	32.72	28.61	690.7	684.4
20	1.794	1.214	84.75	85.72	.00	38.89	31.99	28.20	685.9	680.1
19	1.838	1.218	87.21	88.02	.00	38.85	30.52	27.43	676.3	672.0
18	1.859	1.218	88.66	89.37	.00	39.19	29.11	26.60	666.8	664.3
17	1.867	1.219	89.13	89.80	.00	39.89	27.72	25.63	657.5	656.9
16	1.871	1.220	89.08	89.76	.00	40.78	26.37	24.62	648.2	649.5
15	1.872	1.220	88.90	89.59	.00	41.70	25.07	23.62	638.9	642.1
14	1.869	1.220	88.93	89.62	.00	42.52	23.81	22.69	629.5	634.7
13	1.867	1.218	89.56	90.20	.00	43.05	22.58	21.88	620.1	627.3
12	1.866	1.215	90.89	91.40	.00	43.29	21.39	21.18	610.6	620.0
11	1.867	1.210	92.78	93.13	.00	43.34	20.24	20.59	601.1	612.8
10	1.868	1.206	94.73	94.91	.00	43.46	19.13	20.00	591.5	605.6
9	1.867	1.203	95.98	96.05	.00	43.70	18.30	19.53	584.1	600.1
8	1.865	1.202	96.47	96.49	.00	43.81	17.95	19.32	580.9	597.8
7	1.861	1.199	97.55	97.47	.00	44.07	17.17	18.84	573.6	592.4
6	1.857	1.197	98.03	97.91	.00	44.32	16.69	18.52	568.9	589.0
5	1.853	1.196	98.29	98.15	.00	44.56	16.31	18.24	565.2	586.3
4	1.848	1.195	98.35	98.20	.00	45.00	15.84	17.88	560.5	582.9
3	1.845	1.195	98.26	98.12	.00	45.52	15.44	17.54	556.4	579.8
2	1.847	1.195	97.95	97.84	.00	46.35	14.99	17.14	551.8	576.3
1	1.787	1.227	79.27	80.68	.00	59.56	14.02	14.73	546.9	572.0

1*VECTORS NASA/AE QHSF Fan. Design Point. 22-in rotor LE tip diameter. 97/03/07
Design report geometry. Final core duct flowpath w/ -60 duct loss. 15:44:24
Rotor and stator performance from DAWES models.

STATION 17 FLOW 83.38 CORR. FLOW 58.90 TOTAL PRESSURE 23.03
AREA 243.8 SPEC. FLOW 34.79 TOTAL TEMPERATURE 635.7 GAMMA 1.39816

STL NO.	RADIUS	CORD.	VELOCITIES -*-*-*-*-*-*-*-*-* AXIAL	RADIAL	TANG.	MERID.	ABS.	PRESSURE TOTAL	STATIC	TEMPERATURE TOTAL	STATIC	ABSOLUTE MACH NO.	MERIDINAL DISTANCE	R*VU	PERCENT S P A N	PERCENT F L O W	Q
24	10.690	-8.541	490.	7.	477.	490.	684.	20.92	16.79	638.8	600.0	.570	23.993	5096.5	100.00	100.00	.9510
23	10.549	-8.389	533.	11.	470.	533.	710.	21.30	16.77	635.7	593.8	.595	24.142	4955.3	96.73	96.94	.9607
22	10.419	-8.252	566.	16.	467.	567.	734.	21.65	16.75	633.6	588.9	.617	24.279	4862.6	93.76	93.88	.9683
21	10.294	-8.136	590.	20.	480.	590.	761.	22.03	16.72	635.3	587.3	.641	24.394	4938.0	91.02	90.83	.9705
20	10.172	-8.028	613.	24.	493.	614.	788.	22.42	16.68	637.1	585.6	.664	24.502	5016.6	88.40	87.77	.9726
19	9.936	-7.856	646.	32.	513.	647.	826.	22.97	16.58	638.8	582.3	.699	24.675	5095.1	83.46	81.65	.9767
18	9.701	-7.746	662.	38.	527.	663.	847.	23.22	16.48	639.2	579.7	.718	24.785	5110.9	78.67	75.54	.9792
17	9.460	-7.673	668.	43.	542.	669.	861.	23.33	16.36	639.5	578.0	.731	24.862	5124.9	73.83	69.42	.9800
16	9.213	-7.613	669.	48.	559.	671.	873.	23.38	16.22	640.0	576.7	.742	24.928	5146.6	68.86	63.30	.9798
15	8.956	-7.564	669.	53.	576.	671.	884.	23.38	16.07	640.2	575.4	.752	24.986	5158.9	63.73	57.19	.9795
14	8.689	-7.523	668.	59.	592.	671.	895.	23.35	15.90	640.0	573.5	.763	25.040	5146.1	58.38	51.07	.9796
13	8.410	-7.493	671.	66.	606.	674.	906.	23.33	15.70	638.9	570.8	.775	25.088	5099.4	52.81	44.96	.9809
12	8.119	-7.472	677.	74.	618.	681.	920.	23.31	15.47	637.2	566.9	.789	25.133	5020.8	47.01	38.84	.9834
11	7.817	-7.459	687.	84.	630.	692.	936.	23.32	15.22	634.9	562.3	.806	25.176	4921.9	40.99	32.72	.9870
10	7.504	-7.457	697.	97.	643.	703.	953.	23.33	14.95	632.7	557.4	.824	25.222	4823.5	34.72	26.61	.9905
9	7.252	-7.466	704.	109.	656.	712.	968.	23.32	14.70	631.2	553.5	.840	25.258	4755.5	29.67	21.91	.9927
8	7.141	-7.475	707.	115.	662.	717.	975.	23.30	14.57	630.5	551.6	.848	25.274	4725.4	27.44	19.91	.9936
7	6.881	-7.500	718.	133.	677.	730.	995.	23.25	14.22	629.0	546.8	.869	25.318	4654.8	22.19	15.37	.9954
6	6.709	-7.522	725.	146.	688.	740.	1010.	23.20	13.96	628.0	543.4	.884	25.354	4613.2	18.70	12.50	.9963
5	6.570	-7.543	731.	159.	698.	748.	1023.	23.15	13.72	627.4	540.6	.898	25.391	4583.5	15.87	10.25	.9967
4	6.391	-7.578	737.	177.	713.	758.	1041.	23.08	13.40	626.8	536.9	.917	25.447	4558.3	12.20	7.50	.9968
3	6.229	-7.616	743.	197.	731.	769.	1060.	23.05	13.09	626.6	533.3	.937	25.518	4550.6	8.84	5.12	.9967
2	6.039	-7.666	749.	226.	757.	782.	1088.	23.07	12.68	627.1	528.8	.966	25.652	4572.2	4.87	2.50	.9961
1	5.812	-7.745	583.	215.	915.	621.	1106.	22.32	12.22	643.8	542.4	.969	26.123	5319.7	.00	.00	.9612

STATION 18 FLOW 83.38 CORR. FLOW 58.90 TOTAL PRESSURE 23.03
AREA 244.4 SPEC. FLOW 34.70 TOTAL TEMPERATURE 635.7 GAMMA 1.39816

24	10.804	-6.808	454.	26.	472.	455.	655.	20.92	17.11	638.8	603.2	.545	25.729	5096.5	100.00	100.00	.9510
23	10.660	-6.705	501.	27.	465.	502.	684.	21.30	17.07	635.7	596.9	.572	25.829	4955.3	97.40	96.94	.9607
22	10.526	-6.611	538.	28.	462.	538.	709.	21.65	17.04	633.6	591.9	.595	25.923	4862.6	95.04	93.88	.9683
21	10.399	-6.527	563.	28.	475.	564.	737.	22.03	17.01	635.3	590.2	.619	26.006	4938.0	92.82	90.83	.9705
20	10.274	-6.453	588.	28.	488.	588.	765.	22.42	16.98	637.1	588.6	.643	26.080	5016.6	90.66	87.77	.9726
19	10.031	-6.358	622.	28.	508.	623.	804.	22.97	16.88	638.8	585.2	.678	26.176	5095.1	86.32	81.65	.9767
18	9.788	-6.344	641.	29.	522.	642.	827.	23.22	16.75	639.2	582.4	.700	26.190	5110.9	81.63	75.54	.9792
17	9.540	-6.367	651.	30.	537.	651.	844.	23.33	16.59	639.5	580.4	.715	26.170	5124.9	76.68	69.42	.9800
16	9.286	-6.400	657.	32.	554.	658.	860.	23.38	16.41	640.0	578.6	.730	26.143	5146.7	71.56	63.30	.9798
15	9.024	-6.442	662.	34.	572.	663.	875.	23.38	16.19	640.2	576.7	.744	26.110	5158.9	66.23	57.19	.9795
14	8.753	-6.494	668.	38.	588.	669.	891.	23.35	15.96	640.0	574.2	.759	26.071	5146.1	60.67	51.07	.9796
13	8.471	-6.555	677.	43.	602.	678.	907.	23.33	15.69	638.9	570.7	.775	26.028	5099.4	54.86	44.96	.9809
12	8.180	-6.625	691.	49.	614.	692.	925.	23.31	15.40	637.2	566.1	.794	25.981	5020.8	48.81	38.84	.9834
11	7.879	-6.705	708.	58.	625.	710.	946.	23.32	15.07	634.9	560.7	.815	25.933	4921.9	42.52	32.72	.9870
10	7.568	-6.796	725.	71.	637.	729.	968.	23.33	14.73	632.7	555.0	.839	25.886	4823.5	35.96	26.61	.9905
9	7.318	-6.875	737.	83.	650.	741.	986.	23.32	14.43	631.2	550.6	.857	25.853	4755.5	30.67	21.91	.9927
8	7.209	-6.912	741.	89.	655.	746.	993.	23.30	14.30	630.5	548.7	.866	25.841	4725.4	28.34	19.91	.9936
7	6.953	-7.002	751.	105.	670.	758.	1012.	23.25	13.97	629.0	544.1	.885	25.821	4654.8	22.83	15.37	.9954
6	6.783	-7.065	757.	116.	680.	766.	1024.	23.20	13.74	628.0	541.0	.899	25.818	4613.2	19.16	12.50	.9963
5	6.645	-7.117	761.	127.	690.	771.	1035.	23.15	13.54	627.4	538.6	.910	25.824	4583.5	16.18	10.25	.9967
4	6.470	-7.188	766.	141.	705.	778.	1050.	23.08	13.27	626.8	535.4	.926	25.844	4558.3	12.33	7.50	.9968
3	6.310	-7.256	770.	156.	721.	786.	1067.	23.05	12.99	626.6	532.2	.944	25.887	4550.6	8.83	5.12	.9967
2	6.126	-7.337	779.	177.	746.	799.	1093.	23.07	12.61	627.1	528.0	.971	25.993	4572.2	4.74	2.50	.9961
1	5.914	-7.435	641.	169.	900.	663.	1117.	22.32	12.06	643.8	540.3	.981	26.449	5319.7	.00	.00	.9612

STATION 19 FLOW 83.38 CORR. FLOW 58.90 TOTAL PRESSURE 23.03
AREA 247.2 SPEC. FLOW 34.31 TOTAL TEMPERATURE 635.7 GAMMA 1.39816

24	10.889	-5.075	411.	7.	468.	411.	623.	20.92	17.45	638.8	606.7	.516	27.464	5096.5	100.00	100.00	.9510
23	10.730	-5.043	466.	10.	462.	466.	656.	21.30	17.39	635.7	600.0	.547	27.492	4955.3	97.57	96.94	.9607
22	10.586	-5.014	508.	7.	459.	509.	685.	21.65	17.33	633.6	594.7	.574	27.521	4862.6	95.41	93.88	.9683
21	10.451	-4.978	538.	1.	472.	538.	716.	22.03	17.27	635.3	592.8	.600	27.556	4938.0	93.46	90.83	.9705
20	10.320	-4.957	567.	-5.	486.	567.	747.	22.42	17.21	637.1	590.8	.627	27.577	5016.6	91.48	87.77	.9726
19	10.068	-4.988	606.	-11.	506.	606.	790.	22.97	17.07	638.8	587.1	.665	27.546	5095.1	87.12	81.65	.9767
18	9.824	-5.102	628.	-11.	520.	628.	815.	23.22	16.92	639.2	584.0	.689	27.433	5110.9	82.15	75.54	.9792
17	9.578	-5.240	639.	-6.	535.	639.	834.	23.33	16.74	639.5	581.8	.706	27.298	5124.9	76.92	69.42	.9800
16	9.326	-5.381	648.	-1.	552.	648.	851.	23.38	16.53	640.0	579.8	.722	27.162	5146.6	71.57	63.30	.9798
15	9.066	-5.527	656.	6.	569.	656.	868.	23.38	16.30	640.2	577.7	.737	27.026	5158.9	66.05	57.19	.9795
14	8.795	-5.679	664.	13.	585.	664.	885.	23.35	16.04	640.0	575.0	.753	26.887	5146.1	60.32	51.07	.9796
13	8.515	-5.836	675.	21.	599.	676.	903.	23.33	15.75	638.9	571.3	.771	26.748	5099.4	54.37	44.96	.9809
12	8.224	-5.999	691.	31.	610.	692.	923.	23.31	15.43	637.2	566.5	.791	26.609	5020.8	48.21	38.84	.9834
11	7.924	-6.167	710.	43.	621.	712.	945.	23.32	15.09	634.9	560.9	.814	26.473	4921.9	41.83	32.72	.9870
10	7.612	-6.342	730.	57.	634.	732.	968.	23.33	14.73	632.7	555.0	.839	26.342	4823.5	35.22	26.61	.9905
9	7.362	-6.482	742.	70.	646.	746.	987.	23.32	14.42	631.2	550.5	.858	26.249	4755.5	29.92	21.91	.9927
8	7.253	-6.544	747.	77.	652.	751.	994.	23.30	14.28	630.5	548.5	.867	26.212	4725.4	27.59	19.91	.9936
7	6.995	-6.688	758.	93.	665.	764.	1013.	23.25	13.95	629.0	543.9	.887	26.138	4654.8	22.13	15.37	.9954
6	6.825	-6.784	763.	105.	676.	771.	1025.	23.20	13.73	628.0	540.9	.900	26.102	4613.2	18.51	12.50	.9963
5	6.686	-6.861	767.	115.	686.	776.	1035.	23.15	13.54	627.4	538.5	.911	26.083	4583.5	15.57	10.25	.9967
4	6.510	-6.960	771.	130.	700.	782.	1049.	23.08	13.28	626.8	535.5	.926	26.076	4558.3	11.83	7.50	.9968
3	6.349	-7.050	774.	144.	717.	788.	1065.	23.05	13.02	626.6	532.6	.942	26.096	4550.6	8.43	5.12	.9967
2	6.164	-7.154	780.	161.	742.	797.	1088.	23.07	12.68	627.1	528.8	.966	26.179	4572.2	4.49	2.50	.9961
1	5.952	-7.272	632.	149.	894.	650.	1105.	22.32	12.24	643.8	542.6	.968	26.617	5319.7	.00	.00	.9612

1*VECTORS NASA/AE QHSF Fan. Design Point. 22-in rotor LE tip diameter. 97/03/07
Design report geometry. Final core duct flowpath w/ -60 duct loss. 15:44:24
Rotor and stator performance from DAWES models.

INSIDE VANE 1 AT STATION 20 FLOW 83.38 CORR. FLOW 59.23 TOTAL PRESSURE 22.90
AREA 220.0 SPEC. FLOW 38.76 TOTAL TEMPERATURE 635.7 GAMMA 1.39816

STL NO.	RADIUS	CORD.	VELOCITIES -*-*-*-*-*-*-*-*-* AXIAL	RADIAL	TANG.	MERID.	ABS.	PRESSURE TOTAL	STATIC	TEMPERATURE TOTAL	STATIC	ABSOLUTE MACH NO.	MERIDINAL DISTANCE	R*VU	PERCENT S P A N	PERCENT F L O W	Q
24	10.889	-4.180	518.	0.	235.	518.	568.	21.30	18.32	638.8	612.0	.469	28.360	2555.2	100.00	100.00	.9558
23	10.739	-4.194	518.	5.	233.	518.	567.	21.29	18.31	635.7	609.0	.469	28.342	2498.0	97.45	96.94	.9605
22	10.588	-4.208	536.	2.	231.	536.	584.	21.48	18.30	633.6	605.4	.484	28.327	2450.4	94.88	93.88	.9661
21	10.441	-4.216	556.	-4.	237.	556.	605.	21.71	18.28	635.3	605.0	.502	28.318	2475.4	92.45	90.83	.9665
20	10.300	-4.236	589.	-12.	244.	589.	638.	22.12	18.27	637.1	603.3	.530	28.298	2508.2	90.03	87.77	.9689
19	10.041	-4.324	637.	-21.	255.	638.	687.	22.77	18.24	638.8	599.7	.572	28.210	2557.3	85.11	81.65	.9743
18	9.798	-4.460	656.	-24.	262.	657.	707.	23.05	18.21	639.2	597.7	.591	28.075	2568.6	79.99	75.54	.9771
17	9.556	-4.607	666.	-24.	269.	667.	719.	23.18	18.17	639.5	596.6	.601	27.931	2569.3	74.77	69.42	.9783
16	9.310	-4.758	673.	-21.	277.	674.	728.	23.26	18.11	640.0	596.0	.609	27.786	2576.4	69.46	63.30	.9785
15	9.056	-4.913	679.	-16.	285.	679.	737.	23.28	18.02	640.2	595.2	.617	27.640	2582.2	63.99	57.19	.9783
14	8.793	-5.074	684.	-10.	293.	685.	745.	23.26	17.90	640.0	594.0	.624	27.492	2578.3	58.30	51.07	.9785
13	8.520	-5.241	691.	-4.	300.	691.	754.	23.23	17.75	638.9	591.8	.632	27.343	2558.5	52.41	44.96	.9797
12	8.237	-5.414	701.	2.	306.	701.	765.	23.22	17.58	637.2	588.6	.644	27.194	2521.2	46.30	38.84	.9822
11	7.945	-5.593	715.	9.	311.	715.	780.	23.22	17.36	634.9	584.5	.658	27.048	2468.9	40.00	32.72	.9857
10	7.643	-5.777	734.	19.	315.	734.	799.	23.22	17.08	632.7	579.8	.677	26.908	2411.3	33.49	26.61	.9891
9	7.402	-5.924	751.	29.	320.	751.	816.	23.19	16.81	631.2	575.9	.694	26.808	2367.6	28.29	21.91	.9911
8	7.297	-5.989	758.	34.	322.	759.	825.	23.17	16.67	630.5	574.1	.703	26.768	2349.4	26.02	19.91	.9919
7	7.050	-6.139	777.	50.	328.	779.	845.	23.11	16.32	629.0	569.7	.723	26.689	2311.0	20.70	15.37	.9937
6	6.888	-6.238	790.	62.	332.	792.	859.	23.05	16.08	628.0	566.8	.737	26.651	2289.1	17.20	12.50	.9945
5	6.757	-6.318	800.	73.	336.	803.	871.	23.01	15.88	627.4	564.5	.748	26.630	2273.5	14.38	10.25	.9950
4	6.592	-6.419	812.	90.	343.	817.	886.	22.97	15.62	626.8	561.6	.763	26.624	2260.1	10.82	7.50	.9954
3	6.444	-6.510	823.	108.	350.	830.	901.	22.94	15.39	626.6	559.4	.777	26.645	2256.1	7.62	5.12	.9953
2	6.273	-6.614	829.	130.	362.	839.	913.	22.83	15.14	627.1	557.9	.789	26.730	2269.3	3.92	2.50	.9932
1	6.090	-6.725	798.	162.	432.	814.	922.	22.62	15.06	643.8	573.4	.786	27.181	2628.2	.00	.00	.9649

STL NO.	D-FACTOR	OMEGA BAR	SOLID-ITY	RHO*V RATIO	ABS. ANGLES INLET	ABS. ANGLES EXIT	TURN-ING	ABS MACH NO INLET	ABS MACH NO EXIT	PRESS-URE RATIO	EFFIC IENCY	TEMP RISE	ABS VELOCITY INLET	ABS VELOCITY EXIT	PS RISE	MERID VEL RATIO
24	.2213	-.1073	1.400	1.311	48.72	24.38	24.33	.516	.469	1.909	93.14	.218	623.	568.	.251	1.260
23	.2600	.0028	1.400	1.152	44.72	24.20	20.52	.547	.469	1.768	83.42	.212	656.	567.	.237	1.110
22	.2671	.0405	1.400	1.093	42.09	23.36	18.73	.574	.484	1.740	82.48	.208	685.	584.	.224	1.054
21	.2730	.0663	1.400	1.073	41.28	23.08	18.20	.600	.502	1.744	81.54	.211	716.	605.	.213	1.034
20	.2620	.0579	1.400	1.082	40.63	22.45	18.18	.627	.530	1.772	82.77	.214	747.	638.	.204	1.040
19	.2448	.0336	1.400	1.100	39.84	21.77	18.07	.665	.572	1.820	85.64	.218	790.	687.	.198	1.051
18	.2459	.0276	1.400	1.101	39.66	21.75	17.90	.689	.591	1.839	86.96	.218	815.	707.	.205	1.047
17	.2524	.0218	1.400	1.103	39.92	21.97	17.95	.706	.601	1.848	87.55	.219	834.	719.	.218	1.042
16	.2603	.0168	1.400	1.108	40.41	22.33	18.07	.722	.609	1.854	87.66	.220	851.	728.	.231	1.039
15	.2683	.0141	1.400	1.112	40.95	22.77	18.19	.737	.617	1.856	87.57	.220	868.	737.	.243	1.036
14	.2763	.0129	1.400	1.114	41.39	23.19	18.20	.753	.624	1.854	87.62	.220	885.	745.	.255	1.031
13	.2833	.0124	1.400	1.113	41.55	23.48	18.07	.771	.632	1.851	88.23	.218	903.	754.	.265	1.023
12	.2886	.0124	1.400	1.111	41.42	23.59	17.83	.791	.644	1.850	89.51	.215	923.	765.	.272	1.013
11	.2914	.0129	1.400	1.109	41.11	23.49	17.63	.814	.658	1.850	91.32	.210	945.	780.	.276	1.005
10	.2915	.0137	1.400	1.114	40.89	23.26	17.63	.839	.677	1.850	93.15	.206	968.	799.	.274	1.003
9	.2895	.0146	1.400	1.122	40.90	23.07	17.83	.858	.694	1.848	94.28	.203	987.	816.	.268	1.007
8	.2880	.0151	1.400	1.127	40.93	22.98	17.95	.867	.703	1.846	94.71	.202	994.	825.	.265	1.011
7	.2833	.0155	1.400	1.139	41.07	22.82	18.25	.887	.723	1.841	95.68	.199	1013.	845.	.255	1.020
6	.2799	.0151	1.400	1.149	41.26	22.76	18.50	.900	.737	1.837	96.15	.197	1025.	859.	.249	1.028
5	.2774	.0142	1.400	1.159	41.47	22.73	18.74	.911	.748	1.833	96.43	.196	1035.	871.	.244	1.035
4	.2747	.0116	1.400	1.173	41.86	22.76	19.10	.926	.763	1.830	96.64	.195	1049.	886.	.239	1.046
3	.2746	.0111	1.400	1.186	42.30	22.88	19.43	.942	.777	1.827	96.56	.195	1065.	901.	.237	1.054
2	.2823	.0228	1.400	1.192	42.96	23.33	19.63	.966	.789	1.818	95.28	.195	1088.	913.	.237	1.053
1	.3104	-.0297	1.400	1.459	53.99	27.92	26.07	.968	.786	1.868	85.92	.227	1105.	922.	.280	1.254

STL NO.	CUM.PT RATIO	CUM.TT RATIO	CUM. ADIA.	EFF. POLY.
24	1.705	1.218	75.52	77.08
23	1.704	1.212	77.64	79.04
22	1.719	1.208	80.52	81.72
21	1.738	1.211	81.02	82.21
20	1.770	1.214	82.62	83.73
19	1.822	1.218	85.85	86.77
18	1.845	1.218	87.49	88.28
17	1.856	1.219	88.17	88.91
16	1.862	1.220	88.31	89.05
15	1.864	1.220	88.23	88.98
14	1.862	1.220	88.30	89.04
13	1.860	1.218	88.93	89.61
12	1.858	1.215	90.22	90.79
11	1.859	1.210	92.05	92.46
10	1.858	1.206	93.89	94.14
9	1.856	1.203	95.04	95.19
8	1.854	1.202	95.49	95.59
7	1.849	1.199	96.48	96.50
6	1.845	1.197	96.97	96.94
5	1.842	1.196	97.26	97.21
4	1.839	1.195	97.49	97.41
3	1.836	1.195	97.42	97.34
2	1.828	1.195	96.15	96.19
1	1.811	1.227	81.25	82.54

1*VECTORS NASA/AE QHSF Fan. Design Point. 22-in rotor LE tip diameter. 97/03/07
Design report geometry. Final core duct flowpath w/ -60 duct loss. 15:44:24
Rotor and stator performance from DAWES models.

INSIDE VANE 1 AT STATION 21 FLOW 83.38 CORR. FLOW 59.56 TOTAL PRESSURE 22.78
AREA 220.2 SPEC. FLOW 38.96 TOTAL TEMPERATURE 635.7 GAMMA 1.39816

STL NO.	RADIUS	CORD.	VELOCITIES -*-*-*-*-*-*-*-*-* AXIAL	RADIAL	TANG.	MERID.	ABS.	PRESSURE TOTAL	STATIC	TEMPERATURE TOTAL	STATIC	ABSOLUTE MACH NO.	MERIDINAL DISTANCE	R*VU	PERCENT S P A N	PERCENT F L O W	Q
24	10.889	-3.342	546.	0.	72.	546.	551.	21.64	18.80	638.8	613.7	.454	29.197	785.4	100.00	100.00	.9603
23	10.746	-3.370	511.	5.	68.	511.	516.	21.28	18.80	635.7	613.6	.425	29.166	732.0	97.51	96.94	.9604
22	10.592	-3.401	513.	6.	64.	513.	517.	21.30	18.80	633.6	611.5	.427	29.134	674.7	94.85	93.88	.9638
21	10.439	-3.458	524.	3.	65.	524.	528.	21.40	18.79	635.3	612.2	.435	29.076	678.8	91.94	90.83	.9625
20	10.292	-3.520	563.	-3.	66.	563.	567.	21.82	18.78	637.1	610.4	.468	29.014	684.1	89.08	87.77	.9651
19	10.024	-3.659	623.	-12.	70.	623.	627.	22.57	18.77	638.8	606.2	.520	28.875	697.1	83.63	81.65	.9718
18	9.777	-3.816	645.	-19.	72.	645.	649.	22.87	18.78	639.2	604.2	.539	28.719	701.5	78.30	75.54	.9750
17	9.533	-3.976	658.	-25.	73.	658.	662.	23.04	18.76	639.5	603.1	.550	28.563	700.6	72.99	69.42	.9766
16	9.287	-4.137	667.	-27.	76.	668.	672.	23.15	18.73	640.0	602.5	.559	28.407	701.7	67.66	63.30	.9771
15	9.037	-4.302	671.	-26.	78.	672.	676.	23.18	18.71	640.2	602.3	.562	28.252	703.6	62.21	57.19	.9771
14	8.777	-4.472	671.	-23.	80.	672.	676.	23.17	18.69	640.0	602.0	.563	28.095	704.3	56.56	51.07	.9773
13	8.508	-4.648	671.	-19.	83.	671.	676.	23.14	18.67	638.9	601.0	.563	27.936	702.1	50.71	44.96	.9786
12	8.228	-4.832	672.	-16.	85.	673.	678.	23.12	18.62	637.2	599.0	.565	27.777	695.3	44.63	38.84	.9811
11	7.939	-5.021	680.	-15.	86.	680.	686.	23.11	18.50	634.9	595.9	.573	27.619	681.8	38.35	32.72	.9844
10	7.641	-5.217	693.	-16.	87.	693.	698.	23.10	18.31	632.7	592.3	.586	27.469	661.7	31.88	26.61	.9877
9	7.406	-5.371	705.	-19.	87.	705.	710.	23.06	18.12	631.2	589.4	.597	27.361	642.3	26.76	21.91	.9896
8	7.303	-5.438	710.	-19.	87.	711.	716.	23.03	18.02	630.5	588.0	.603	27.319	634.5	24.53	19.91	.9903
7	7.065	-5.594	726.	-13.	88.	726.	731.	22.96	17.76	629.0	584.6	.617	27.235	620.8	19.36	15.37	.9919
6	6.910	-5.696	738.	-7.	89.	738.	743.	22.91	17.56	628.0	582.3	.628	27.194	613.6	15.99	12.50	.9928
5	6.786	-5.778	749.	1.	90.	749.	754.	22.87	17.38	627.4	580.2	.639	27.172	608.8	13.28	10.25	.9933
4	6.630	-5.880	767.	13.	91.	767.	772.	22.86	17.12	626.8	577.3	.656	27.164	605.3	9.90	7.50	.9940
3	6.492	-5.970	784.	28.	93.	785.	790.	22.83	16.86	626.6	574.8	.673	27.187	605.0	6.90	5.12	.9939
2	6.334	-6.074	795.	48.	96.	797.	803.	22.60	16.53	627.1	573.7	.684	27.274	610.2	3.46	2.50	.9903
1	6.174	-6.178	842.	84.	114.	846.	854.	22.91	16.20	643.8	583.3	.722	27.735	705.8	.00	.00	.9684

STL NO.	D-FACTOR	OMEGA BAR	SOLID-ITY	RHO*V RATIO	ABS. ANGLES INLET	ABS. ANGLES EXIT	TURN-ING	ABS MACH NO INLET	ABS MACH NO EXIT	PRESS-URE RATIO	EFFIC IENCY	TEMP RISE	ABS VELOCITY INLET	ABS VELOCITY EXIT	PS RISE	MERID VEL RATIO
24	.3429	-.2075	1.400	1.414	48.72	7.53	41.19	.516	.454	1.941	95.70	.218	623.	551.	.388	1.328
23	.4285	.0056	1.400	1.158	44.72	7.59	37.12	.547	.425	1.767	83.34	.212	656.	516.	.361	1.096
22	.4519	.0811	1.400	1.064	42.09	7.08	35.01	.574	.427	1.726	81.16	.208	685.	517.	.340	1.009
21	.4664	.1323	1.400	1.025	41.28	7.08	34.21	.600	.435	1.719	79.23	.211	716.	528.	.319	.973
20	.4420	.1153	1.400	1.049	40.63	6.74	33.89	.627	.468	1.748	80.64	.214	747.	567.	.302	.993
19	.4039	.0672	1.400	1.095	39.84	6.37	33.48	.665	.520	1.804	84.28	.218	790.	627.	.289	1.028
18	.4011	.0553	1.400	1.102	39.66	6.35	33.31	.689	.539	1.825	85.78	.218	815.	649.	.295	1.028
17	.4042	.0435	1.400	1.112	39.92	6.37	33.55	.706	.550	1.837	86.58	.219	834.	662.	.306	1.029
16	.4112	.0335	1.400	1.123	40.41	6.46	33.95	.722	.559	1.845	86.90	.220	851.	672.	.321	1.030
15	.4238	.0282	1.400	1.128	40.95	6.61	34.34	.737	.562	1.848	86.90	.220	868.	676.	.340	1.024
14	.4396	.0257	1.400	1.126	41.39	6.81	34.58	.753	.563	1.846	87.00	.220	885.	676.	.363	1.012
13	.4557	.0248	1.400	1.119	41.55	7.01	34.54	.771	.563	1.844	87.60	.218	903.	676.	.385	.993
12	.4688	.0248	1.400	1.109	41.42	7.16	34.26	.791	.565	1.842	88.84	.215	923.	678.	.404	.972
11	.4762	.0256	1.400	1.103	41.11	7.19	33.92	.814	.573	1.842	90.58	.210	945.	686.	.414	.956
10	.4798	.0272	1.400	1.104	40.89	7.12	33.77	.839	.586	1.841	92.32	.206	968.	698.	.417	.947
9	.4817	.0291	1.400	1.110	40.90	7.01	33.88	.858	.597	1.837	93.35	.203	987.	710.	.416	.945
8	.4819	.0299	1.400	1.113	40.93	6.97	33.96	.867	.603	1.835	93.74	.202	994.	716.	.415	.946
7	.4803	.0308	1.400	1.126	41.07	6.90	34.17	.887	.617	1.829	94.63	.199	1013.	731.	.410	.951
6	.4781	.0299	1.400	1.138	41.26	6.86	34.40	.900	.628	1.825	95.10	.197	1025.	743.	.405	.957
5	.4751	.0283	1.400	1.151	41.47	6.83	34.64	.911	.639	1.822	95.41	.196	1035.	754.	.400	.965
4	.4688	.0230	1.400	1.174	41.86	6.79	35.07	.926	.656	1.821	95.79	.195	1049.	772.	.392	.981
3	.4641	.0220	1.400	1.195	42.30	6.77	35.53	.942	.673	1.818	95.72	.195	1065.	790.	.383	.996
2	.4706	.0454	1.400	1.202	42.96	6.89	36.07	.966	.684	1.800	93.50	.195	1088.	803.	.370	1.000
1	.4731	-.0588	1.400	1.604	53.99	7.69	46.29	.968	.722	1.892	87.86	.227	1105.	854.	.393	1.303

STL NO.	CUM.PT RATIO	CUM.TT RATIO	CUM. ADIA.	EFF. POLY.
24	1.732	1.218	78.01	79.42
23	1.703	1.212	77.57	78.96
22	1.705	1.208	79.21	80.48
21	1.713	1.211	78.71	80.04
20	1.746	1.214	80.49	81.73
19	1.807	1.218	84.50	85.50
18	1.831	1.218	86.31	87.19
17	1.844	1.219	87.20	88.02
16	1.853	1.220	87.55	88.35
15	1.856	1.220	87.57	88.37
14	1.854	1.220	87.68	88.47
13	1.852	1.218	88.29	89.03
12	1.851	1.215	89.55	90.17
11	1.850	1.210	91.31	91.78
10	1.849	1.206	93.06	93.38
9	1.846	1.203	94.11	94.33
8	1.844	1.202	94.51	94.69
7	1.838	1.199	95.43	95.53
6	1.834	1.197	95.91	95.97
5	1.831	1.196	96.24	96.27
4	1.830	1.195	96.64	96.63
3	1.827	1.195	96.58	96.58
2	1.809	1.195	94.37	94.54
1	1.834	1.227	83.17	84.33

1*VECTORS NASA/AE QHSF Fan. Design Point. 22-in rotor LE tip diameter. 97/03/07
Design report geometry. Final core duct flowpath w/ -60 duct loss. 15:44:24
Rotor and stator performance from DAWES models.

VANE 1 STATION 22 FLOW 83.38 CORR. FLOW 59.89 TOTAL PRESSURE 22.65
AREA 231.2 SPEC. FLOW 37.31 TOTAL TEMPERATURE 635.7 GAMMA 1.39816

STL NO.	RADIUS	CORD.	VELOCITIES -*-*-*-*-*-*-*-*-* AXIAL	RADIAL	TANG.	MERID.	ABS.	PRESSURE TOTAL	STATIC	TEMPERATURE TOTAL	STATIC	ABSOLUTE MACH NO.	MERIDINAL DISTANCE	R*VU	PERCENT S P A N	PERCENT F L O W	Q
24	10.889	-2.389	548.	0.	0.	548.	548.	22.04	19.17	638.8	613.9	.452	30.150	.0	100.00	100.00	.9652
23	10.757	-2.480	471.	7.	0.	471.	471.	21.27	19.18	635.7	617.3	.387	30.056	.0	97.19	96.94	.9602
22	10.607	-2.584	452.	19.	0.	453.	453.	21.12	19.20	633.6	616.6	.372	29.951	.0	93.98	93.88	.9615
21	10.448	-2.694	448.	26.	0.	449.	449.	21.08	19.20	635.3	618.6	.369	29.841	.0	90.60	90.83	.9584
20	10.293	-2.801	499.	32.	0.	500.	500.	21.52	19.16	637.1	616.3	.411	29.733	.0	87.29	87.77	.9613
19	10.015	-2.993	587.	39.	0.	588.	588.	22.37	19.04	638.8	610.1	.486	29.542	.0	81.37	81.65	.9694
18	9.760	-3.170	622.	40.	0.	623.	623.	22.70	18.93	639.2	607.0	.516	29.366	.0	75.91	75.54	.9729
17	9.509	-3.343	645.	37.	0.	646.	646.	22.90	18.83	639.5	604.9	.536	29.196	.0	70.57	69.42	.9748
16	9.260	-3.515	660.	33.	0.	661.	661.	23.03	18.77	640.0	603.7	.549	29.030	.0	65.25	63.30	.9757
15	9.008	-3.689	667.	30.	0.	668.	668.	23.08	18.73	640.2	603.2	.555	28.865	.0	59.89	57.19	.9759
14	8.751	-3.867	669.	29.	0.	669.	669.	23.07	18.70	640.0	602.8	.556	28.700	.0	54.40	51.07	.9762
13	8.486	-4.050	667.	29.	0.	668.	668.	23.04	18.69	638.9	601.9	.556	28.534	.0	48.74	44.96	.9775
12	8.209	-4.241	659.	28.	0.	659.	659.	23.02	18.76	637.2	601.1	.549	28.367	.0	42.85	38.84	.9799
11	7.920	-4.442	643.	25.	0.	644.	644.	23.01	18.92	634.9	600.6	.536	28.199	.0	36.68	32.72	.9831
10	7.616	-4.651	632.	20.	0.	632.	632.	22.98	19.02	632.7	599.6	.527	28.034	.0	30.21	26.61	.9862
9	7.373	-4.820	622.	13.	0.	622.	622.	22.93	19.09	631.2	599.1	.519	27.914	.0	25.01	21.91	.9880
8	7.268	-4.892	623.	-20.	0.	623.	623.	22.90	19.05	630.5	598.4	.520	27.866	.0	22.78	19.91	.9886
7	7.031	-5.056	642.	-17.	0.	642.	642.	22.82	18.75	629.0	594.8	.537	27.774	.0	17.72	15.37	.9902
6	6.879	-5.161	657.	-14.	0.	657.	657.	22.77	18.53	628.0	592.2	.551	27.729	.0	14.48	12.50	.9910
5	6.759	-5.244	671.	-13.	0.	671.	671.	22.74	18.33	627.4	590.0	.564	27.706	.0	11.91	10.25	.9917
4	6.611	-5.346	695.	-10.	0.	695.	695.	22.75	18.04	626.8	586.8	.585	27.698	.0	8.77	7.50	.9926
3	6.483	-5.435	716.	-5.	0.	716.	716.	22.72	17.76	626.6	584.2	.604	27.722	.0	6.03	5.12	.9926
2	6.338	-5.535	722.	1.	0.	722.	722.	22.37	17.40	627.1	583.9	.610	27.812	.0	2.94	2.50	.9874
1	6.200	-5.630	809.	16.	0.	810.	810.	23.20	17.02	643.8	589.5	.681	28.283	.0	.00	.00	.9719

STL NO.	D-FACTOR	OMEGA BAR	SOLID-ITY	RHO*V RATIO	ABS. ANGLES INLET	ABS. ANGLES EXIT	TURN-ING	ABS MACH NO INLET	ABS MACH NO EXIT	PRESS-URE RATIO	EFFIC IENCY	TEMP RISE	ABS VELOCITY INLET	ABS VELOCITY EXIT	PS RISE	MERID VEL RATIO
24	.2914	-.3218	2.191	1.448	48.72	.00	48.72	.516	.452	1.976	98.58	.218	623.	548.	.494	1.334
23	.4488	.0085	2.107	1.084	44.72	.00	44.72	.547	.387	1.766	83.25	.212	656.	471.	.459	1.010
22	.5055	.1222	2.014	.951	42.09	.00	42.09	.574	.372	1.712	79.82	.208	685.	453.	.433	.890
21	.5460	.1988	1.905	.889	41.28	.00	41.28	.600	.369	1.693	76.88	.211	716.	449.	.405	.835
20	.5096	.1730	1.818	.942	40.63	.00	40.63	.627	.411	1.724	78.48	.214	747.	500.	.374	.882
19	.4424	.1010	1.717	1.041	39.84	.00	39.84	.665	.486	1.788	82.91	.218	790.	588.	.333	.970
18	.4252	.0832	1.689	1.069	39.66	.00	39.66	.689	.516	1.811	84.59	.218	815.	623.	.319	.993
17	.4172	.0654	1.679	1.093	39.92	.00	39.92	.706	.536	1.826	85.61	.219	834.	646.	.318	1.010
16	.4178	.0503	1.673	1.112	40.41	.00	40.41	.722	.549	1.836	86.13	.220	851.	661.	.326	1.020
15	.4274	.0423	1.670	1.121	40.95	.00	40.95	.737	.555	1.840	86.23	.220	868.	668.	.343	1.019
14	.4418	.0386	1.674	1.121	41.39	.00	41.39	.753	.556	1.839	86.37	.220	885.	669.	.364	1.008
13	.4573	.0373	1.686	1.113	41.55	.00	41.55	.771	.556	1.836	86.96	.218	903.	668.	.388	.988
12	.4793	.0374	1.709	1.092	41.42	.00	41.42	.791	.549	1.834	88.16	.215	923.	659.	.422	.953
11	.5071	.0386	1.745	1.059	41.11	.00	41.11	.814	.536	1.833	89.84	.210	945.	644.	.465	.904
10	.5286	.0409	1.799	1.033	40.89	.00	40.89	.839	.527	1.831	91.48	.206	968.	632.	.499	.864
9	.5457	.0435	1.854	1.015	40.90	.00	40.90	.858	.519	1.827	92.42	.203	987.	622.	.525	.835
8	.5475	.0447	1.882	1.014	40.93	.00	40.93	.867	.520	1.825	92.76	.202	994.	623.	.529	.829
7	.5337	.0459	1.954	1.034	41.07	.00	41.07	.887	.537	1.818	93.58	.199	1013.	642.	.516	.841
6	.5226	.0446	2.008	1.051	41.26	.00	41.26	.900	.551	1.814	94.05	.197	1025.	657.	.507	.853
5	.5118	.0421	2.057	1.069	41.47	.00	41.47	.911	.564	1.812	94.41	.196	1035.	671.	.499	.865
4	.4937	.0343	2.127	1.102	41.86	.00	41.86	.926	.585	1.812	94.95	.195	1049.	695.	.486	.889
3	.4796	.0328	2.197	1.130	42.30	.00	42.30	.942	.604	1.810	94.89	.195	1065.	716.	.472	.909
2	.4841	.0677	2.279	1.127	42.96	.00	42.96	.966	.610	1.781	91.72	.195	1088.	722.	.455	.906
1	.4337	-.0876	2.381	1.596	53.99	.00	53.99	.968	.681	1.916	89.76	.227	1105.	810.	.474	1.246

STL NO.	CUM.PT RATIO	CUM.TT RATIO	CUM. ADIA.	EFF. POLY.
24	1.764	1.218	80.80	82.05
23	1.702	1.212	77.48	78.88
22	1.691	1.208	77.87	79.22
21	1.688	1.211	76.36	77.82
20	1.722	1.214	78.33	79.70
19	1.791	1.218	83.12	84.22
18	1.817	1.218	85.11	86.08
17	1.833	1.219	86.23	87.12
16	1.844	1.220	86.78	87.63
15	1.848	1.220	86.90	87.75
14	1.847	1.220	87.05	87.88
13	1.845	1.218	87.65	88.43
12	1.843	1.215	88.87	89.54
11	1.842	1.210	90.56	91.09
10	1.840	1.206	92.22	92.60
9	1.836	1.203	93.17	93.47
8	1.833	1.202	93.53	93.79
7	1.827	1.199	94.38	94.57
6	1.823	1.197	94.86	95.00
5	1.820	1.196	95.23	95.34
4	1.821	1.195	95.79	95.85
3	1.819	1.195	95.75	95.81
2	1.790	1.195	92.58	92.90
1	1.857	1.227	85.06	86.08

REPORT DOCUMENTATION PAGE

Form Approved
OMB No. 0704-0188

1. AGENCY USE ONLY (*Leave blank*)	2. REPORT DATE	3. REPORT TYPE AND DATES COVERED
	July 2003	Final Contractor Report

4. TITLE AND SUBTITLE

Design and Test of Fan/Nacelle Models Quiet High-Speed Fan Design

5. FUNDING NUMBERS

WU–781–30–11–00
NAS3–27752

6. AUTHOR(S)

Russ Repp, David Gentile, David Hanson, and Srinivas Chunduru

7. PERFORMING ORGANIZATION NAME(S) AND ADDRESS(ES)

Honeywell Engines, Systems and Services
111 S. 34th Street
Phoenix, Arizona 85072-2181

8. PERFORMING ORGANIZATION REPORT NUMBER

E–13945

9. SPONSORING/MONITORING AGENCY NAME(S) AND ADDRESS(ES)

National Aeronautics and Space Administration
Washington, DC 20546–0001

10. SPONSORING/MONITORING AGENCY REPORT NUMBER

NASA CR—2003-212369

11. SUPPLEMENTARY NOTES

Project Manager, Christopher J. Miller, Structures and Acoustics Division, NASA Glenn Research Center, organization code 5940, 216–433–6179.

12a. DISTRIBUTION/AVAILABILITY STATEMENT

Unclassified - Unlimited
Subject Category: 07 Distribution: Nonstandard

Available electronically at http://gltrs.grc.nasa.gov

This publication is available from the NASA Center for AeroSpace Information, 301–621–0390.

12b. DISTRIBUTION CODE

13. ABSTRACT ***(Maximum 200 words)***

The primary objective of the Quiet High-Speed Fan (QHSF) program was to develop an advanced high-speed fan design that will achieve a 6 dB reduction in overall fan noise over a baseline configuration while maintaining similar performance. The program applies and validates acoustic, aerodynamic, aeroelastic, and mechanical design tools developed by NASA, U.S. industry, and academia. This technology is needed to maintain U.S. industry leadership in the regional turbofan engine market.

14. SUBJECT TERMS

Jet aircraft noise; Compressor blades; Turbofans; Turbomachinery

15. NUMBER OF PAGES

245

16. PRICE CODE

17. SECURITY CLASSIFICATION OF REPORT	18. SECURITY CLASSIFICATION OF THIS PAGE	19. SECURITY CLASSIFICATION OF ABSTRACT	20. LIMITATION OF ABSTRACT
Unclassified	Unclassified	Unclassified	